RAMAN SPECTROSCOPIC CHARACTERISATION OF INORGANIC FIBRES AND PARTICLES AND THEIR COVERAGE BY WETTING AGENTS.

Delphine Bard

A thesis submitted in part fulfilment of the requirement of
Sheffield Hallam University
for the degree of Doctor of Philosophy

November 1998

Collaborating Organisation: Health and Safety Laboratory

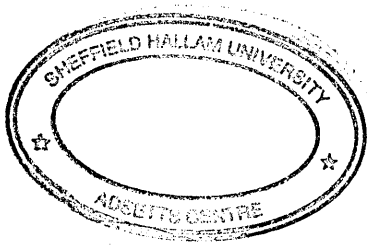
SHEFFIELD HALLAM UNIVERSITY
ADSETTS CENTRE

Acknowledgements.

I would like to specially thank my supervisors Prof. Jack Yarwood (Sheffield Hallam University) and Mr. Barry Tylee (Health and Safety Laboratory) for their support, advice and encouragement. Big thanks also go to:

-the staff at the Health and Safety Laboratory who helped me throughout this work, especially Russell Atkinson for his help on the rotating drum tester.

-Mr Graham Gwilliam at Asbestostrip Innovations for his collaboration.

-Susanne Stich for her precious help and work on gunshot residues

-Stephanie Terrier for her help on the wetting process on inorganic fibres.

I would like to gratefully acknowledge my colleagues and friends at Sheffield Hallam University; Jean-Philippe, Claudia, Peter, Carine, Sohail, Chris (from Baaaaarnsley), Franny, Sandry, Jane, Chris (from Sheffield), Jeff and Pierre, for making life more sunny in Sheffield.

A very special thanks go to my parents for their precious support and encouragement throughout my academic career.

ABSTRACT:

Inorganic fibres especially asbestos have been widely used as a raw material in the construction industries. However, asbestos is now recognised as a carcinogenic material. Therefore, asbestos removal is being widely undertaken. But the hazards increase at this stage as the material is disturbed. Dry removal was found to be an exhausting operation producing a high concentration of fibres. The spraying or injection of wetting agent into the material reduces the hazard associated with the removal process by aggregating the fibres together. The airborne concentration of fibres is then considerably reduced.

Raman microspectroscopy has been shown to be a very powerful technique for the identification of micrometer-sized fibres and particles, with little or no sample preparation. Such spectra are sensitive to the composition of the material and can often be used to distinguish between similar species. Raman microscopy also provides important information about surface coverage of such materials with a spatial resolution between 2 and 4 μm.

Raman spectra were obtained from five asbestos reference standards in comparison with four non-fibrous analogues. The different species such as amosite, anthophyllite, chrysotile, crocidolite and tremolite gave distinct spectra. There were no very distinct differences between the spectra of asbestos fibres and their non-fibrous forms except sometimes in the ν(OH) stretching region or band width in the case of tremolite. The reference spectra have been used for identification of known and unknown (industrial samples) fibres on cellulose filters. Moreover, other inorganic particles on cellulose filters have been identified.

The discrimination between pure diesel and coal particles on quartz filters and the identification of gunshot residues on paper substrates were also successfully achieved.

The coverage of wetting agents on the surface of inorganic fibres connected with asbestos removal operations have been also investigated. Basic laboratory experiments were undertaken. Several inorganic fibres such as man made and asbestos fibres as well as calcium silicate were wetted using different processes: spraying, dipping and capillary adsorption in order to measure the distribution of wetting agents on individual fibres. Insulation materials, usually composed of calcium silicate and asbestos fibres from asbestos removal sites, were collected and also analysed by Raman microspectroscopy. Finally, the effectiveness of suppressing dust was measured on wet industrial samples using a rotating drum tester and the data correlated with Raman measurements.

CONTENTS.

1. Introduction.

The characterisation of pollutants such as asbestos fibres or diesel particles in the atmosphere is very important due to the hazards arising from the inhalation of these carcinogenic particles. Health and Safety Laboratory (HSL) in Sheffield possesses a large number of instruments (optical and electron microscopes, chromatographs, infrared and x-ray spectrometers) allowing the identification of fibres and particles. Nevertheless, Raman microspectroscopy, which is now a well established research technique in the Materials Research Institute at Sheffield Hallam University, can also provide useful information, at the molecular level, from micrometer size particles. HSL was very interested in using this powerful technique for a research project based on 'dust control' especially from silicate fibres. Therefore, the research work discussed in this thesis is a project, based at Sheffield Hallam University and associated with and sponsored by the Health and Safety Executive (parent body of HSL).

1.1. Fibre definition.

Fibres are found everywhere around us from hairs, wool and textile fibres, nylon used for making tights, to asbestos and glass fibres used in insulation materials. The fibres can be classified into natural-occurring and man-made fibres, which can themselves divide into organic and inorganic fibres as shown in figure 1.1.

A fibre is "a slender, elongated structure"[1]. Moreover, fibres possess parallel sides, distinguishing them from dust. A fibre is also characterised by a minimum length and a minimum aspect ratio (the ratio of length to diameter or width). The World Health Organisation has defined a fibre as a particle which has a length greater than 5 μm and an aspect ratio equal or greater than 3:1[2]. The fibres having a diameter less than 3 μm are considered to be respirable[2]. Respirable fibres are fibres which can be inhaled deep into the lungs. The length of a fibre has little influence on its aerodynamic properties. It is agreed that fibres having a length greater than 200 to 250 μm are non-respirable since they are too long to deposit in the lung.

Asbestos fibres can be split into very thin fibres having a diameter of less than 0.05 μm[3]. The Man Made Vitreous Fibres (MMVF) which are synthetic glass fibres, have typical diameter greater than 3 μm. The average diameter is 5 μm with some fibres

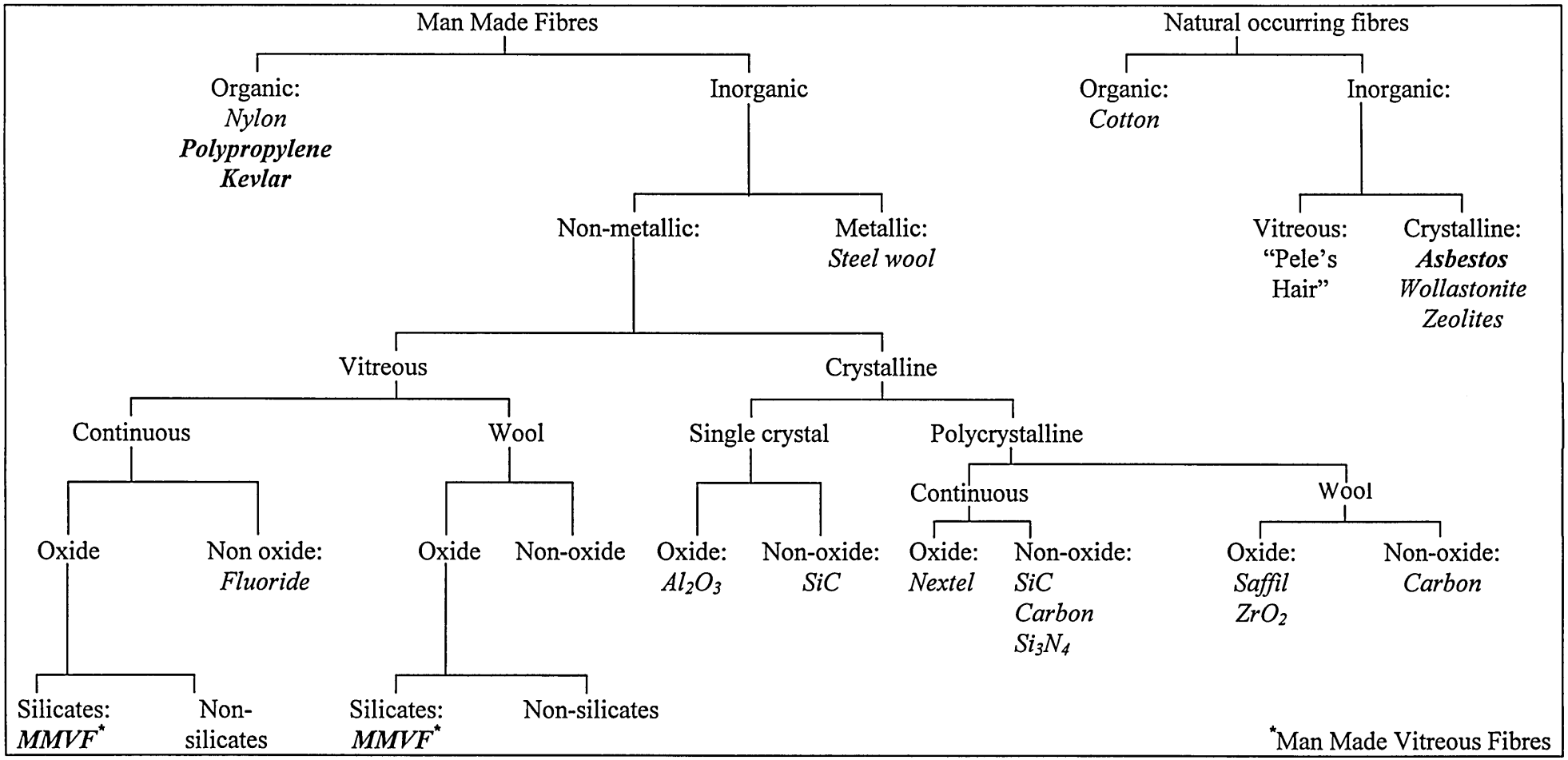

Figure 1.1. Tree of the family fibres.

thinner than 1 and thicker than 20 μm[4]. Organic fibres such as hairs possess a diameter many hundred times thicker than asbestos.

1.2. Asbestos and man made mineral fibres.

The most familiar inorganic fibres are probably asbestos. The term asbestos is derived from the Greek word meaning inextinguishable or unquenchable. Asbestos fibres are naturally occurring silicate minerals which were mined for their useful chemical and physical properties including high tensile strength, flexibility, incombustibility, low thermal conductivity and chemical inertia[5]. In general, asbestos does not degrade below a temperature of 500°C. Only six minerals, belonging to two broad groups, serpentine and amphibole, are classified as asbestos. Actinolite, amosite, anthophyllite, crocidolite and tremolite are amphiboles while chrysotile is a serpentine member. All asbestos minerals can also occur with a different morphology as mineral fragments which are non-fibrous varieties. Compared with asbestos fibres, these crystals are not hazardous.

The man-made vitreous silicate fibres are manufactured fibres from glass or rock. They are oxides, mainly silica SiO_2 and are called silicate glasses. They include textile glass fibres, glass fibres produced for air and liquid filtration and fibres used in insulating and ceiling tile products (glass wool, rock and slag wool and refractory ceramic fibres) which are often called "mineral" fibres in the literature.

The properties of asbestos have been known for over 4000 years. The embalmed bodies of the Pharaohs were wrapped in asbestos clothes to preserve them against the ravages of time. Asbestos was also incorporated to clay for strengthening pots. The first written mention of asbestos by Theophrastus, one of Aristotle's students, appears around 300 B.C in the Greek text "On Stones". It is described as a substance that looks like rotten wood and burns without harm when doused with oil[6]. But, it is only in the mid 19th century, that asbestos was first mined commercially in significant quantities when high pressure and temperature engines become more common and therefore a more effective insulant and packing material was needed. During the first half of the 20th century, asbestos was widely used as an insulating materials in army ships and after the Second World War in the building construction. It is mixed with cement and sprayed as asbestos coatings to protect steel structures against fire in high rise buildings.

Asbestos is combined with plastic to be used in buttons, telephones and electrical panels. Vinyl asbestos floor tiles are also produced. Asbestos finds other applications such as automobile brake shoes or filters to purify fruit juice, wine and sugar. The fibres are also woven into cloth used for fire-proof suits and parachute flares. Chrysotile is the most commercially valuable asbestos because of its silky flexibility and, in general, greater fibre length than amphiboles. In general, 95 % of the world-wide deposits of asbestos are chrysotile and only 5 % are amphiboles[7]. The largest deposits of chrysotile are in Canada and Russia while those of amphiboles are in South Africa. In the 1970s, there was public concern about the health hazards of asbestos and asbestos production reached its maximum at 5 million tons per year[8].

The production of glass wool and refractory ceramic fibres began in the 1930s and 1940s, respectively. In 1985, the world-wide production of man-made mineral fibres (MMMF) exceeded 6 million tons which was more important than the peak of asbestos production in 1970s. MMMF is now used to replace asbestos in industrialised countries[8]. However, in 1997, 2 million tons of asbestos was still used, mostly for asbestos-cement products in Asian, eastern European and developing countries[6].

Silica, asbestos and man made mineral fibres (MMMF) are inorganic particles mainly composed of silicon and oxygen, and all three are known or suspected carcinogens.

Relatively high concentrations of crystalline silica show a risk for lung cancer. From epidemologic studies, there is little evidence for lung cancer induced by Man-Made Mineral Fibres. The International Agency for Research determines that glass wool, rock and slag wool and refractory ceramic fibres are only possibly carcinogenic. Nevertheless, it is now well established that asbestos is associated with the development of pulmonary and pleural diseases, such as asbestosis, lung cancer and mesothelioma[9,10]. One of the properties of asbestos is to break down into millions of fine invisible fibres which can be breathed deeply and retained in the lungs indefinitely. These fine fibres can cause irreparable damage and be responsible for the development of incurable diseases. Since the beginning of the 20th century, asbestosis, which is a pulmonary fibrosis, is recognised as a disease connected with the exposure of asbestos. Mesothelioma, a cancer which affects the membrane lining of the chest or abdomen, was identified in the 1950s. Other cancers of the gastro-intestinal tract and larynx are

also related to asbestos exposure. In the mid 1960s, it became apparent that even low concentrations of asbestos represent a health hazard. The risk of contracting diseases related to asbestos depends on several factors:

- the cumulative dose or total exposure to which the person is exposed,
- the time since the first exposure,
- and the type and size of the asbestos fibres.

Both MMMF and silica are classified in Group 2B whereas asbestos belongs to the Group 1 in terms of toxicity. However, chrysotile is considered less carcinogenic than the amphiboles. Chrysotile fibres, the only asbestos which belongs to the serpentine group, are retained in the lungs for a shorter time than amphiboles[11].

From the end of the World War II up to 1980, asbestos was the material of choice against fire and as a thermal and acoustic insulator, was used in schools, homes, industries, office and public buildings. The asbestos containing materials used in building construction are: asbestos cement, insulation boards, fire proofing panels, floor and ceiling tiles, lagging for boilers and pipes, sprayed coatings... These products are mainly made of chrysotile, which is still used in the production of various asbestos containing materials, and amosite and crocidolite which have been prohibited since 1987[12]. Asbestos encapsulated, or bonded in a matrix, does not show a potential health risk. Risks arise during mining, manufacture of asbestos containing materials (drilling, sawing...) or when the products are damaged or disturbed. In the case of asbestos cement, for example, the concentration of fibres released in the atmosphere is in general very low during the working life time. However, friable materials such as asbestos pipe lagging tend to release a greater number of free fibres as they can be reduced to dust just under hand pressure. In 1984, there was evidence that asbestos cement pipes can pollute the water distribution system with asbestos fibres. Because of the potential risk associated with the presence of asbestos fibres in the air of public buildings, chemical industries and schools[13,14], asbestos is now being progressively removed. But the hazards increase during this process as the material is disturbed. Dry removal is found to be an exhausting operation. The operators have to wear protective clothing and high efficiency respirators making work conditions difficult when the ambient temperature is high. The concentration of fibres in the atmosphere is extremely high and decontamination of the site after removal is difficult and costly. The removal of

contaminated cloths and respiratory equipment by the operators is also a very hazardous operation. The spraying or injection of wetting agent inside the material reduces the hazard associated with the removal process by aggregating the fibres together. The concentration of fibres in the atmosphere is therefore considerably reduced. Indeed, the level of airborne fibres can be reduced from hundreds to less than 1 fibres/ml by using wetting and penetrating agents[15]. In the UK, the Approved Code of Practice 'Work with Asbestos Insulation, Asbestos Coating and Asbestos Insulation Board' imposed the use of dust suppression methods during asbestos removal. An alternative to asbestos removal, is encapsulation. The asbestos material is sprayed with a solution when dry, this forms a coating over the material. In this case the material is not removed.

It is estimated that 0.5 million tons per year of asbestos containing materials are removed from buildings (in the UK). These materials are either double bagged and disposed of underground in landfill sites or resold , in many cases where only chrysotile asbestos is present, as chrysotile is less carcinogenic than amphibole asbestos.

No material as good as asbestos is available to replace it. MMMF such as glass wool are now used, exchanging one risk for another. MMMF does not possess incombustibility properties as good as asbestos, increasing the risk of fire. Moreover, the risk of such fibres is currently a topic of debate.

It should be noted that asbestos exposure can arise from fibrous contamination of other products. Talc, for example, sometimes contains small amounts of asbestos such as tremolite or anthophyllite and the use of cosmetic talcum powders may produce a significant asbestos exposure.

1.3. The UK regulations concerning asbestos fibres.

Concerning the exposure of workers to asbestos fibres, the Control of Asbestos at Work Regulations (CAWR) established limits for short and long work periods, called control limits and action levels respectively[16].

The control limits, for short time exposure, are as follows:

- for the five amphibole asbestos materials or any mixture of any of these five amphiboles with chrysotile: 0.2 fibres/ml during 4 hours or 0.6 fibres/ml during 10 minutes.

- for chrysotile alone: 0.5 fibres/ml during 4 hours or 1.5 fibres/ml during 10 minutes.

The action levels for long time exposure, over a period of 12 weeks, are as follows:

- for the five amphibole asbestos materials or any mixture of any of these five amphiboles with chrysotile: 48 fibre-hours/ml.
- for chrysotile alone: 96 fibre-hours/ml.

Moreover, after asbestos is removed or encapsulated, the concentration of asbestos fibres, called the clearance indicator, established by the Approved Code of Practice Work, cannot exceed 0.01 fibres/ml[16].

There is no regulation in the UK concerning the exposure of workers to MMVF. Typically, man made fibres are not respirable since their diameters are greater than 3 μm.

1.4. HSL techniques for asbestos identification and fibre counting.

Since the inhalation of asbestos dust is associated with lung and other diseases, it is therefore necessary to identify the asbestos and measure the concentration of airborne fibres.

For bulk fibre samples, the simplest and cheapest identification procedure is the Polarised Light Microscopic (PLM) method[17]. Transmission and scanning electron microscopies (TEM, SEM) are also very useful in the case of very small samples or short fibres, especially when coupled with Energy Dispersive X ray (EDX) analysis[17].

For asbestos monitoring, measurements are taken by drawing a known volume of air through a membrane, generally a cellulose filter of 0.8 to 1.2 μm pore size. The filter is placed in a holder fitted with an electrically conducting cowl (figure 1.2). The holder is connected to an adjustable pump by a flexible tube (figure 1.2). A cap is used to protect the filter from contamination during transport. The airborne concentration of asbestos fibres on filters is then measured using the Phase Contrast Microscopic (PCM)[16] method.

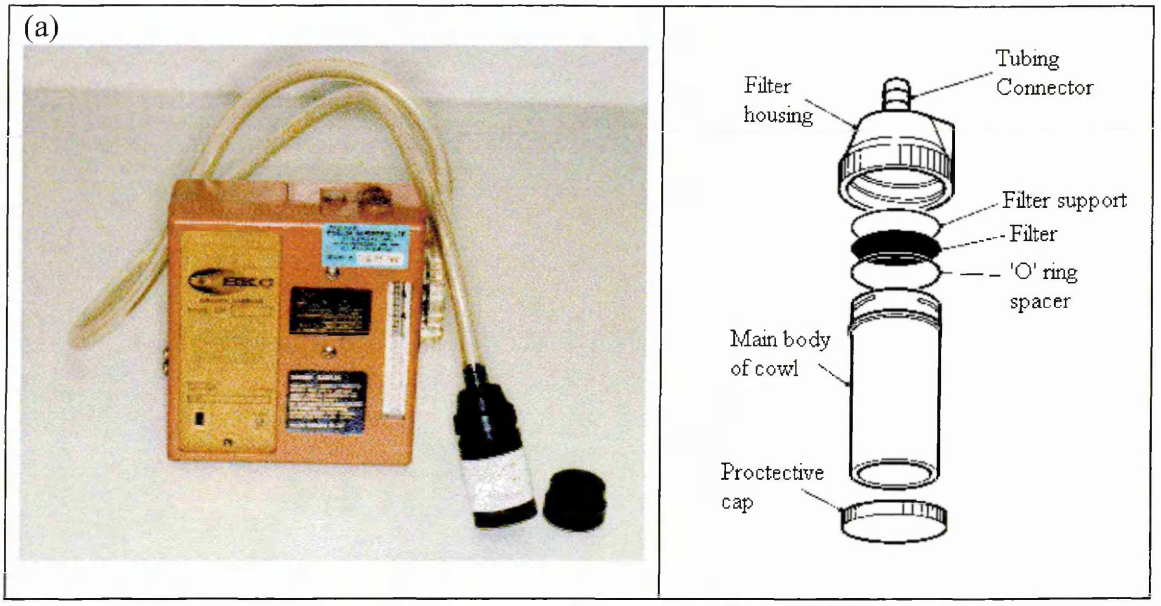

Figure 1.2. Equipment used to collect and monitor airborne fibres. (a) Sample head connected to a pump. (b) Sample head scanned from MDHS 39/4[16].

1.4.1. Polarised Light Microscopic method.

split up using tweezers, immersed in a liquid of known refractive index (RI) and a glass slide,

split up using tweezers, immersed in a liquid of known refractive index (RI) and covered with a glass slip. For a successful analysis, the RI of the liquid needs to be close to one of the two observable RI of the asbestos fibres. The physical properties and appearance of the fibres, under the stereo microscope, are used to choose the RI liquid. Using plane polarised light, the relief and Becke line test can confirm the appropriate RI liquid. The relief which is the contrast observed between the fibre and its liquid has to be small for a correct RI. The Becke line test is performed by partially closing the condenser iris. In this case, a bright halo or Becke line can be observed at the edge of the particle if a difference in RI between the liquid and the fibre exists. If the halo moves into or away from the fibre when the microscope stage is raised, it indicates a lower or greater RI of the liquid than of the fibre respectively. The typical RI liquid are reported in table 1.2.

The identification of asbestos using plane polarised light can now be performed and is based on the morphology, colour and pleochroism, birefringence, extinction characteristics, sign of elongation and dispersion staining which are briefly described below[18]. The microscope is equipped with a polariser which is inserted below the condenser. For observation under crossed polars, an analyser, which transmits only light having passed through an anisotropic object such as asbestos, is inserted. In this case, the fibres are observed against a dark background. This analyser is inserted to observe

birefringence, the extinction and sign of elongation characteristics. A first order red compensator also needs to be inserted to determine the elongation sign of fibres.

a. Morphology.

The asbestos fibres occur in an asbestiform habit which is defined by the following characteristics:

- an length width aspect ratio from 20:1 to 100:1 or higher for fibres longer than 5 μm.
- the ability to split into very thin fibrils.
- two or more of the following characteristics: closely packed bundles of fibrils, fibre bundles with frayed ends, fibres in the form of thin needles, matted masses of individual fibres and curved fibres.

b. Pleochroism.

The colour of asbestos may change depending on the orientation of the fibres parallel or perpendicular to the polariser. Crocidolite gives a dark blue colour when the fibres are parallel to the polariser changing to blue grey when the fibres are perpendicular to the polariser. Actinolite has a green colour when the fibres are parallel to the polariser, changing to pale green, grey or yellow when the fibres are perpendicular to the polariser. However, the other asbestos fibres show little changes in colour using plane polarised light.

c. Birefringence.

The birefringence is the magnitude difference between the highest and lowest RI of a mineral. Asbestos fibres show specific interference colours depending on their birefringence and thickness when they are orientated between crossed polars at about 45^{o} to the polariser. The birefringence magnitude and interference colours for asbestos are reported in table 1.2. It should be noted that glass fibres which are usually isotropic materials appear dark in all directions between crossed polars.

d. Angle of extinction.

Asbestos, as many fibres, shows complete extinction when the fibres are parallel or nearly parallel to the polariser or the analyser (see table 1.2).

e. Sign of elongation.

The sign of elongation expresses the relationship between the shape of the fibre and the optical characteristics. The fibre is called length slow (positive elongation) when the high RI vibration plane is parallel to the long axis. The fibre is called length fast (negative elongation) when the low RI vibration plane is parallel to the long axis. Between crossed polars with a compensator inserted at 45°, the sign of elongation is determined by looking at the colours of the fibres orientated NE-SW (North East - South West) or NW-SE (North West - South East) (see table 1.2). Crocidolite is the only asbestos having a negative elongation .

f. Dispersion staining.

Using white light, dispersion colours are observed when a particle and its liquid medium have a similar RI at one wavelength but a significantly different RI at other wavelengths. Intense dispersion staining colours can be produced by using a dispersion staining objective or a phase contrast objective. The different colours observed when fibres are oriented parallel or perpendicular to the polariser are summarised in table 1.2.

Using the PLM method, it can become difficult to identify the varieties of asbestos if the specimens are exposed to a temperature of over 500 °C for a prolonged period of time since changes in colour, birefringence, sign of elongation, pleochroism can occur[19,20].

1.4.2. Electron Microscopy.

Microscopes using visible light as a source of illumination have a limited resolution. Diffraction effects make it impossible to observe details smaller than 0.1 μm[21]. A typical laboratory microscope with x 40 objective of numerical aperture (NA) 0.7 has its resolution limit at about 0.5 μm[21]. The resolution limit for phase contrast microscopy, using the X 40 objective (NA: 0.65 - 0.7) and eyepieces with a magnification of 12.5, is 0.2 μm[16].

In electron microscopy, an accelerated electron beam is used as a source of illumination. The electron beam possesses a wavelength many times shorter than that of light photons and therefore electron microscopy has a smaller diffraction-limited resolving power.

			Chrysotile	*Amosite*	*Anthophyllite*	*Tremolite*	*Actinolite*	*Crocidolite*
Refractive Index ranges		nα	1.537-1.554	1.670-1.675	1.596-1.654	1.599-1.620	1.619-1.658	1.680-1.692
		nγ	1.545-1.557	1.683-1.694	1.625-1.667	1.622-1.641	1.641-1.677	1.683-1.700
Stereo microscopy observations	colour		colourless and white	colourless and white to grey brown	colourless and white to grey brown	colourless and white to grey brown	green-grey	blue
	appearance		flexible fibres	straight fibres	straight fibres	straight fibres	straight fibres	straight fibres
	lustre		silky	vitreous	vitreous	vitreous	vitreous	metallic
Polarised light microscopy observations	RI liquid		1.550	1.670	1.605	1.605	1.640	1.700
	pleochroism	fibre parallel and perpendicular to the polariser	none	none	none	none	green grey	blue grey
	birefringence		low grey interference colour for thin fibres and white or higher first order colour for thick fibres.	moderate white interference colours for thin fibres and higher first or second order colours for thick fibres	moderate white interference colours for thin fibres and higher first or second order colours for thick fibres	moderate white interference colours for thin fibres and higher first or second order colours for thick fibres	moderate white interference colours for thin fibres and higher first or second order colours for thick fibres	low anomalous interference colours from grey to blue pale or brown
	extinction		complete or undulose with curved fibres when fibres parallel to polariser or analyser	complete when fibres parallel to polariser or analyser	complete when fibres are parallel to polariser or analyser	complete when fibres are parallel or nearly parallel to polariser or analyser	complete when fibres are parallel or nearly parallel to polariser or analyser	complete when fibres are parallel to vibration planes of polariser or analyser
	sign of elongation	compensator at 45° with the slow direction in the NE-SW direction	positive colour blue green with fibre NE-SW colour orange-yellow with fibre NW-SE	positive colour blue green with fibre NE-SW colour orange-yellow with fibre NW-SE	positive colour blue green with fibre NE-SW colour orange-yellow with fibre NW-SE	positive colour blue green with fibre NE-SW colour orange-yellow with fibre NW-SE	positive colour blue green with fibre NE-SW colour orange-yellow with fibre NW-SE	negative colour orange yellow with fibre NE-SW colour blue green with fibre NW-SE
	colours with dispersion staining objective	fibre parallel and	purple	yellow	yellow	yellow	yellow brown	blue
		perpendicular to the polariser	blue	purple-red	orange	blue	blue purple	blue
	colours with phase contrast objective	fibre parallel and	pale blue (fibre) orange (halo)	grey (fibre) yellow (halo)	dark grey (fibre) orange (halo)	dark grey (fibre) yellow (halo)	dark grey (fibre) yellow (halo)	blue (fibre) red brown (halo)
		perpendicular to the polariser	pale blue (fibre) orange (halo)	blue (fibre) orange (halo)	blue (fibre) orange yellow (halo)	blue (fibre) orange (halo)	blue (fibre) orange (halo)	blue (fibre) red brown (halo)

Table 1.2. Asbestos properties for identification by PLM.

The electron microscopes can be classified in two categories: the transmission and reflection light microscopes. The transmission light microscopes such as the TEM (Transmission Electron Microscope) look at the internal structure of translucent specimens whereas the reflection light microscopes such the SEM (Scanning Electron Microscope) look at the outside features.

1.4.2.1. The basic principle of SEM and TEM.

In SEM, an electron beam with energies up to 30-40 keV is focused on the surface of the sample and scanned across it. The electrons can interact with the matter in many ways. Only the emitted secondary electrons and backscattered electrons (or reflected primary electrons) are normally used in the SEM image formation. The intensity of the emitted and reflected electrons is very sensitive to the angle between the incident beam and the sample surface and therefore changes with the topography. The scattered electrons are detected, amplified and used to vary the brightness of a second beam of electrons scanned in synchronism with the first beam on a cathode ray tube display.

In TEM, the electron beam is concentrated on the sample by a condenser lens. The transmitted electrons passing through the sample are focused by the objective lens to produce a magnified primary image. A projector lens enlarges this image which forms the final image on a fluorescent screen or a photographic film.

SEM and TEM can be coupled with Energy Dispersive X-ray analysis. Indeed, under electron bombardment, X-ray photons with wavelength and energy characteristics of the elements in the sample are emitted. This spectrum can then be used for elemental analysis.

1.4.2.2. The SEM and TEM applied to asbestos fibres.

For SEM analysis, the specimens are mounted onto pin stubs and then sputter coated with a thin layer of gold or carbon which gives a conducting surface and dissipates the static charge from the electron beam. SEM instruments give an image showing the morphology of the specimen under study and with an X-ray analytical attachment (EDX) can provide qualitative and quantitative analysis of the elements present.

In SEM, the resolution is mainly limited by the diameter of the electron beam which scans the samples. Modern SEMs can achieve a resolution of about 5 nm with an idealised sample, but in practice the resolution is much smaller [22]. The identification in SEM-EDX is limited to fibres with diameters thicker than 0.1 μm[22]. The EDX spectrum from fibres with diameters less than 0.1 μm are difficult to interpret because of the gold peak. Nevertheless, thin asbestos fibres as small as 0.01 μm can be observed on SEM micrographs[17].

The principal elements in the EDX spectrum of asbestos are silicon, oxygen, magnesium, manganese, calcium, aluminium, sodium and iron, found in different proportion, depending on the varieties. Typical values for the six varieties of asbestos are listed in table 1.3.

	Actinolite	*Amosite*	*Anthophyllite*	*Chrysotile (Cassiar)*	*Chrysotile (Zimbabwe)*	*Crocidolite*	*Tremolite*
Si	20	21	21	17	15	21	21
O	61	63	61	59	59	61	61
Mg	7	5	16	24	21	3	13
Mn	-	1	-	-	0.5	-	-
Fe	5	11	2	0.4	-	9	0.4
Ca	4	-	-	-	-	-	5
Al	1	-	-	0.5	4	-	0.5
Na	-	-	-	-	-	5	-

Table 1.3. Percentage of elements from EDX analysis for the six varieties of asbestos. Analysis made at HSL, Sheffield, as of 22/03/96.

Recently, HSL staff investigated a better way to discriminate asbestos of non-asbestos fibres (crystals) by SEM[23]. In this work, the range of chemical variations and morphologies of tremolite fibres are studied. The detailed examination of the large fibres can help to decide whether if the fibres are asbestiform (having a fibrillar structure) or not. The criterion to classify a material as asbestos is based on the ability of large fibres to split into fine fibrils.

SEM micrographs of four varieties of asbestos are shown in figure 1.3.

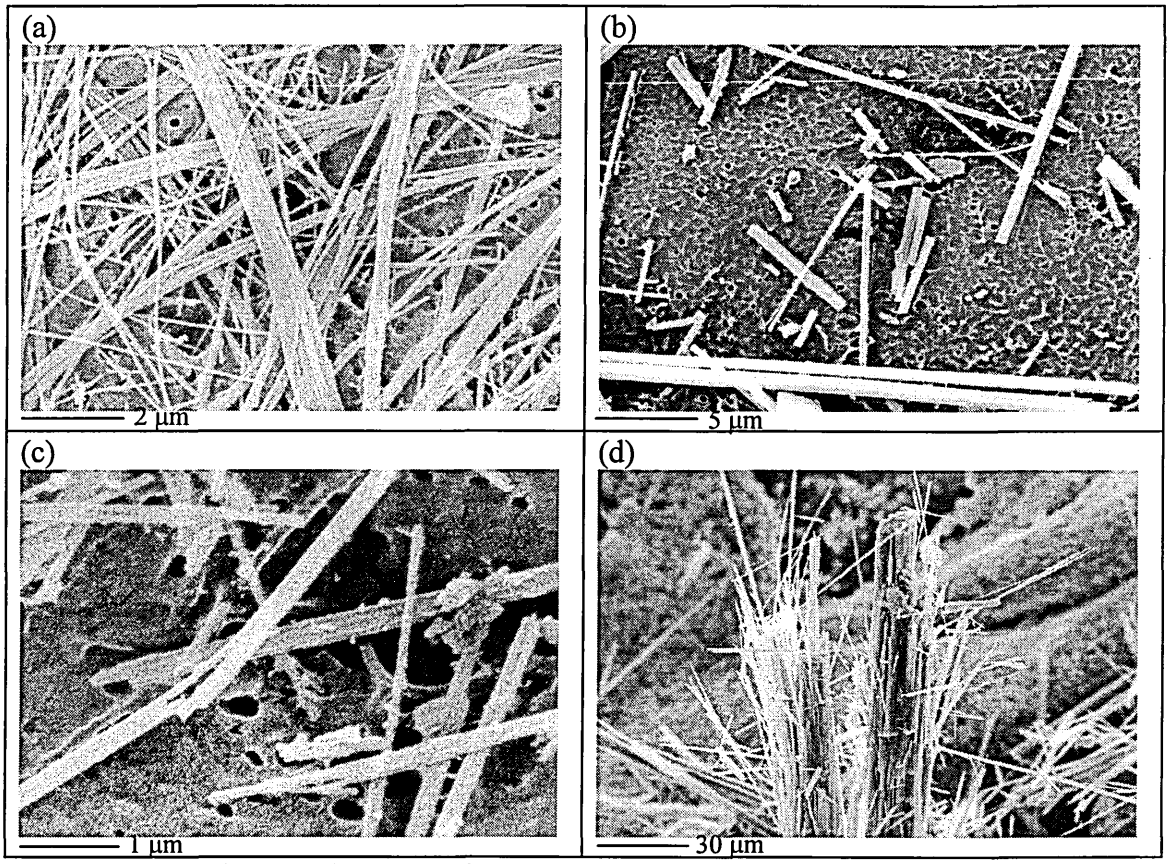

Figure 1.3. SEM images of asbestos fibres. (a) chrysotile, (b) amosite, (c) crocidolite, (d) tremolite. Analysis was made by G.Revell at HSL, Sheffield.

For TEM analysis, the specimen has to be thin enough (few hundred Å thick) for electrons to be transmitted. Bulk samples are ground under liquid or dispersed using ultrasound and then transferred onto a vapour deposited carbon film on a microscope grid. TEM gives an image of the specimen as well as an electron diffraction pattern used to determine the crystal structure and a quantitative analysis with EDX.

The identification limit in TEM is approximately 0.0025 µm (fibre diameter)[22]. Nevertheless images on the few nm scale can be observed. The TEM micrograph of chrysotile fibres gives the image of fibrils having a characteristic tubular morphology with typical diameters of about 250 Å (see chapter 2)[24]. This characteristic appearance and the diffraction pattern are used to identify unambiguously chrysotile from non-fibrous analogues or amphiboles asbestos.

Identification of varieties of asbestos amphiboles from diffraction patterns may be possible. However, the measurements are time consuming and depend strongly on the skills of the manipulator. In fact, TEM is the ultimate technique for asbestos discrimination.

X-ray diffraction analysis can be also employed on its own for the identification of asbestos.

1.4.3. Phase Contrast Microscopic method.

To count the fibres, the filters need previously to be mounted on clean microscope slides using the acetone-triacetin method[16]. The cellulose filter is first attached and cleared onto a glass slide using hot acetone vapour. Then, a drop of glycerol triacetate, called triacetin, is placed onto it and covered with a cover slip.

The microscope is equipped with a positive phase contrast par focal objective X 40 and two eyepieces with magnification of 12.5 X, giving a total magnification of 500 X. One of the eyepieces is fitted with a Walton-Beckett graticule having a diameter of 100 ± 2 μm (figure 1.2). This graticule, having a definite area, is used to count randomly the fibres.

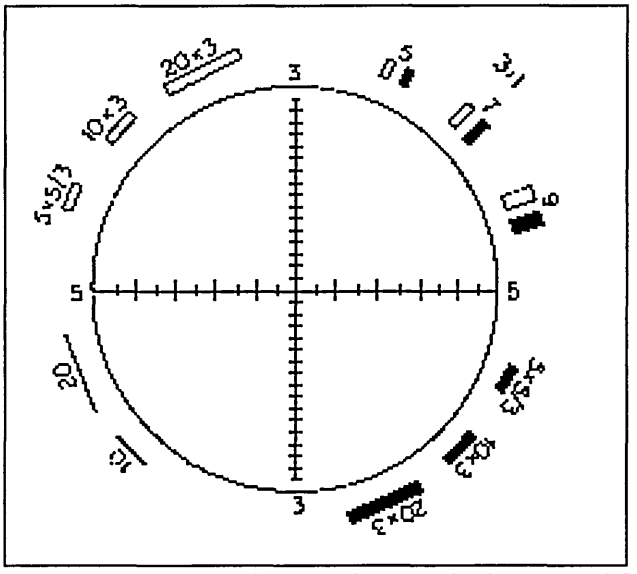

Figure 1.2. The Walton-Beckett graticule scanned from Walton[25].

A countable fibre is defined as an object having a length ≥ 5 μm, a width ≤ 3 μm and an aspect ratio > 3:1 μm. Fibres are not counted when they touch any particle having a size greater than 3 μm. Split fibres are counted as one fibre if they are in agreement with the criteria above (the width is measured across the undivided part). Bundles of fibres are counted as one fibre; otherwise as several individual fibres if they can be distinguished (if they meet the criteria above).

A fibre having two ends in the graticule area is counted as one, a fibre having only one end in the area is counted as half and a fibre passing through the graticule with no end in that area is not recorded. The counting is stopped when either:

- 100 (for clearance indicator) and 200 (for assessment of respiratory protection) are examined.
- or 100 fibres are counted and at least 20 graticules are inspected.

The airborne concentration in fibres/ml is then calculated using the formula:

$$C = 1000\ N\ D^2 / V\ n\ d^2 \qquad 1.1$$

where N is the number of fibres counted, n is the number of graticules area examined, D is the diameter of the exposed filter area (22 mm), d is the diameter of the Walton Beckett graticule (100 μm) and V (in litres) is the volume of air sampled.

It has to be noted that using PCM method, fibres having a diameter smaller than 0.2 μm may not be visible. In practice, this method cannot detect fibres smaller than 0.3 μm[26].Therefore, the airborne concentration is only representative of a part of the total number of fibres. Moreover, since this method does not determine the chemical composition or crystallographic structure, all fibres meeting the size definition, including other varieties of fibres as well as the non-asbestiform mineral fragments, are counted.

The precision of the method depends on the numbers of fibres counted and the uniformity of the fibre distribution on the filter. The limit of detection is 0.01 fibres/ml[16].

1.5. Literature review.

The potential of using Raman spectroscopy for identification and structural characterisation of polymers but also minerals has been recognised for a long time. Raman spectra are fingerprints of the molecular structure of the compounds under study. Because Raman spectroscopy uses optical wavelengths, samples as small as 1 μm can be analysed. The Raman spectra from μm sized regions of crystalline or amorphous solids, from powders or single crystals can be obtained. This attractive technique was used for corrosion studies[27,28], the investigation of inclusions in minerals[29], the identification of contaminants in polymers[30] or also the study of polymer morphology[31].

It was used in the structural studies of silicate glass fibres[32], silicate glasses and melts[33], as well as for the discrimination of silicates[34], feldspars[35] and fibrous natural zeolites[36]. It is an excellent technique to distinguish among crystalline polymorphs such as aluminium hydroxide[37], Al_2SiO_5[38] or high pressure polymorphs of SiO_2[39]. An other area of interest came from planetary and environmental science with the identification of pesticides, vanadium pentoxide particles[40], carbonaceous material associated with urban airborne particles[41] or lunar rock fragments[42]. Raman microscopy was also a useful tool for the study of graphite related carbonaceous compounds[43,44,45] as well as coke, coal and diesel particles[46,47].

In recent years, vibrational spectroscopic techniques have become more and more important for the examination of fibres. Fourier Transform infrared microscopes have proved to be very useful in forensic science, especially for the identification of fibres such as acrylic, wool, nylon fibres[48-51]. However, the direct analysis of fibres may produce a noisy and distorted spectrum due to their circular or elliptical cross section. The fibres needed to be first prepared by rolling flat or by flattening them under high pressure in a diamond anvil cell. It can be also an advantage to increase the sampling area of fibres less than 50 μm because then diffraction effects are reduced, and the signal to noise ratio is improved[52]. But, this method can alter the morphology of the fibre and certain information may be lost. Moreover, infrared microspectroscopy can only analyse samples having a size of at least 10 μm. The non-destructive technique of Raman microspectroscopy is then a very good alternative for the analysis of fibres with little or no sample preparation and a much higher spatial resolution. The spectra extend to low wavenumbers and generally exhibit fewer and narrower bands in comparison with infrared. The only limits are the fluorescence (which may swamp the Raman signal) and the degradation of the specimen under heat of the laser irradiation .The fluorescence can be overcome or diminished by leaving the sample under the laser for few minutes and using a different laser wavelength or a FT Raman spectrometer. The laser power can be reduced using an attenuation filter. The Raman microprobe was also very useful for forensic characterisation of organic fibres such as wool, polyester and polyacrylic fibres[51,53]. Synthetic fibres of different structure showed very different Raman spectra and were easily distinguished. Raman spectra of dyed fibres showed

distinctive bands from the dye and from the fibres[54,55]. Another field of interest was the investigation of the stress in single fibres[56,57,58]

However, the fibres of main interest in this thesis are silicate fibres, especially asbestos fibres. The literature concerning the study of asbestos using vibrational spectroscopy analysis is relatively limited. No articles referring to MMVF could be found in literature.

For infrared analysis, transmission, or more recently diffuse reflectance infrared Fourier transformed spectroscopy (DRIFTS) were the technique of choice for the study of asbestos. These techniques involved the grinding of asbestos with KBr. The infrared spectra of the varieties of asbestos in the 250-1300 cm^{-1} region, showed distinctive spectra[59-61]. Chrysotile was the most investigated asbestos. The characterisation[62,63] and thermal degradation of chrysotile[64,65] were the principal studies by infrared spectroscopy. The analysis and quantification of mixtures of two varieties of asbestos seemed to be possible; but the detection limit depended on the type of mixtures (for example, 3% of crocidolite in chrysotile but 15% of crocidolite in amosite)[60,61]. Recently, DRIFTS was used to identify and quantitate asbestos and asbestos mixtures such as 0.01 % by weight of asbestos in cellulose and 5μg of amosite in 20μg of chrysotile[66]. The application of infrared for the identification of asbestos of insulation materials was also performed by removing individual fibres with tweezers, washing them with dilute acid and mixing them with KBr[60]. The analysis of asbestos containing materials directly mixed with KBr can be difficult and limited due to the presence of the matrix bands[67]. However, these articles did not mention the percentage of fibres in the asbestos containing materials.

Very few articles were published on the investigation of asbestos using Raman microspectroscopy and most work is concerned with the identification of the different asbestos varieties from pure fibres[68-71]. Recently, near infrared and mid infrared diffuse reflection (NIR DR, MIR DR) and Raman spectroscopy were applied to the analysis of four asbestos and non-fibrous forms of serpentine and amphibole minerals[72]. The NIR diffuse reflection and Raman spectra were directly obtained from the fibres using a fibre optic probe and a microspectrometer respectively. To minimise the distortions in the MIR DR spectra, the fibres were ground with dried KBr. It was shown that NIR

spectroscopy might be able to distinguish between asbestos and non-fibrous mineral forms. An asbestos waste was also investigated. An attempt to identify the unknown fibres by Raman spectroscopy, was not very successful. However, the spectra from the waste material was collected only in the 400-1200 cm^{-1} region. The identification was only successfully achieved using NIR DR. The article did not mention either the size of the sample under study or the composition or percentage of asbestos in the waste material.

No articles referring to the study of wetting agents for removal operations on asbestos using Raman or infrared could be found at this date. However, infrared spectroscopy has been used to study the adsorption of molecules on asbestos in a biological context: adsorption of ammonia[73], stearic acid[74], phenanthrene and CO_2[75] on chrysotile, of various probe molecules on amphiboles and chrysotile[76], interaction of chrysotile albumin[77]. Infrared spectroscopy was also employed to look at the modification of asbestos by siliconates[78].

There are general reviews from books or articles on Raman spectra of inorganic or materials which are very useful[79-83].

1.6. Aims and objective.

The principal aim of the work described in this thesis was to explore the value of Raman microspectroscopy for the study of minerals and fibres. In particular, we wanted to address the following questions in connection with the ability of Raman microspectroscopy for:

(1) the identification of inorganic fibres: man-made mineral fibres and varieties of asbestos.

(2) the discrimination of asbestos and mineral fragments; coal and diesel particles.

(3) the identification of μm size fibres or particles on filters or paper substrates, from asbestos containing materials, air monitoring measurements and gun shots.

(4) the detection and coverage measurement of commercial wetting agents on the surface of individual inorganic fibre. Indeed, none of the HSL current techniques, optical microscopy, SEM or TEM can provide information about the distribution of wetting agents on individual fibres during asbestos removal.

This thesis is divided in eight chapters:

Chapter 1 is the general introduction to the research project.

Chapter 2, 3 and 4, cover the theoretical backgrounds. They give a brief overview of Raman spectroscopy, the chemistry of asbestos fibres and MMVF and the wetting process of asbestos-containing materials.

Chapter 5 deals with the discrimination of some reference inorganic fibres and the ability of Raman microspectroscopy to identify individual fibres or particles on filter or paper substrate.

Chapter 6 and 7 deal with the distribution of wetting agents on the surface of inorganic fibres for asbestos removal operations. Chapter 6 concentrates on basic laboratory experiments in order to establish a method for the measurement of the coverage of wetting agents on fibres by Raman microspectroscopy.

Chapter 7 outlines the application of the method for the investigation of wet asbestos containing materials and our attempts to correlate the Raman measurements with the effectiveness of the wetting agents to suppress dust.

Chapter 8 is the conclusion chapter. It gives a summary of these three years of research, the achievements and the future work.

[1] American Heritage Dictionary. Second College Edition, Houghton Mifflin, Boston, 1982.
[2] V. Timbrell. Ann. Occup. Hyg., 26, 347-369, 1982.
[3] R.Derricott. In Asbestos, Eds. L.Michaels and S.S.Chissick, John Wiley and Sons, NewYork, 305-337, 1979.
[4] Nomenclature Committee of TIMA Inc. Nomenclature of Man-Made Vitreous Fibers. Ed. W.Eastes, Owens-Corning Fiberglass, 72 pp, 1991.
[5] Glossary of Geology. American Geological Institute, Washington, Eds. D.C. M.Gary, R.McAffee and C.Wolf, 805 pp, 1974.
[6] J.E. Alleman and B.T. Mossman. Sci. Am., 277, 54-57, 1997.
[7] W.Büchner, R.Schliebs, G.Winter and K.H.Büchel. Industrial Inorganic Chemistry, Eds. H.F. Ebel and C.Dyllick-Brenzinger, VCH Verlagsgeselschaft,Weiheim and VCH Publishers, NewYork, 614 pp, 1989.
[8] K. Steenland and L.Stayner. Canc. Causes Control, 8, 491-503, 1997.
[9] W.H.Walton. Ann. Occup. Hyg., 25, 117, 1982.
[10] K.BéruBé, B.Mossman, T.Quinlan and D.Taatjees. Microsc. Anal., 13-15, 1998.
[11] A.Morgan and A.Holmes. Environ. Res., 39, 475-484, 1986.
[12] The Control of Asbestos at Work Regulations 1987, SI No.2115, HMSO, London.
[13] E.Ganor, A.Fischbein, S.Brenner and P.Froom. Br. J. Ind. Med., 49, 486-488, 1992.
[14] M.A.Mehlman. Ann. N.Y. Acad. Sci., 643, 368-389, 1991.
[15] G.Burdett and G.Revell. Wet Removal of Asbestos: Final Report. Internal report, IR/L/MF/95/08, Health and Safety Laboratory, 11 pp, 1995.
[16] Health and Safety Executive. Asbestos fibres in air. Methods for the Determination of Hazardous Substances, MDHS 39/4, HSE Books, 20 pp, 1995.
[17] D.Cam and M.Staiano. Microsc. Anal., 37-40, 1996.
[18] Health and Safety Executive. Asbestos in Bulk Materials. Methods for the Determination of Hazardous Substances, MDHS 77, HSE Books, 24 pp, 1994.
[19] J.Prentice and M.Keech, Microsc. Anal., 7-12, 1989.
[20] G.J.Laughlin and W.C.McCrone. Microscope, 37, 9-15, 1989.
[21] I.M.Watt. The Pinciple and Practice of Electron Microscopy. Eds. The Press Syndicate of the University of Cambridge, 304 pp, 1985.
[22] K.R.Spurny. Analyst, 119, 41-51, 1994.
[23] G.Revell and G.Burdett. Tremolite: Scanning Electron Microscope Examination of Various Tremolites. Internal report, IR/L/MF/96/06, Health and Safety Laboratory, 7 pp, 1996.
[24] J.E.Chisholm. In Asbestos, Eds. S.S.Chissick and R.Derricott, John Wiley and Sons, NewYork, 85-167, 1983.
[25] W.H.Walton and S.T.Beckett. Ann. Occup. Hyg., 20, 19-23, 1977.
[26] D.K.Verma and N.E.Clark. Am. Ind. Hyg. Assoc. J., 56, 866-873, 1995.
[27] S.J.Oh, D.C.Cook and H.E.Townsend. Hyp. Interact., 112, 59-65, 1998.
[28] H.E.Townsend, T.C.Simpson and G.L.Johnson. Corros. Sci., 50, 546-554, 1994.
[29] B. Wopenka and J.D Pasteris. Appl. Spectrosc., 40, 144-151, 1986.
[30] H.Boyer. Microbeam Anal., 265-268, 1983.

[31] M.Glotin and L.Mandelkern. Colloid Polym. Sci., 260, 182-192, 1982.
[32] C.T.Ho, W.C.LaCourse, R.A.Condrate Sr., A.Jillavenkatesa. Mater. Lett., 23, 237-240, 1995.
[33] P.F.McMillan. Am. Mineral., 69, 622-644, 1984.
[34] A.Wang, J.Han, L.Guo, J.Yu and P.Zeng. Appl. Spectrosc., 48, 959-968, 1994.
[35] T.P.Mernagh. J. Raman Spectrosc., 22, 453-457,1991.
[36] B.Wopenka, J.J.Freeman and T.Nikischer. Appl. Spectrosc., 52, 54-63, 1998.
[37] K.A.Rodgers. Clay Miner., 28, 85-89, 1993.
[38] T.P.Mernagh and L.G.Liu. Phys. Chem. Minerals, 18, 126-130, 1991.
[39] H.Boyer, D.C.Smith, C.Chopin and B.Lasnier. Phys. Chem. Minerals, 12, 45-48, 1985.
[40] E.S.Etz, G.J.Rosasco and J.J.Blaha. In Environmental Pollutants, Eds. T.Y.Toribara and J.R.Coleman, Plenum Publishing Corp., New York, 413-458, 1978.
[41] J.J.Blaha, G.J.Rosasco and E.S.Etz. Appl. Spectrosc., 32, 292-297, 1978.
[42] A.Wang, B.L.Jolliff and L.A.Haskin. J. Geophys. Res., 100, 189-199, 1995.
[43] Z.Zheng and X.Chen. Sci. China, Ser. B, 38, 97-106, 1994.
[44] R.M.Bustin, J.N.Rouzaud and J.V.Ross. Carbon, 33, 679-691, 1995.
[45] J.D.Pasteris and B.Wopenka. Can. Mineral., 29, 1-9, 1991.
[46] P.D.Green, C.A.Johnson and K.M.Thomas. Fuel, 62, 1013-1023.
[47] L.Suhartono, B.C.Cornilsen, J.H.Johnson and D.H.Carlson. Appl. Occup. Environ. Hyg., 11, 790-798, 1996.
[48] M.C. Grieve. Sci. Justice, 35, 179-190, 1995.
[49] T.Gal, I.Ambrus and S.Urszu. Acta Chim. Hungarica, 128, 919-928, 1991
[50] T.J.Hopen and G.D.Schubert. Microscope, 43, 109-113, 1995.
[51] P.L.Lang, J.E.Katon, J.F. O'Keefe and D.W.Schiering. Microchem. J., 34, 319-331, 1986.
[52] E.G.Bartick. In The Design, Sample Handling and Applications of Infrared Microscopes, Ed. P.B.Roush, American Society for Testing and Materials, Philadelphia, 64-73, 1987.
[53] L.E.Jurdana, K.P.Ghiggino and K.W.Nugent. Textile Res. J., 65, 593-600, 1995.
[54] I.P.Keen, G.W.White and P.M.Fredericks. J. Forensic Sci., 43, 82-89, 1998.
[55] S.P.Bouffard, A.J.Sommer, J.E.Katon and S.Godber. Appl. Spectrosc., 48, 1387-1393, 1994.
[56] N.Everall and J.Lumsdon. J. Mater. Sci., 26, 5269-5274, 1991.
[57] K.Prasad and D.T.Grubb. J. Appl. Polym. Sci., 41, 2189-2198, 1990.
[58] M.C.Andrews and R.J.Young. J. Raman Spectrosc., 24, 539-544, 1993.
[59] M.J.Luys, G.De Roy, E.F.Vansant and F.Adams. J. Chem. Soc. Faraday Trans. 1, 78, 3561-3571, 1982.
[60] A.Marconi. Ann. Ist. Sup. Sanità, 19, 629-638, 1983.
[61] G.A.Luoma, L.K.Yee and R.Rowland. Anal. Chem., 54, 2140-2142, 1982.
[62] C.Viti and M.Mellini. Eur. J. Mineral., 9, 585-596, 1997.
[63] M.K.Titulaer, J.C.Van Miltenburg, J.B.H.Jansen and J.W.Geus. Clay. Clay Miner., 41, 496-513, 1993.
[64] C.Jolicoeur and D.Duchesne. Can. J. Chem., 59, 1521-1526, 1981.

[65] A.K.Datta. J. Mater. Sci. Lett., 10, 870-871, 1991.
[66] P.L.Lang, V.V.Chu, K.McCune, S.Franssen, M.Goodnight-Schmidt, R.Mendenhall and W.Conner. Appl. Spectrosc., 52, 212-217, 1998.
[67] D.Balducci and F.Valerio. Intern. J. Environ. Anal. Chem., 27, 315-323, 1986.
[68] J.J.Blaha and G.J.Rosasco. Anal. Chem., 50, 892-896, 1978.
[69] M.Delhaye, P.Dhamelincourt and F.Wallart. Toxicol. Env. Chem. Rev., 3, 73-87, 1979.
[70] J.J.Blaha, E.S.Etz and W.C.Cunningham. Scanning Electron Microsc.I, SEM Inc., 1, 93-102, 1979.
[71] A.Wang, P.Dhamelincourt and G.Turrell. Appl. Spectrosc. 42, 1441-1450, 1988.
[72] I.R.Lewis, N.C.Chaffin, M.E.Gunter and P.R.Griffiths. Spectrochim. Acta, 52A, 315-328, 1996.
[73] B.Fubini and L.Mollo. Langmuir, 13, 919-927, 1997.
[74] V.E.Berkheiser. Clay. Clay Miner., 30, 91-96, 1982.
[75] H.Suquet. Can. J. Chem., 67, 202-207, 1988.
[76] L.Bonneau, H.Suquet, C.Malard and H.Pezerat. Environ. Res., 41, 251-267, 1986.
[77] R.Dimitru-Stanescu, C.Mandravel and C.Bercu. Analyst, 119, 689-691, 1994.
[78] Y.Pelovski, M.Petkova, I.Dombalov and G.Liptay. J. Therm. Anal., 42, 485-490, 1994.
[79] W.P.Griffith. In Spectroscopy of Inorganic Based Materials, Eds. R.J.H.Clark and R.E.Hester, John Wiley and Sons, 119-185, 1987.
[80] K.Nakamoto. Infrared and Raman spectra of inorganic and Coordination Compounds, 4th Ed., a Wiley-Interscience publication, New York, 484 pp, 1986.
[81] I.A.Degen and G.A.Newman. Spectrochim. Acta, 49A, 859-887, 1993.
[82] W.P.Griffith. J. Chem. Soc. (A), 286-291, 1970.
[83] E.E.Coleyshaw and W.P.Griffith. Spectrochim. Acta, 50A, 1909-1918, 1994.

2. Raman spectroscopy.

2.1. Raman theory.

2.1.1. Introduction.

The Raman effect was first observed by Raman in 1928 using focused sunlight and filters and relied on visual observation of colour changes in the scattered light[1,2].

The Raman scattered light is due to rotations and vibrations of the molecule under study. If a sample is illuminated with a monochromatic light (ν_0) which has an energy too low to excite an electronic transition of the molecules, most of the light is transmitted, 1 to 5 % is reflected[3], and a very small quantity (less than 0.1 %)[4] is scattered in all the directions. Most of the scattered light possess the same frequency as the incident light (ν_0) and is called elastic or Rayleigh scattering. About 10^{-6} [4] of the incident light is scattered at different frequencies[4]. The Raman scattering is an inelastic process.

($\nu_0 - \nu_v$) referred as Raman Stokes scattering frequency and ($\nu_0 + \nu_v$) to as Raman anti-Stokes scattering frequency. The differences in frequency $\Delta\nu = |\nu_o - (\nu_o \pm \nu_{vib})| = |\pm\nu_v|$ are independent of the incident light frequency ν_o and are characteristic of the molecules. At normal temperature, the anti-Stokes lines intensity is weaker than the Stokes lines. Since the Stokes and anti-Stokes Raman spectra are identical in frequency, it is usually the Stokes Raman scattering which is recorded.

2.1.2. Classical theory.

According to the classical theory[1,3,5,6], when a molecule is placed in an electric field ($\vec{E}$), the electrons moved to follow the field thus creating an electric dipole moment. For small field, the induced dipole moment ($\vec{P}$) is proportional to the applied field ($\vec{E}$):

$$\vec{P} = \vec{\vec{\alpha}}\ \vec{E} \qquad 2.1$$

$\vec{\vec{\alpha}}$ is the polarisability of the molecule and is characteristic of the ease with which the electron cloud of the molecule can be distorted. α is a tensor and can be expressed in the xyz directions of the Cartesian system as:

$$\begin{pmatrix} \vec{P}_x \\ \vec{P}_y \\ \vec{P}_z \end{pmatrix} = \begin{pmatrix} \alpha_{xx} & \alpha_{xy} & \alpha_{xz} \\ \alpha_{yx} & \alpha_{yy} & \alpha_{yz} \\ \alpha_{zx} & \alpha_{zy} & \alpha_{zz} \end{pmatrix} \begin{pmatrix} \vec{E}_x \\ \vec{E}_y \\ \vec{E}_z \end{pmatrix} \qquad 2.2$$

$\vec{E}$, the electric field associated with the electromagnetic radiation, is given by:

$$\vec{E} = \vec{E}_o \cos(2\pi t\nu_o) \qquad 2.3$$

$\vec{E}_o$ is the equilibrium field strength and ν_o is the angular frequency of the radiation. In the case of a diatomic molecule which vibrates with a frequency ν_v at time t, the normal coordinate q_v is given by:

$$q_v = q_o \cos(2\pi\nu_v t) \qquad 2.4$$

The tensor $\vec{\vec{\alpha}}$ depends on the geometry of the molecule and then varies with the normal coordinates. In the harmonic case, we can write:

$$\vec{\vec{\alpha}} = \vec{\vec{\alpha}}_o + \left(\frac{\partial\vec{\vec{\alpha}}}{\partial q_v}\right)_o q_v \qquad 2.5$$

If there is interaction between the incident radiation, of frequency ν_o, and the molecule, then from equation 2.1 and equation 2.5:

$$\vec{P} = \vec{\vec{\alpha}}_o \vec{E} + \left(\frac{\partial\vec{\vec{\alpha}}}{\partial q_v}\right)_o q_v\vec{E} \qquad 2.6$$

Substitution of equation 2.3 and 2.4 in equation 2.6 yields:

$$\vec{P} = \vec{\vec{\alpha}}_o \vec{E}_o \cos(2\pi\nu_o t) + \left(\frac{\partial\vec{\vec{\alpha}}}{\partial q_v}\right)_o q_o \vec{E}_o \cos(2\pi\nu_o t)\cos(2\pi\nu_v t) \qquad 2.7$$

$$\text{since: } \cos(2\pi\nu_o t)\cos(2\pi\nu_v t) = \frac{1}{2}\left[\cos(2\pi(\nu_o+\nu_v)t) + \cos(2\pi(\nu_o-\nu_v)t)\right] \qquad 2.8$$

then:

$$\vec{P} = \vec{\vec{\alpha}}_o \vec{E}_o \cos(2\pi\nu_o t) + \frac{1}{2}\left(\frac{\partial\vec{\vec{\alpha}}}{\partial q_v}\right)_o q_o \vec{E}_o \left[\cos(2\pi(\nu_o+\nu_v)t) + \cos(2\pi(\nu_o-\nu_v)t)\right] \qquad 2.9$$

The first term in equation 2.9 describes the Rayleigh scattering (ν_o) and the other terms describe the Stokes (ν_o-ν_v) and the anti-Stokes Raman scattering (ν_o+ν_v).

2.1.3. The quantum theory.

In the case of a diatomic molecule treated as a simple harmonic vibrator, the energy (E_v) of each of its vibrations is quantised:

$$E_v = h\nu\left(v+\frac{1}{2}\right) \qquad 2.10$$

where v is the vibrational quantum number which have the values 0,1, 2, 3, 4....

The quantum theory[1,4,5] considers the monochromatic radiation of frequency ν_o as a stream of photons having an energy $h\nu_o$. In the Rayleigh scattering (figure 2.1), the photons are scattered without change in frequency and energy ($h\nu_o$). Raman scattering occurs as a result of the interaction of the light with a molecule. The result is a transfer of energy between the light the incident photons and the molecule. In the Stokes Raman scattering (figure 2.1), the molecule is undergoing a vibrational transition from the ground state (v=0) to the first excited state (v=1). The scattered photons have a diminished energy $h(\nu_o-\nu_v)$ and so lower frequency than the incident light. In the anti-Stokes Raman scattering, the molecule is undergoing a vibrational transition from the excited state (v=1) to the ground state (v=0). The scattered photons have an enhanced energy $h(\nu_o+\nu_v)$ and so higher frequency than the incident light.

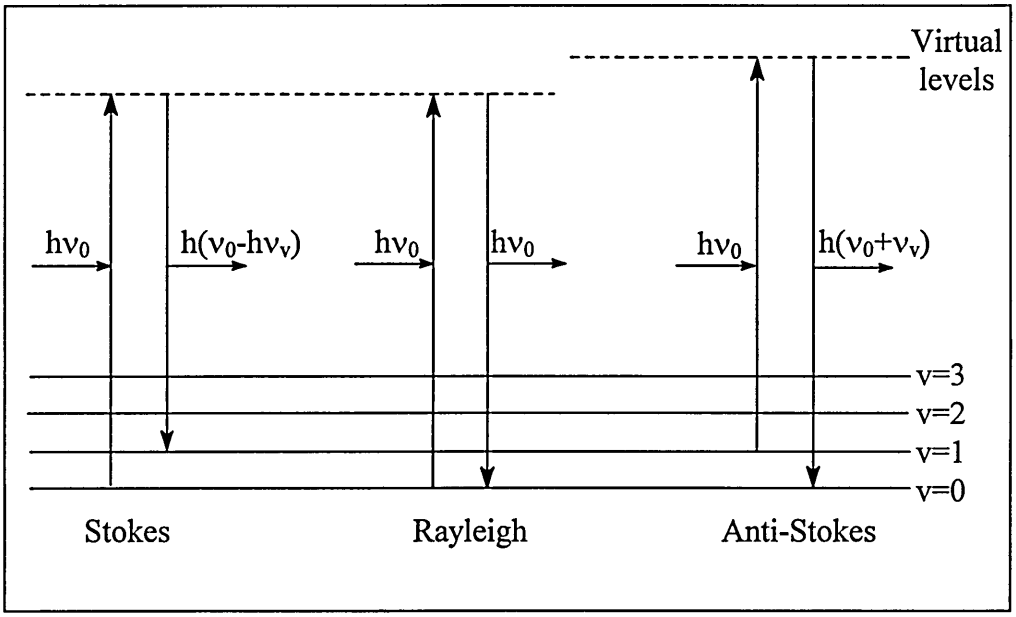

Figure 2.1: Energy level diagram of Raman and Rayleigh scattering effect.

According to the Boltzmann distribution law[7],the ratio of the number of molecules (N_i) in state i, having energy E_i, to the number molecules (N_j) in state j, having energy Ej, at thermal equilibrium, is given by:

$$\frac{N_j}{N_i} = \frac{g_j}{g_i} e^{-\left(\frac{Ej-E_i}{k_B T}\right)} \qquad 2.11$$

g_i and g_j are the degeneracies of the two states i and j.

At ordinary temperature, from equation 2.11, the number of molecules in the ground state N_i will be greater than that of the excited state N_j. Since the intensity of a transition is dependent on the number of molecules which are in the state corresponding to the starting point of transition, the Stokes lines intensity will be higher than that of anti-Stokes lines at ordinary temperature.

2.1.4. Selection rules.

A transition is allowed if the polarisability of transition is different from zero[3] which can be expressed as:

$$[P_{ij}] = \int \psi_j^* \vec{P} \psi_i \, dq_v \qquad 2.12$$

where ψ_i and ψ_j are the wave functions of the states i and j, $\vec{P}$ is the induced dipole moment operator.

In the harmonic case, $\vec{P}$ can be expressed as:

$$\vec{P} = \vec{\vec{\alpha}}_o \vec{E} + \left(\frac{\partial \vec{\vec{\alpha}}}{\partial q_v}\right)_o q_v \vec{E} \qquad 2.6$$

Substitution of equation 2.6 in equation 2.12 yields:

$$[P_{ij}] = \vec{\vec{\alpha}}_o \vec{E} \int \psi_j^* \psi_i \, dq_v + \left(\frac{\partial \vec{\vec{\alpha}}}{\partial q_v}\right)_0 \vec{E} \int \psi_j^* q_v \psi_i \, dq_v \qquad 2.13$$

The first term of equation 2.13 is zero because of the orthogonality of the wave functions unless i=j. It is the case of the Rayleigh scattering which is not dependant of the polarisability change.

The second term is different from zero if:

$\int \psi_j^* q_v \psi_i \, dq_v \neq 0$, in the harmonic case, $j=i \pm 1$ or $\Delta v = \pm 1$

or if $\left(\frac{\partial \vec{\vec{\alpha}}}{\partial q_v}\right)_0 \neq 0$, i.e. if there is change in the polarisability tensor against the vibrational coordinates.

The general harmonic rule for Raman vibrational transitions is $\Delta v = \pm 1$ but overtone transitions can be allowed with $\Delta v = \pm 2, 3...$ and combination bands can occur when one photon is absorbed and more than one vibration is excited. However, these bands are extremely weak in most Raman spectra.

2.1.5. Raman intensities.

The intensity per solid angle of scattered light [1,6] corresponding to a transition between two vibrational states i and j is given by:

$$I_{i \to j} = \text{const}\, I_0 (\nu_0 + \nu_{ij})^4 \left| (P_{\rho\sigma})_{ij} \right|^2 \qquad 2.14$$

$$\text{where } (P_{\rho\sigma})_{ij} = \sum_{\rho\sigma} (\alpha_{\rho\sigma})_{ij} E_\rho \qquad 2.15$$

I_0 and ν_0 are the intensity and frequency of the incident light, ν_{ij} is the frequency corresponding to the energy difference between the states i and j, $P_{\rho\sigma}$ are the components of the induced dipole moment, $\alpha_{\rho\sigma}$ are the components of the polarisability tensor, E_ρ are the components of the electric field of the incident light, σ and ρ denote x, y, z Cartesian components.

$\alpha_{\rho\sigma}$ can be written in the form:

$$(\alpha_{\rho\sigma})_{ij} = \frac{1}{h} \int \psi_j^* \alpha_{\rho\sigma} \psi_i \, dq_v \qquad 2.16$$

ψ_i and ψ_j are vibrational state wave functions.

The $\alpha_{\rho\sigma}$ terms can be expanded in a Taylor series as a function of vibrational coordinate q_v:

$$\alpha_{\rho\sigma} = (\alpha_{\rho\sigma})_0 + \left(\frac{\partial \alpha_{\rho\sigma}}{\partial q_v} \right)_0 q_v + \ldots \qquad 2.17$$

Substitution of equation 2.17 in equation 2.16 yields:

$$(\alpha_{\rho\sigma})_{ij} = \frac{1}{h} (\alpha_{\rho\sigma})_0 \int \psi_j^* \psi_i \, dq_v + \frac{1}{h} \left(\frac{\partial \alpha_{\rho\sigma}}{\partial q_v} \right)_0 \int \psi_j^* q_v \psi_i \, dq_v \qquad 2.18$$

The first term of equation 2.18 is zero unless i=j and is responsible for Rayleigh scattering. The second term describes the Raman scattering and is different from zero for a harmonic oscillator if i=j±1.

If we consider a Stokes transition from v to (v+1), $\alpha_{\rho\sigma}$ can be expressed as:

$$(\alpha_{\rho\sigma})_{v \to v+1} = \frac{1}{h} \left(\frac{\partial \alpha_{\rho\sigma}}{\partial q_v} \right)_0 \sqrt{\frac{(v+1)h}{8\pi^2 \mu \nu_v}} \qquad 2.19$$

μ is the reduced mass and ν_v is the Stokes frequency.

An expression of the intensity of a Stokes Raman band for N molecules can be given by:

$$I_{i \to j} = \text{const}\, I_0 \frac{(\nu_0 - \nu_v)^4 N}{\left(1 - e^{-h\nu_v/kT}\right)} \frac{\sum_{\rho\sigma}\left(\frac{\partial \alpha_{\rho\sigma}}{\partial q_v}\right)^2 E_\rho^2 (v+1)h}{h^2 8\pi^2 \mu \nu_v} \qquad 2.20$$

By summation over $\sigma\rho$ for a polarised incident light:

$$I_{i \to j} = K\, I_0 \frac{(\nu_0 - \nu_v)^4 N}{\left(1 - e^{-h\nu_v / kT}\right)\mu\nu_v} \left[45\bar{\alpha}^2 + 13\gamma^2\right] \qquad 2.21$$

$\bar{\alpha}$ (mean value) and γ (anisotropy) are two invariant quantities related back to $\vec{\vec{\alpha}}$ tensor given in equation 2.2.

2.1.6. Raman spectroscopy of crystals.

A crystal is characterised by a primitive cell which is the smallest unit, repeated in three dimensions. The site symmetry of a molecule in the crystalline state is, in general, lower than in the isolated molecule. The reduction in symmetry may split the degenerate vibrations. In addition, crystals can present lattice modes resulting from translatory and rotatory motions. However, these "external" modes give bands usually in the low frequency region or as the combination bands with internal modes in the high frequency region.

In the case of caesium chloride[4] primitive cell, in body centred cubic symmetry, a typical vibration occurs as shown in figure 2.2.

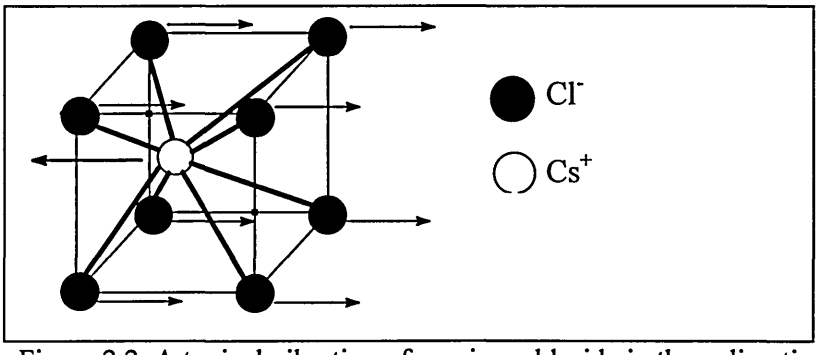

Figure 2.2. A typical vibration of caesium chloride in the y direction.

This vibration can appear in any of the three Cartesian x, y, z directions. These three vibrations have the same frequency, then are said to be triple degenerate. If the caesium chloride symmetry is reduced from cubic to orthorhombic, the three vibrations are no longer equivalent. They appear at three different frequencies and are referred to as lattice modes.

The free CO_3^{2-} ion presents internal modes of vibration when calcite or aragonite[4] exhibits internal and external or lattice modes. The calcite crystal possesses two molecules (Ca^{2+} CO_3^{2-}) in the unit cell while aragonite has four molecules per unit cell. As we have seen, the symmetry of carbonate ions placed in a "crystal" may be lower than that of the free ions. The four internal modes of the carbonate ion are shown in figure 2.3

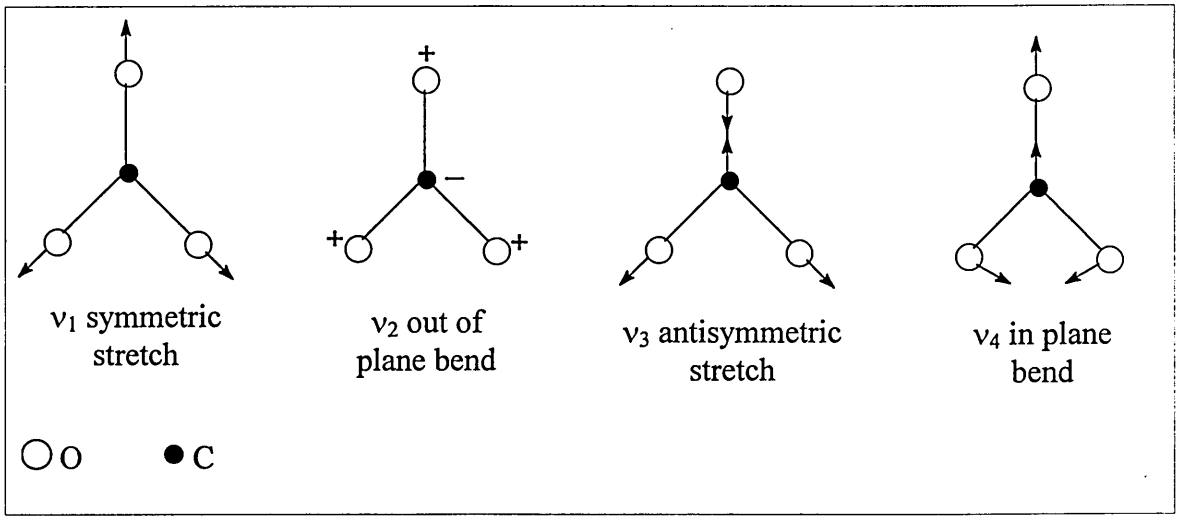

Figure 2.3. Internal modes of vibration of ion CO_3^{2-}

ν_1, ν_3 and ν_4 are Raman active. ν_3 (antisymmetric stretch) and ν_4 (in plane blend) have a degeneracy of two. Placing carbonate ions in a crystal structure may remove the degeneracy. This does not occur for calcite because the carbonate vibrations from the two CO_3^{2-} in the primitive cell can couple as shown in figure 2.4 for vibration ν_1. The internal calcite modes are observed at 1088 cm^{-1} (symmetric stretch), 1443 cm^{-1} (antisymmetric stretch) and 714 cm^{-1} (in plane bend)[4].

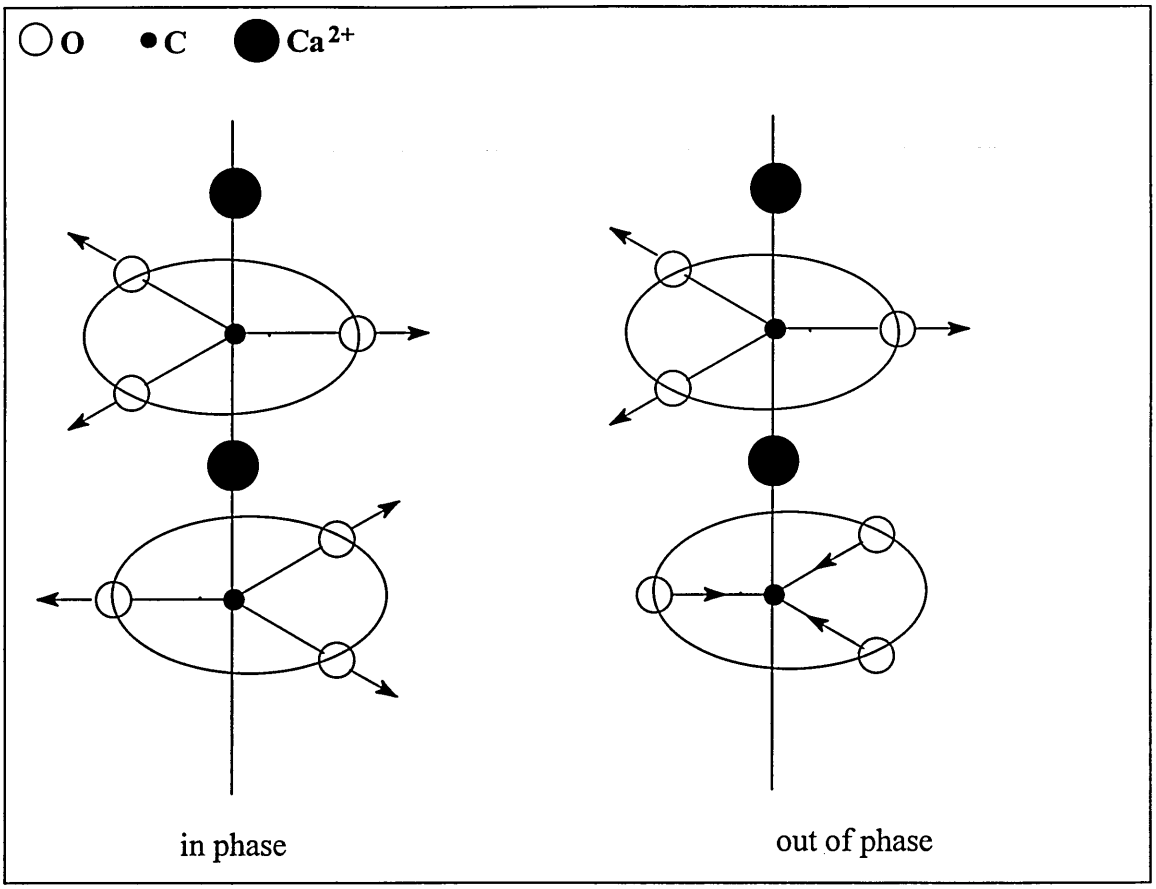

Figure 2.4. ν_1 vibrations coupled in phase and out of phase from the calcite unit cell.

In the case of aragonite, which has four molecules to a unit cell, the loss of the C_3 axis removes the degeneracy of the vibrations ν_3 and ν_4. Doublets appear if the magnitude of the splitting is sufficient. Calcite and aragonite show also lattice modes in low frequency at ~ 153, 283 cm^{-1} and 150, 180, 190, 206 cm^{-1} respectively[4].

2.2. Renishaw Ramanscope 2000 spectrometer.

2.2.1. Introduction.

The main difficulty in Raman spectroscopy has been the very low intensity of Raman scattered light and the high intensity of unwanted Rayleigh scattered light. The function of the spectrometer (figure 2.5) is to excite a sample with a suitable powerful laser light, to remove the Rayleigh scattered light in order to leave the Raman scattered light and then to detect photons at the shifted wavenumbers.

2.2.2. General description of the Renishaw spectrometer.

The excitation light is usually provided by a visible laser. The first component of the spectrometer is the plasma line rejection filter (1). The filter blocks the unwanted

Figure 2.5. Renishaw Ramascope 2000 spectrometer

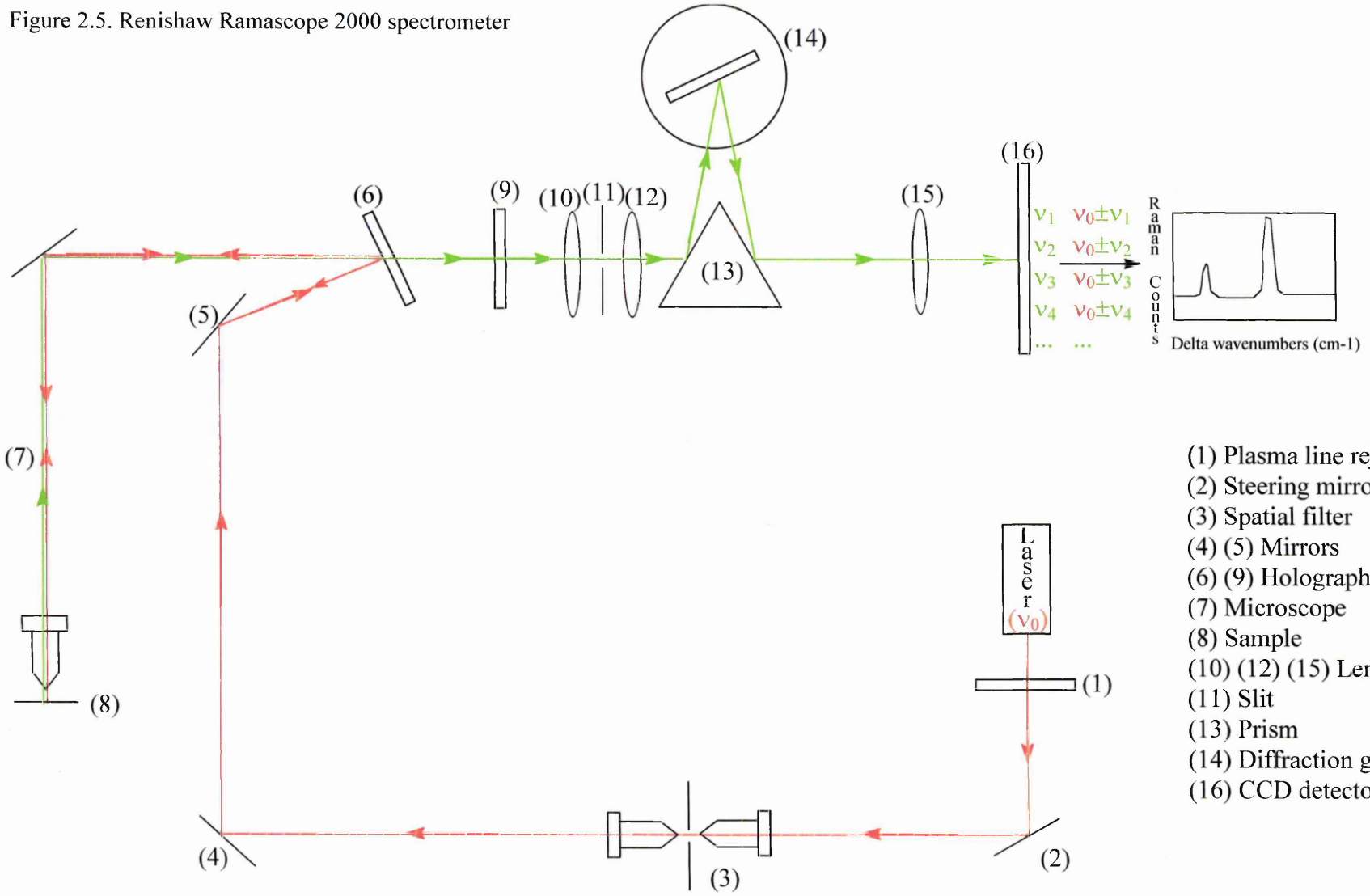

(1) Plasma line rejection filter
(2) Steering mirror
(3) Spatial filter
(4) (5) Mirrors
(6) (9) Holographic notch filter
(7) Microscope
(8) Sample
(10) (12) (15) Lenses
(11) Slit
(13) Prism
(14) Diffraction grating
(16) CCD detector

plasma lines from the laser and transmits the main laser line. The first steering mirror (2) sends the monochromatic light through the spatial filter (3) which consists of two objectives and a pinhole. In microprobe mode, the X 20 objective focuses the beam onto the pinhole and then onto a second objective (X 4) in order to produce a collimated beam. The collimated beam is deflected by mirrors (4,5) onto a holographic notch filter (6). Since the filter reflects the laser wavelength, the beam passes into the microscope (7) to be focus onto the sample (8) using the objectives X 10, X 20, X 50 and X 100. The 180° scattered light comes back into the microscope and arrives on the holographic notch filters (6,9) which filter out the Rayleigh component and transmit Raman shifted wavelengths. A first lens (10) focused the Raman light through an adjustable entrance slit (11). A second lens (12) recollimates the beam before deflecting it by a prism (13) onto a diffraction grating (14) which separates the beam constituent wavelengths. The prism deflects the dispersed light through a lens (15) on a CCD (charge coupled device) detector (16).

2.2.3. Optics.

2.2.3.1. Lasers.

Three lasers having different wavelengths were available: helium neon (633 nm), argon ion (514 nm) and a diode laser (782 nm). They possess different polarisation; the HeNe laser has a horizontal polarisation (resulting in a east-west orientation of the laser on the sample) since the Ar+ and diode lasers have a vertical polarisation (resulting in a north-south orientation of the laser on the sample).

These lasers have a power of 25 mW which can be reduced to 50, 25, 10 and 1% using neutral density filters.

Photons may be emitted spontaneously, from the lasers, over a small range of wavelengths as the collision between atoms may change their energy levels. Therefore, a plasma line rejection filter, which is a narrow band filter centred on the laser wavelength, is placed after the laser in order to block the unwanted plasma lines.

2.2.3.2. Holographic Notch Filters.

The main function of the holographic notch filters (HNF) is to remove the Rayleigh light. The HNF[8] can be described as wavelength specific mirrors. In fact, they reflect light on a narrow band of wavelengths, with a high degree of efficiency. The

result is a notch in the HNF transmission spectrum. The filters are of photosensitive organic material sandwiched between transparent substrates. A laser wavelength is used to write a hologram into the material to produce sinusoidal variation in the refractive index through the photosensitive material. The change in refractive index is necessary to diffract the light. The hologram can be written in order to reflect or reject a narrow band of wavelengths.

2.2.3.3. Diffraction grating.

The diffraction grating[8,9] disperses spatially the incident polychromatic light into its constituent wavelengths. The surface of the diffraction grating is made of a series of n parallel lines "grooves" spaced each other by the same value d.

The grating equation describing the dispersion of the spectrum produced by a grating as shown in figure 2.5 is:

$$m\lambda = d(\sin\theta_i + \sin\theta_o) \qquad 2.22$$

where θ_i is the input angle or angle of incidence, θ_o output angle or angle of diffraction, d the groove spacing and m order of diffraction. m can take the values ±1 ±2 ±3...

Using the angles α and γ, the equation can be written as:

$$m\lambda = d\left[\sin(\alpha+\gamma/2)+\sin(\alpha-\gamma/2)\right] \qquad 2.23$$

$$\text{or } m\lambda = 2d \sin\alpha \cos\gamma/2 \qquad 2.24$$

This general equation applies only to the central on axis ray. In the case of the off axis ray, an angle δ as shown in figure 2.5 needs to be introduced:

$$m\lambda = 2d \sin(\alpha+\delta/2) \cos(\alpha/2-\delta/2) \qquad 2.25$$

The absolute wavenumber is now given by :

$$\bar{\nu} = \frac{5gm}{\sin(\alpha+\delta/2)\ \cos(\frac{\gamma-\delta}{2})} \qquad 2.26$$

where g is the groove density or number of rulings per millimetre.

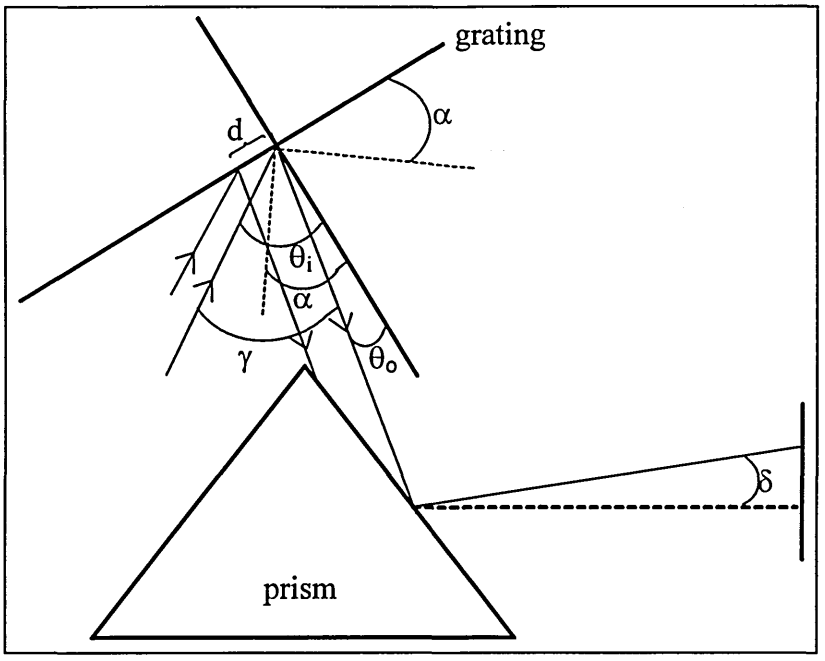

Figure 2.6: schema of the diffraction grating

The resolving power R of the grating is given by:

$$R=mN=\lambda/\Delta\lambda \qquad 2.26$$

where N is the number of lines illuminated on the diffraction grating , m the spectral order and $\Delta\lambda$ is the minimum band width resolvable at a given spectral position.

The Renishaw Ramanscope 2000 is equipped with a holographic grating of 1800 grooves/mm.

2.2.3.4. Detector.

The CCD (Charge Coupled Device) detector is made of many independent silicon pixels arranged in a 2 dimensional array. The surface of the detector is form of integrated circuit which has a metal oxide semiconductor structure. A photon is detected by generating a photoelectron in the silicon which is trapped on the pixel. For a given exposure time, photons incident on the pixel therefore electrons increased creating a charge on the pixel. The CCD is an ideal detector for Raman spectroscopy because of the low noise characteristic and high quantum efficiency. There are two limitations to the CCD detector[10]. First, the CCD are sensitive to high energy photons such as cosmic rays. Second, this detector may saturate before the signal to noise ratio is acceptable. The CCD is thermo-electrically cooled to -70 °C. The size of the 2 dimensional detector is 578 x 385 pixels. One pixel is 22 micron each side.

2.2.4. Confocal vs microprobe mode.

The adjustable slit mounted before the diffraction grating is a very important part of the spectrometer. The collimated light from the microscope is focused to the slit by a lens. The nature of the image at the CCD depends on the sample as well as on the width of the slit.

In Raman microscopy, the spatial resolution in the lateral plane (x,y) axis is of the order of 1-2 μm. Using X 100 and X 50 short-working length objectives, the illuminated sample area is about between 2 and 5 μm. Good spatial resolution along the z axis is obtained by confocal Raman microspectroscopy[11]. The instrument is set up in confocal mode using a X 100 objective, a slit width closed down to 15 μm and a CCD area of 4 x 576 pixels. The resolution is maximised in confocal mode when the slit is closed. However, the amount of radiation at the detector, as the signal to noise ratio in the spectrum is lower than if the spectrum, had been recorded in microprobe mode (slit open 50 μm, CCD area of 15 x 576 pixels) at lower resolution[10,11]. When the Renishaw Ramanscope 2000 is set up in confocal mode, the resolution is about 2-3 cm^{-1}.

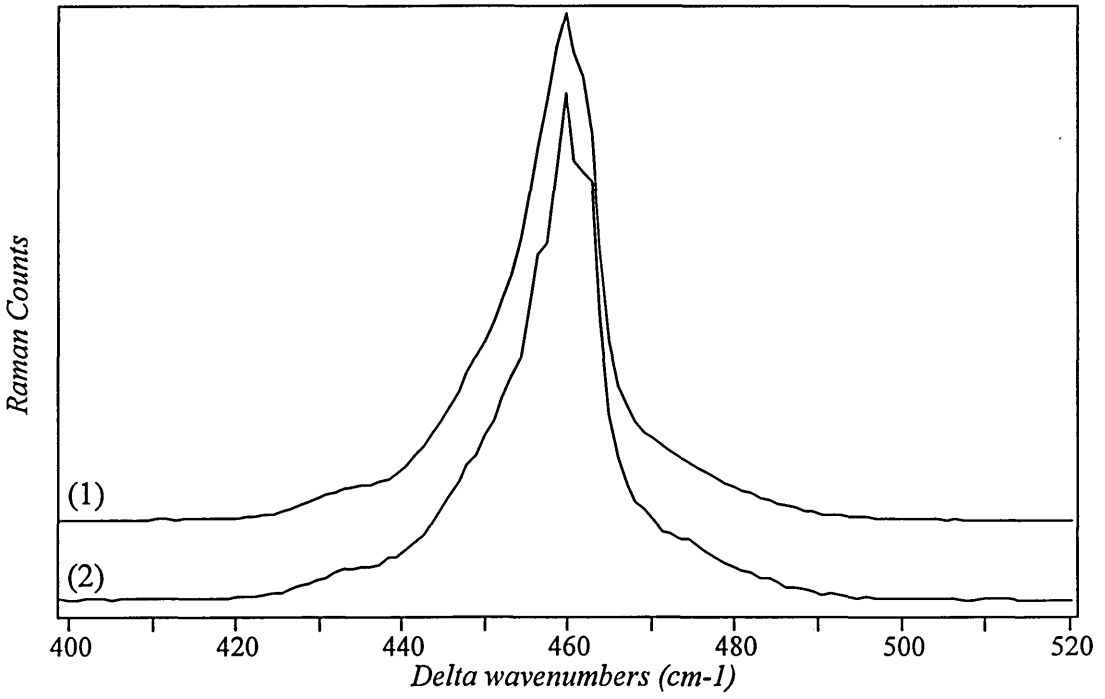

Figure 2.7. Raman spectra of CCl_4 in a quartz cuvette, (1) slit width of 50 μm and CCD area of 15 x 576 pixels, red laser, X 20 objective, T_{aq}=10 s; (2) slit width of 15 μm and CCD area of 4 x 576 pixels, red laser, X 20 objective, T_{aq}=10 s.

[1] Practical Raman Spectroscopy, Eds. D.J.Gardiner and P.R.Graves, Springer-Verlag Berlin Heidelberg, 157 pp, 1989.
[2] J.R Ferraro. Spectroscopy, 11, 18-25, 1996.
[3] Session d'initiation. Spectromètries Infrarouge à Transformée de Fourier et Raman.(1992), Internal report, Ed. Laboratoire de Spectroscopie Moléculaire et Cristalline, Université de Bordeaux I, 1992.
[4] S.Roberts and I.Beattie. In Microprobe Techniques in the Earth Sciences, Eds. P.J.Potts, J.F.W.Bowles, S.J.B.Reed and M.R.Cave, Chapman and Hall London, 387-408, 1995.
[5] Infrared and Raman spectroscopy. Methods and applications, Ed. B Schrader, VCH Verlagsgesellshaft, 787 pp, 1995.
[6] K.Nakamoto. Infrared and Raman Spectra of Inorganic and Coordination Compounds, 4th Edition, A Wiley-Interscience Publication, NewYork, 484 pp, 1986.
[7] Spectroscopy, volume 2. Eds. B.P.Straughan and S.Walker, Chapman and Hall London, 362 pp, 1976.
[8] Renishaw Raman Imaging Microscope; Background to the System-Grating Lightpath. Ed. Renishaw plc transducer systems division, 25 pp, 1996.
[9] Optics second edition. Eds. F.G.Smith and J.H.Thomson, John Wiley and Sons, 350 pp, 1988.
[10] P.J Hendra and J.K Agbeneyega. The Raman Spectra of Polymers, John Wiley and Sons, 1993.
[11] K.P.J.Williams, G.D.Pitt, D.N.Batchelder and B.J.Kip. Appl. Spectrosc., 48, 232-235, 1994.

3. Inorganic fibres.

Asbestos, quartz and man-made vitreous fibres (MMVF) are the inorganic fibres described in this chapter in term of chemistry, structure and surface properties. These fibres, which are all predominantly composed of silicon and oxygen, are known or suspected carcinogens. Asbestos and quartz fibres are mined from the earth whereas MMVF are manufactured fibres from glass or rock and used to replace asbestos in most industrialised countries.

3.1. Asbestos.

3.1.1. Introduction.

Asbestos is the common name given to the fibrous forms of several naturally occurring silicate minerals which have been mined for their useful chemical and physical properties including high tensile strength, flexibility, incombustibility, low thermal conductivity and chemical inertia[1]. Only six minerals with an asbestiform habit have been classified as asbestos. The characteristics of the asbestiform habit are the fibrillar structure and the fibre flexibility and strength[2]. All asbestos types can also occur in a different habit as mineral fragments which are non-asbestos varieties. These amphibole mineral fragments do not break down to form fibrous particles. The name given to the six varieties of asbestos as well as to their non-asbestiform mineral analogues are amosite and grunerite, fibrous actinolite and actinolite, fibrous anthophyllite and anthophyllite, chrysotile and lizardite, crocidolite and riebeckite, fibrous tremolite and tremolite, respectively.

Chrysotile is a sheet silicate in the serpentine group while the other types of asbestos are chain silicates in the amphibole group. The difference between the five asbestos amphiboles is in the cation composition. The amphibole minerals are common rock forming minerals referred to as solid solutions[3] and are well known for their chemical variation. The definition of a solid solution from Reviews in Mineralogy, volume 28, is: "a mineral structure in which specific atomic site(s) are occupied in variable proportions by two or more different chemical elements (or ionic groups)"[4]. Moreover, the structure of amphibole asbestos is never perfect and faults can regularly occur in single asbestos fibres. Chrysotile , the only serpentine mineral classified as asbestos, has a fairly constant composition. However, structural faults and minor chemical variations can occur.

The physical and chemical properties, and the complex surface chemistry of amphibole asbestos minerals are different from that of serpentine asbestos chrysotile. These differences are reported below.

3.1.2. Amphibole asbestos.

3.1.2.1. Crystal structure.

The basic structure sometimes called I beam (figure 3.1), is composed of a octahedral band of cations sandwiched between two double tetrahedral silicate chains[5]. The double chain consists of two juxtaposed pyroxene chains extended along the c direction. A chain has a Si:O or Si+Al:O ratio of 4:11, since Al may substitute for Si in the tetrahedral sites. These chains are stacked along the a-axis direction apex to apex (figure 3.2). Hydroxyl groups (or sometimes F, Cl or O) occupy anion position O(3) in the plane of the apical oxygen atoms. By stacking two double silicate chains apex to apex, five octahedral sites referred to as M(1), M(2), and M(3) sites are formed. M(4) sites at the edge of the double chains link adjacent silicate chains in the b direction. The octahedral band (figure 3.3), thus, consists of 2 M(1), 2M(2), 1M(3) and 2M(4) sites. Some amphiboles contain an atom in the site (A) in order to balance the charge from the hydroxyls.

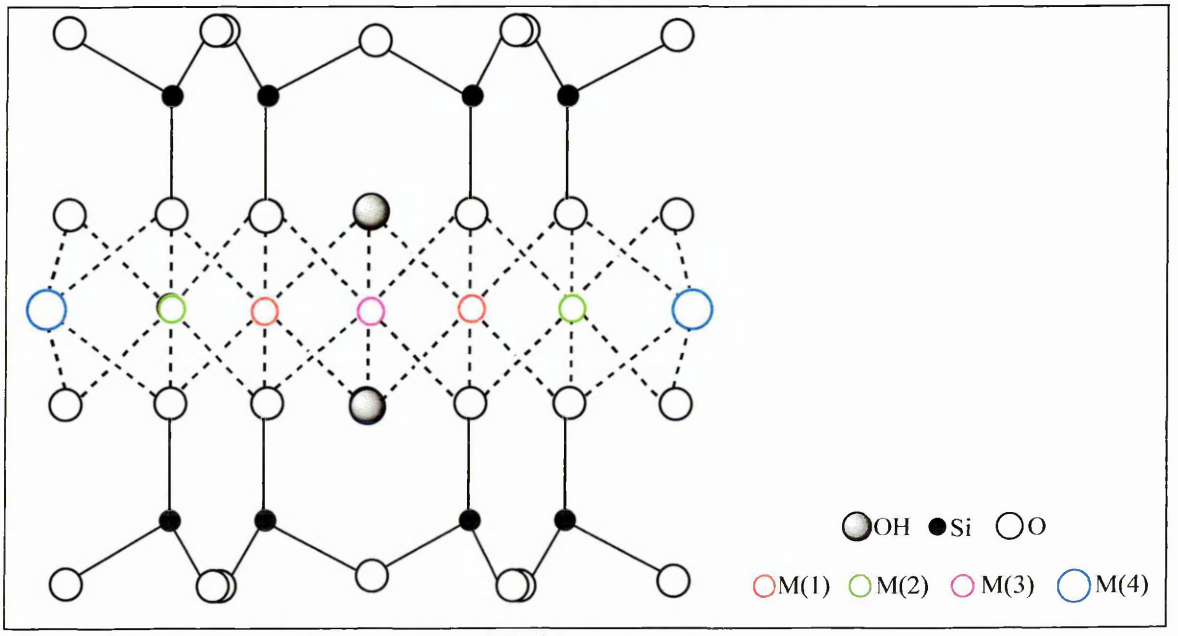

Figure 3.1: The I beam structure of amphiboles.

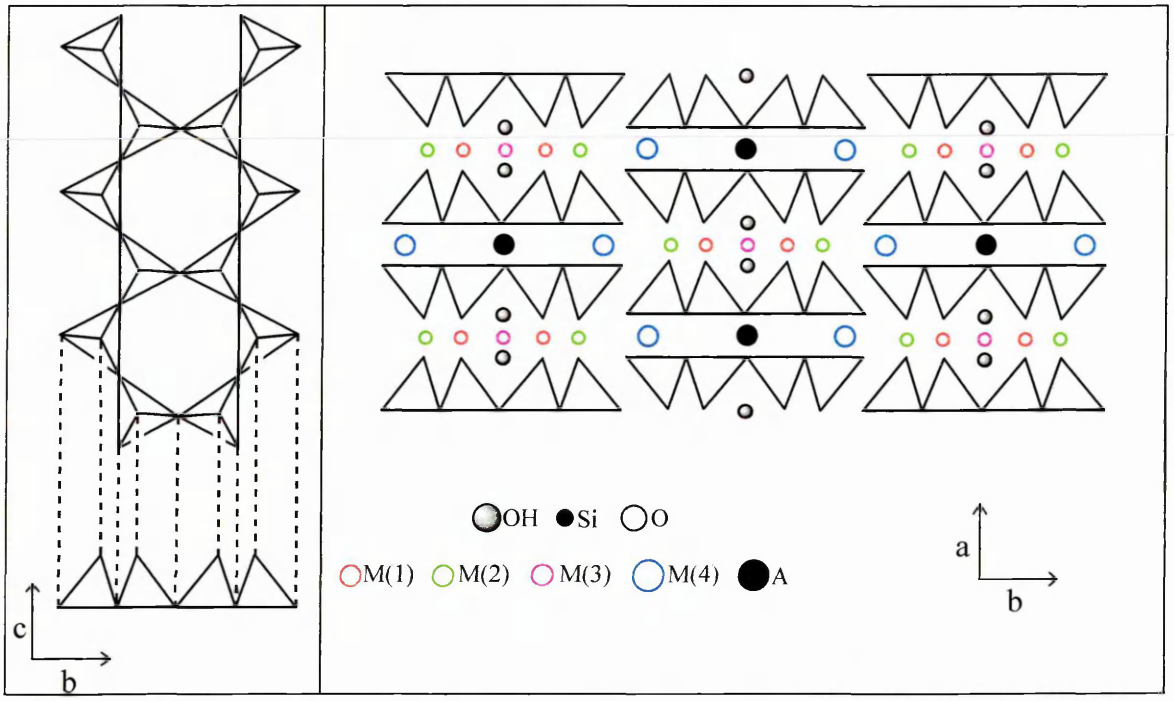

Figure 3.2: The amphibole structure.

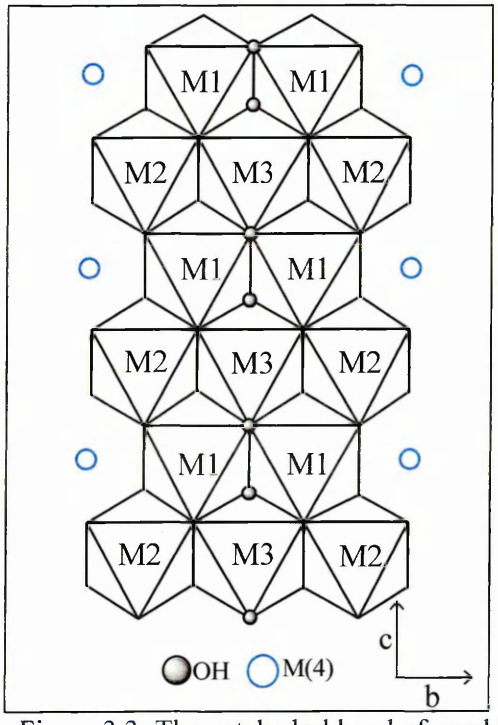

Figure 3.3: The octahedral band of amphiboles.

The amphibole structure can also be visualised by assembling two different types of slabs called M and P[6,7,8]. M and P are related to the structures of pyroxenes and micas[5]. A mica can be constructed purely of M slabs, a pyroxene of P slabs. The idealised amphibole structure can be thought as an alternation of slabs of mica and pyroxene structure MPMPMP (figure 3.4).

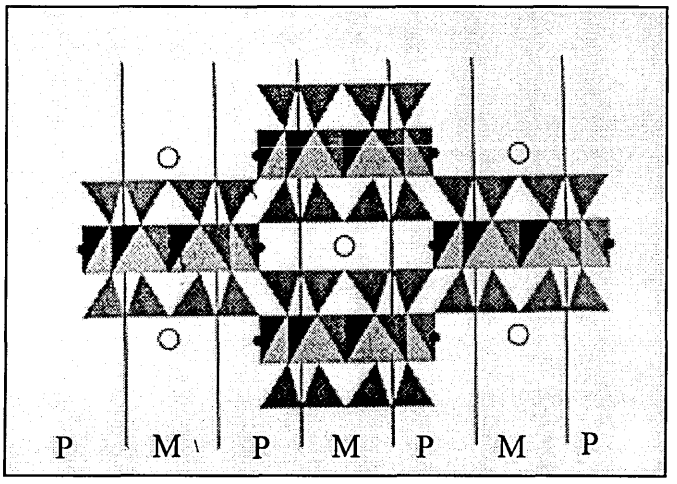

M: mica
P: pyroxene

Figure 3.4: MPMPMP structure scanned from D.T.Griffen[9].

There three basic ways of stacking the I beams which are called clinoamphiboles, orthoamphiboles and protoamphiboles[5]. These three structures are ideal polytypes. Amosite, crocidolite, tremolite and actinolite are clinoamphiboles with a monoclinic symmetry. Anthophyllite is orthoamphibole with a orthorhombic symmetry.

3.1.2.2. Chemistry and nomenclature.

The general formula of the amphiboles is: $A_{0-1}B_2C_5T_8O_{22}(OH, F, Cl, O)_2$[10]. T represents Si and Al which are in tetrahedral coordination in the double silicate chains. C corresponds to the cation sites Mg, Fe^{2+}, Mn, Al, Fe^{3+} and Ti which occupy regular octahedral sites. B refers to Na, Li, Ca, Mn, Fe^{2+}, Mg in less regular octahedral sites or 8 coordinated cation sites. A cations such as Na and K occupy 6 to 12 coordinated sites. The idealised formula of mineral and asbestos amphiboles are listed in table 3.1.

Amphiboles are divided into four principal groups on the basis of the number of atoms of (Ca+Na) and Na in the B position in the formula[10,11,12].

1. Iron-magnesium-manganese amphiboles have $(Ca+Na)_B<1.34$ atoms.
2. Calcic amphiboles have $(Ca+Na)_B\geq1.34$ atoms but $Na_B<0.67$ atoms.
3. Sodic-calcic amphiboles have $(Ca+Na)_B\geq1.34$ atoms and $0.67<Na_B<1.34$ atoms.
4. Alkali amphiboles have $Na_B\geq1.34$ atoms.

This nomenclature was applied from 1978 to 1997. The 1978 nomenclature of mineral

and asbestos amphiboles is summarised in table 3.2[10,11,12].

The new nomenclature approved by the International Mineralogical Association is as follows[13]:

1. Magnesium-iron-manganese-lithium amphiboles have $(Ca+Na)_B<1.00$ atoms and $(Mg+Fe+Mn+Li)_B\geq1.00$ atoms.

2. Calcic amphiboles have $(Ca+Na)_B\geq1.00$ atoms and $Na_B<0.50$ atoms, but $Ca_B>1.50$ not in every case.

3. Sodic calcic amphiboles have $(Ca+Na)_B \geq 1.00$ atoms and $0.50<Na_B<1.50$ atoms.

4. Sodic amphiboles have $Na_B\geq1.00$ atoms.

The 1997 nomenclature of mineral and asbestos amphiboles is summarised in table 3.3[13]. Within these 4 groups, there are a large number of amphibole names using adjectival prefixes (such as ferro, alumino...) to keep the number of fundamental amphibole names to a minimum.

name	idealised formula
fibrous actinolite (actinolite)	$Ca_2(Mg,Fe^{2+})_5(Si_8O_{22})(OH)_2$
amosite (grunerite)	$(Fe^{2+},Mg)_7(Si_8O_{22})(OH)_2$
fibrous anthophyllite (anthophyllite)	$(Mg,Fe^{2+})_7(Si_8O_{22})(OH)_2$
crocidolite (riebeckite)	$Na_2Fe^{3+}{}_2(Fe^{2+},Mg)_3(Si_8O_{22})(OH)_2$
fibrous tremolite (tremolite)	$Ca_2Mg_5(Si_8O_{22})(OH)_2$

Table 3.1: The idealised formula of mineral and asbestos amphiboles.

name	group	nomenclature
fibrous actinolite (actinolite)	calcic amphibole	$(Ca+Na)_B\geq1.34$; $Na_B<0.67$; $(Na+K)_A<0.50$; $Si\geq7.50$; $0.50\leq Mg/(Mg+Fe^{2+})\leq0.89$
amosite (grunerite)	Fe-Mg-Mn amphibole	$(Ca+Na)_B<1.34$; $Li<1.00$; $Mn<5.00$; $Mg/(Mg+Fe^{2+})<0.30$
fibrous anthophyllite (anthophyllite)	Fe-Mg-Mn amphibole	$(Ca+Na)_B<1.34$; $Li<1.00$; $Si\geq7.00$; $0.10\leq Mg/(Mg+Fe^{2+})\leq0.89$
crocidolite (riebeckite)	alkali amphibole	$Na_B\geq1.34$; $Fe^{2+}/(Fe^{2+}+Mg)\geq0.50$; $Fe^{3+}/(Fe^{3+}+Al^{VI})\geq0.70$
fibrous tremolite (tremolite)	calcic amphibole	$(Ca+Na)_B\geq1.34$; $Na_B<0.67$; $(Na+K)_A<0.50$; $Si\geq7.50$; $Mg/(Mg+Fe^{2+})\geq0.90$

Table 3.2: 1978 nomenclature of mineral and asbestos amphiboles.

name	group	nomenclature
fibrous actinolite (actinolite)	calcic amphibole	$(Ca+Na)_B \geq 1.00$; $Ca_B \geq 1.50$; $0.50 < Na_B < 1.50$; $(Na+K)_A < 0.50$; $Ca_A < 0.50$; $Si \geq 7.50$; $0.50 \leq Mg/(Mg+Fe^{2+}) < 0.90$
amosite (grunerite)	Mg-Fe-Mn-Li amphibole	$(Ca+Na)_B < 1.00$; $Li < 1.00$; $Si > 7.00$; $(Mg+Fe+Mn+Li) \geq 1.00$; $Mg/(Mg+Fe^{2+}) < 0.5$
fibrous anthophyllite (anthophyllite)	Mg-Fe-Mn-Li amphibole	$(Ca+Na)_B < 1.00$; $Li < 1.00$; $Si > 7.00$; $(Mg+Fe+Mn+Li) \geq 1.00$; $Mg/(Mg+Fe^{2+}) \geq 0.5$
crocidolite (riebeckite)	alkali amphibole	$Na_B \geq 1.50$; $(Na+K)_A < 0.50$; $Li < 0.5$; $(Mg+Fe^{2+}+Mn^{2+}) > 2.5$; $(Fe^{2+}$ or $Mg) > Mn^{2+}$; $(Fe^{3+}$ or $Al^{VI}) > Mn^{3+}$; $Mg/(Mg+Fe^{2+}) \geq 0.5$; $Fe^{3+} > Al^{VI}$
fibrous tremolite (tremolite)	calcic amphibole	$(Ca+Na)_B \geq 1.00$; $Ca_B \geq 1.50$; $0.50 < Na_B < 1.50$; $(Na+K)_A < 0.50$; $Ca_A < 0.50$; $Si \geq 7.50$; $Mg/(Mg+Fe^{2+}) \geq 0.90$

Table 3.3: 1997 nomenclature of mineral and asbestos amphiboles.

3.1.2.3. Defects and grain boundaries in amphiboles.

The amphiboles structure is not perfect and can present a variety of structural defects: chain width errors, exsolution lamellae and grain boundaries. Other defects such as twinning and stacking faults resulting from errors in the orientation of the I beam[14], and dislocation may also appear[15,16,17].

3.1.2.3.1. Chain-width errors.

These defects involve aperiodicity in the widths of the silicate chains[15, 18,19]. A single slab of triple, quadruple, quintuple, etc... silicate chains may insert into the silicate double-chain. In fact, the idealised amphibole structure is a regular alternation of slabs M and P. A mistake in the structure occurs if for example, an extra mica slab (M) is inserted in the (MP) sequence as: MPMPMMPMP. Therefore, this structure would have a triple silicate slab in the double-chain silicates. Single chain defects may also occur.

3.1.2.3.2. Exsolution lamellae.

Exsolution lamellae are non-periodic hosts in amphiboles having an amphibole structure with a different chemical composition from the host amphiboles[14,20]. They form by solid state precipitation when a high temperature amphibole solid-solution cools slowly.

3.1.2.3.3. Grain boundaries.

Grain boundaries define the limits where the structure of a crystal stops and can

be considered as a type of crystal defect. The most important observation is that, sheet silicates occur in amphiboles at the boundaries between the fibrils.

3.1.2.4. Compositional variations in amphiboles asbestos.

The amphibole mineral group is well known for its chemical variation[4,21-24].For example, the composition of crocidolite (or riebeckite) can be so far from the idealised formula that it does no longer fall in the category associated to the crocidolite name. The main variation in asbestos amphiboles are as follows:
There is partial substitution of F, Cl and O for OH in the hydroxyl sites. Fe^{2+} and Mg mix freely in octahedral sites. There are substitutions of Al in the octahedral site as well as Al for Si in the tetrahedral silicate sheet. Some K, Na and Ca can be observed in the empty A sites of asbestos amphiboles. Limited solid solution belonging to the calcic amphibole group arises in crocidolite, amosite and anthophyllite. Some Fe^{3+} occurs in amosite and anthophyllite. Mn substitution can occur in amosite.

Moreover, amphiboles have intergrown layer silicates which have been observed by electron microscopy[5]. Any bulk analysis is therefore contaminated by these additional minerals.

3.1.2.5. Surface properties.

3.1.2.5.1. Surface chemistry.

The I beam are connected together with weaker bonds than those inside the I beam unit itself. Therefore, it has been assumed that the cleavage surface of pure amphibole asbestos leaves the I beam intact. In fact, a solution would have an easy access to tetrahedral, M(4) and A sites and has however, a more limited access to M(2) cation sites. The other cation sites M(1) and M(3) have no direct contact with the environment but they might interact if there is dissolution. However, the amphiboles structure is not perfect. Most workers believe that there is parting surfaces which occur along defects (such as twinning and chain width errors)[5]. The surface of asbestos fibres are mainly made by the planes (100), (110) and (010), planes parallel to c as shown in figure 3.5, as well as the terminal planes which cut the fibres axis[25]. The planes parallel to c form the majority of all surface of a single fibre. The parting surface (figure 3.5) would still be very similar to those of pure amphibole asbestos leaving the I beam intact. However, it is possible that the (100) parting surface cuts the I beam in half through the

octahedral strips leaving access to all the M sites. The other possibility for the (100) surface is an up and down stepped surface by cutting the structure between opposite set of silica double chains. The (010) surface consists of M(4) sites and the edges of silica chains. The (110) surface is not planar but a stepped (100)/(010). Planes which cut the end of a fibre are not specifically known.

However, other irregular surface also occur and all amphibole asbestos observed by TEM with the electron beam parallel to the c axis had layer silicates intergrown between the amphibole fibrils[15]. Therefore, no generalisation about the surfaces of asbestos fibres is possible. It is likely to have many different types of surfaces that vary in structure, orientation and chemistry.

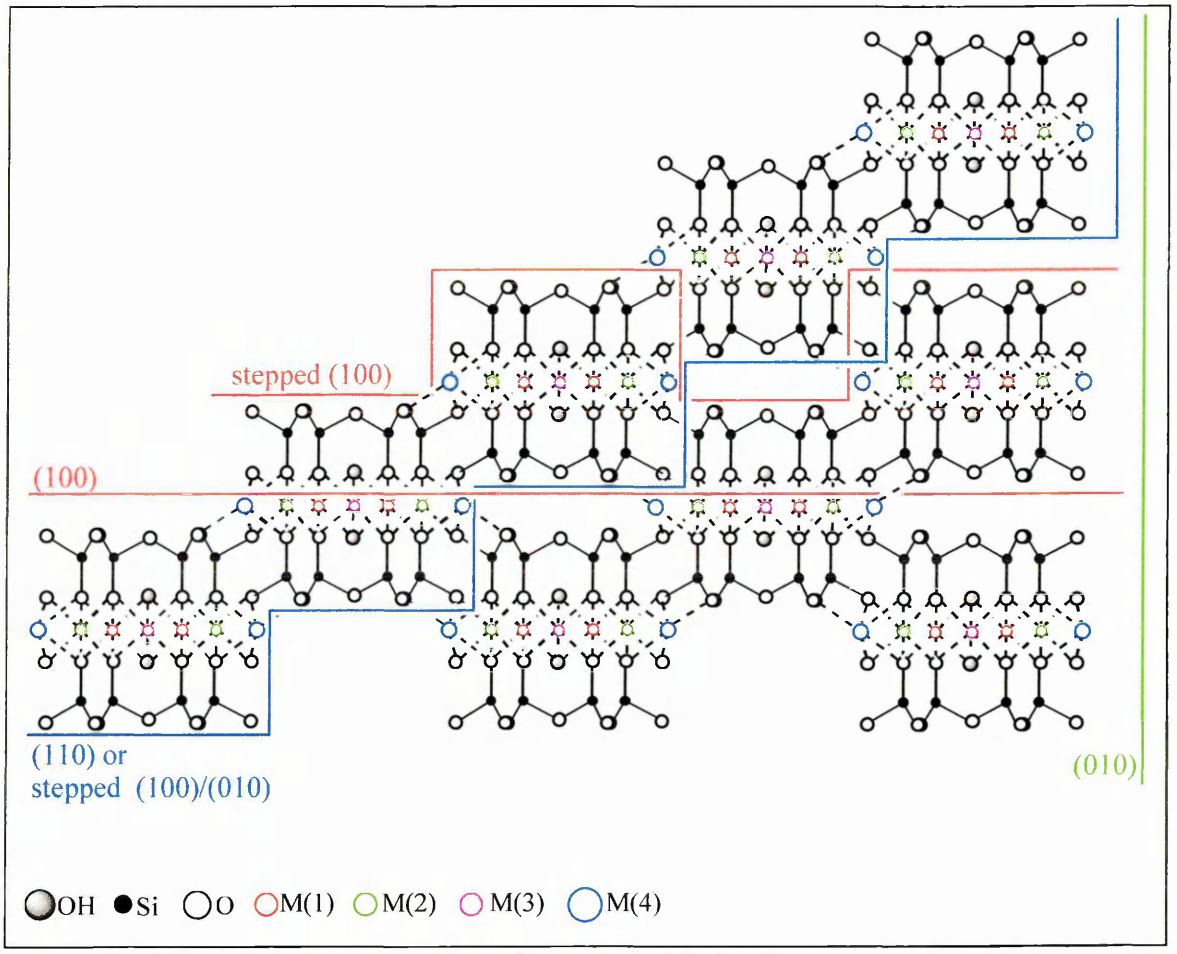

Figure 3.5: Planes defining the parting surfaces of amphibole asbestos.

3.1.2.5.2. Surface character and surface charge.

In air or solution, the surfaces parallel to c, complete their coordination with hydroxyls and present a basic character. For the end of fibres, the small part of all surface of a single fibre, the silica chains must be cut giving SiO^- groups which may

accept H^+ from solution and present a weak Brønsted acid character.

Schiller et al suggest that the ends of the amphibole fragments or fibres are positively charged whereas the surfaces parallel to c are negatively charged[26]. Therefore, the surface net charge of amphiboles measured by zeta potential is negative as shown for several amphibole asbestos in table 3.4[27]. The definition of the zeta potential from the Penguin dictionary of chemistry[28] is: "the potential difference across the diffuse part of a double layer, i.e. between the rigid solution layer and the mobile part of the solution adjacent to the bulk solution." The negative net charge for pH greater than 3 can be explained by the dissolution of silanol surface groups[29].

	Zeta potential at room temperature in distilled water with pH=7.4
Crocidolite	- 50.5 mV
Amosite	- 58.5 mV
Anthophyllite	- 54.0 mV

Table 3.4: Zeta potential for several asbestos amphiboles.

3.1.3. Chrysotile and lizardite.

3.1.3.1. Crystal structure.

Chrysotile and lizardite, which have a 1:1 layer structure, belong to the serpentine group[5]. The 1:1 layer structure of chrysotile and lizardite (figure 3.6) consists of one tetrahedral silicate sheet, which is linked to one octahedral magnesium hydroxide sheet (figure 3.7), by sharing of the apical oxygen of the silicate sheet. Indeed, in serpentine, there is a tetrahedral sheet only on one side of the octahedral sheet. Chrysotile and lizardite are called trioctahedral species because all of the octahedral sites are occupied.

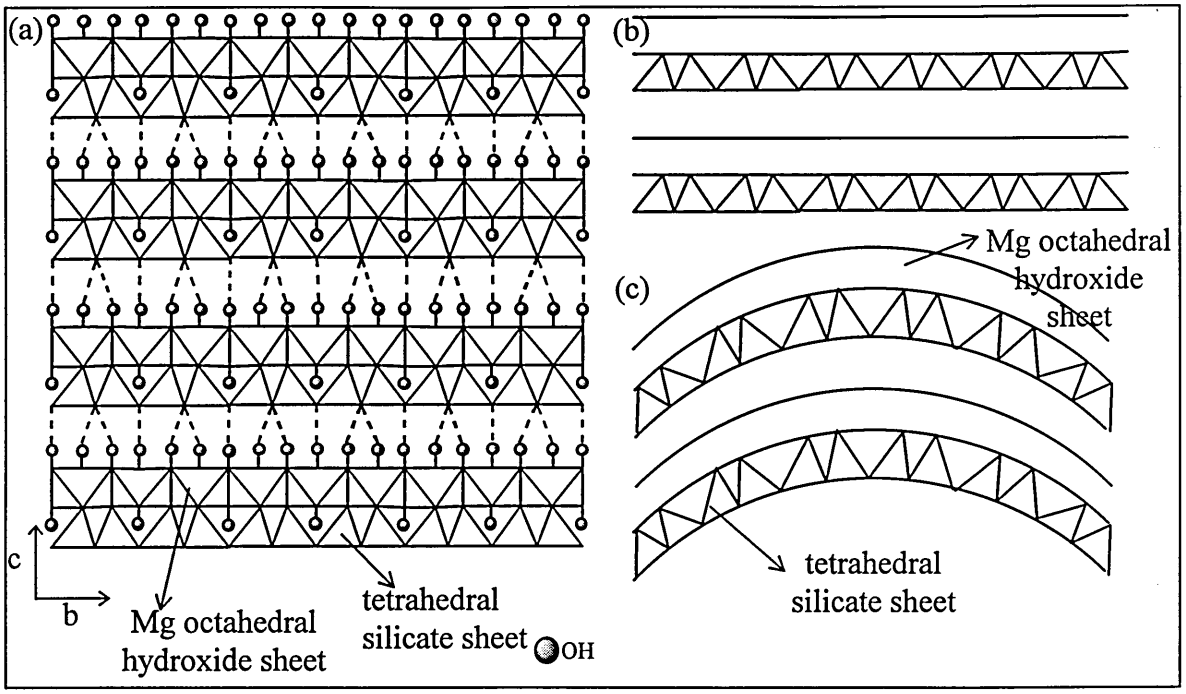

Figure 3.6: 1:1 layer structure of lizardite (a and b) and chrysotile (c).

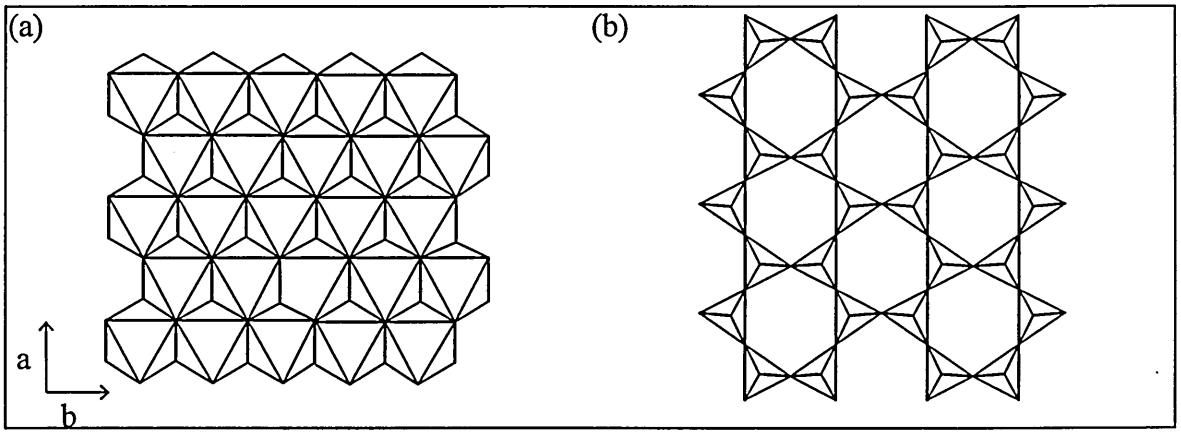

Figure 3.7: Magnesium octahedral (a) and silicate tetrahedral sheet (b) of the 1:1 layer structure.

However, in chrysotile, due to a misfit between the octahedral and tetrahedral layers, the 1:1 layers are, at least locally, curled[30,31] whereas lizardite has quite planar layers (figure 3.6). Moreover, in chrysotile, the 1:1 layers can take the form of concentric tubes (figure 3.8) having a cylinder, ellipse or less regular shape[32,33,34]. A fibril is defined as a cylinder increasing in diameter away from the fibril axis. Another type of fibril consists of one or more 1:1 layers rolled up like a carpet (figure 3.8). The fibrils are closed packed and possess inner spaces as well as gaps between them[35]. These gaps may be completely , partially, or not at all filled with materials such as amorphous silica or curved strips of 1:1 layers[18]. The diameter of a fibril is about 250 Å

with an inner tube of about 70 Å[18]. The length of the chrysotile fibres is on the order of cm or less.

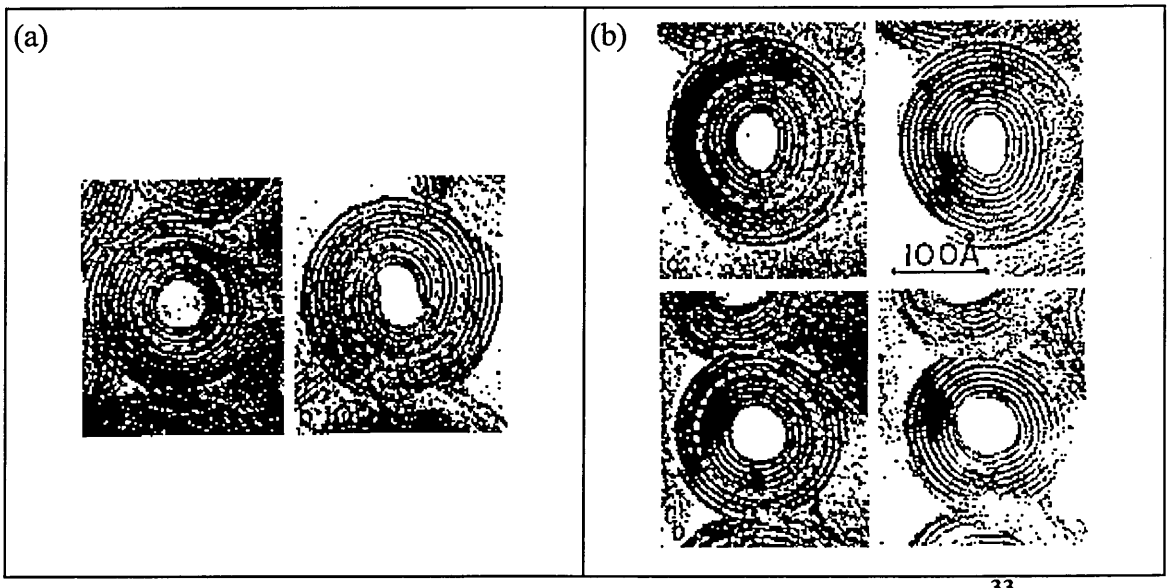

Figure 3.8: Concentric (a) and spiral structure (b) of chrysotile scanned from Yada[33].

3.1.3.2. Nomenclature.

The general formula of the 1:1 layer silicate in the trioctahedral case is[5]: $M_3[T_2O_5](OH)_4$. M corresponds to Mg cations in 6 coordinated cations sites and T represents Si in 4 coordinated cations sites. The idealised formula for chrysotile and lizardite is $Mg_3(Si_2O_5)(OH)_4$.

3.1.3.3. Chemical variations in chrysotile and lizardite.

In contrast to amphibole asbestos, the composition of the chrysotile asbestos and lizardite are close to its idealised formula. There are minor chemical variations in the natural species such substitutions of Al and Fe^{3+} for Si and Al, Fe^{2+} and Fe^{3+} for Mg[4,21,22,31]. However, these substitutions seem to be more limited in chrysotile than in lizardite[36]. In fact, the substitutions (except Fe^{2+}) reduce the misfit between the tetrahedral and octahedral sheet and then, the tendency for the 1: 1 layers to curl is reduced. Lizardite and chrysotile may contain traces of Ni, Co, Mn, Cr, Zn, Cu and Pb[5,24]. Lizardite and chrysotile commonly contains excess H_2O[37].

3.1.3.4. Structural variations in chrysotile and lizardite.

Most normal chrysotile samples have the a axis direction parallel to the fibril axis. However, some samples called parachrysotile have the b axis direction parallel to the cylinder axis and generally occur in small amounts with other chrysotile structure. Chrysotile and lizardite occur in different polytypes depending on the way of stacking the layers together. Chrysotile presents polytypes defined by the number of 1:1 layers per unit cell (for example 1, 2), the structure of the layers per unit cell (for example orthorhombic, monoclinic) and the shape of the lattice (for example cylindrical lattice)[31]. However, more complicated polytypes can occur as well as chrysotile having disordered layer stacking. Hydrogen bondings occur between layers and are variable from place to place along the b direction.

Lizardite presents polytypes defined by the number of 1:1 layers per unit cell and the symmetry of the 1:1 layers (for example trigonal, hexagonal)[31,38,39]. In lizardite polytypes, some hydrogen atoms of one layer are involved in hydrogen bonding with an adjacent layer.

3.1.3.5. Surface chemistry.

Because of the misfit between silicate sheet on the inside and Mg hydroxide sheet on the outside, the 1:1 layers of chrysotile are curled. The dominant surface of an ideal chrysotile fibre is the Mg hydroxide sheet ($Mg(OH)_2$). Therefore, the basic surface structure of chrysotile as well as lizardite (figure 3.9) comprises hydroxyl groups with the sheet of Mg atoms underlying and presents a basic character[40,41]. In an aqueous solution, the hydrogen of chrysotile surface can form hydrogen bonds with a relatively organised layers of H_2O. The ends of the fibrils, although a small part of the surface of a single fibre, must cut the tetrahedral silicate and magnesium sheets. In the case of silica chains, we have SiO^- group which accepts H^+ from solution. In the case of magnesium hydroxide sheet, we have octahedral sites which would like to complete their Mg coordination with water from the air or solution. These sites, at the end of fibrils, possess a weak Brønsted acidity. However, several complications in the surface chemistry and structure of chrysotile can appear because of the shape of fibrils. Indeed, fibrils with cylindrical layers should have a continuous Mg hydroxide surface. This not the case for fibrils with layers in spiral conformation (rolled up like a carpet) which present a "ledge". Moreover, the chrysotile possesses inner spaces and gaps between

them. These spaces can be filled by materials other than serpentine. Therefore, the surface may be in part a coating material rather than the Mg hydroxide sheet. The surface of the unfilled inner space of a fibril is the silicate sheet where a solution will have access. But the interactions of a fluid with the interior fibril surface may be minor compared to interactions with the exterior fibril surface.

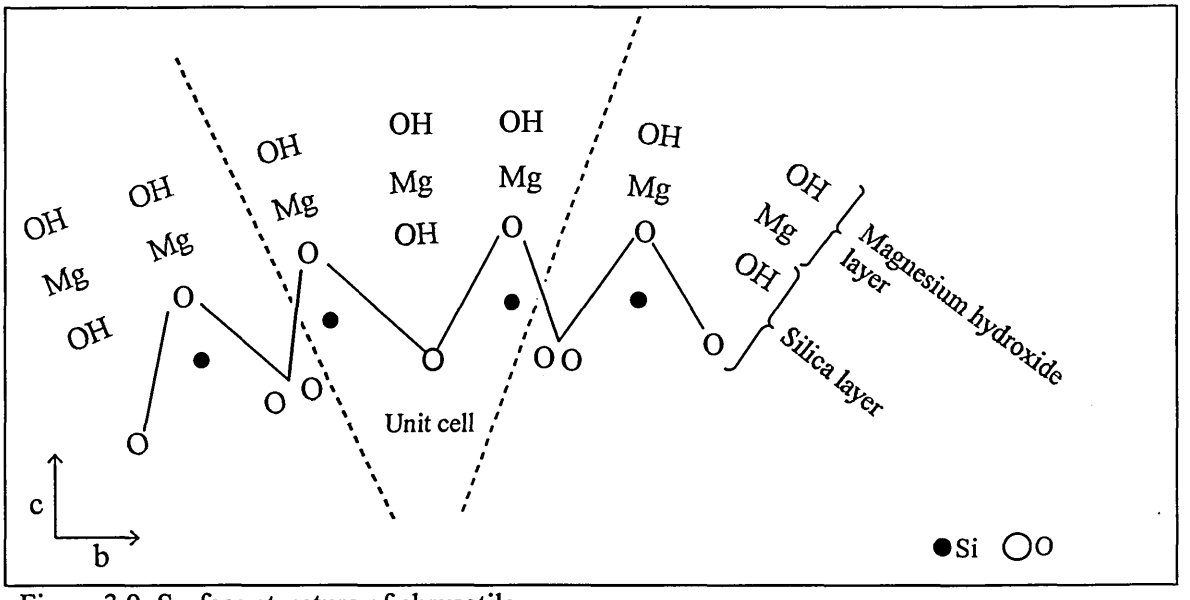

Figure 3.9: Surface structure of chrysotile.

3.1.3.6. Surface charge.

In aqueous solution, the octahedral sheet of the outer surface of chrysotile fibrils has a positive net charge. The silicate sheet of the inner tube of a fibril has a negative net charge. However, the size of the exterior surface of a fibre is larger than the interior, resulting in a positive zeta potential for chrysotile. Typical values for two chrysotile samples are +40.5 and 52.5 mV in distilled water for pH=7.4 at room temperature[27].

3.1.4. Surface site reactivity of chrysotile and amphiboles.

Bonneau et al[29] used probe molecules to study the acid base properties of amphibole asbestos. Pyridine, which is used to probe acid sites, was only physisorbed on chrysotile and amphibole asbestos indicating that acid sites on the surface are few or weak. Fluoride, phosphate, CO_2 and benzoic acid, which are reactive with basic sites were chemisorbed to surface hydroxyls. Therefore, the majority of reactive sites on chrysotile and amphibole asbestos have Lewis base character.

It is also reported in literature that chrysotile possesses hydrophilic character[42] as

distinct from the amphiboles amosite and crocidolite which show a degree of hydrophobicity due to naturally occurring organic impurities such as oils[43,21].

The amphiboles asbestos show various degrees of relative resistance to reaction with acids whereas strong acids decompose rapidly chrysotile. All varieties of asbestos amphiboles as well as chrysotile show a good stability toward alkali.

3.2. Man Made Vitreous Fibres (MMVF).

3.2.1 Introduction.

The man-made vitreous silicate fibres include textile glass fibres, glass fibres used for air and liquid filtration as well as fibres used in insulating and ceiling tile products which are often called mineral fibres in the literature. The name mineral fibres comes from the mineral starting materials mostly used for their production and includes glass wool, rock and slag wool and refractory ceramic fibres. Typically, most man made fibres are not respirable since their diameter are greater than 3 μm.

The man-made vitreous fibres are non-metallic inorganic fibres which are in glassy or vitreous state when produced. They are oxides, mainly silica SiO_2 and are called silicate glasses.

3.3.2. Chemistry.

Many oxides could be used in commercial glasses. However, their number is limited by their cost. Therefore, most man made vitreous fibres contain SiO_2 as the largest component. Indeed, SiO_2 is the second most abundant mineral compound in nature (after the feldspars).

To form a glass, a glass former such as SiO_2, B_2O_3, P_2O_5 or GeO_2 is required. These compounds can be melted and quenched into a glass state. Quartz fibres consist of purely SiO_2. However, modifiers and intermediate oxides are added to enable the glasses to melt and be worked at lower temperatures. Oxides such as Al_2O_3, TiO_2 and ZnO are usually classified as intermediate oxides or stabilisers. Oxides such as MgO, Li_2O, BaO, CaO, Na_2O and K_2O are usually classified as modifiers and can be called fluxes. The fluxes allow the SiO_2 network to break down. The intermediate oxides help to obtain a silicate glass with a high degree of chemical resistance. They also control, with the fluxes, the viscosity of the melt. The melt must possess a viscosity allowing it to cool rapidly into a vitreous state.

Three types of raw materials are used to make MMVF:

- Mined or quarried materials: sand, clay, limestone, dolomite and basalt or other mined rocks.
- Manufactured chemicals: soda ash, borax, boric acid and calcined alumina.
- Waste glass from other industries.

The fibres are produced using different process[44]. The continuous drawing process is used to make continuous glass fibres often called textile fibres; the rotary process to make most of the insulating glass fibres; the flame attenuation process to make glass fibres for special uses like filtration; the fibre blowing process to make refractory ceramic fibres and the wheel centrifuge and Downey process to make refractory ceramic fibres as well as rock and slag wool fibres.

The chemical composition for typical fibres of textile glass, glass wool, rock and slag wool as well as refractory ceramic fibres are shown in table 3.5[44]. It has to be noted that the compounds reported in table 3.5 are oxides which do not exist as individual crystals in the fibres.

Three typical textile glass fibres are reported: E glass which is a calcium aluminium silicate glass; S glass which is a magnesium aluminium silicate glass and AR glass produced with a high content of ZrO_2 oxide in order to improve its stability to alkalis.

Glass wool fibres have typical composition with more Na_2O and K_2O alkaline oxides as well as B_2O_3 and less CaO and MgO than rock and slag wool fibres resulting in a low and high melting temperature respectively.

Ceramic refractory fibres have a composition of about 50/50 in weight Al_2O_3 and SiO_2. Other oxides such as ZrO_2, TiO_2 and Cr_2O_3 can be added to change the fibres properties.

The fibres have binders or other materials sprayed onto them (table 3.6) at the last stage when they are formed[44]. After spraying, glass wool fibres and slag and rock wool fibres are bring into a curing oven.

	Textile glass fibres E-Glass	*Textile glass fibres S-Glass*	*Textile glass fibres AR-Glass*	*Glass wool (insulating glass fibres)*	*Rock wool made from basalt melted in a furnace*	*Rock wool made from basalt and other materials melted in a cupola*	*Slag wool made from slag melted in a cupola*	*Refractory ceramic fibres Kaolin aluminosili--cate*	*Refractory ceramic fibres High purity aluminosili--cate*	*Refractory ceramic fibres Zirconia aluminosili--cate*
SiO_2	52-56	65	60-70	55-70	45-48	41-53	38-52	49.5-53.5	48.5-54	47.5-50
Al_2O_3	12-16	25	0-5	0-7	12-13.5	6-14	5-15	43.5-47	45.5-50.5	35-36
B_2O_3	5-10	-	-	3-12	-	-	-	-	-	-
Na_2O)				13-18	2.5-3.3	1.1-3.5	0-1	0.5	0.2	<0.3
K_2O)	0-2	-	11-20	0-2.5	0.8-2	0.5-2	0.3-2	<0.01	<0.01	<0.01
MgO)	0-5	10	1-10	0-5	8-10	6-16	4-14	<0.1	<0.01	0.01
CaO	16-25	-	-	5-13	10-12	10-25	20-43	<0.1	<0.05	<0.05
TiO_2	0-1.5	-	-	0-0.5	2.5-3	0.9-3.5	0.3-1	2	0.02	0.04
Fe_2O_3	0-0.8	-	0-0.5	0.1-0.5	-	-	-	1	<0.2	<0.05
F_2	0-1	-	-	0-1.5	-	-	-	-	-	-
ZrO_2	-	-	10-18	-	-	-	-	0.1	0.2	15-17
Li_2O	-	-	-	0-0.5	-	-	-	-	-	-
$S0_3$	-	-	-	0-0.5	-	-	-	-	-	-
BaO	-	-	-	0-3	-	-	-	-	-	-
FeO	-	-	-	-	11-12	3-8	0-2	-	-	-
S	-	-	-	-	0-0.2	0-0.2	0-2	-	-	-
P_2O_3	-	-	-	-	-	-	0-0.5	-	-	
Cr_2O_3								<0.03	<0.01	<0.01

Table 3.5: Composition in percentage weight of some typical MMVF.

Type of fibres	Coating
Textile glass fibres	Chemical sizing to protect and lubricate the fibres.
Glass wool fibres	Binders mainly phenol formaldehyde resins. Other agents including melamine resins, silicones, oils for lubrication, wetting agents, antistatic agents and stabilisers.
Rock and slag wool fibres	Lubricant or dedusting agents (water based emulsions of mineral oil, polypropylene glycol or related compounds). Binders (phenolic resins). Antistatic agents, wetting agents and hydrophobic agents.
Refractory ceramic fibres	none

Table 3.6: Binders and other materials sprayed onto MMVF.

3.3.3. Structure.

The MMVF are synthetic fibres with a glass like structure. A glass is an inorganic non-crystalline (amorphous) material formed after solidification from a molten product[45]. In contrast with crystalline materials, it shows a diffuse x-ray diffraction diagram. Silicate glasses consist of three dimensional network of SiO^{4-} tetrahedra linked by sharing a common bridging oxygen (figure 3.10). Oxides or other elements or cations can remain in the interstitial spaces of the network. In other words, glasses possess a short range order and a long range disorder. They do not have lattice order or orientational order.

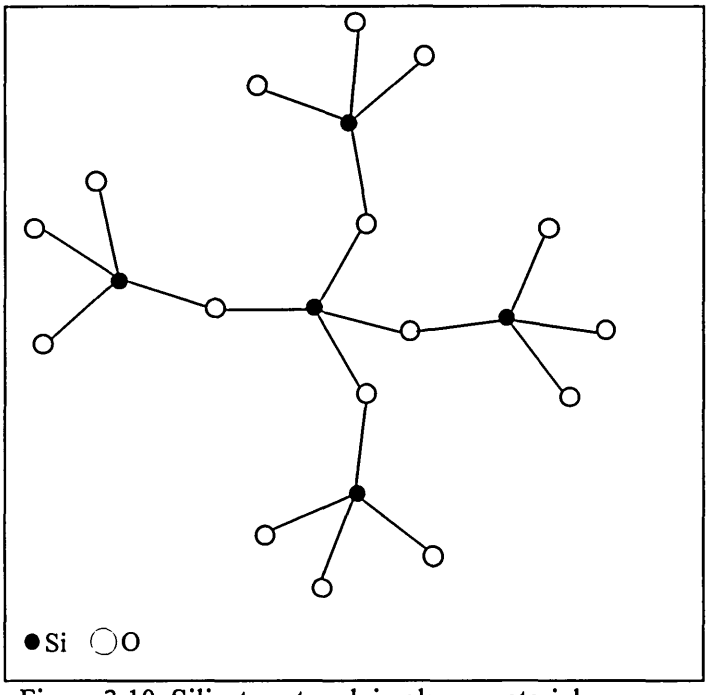

Figure 3.10. Silicate network in glassy material.

Glasses have conchoidal fracture properties and break with dish or shell like surfaces. Consequently, MMVF, do not split longitudinally or along their length like asbestos but across. Indeed, asbestos fibres can split longitudinally or along their length into many thin fibres which can split again into thinner fibres called fibrils. This is due to structural features. MMVF do not exhibit fibres with diameters as thin as most of asbestos fibres. The fibres have no planes of cleavage and break almost cleanly across becoming shorter and not thinner.

MMVF are vitreous when manufactured. However, for special applications ceramic fibres as well as rock and slag wool fibres can be partially crystalline when they are exposed to high temperatures. Moreover, small unmelted grains such as silica, alumina, mullite, olivine or anorthite can be found in MMVF. Some refractory ceramic fibres can also show very small amount of tiny mullite crystals. Finally, small amounts of inorganic crystallites (especially calcium compounds) are often found in the binder coating the fibres.

3.3.4. Dissolution behaviour.

MMVF are rapidly dissolved by alkaline solutions[44]. In acid solution, atoms such as Na, Ca and Mg are removed from the network leaving an open silicate structure which dissolves more slowly[44]. E glass and refractory ceramic fibres which have high alumina and silica content possess lower dissolution rates than slag, rock and glass wool fibres.

[1] Glossary of Geology. American Geological Institute, Washington, Eds. D.C. M.Gary, R.McAffee and C.Wolf, 805 pp, 1974.
[2] T.Zoltai. In Amphiboles and Other Hydrous Pyriboles-Mineralogy, Ed. D.R.Veblen, Rev. Mineral., 9A, 237-278, 1981.
[3] C.Klein and C.S.Hurlbut Jr. In Manual of Mineralogy. 21st Eds. John Wiley and Sons, NewYork, 1993.
[4] C.Klein. In Heath Effects of Mineral Dusts, Eds. G.D.Guthrie Jr. and B.T.Mossman, Rev. Mineral., 28, 7-56, 1993.
[5] D.R.Veblen and A.G.Wylie. In Heath Effects of Mineral Dusts, Eds. G.D.Guthrie Jr. and B.T.Mossman, Rev. Mineral., 28, 61-131, 1993.
[6] J.B.Thompson Jr. Amer. Mineral., 63, 239-249, 1978.
[7] D.R.Veblen. Amer. Mineral., 76, 801-826, 1991.
[8] D.R.Veblen. In Minerals and Reactions at the Atomic Scale: Transmission Electron microscopy, Ed. P.R.Buseck, Rev. Mineral., 27, 181-229, 1992.
[9] D.T.Griffen. Silicate Crystal Chemistry, Ed. Oxford University Press, Inc., 1992.
[10] F.C.Hawthorne. In Amphiboles and Other Hydrous Pyriboles-Mineralogy, Ed. D.R. Veblen, Rev. Mineral., 9A, 1-102, 1981.
[11] B.E.Leake. Amer. Mineral., 63, 1023-1053, 1978.
[12] F.C. Hawthorne. Can. Mineral., 21, 173-480, 1983.
[13] B.E.Leake, A.R.Woolley, C.E.S.Arps, W.D.Birch, M.C.Gilbert, J.D.Grice, F.C.Hawthorne, A.Kato, H.J.Kisch, V.G.Krivovichev, K.Linthout, J.Laird, J.A.Mandarino, W.V.Maresch, E.H.Nickel, N.M.S.Rock, J.C.Schumacher, D.C.Smith, N.C.N.Stephenson, L.Ungaretti, E.J.W.Whittaker, Y.Guo. Amer. Mineral., 82, 1019-1037, 1997.
[14] E.A.Smelik and D.R.Veblen. Amer. Mineral., 78, 511-532, 1993.
[15] J.H.Ahn and P.R.Buseck. Amer. Mineral., 76, 1467-1478, 1991.
[16] E.J.W.Whittaker, B.A.Cressey and J.L.Hutchison. Mineral. Mag., 44, 287-291, 1981.
[17] B.A.Cressey, E.J.W.Whittaker and J.L.Hutchison. Mineral. Mag., 46, 77-87, 1982.
[18] J.E.Chisholm. In Asbestos, Eds. S.S.Chissick and R.Derricott, John Wiley and Sons, NewYork, 85-167, 1983.
[19] M.Dorling and J.Zussman. Lithos, 20, 469-489, 1987.
[20] Y.H.Shau, D.R.Peacor, S.Ghose and P.P.Phakey. Amer. Mineral., 78, 96-106, 1993.
[21] A.A. Hodgson. In Asbestos, Eds. L.Michaels and S.S.Chissick, John Wiley and Sons, NewYork, 67-114, 1979.
[22] M.Ross. In Amphiboles and Other Hydrous Pyriboles-Mineralogy, Ed. D.R.Veblen, Rev. Mineral., 9A, 279-323, 1981.
[23] K.Kullerud. Eur. J. Mineral., 8, 355-370, 1996.
[24] D.R.Bowes and C.M.Farrow. Am. J. Ind. Med., 32, 592-594, 1997.
[25] M.F.Hochella Jr. In Heath Effects of Mineral Dusts, Eds. G.D.Guthrie Jr. and B.T.Mossman, Rev. Mineral., 28, 275-305, 1993.
[26] J.E.Schiller, S.L.Payn and S.E.Khalafalla. Science, 209, 1530-1532, 1980.
[27] W.G.Light and E.T.Wei. Environ. Res.,13, 135-145, 1977.
[28] The Penguin Dictionary of Chemistry. Ed. Penguin Books, 434 pp, 1983.

[29] L.Bonneau, H.Suquet, C.Malard and H.Pezerat. Environ. Res., 41, 251-267, 1986.
[30] L.Pauling. Proc. Nat. Acad. Sci., 16, 578-582, 1930.
[31] F.J.Wicks and D.S.O'Hanley. In Hydrous Phyllosilicates, Ed. S.W.Bailey, Rev. Mineral., 19, 91-167, 1988.
[32] K.Yada. Acta Crystallogr., 23, 704-707, 1967.
[33] K.Yada. Acta Crystallogr., A27, 659-664, 1971.
[34] K.Yada. Can. Mineral., 17, 679-691, 1979.
[35] A.Baronnet. In Minerals and Reactions at the Atomic Scale: Transmission Electron Microscopy, Ed. P.R.Buseck, Rev. Mineral., 27, 231-288, 1992.
[36] C.Viti and M.Mellini. Eur. J. Mineral., 9, 585-596, 1997.
[37] E.J.W.Whittaker and F.J.Wicks. Amer. Mineral., 55, 1025-1047, 1970.
[38] F.J.Whicks and E.J.W. Whittaker. Can. Mineral., 13, 227-243, 1975.
[39] S.H.Hall, S.Guggenheim, P.Moore and S.W.Bailey. Can. Mineral., 14, 314-321, 1976.
[40] F.J.Whicks, K.Kjoller and G.S.Henderson. Can. Mineral., 30, 83-91, 1992.
[41] M.Mellini. Amer. Mineral., 67, 587-598, 1982.
[42] I.Choi and R.W.Smith. J. Colloid Interface Sci., 40, 253-262, 1972.
[43] J.Ralston and J.A.Kitchener. J. Colloid Interface Sci., 50, 242-249, 1975.
[44] Nomenclature Committee of TIMA Inc. Nomenclature of Man-Made Vitreous Fibers. Ed. W.Eastes, Owens-Corning Fiberglass, 72 pp, 1991.
[45] W.Büchner, R.Schliebs, G.Winter and K.H.Büchel. Industrial Inorganic Chemistry, Eds. H.F. Ebel and C.Dyllick-Brenzinger, VCH Verlagsgeselschaft,Weiheim and VCH Publishers, NewYork, 614 pp, 1989.

CHAPTER 4

BACKGROUND ON WET REMOVAL ASBESTOS CONTAINING MATERIALS

4. Background on wet removal asbestos containing materials.

4.1. Introduction.

The tendency of asbestos containing materials to generate fibres during a disturbance, depends significantly on the type of materials. Products where asbestos fibres are bound in a matrix such as friction materials (e.g.: brake lining for lorries) and cement, release in general less fibres into the atmosphere during their working time than friable asbestos lagging. However, the risk associated with asbestos material conducted to their progressive removal.

Dry removal was found to be a hazardous operation, contaminating the site with a high concentration of asbestos fibres. On the other hand, the wetting of the material reduces the hazard associated with the removal process by aggregating the fibres together. The concentration of fibres in the atmosphere is therefore considerably reduced[1]. As wet removal is now in widespread use in the UK, tests were needed for assessing the effectiveness to suppress or reduce airborne fibre levels. HSL designed, a few years ago, a rotating drum dust generation tester, which was used to estimate the concentration of fibres released during disturbance of wet asbestos materials.

4.2. Wetting process.

The application of wetting agents on asbestos containing materials where the outer surface is sealed, covered or armoured, using handsprays, are usually unsuccessful and superficial. Therefore, systems were developed in order to improve the wetting process. Asbestostrip Innovations designed a system called The Safestrip Injection System, able to inject the liquid directly inside the material (figure 4.1). In this system, the water passes through a filter, a pressure regulator, a pump and a mixer where the wetting agent is mixed with water. The diluted wetting agent is then distributed directly inside the material with a set of needles creating multipoint injections. The pressure at the needles is about 2 bars. Long needles up to 50 cm for injection into inaccessible flock coated steel work or concrete can be used. The injection is usually carried on from the top, since gravity helps penetration. After a soaking time, removal proceeds. Handsprays then provide additional wetting where dry areas exist.

The amount of liquid necessary for a complete wetting varies from 40 to 60 % of the asbestos material volume.

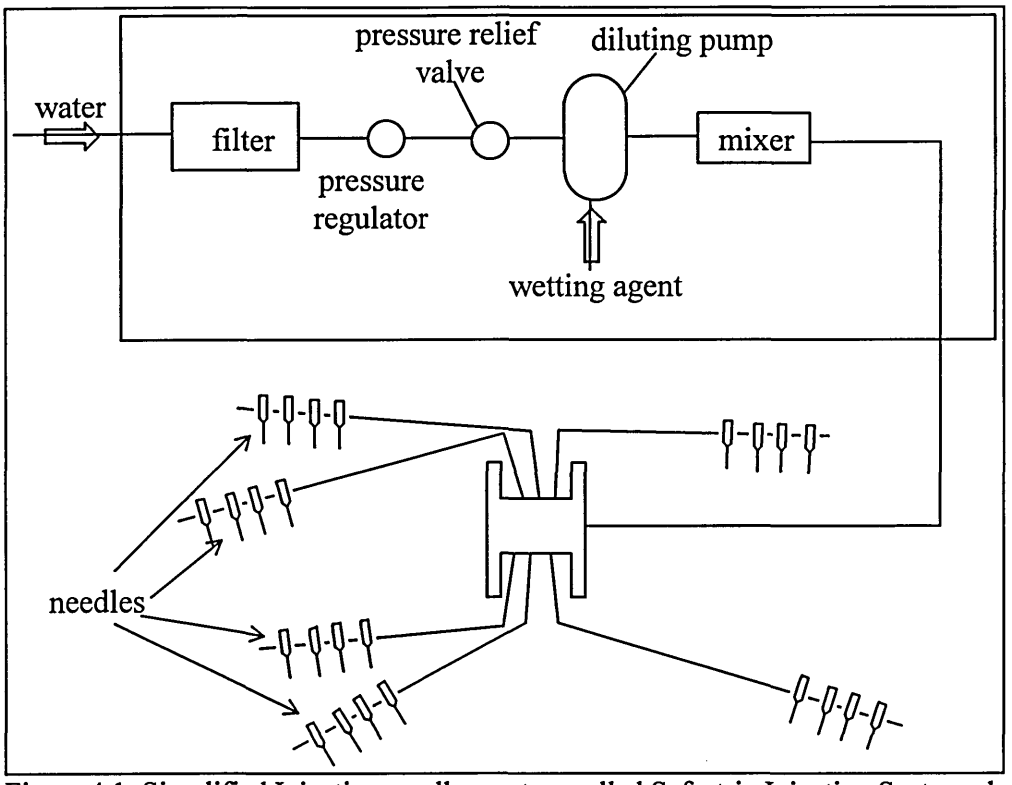

Figure 4.1: Simplified Injection needles system called Safestrip Injection System, developed by Asbestostrip Innovations (Cinderford).

4.3. Wetting and encapsulating agents.

There are two types of products: wetting and encapsulating agents. The wetting agents penetrate and saturate asbestos containing materials, while the encapsulating agents penetrate them and harden, forming a less friable material.

Wetting and encapsulating agents are generally developed from "hands on experience" rather than from the study of chemistry and properties of asbestos containing materials. Water was proved to be a good wetting agent but non-applicable due to its fast rate of evaporation. Wetting and encapsulating agents were also used in order to improve the wetting process . However, a lot of wetting agents are water based products.

The literature reported the investigation of the penetration of water, solution of surfactants in water, commercial asbestos removal solutions and analytical reagent grade

organic liquids into asbestos containing materials. It was found that in most cases the addition of wetting agent to water caused no improvement in wetting levels with the exception of amosite / calcium silicate[2].

HSL found that different agents are required depending on the composition of asbestos containing materials. For example, water appears to be an adequate wetting agent for hydrophilic asbestos containing materials (pre-formed tiles and pipe lagging composed of primarily calcium carbonate and quartz mixture with 18 % of amosite). The addition of wetting agents to remove hydrophobic asbestos containing materials (loose amosite material) appears to be beneficial[3].

Three products called penetrant n°1, astrip and hotstrip were supplied and described in the following paragraphs.

4.3.1. Penetrant n°1.

Eppert penetrant n°1 from Eppert Europe Limited (Rugeley) was provided by the Health and Safety Laboratory (Sheffield). Penetrant n°1 is a white solution or emulsion in water which forms a film when dry. It is an encapsulating agent. However, the concentration and chemistry are not officially known.

The Raman spectrum displays bands characteristic of n-alkane and two bands (at 670 and 615 cm^{-1}) assigned to the C-Cl stretching vibrations. The major compound is probably a long chain alkane with chlorine. In fact, the Raman spectrum of this wetting agent is very similar to the spectrum of polyvinylchloride (PVC).

The infrared spectrum (dry film cast on ZnSe) shows also bands characteristic of n-alkane and C-Cl stretching vibrations.

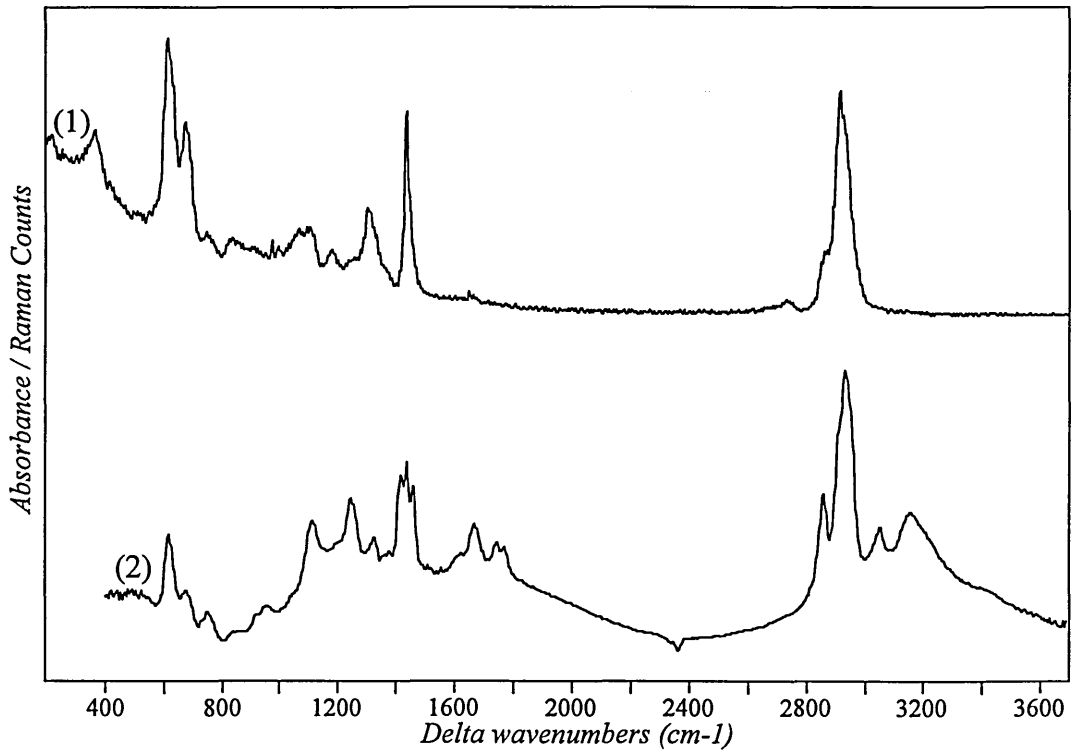

Figure 4.1. Raman (1) and infrared (2) spectra of penetrant n°1. (1) wetting agent cast on quartz slide, red laser; (2) wetting agent cast on ZnSe, transmission mode.

4.3.2. Astrip.

Astrip was provided by Asbestostrip Innovations (Cinderford). This product was designed by B.P chemicals, 1986-87, specifically to wet asbestos containing materials. This wetting agent was developed to be used at ambient temperature (between O° and 80°C). It possesses a viscosity of 2.0 centistokes at 40°C.

The composition of Astrip is as follows:

- 39.65% w/w of deionized water

- 50% polyalkylene glycol

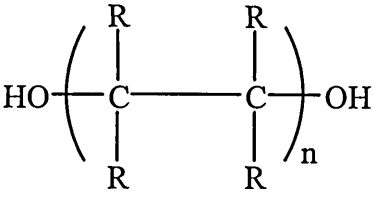

- 10 % additives.

- 0.25% optional dye.

4.3.2.3. Hotsrip and emulsions.

Hotstrip was provided by Asbestostrip Innovations (Cinderford). It is a clear non-aqueous solution, composed of pure polydimethylsiloxane (PDMS), having a viscosity of 50 centistokes.

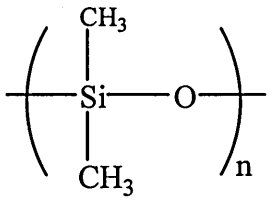

This wetting agent is used on asbestos removal sites at high temperature conditions (between 90 °C and more than 200 °C)

PDMS consists of Si-O-Si siloxane backbone with methyl side groups. The siloxane backbone is one of the most flexible polymers due to:

- the Si-O bond length (1.64 Å) which is longer than the C-C bond (1.53 Å)[4]
- The Si-O-Si angle which is more variable (105-180°) and more open than the tetrahedral bonding (~110°)[5].

The siloxane bonds rotate freely requiring almost zero rotational energy[6]. The flexibility of the siloxane backbone permits the orientation of the methyl groups at the surface or interfaces (figure 4.2).

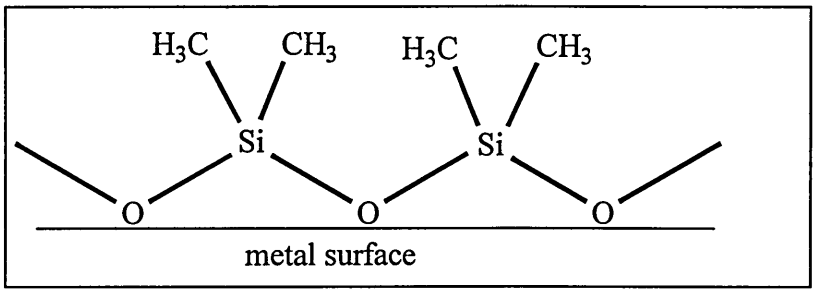

Figure 4.2. Orientation of PDMS on metal substrate.

PDMS has also a very low surface energy of 20 mN/m[6] and possesses a spreading or creep behaviour[5].

Silicone ($R_nSiO_{(4-n)}$) in water emulsions were provided by Dow Corning. The particles of silicone possess a size of 15 to 20 μm. The emulsions are composed of:

- 97 % w/w of water and silicone (40 % w/w of water for 60 % w/w of silicone).
- very small amount of additives (3 to 6 % w/w).

4.4. Rotating drum dust generation tester.

Literature reported tests which were developed to measure the concentration of fibres released from the surfaces of material containing asbestos untreated and encapsulated, when exposed to an air stream and brush[7].

The rotating drum tester, developed by HSL, was previously used in order to test a variety of materials for their dustiness such as sand, cement, silicon carbide, coal dust talc and reactive dyestuff. Burdett et al tested and compared the dust generation of man made vitreous fibres in correlation with the removal of MMVF material[8]. Most recently, Atkinson used the drum in order to measure the release of fibres from different asbestos containing materials[9].

4.4.1. Description of the tester.

The schema of the rotating drum tester is given in figure 4.3. The 50 litre stainless steel drum of the dust generation tester is composed of a main cylinder body and two removal conical end pieces. Six vanes of 2.5 cm height are found along the internal surface of the main cylinder in order to facilitate the breaking of the sample and provide a homogenous dust distribution. The rotation of the drum standing on two rollers is activated by a variable speed motor. The released fibres are collected on cellulose filters which are fitted in a sampling cassette and connected to a variable flow rate pump. The air flow rate is measured using a calibrated rotameter. The cassettes fit onto the outlet of the drum by silicone tubing which permits quick and easy exchange. The rotating drum is placed in a glove box due to the hazardous nature of the samples that are being investigated.

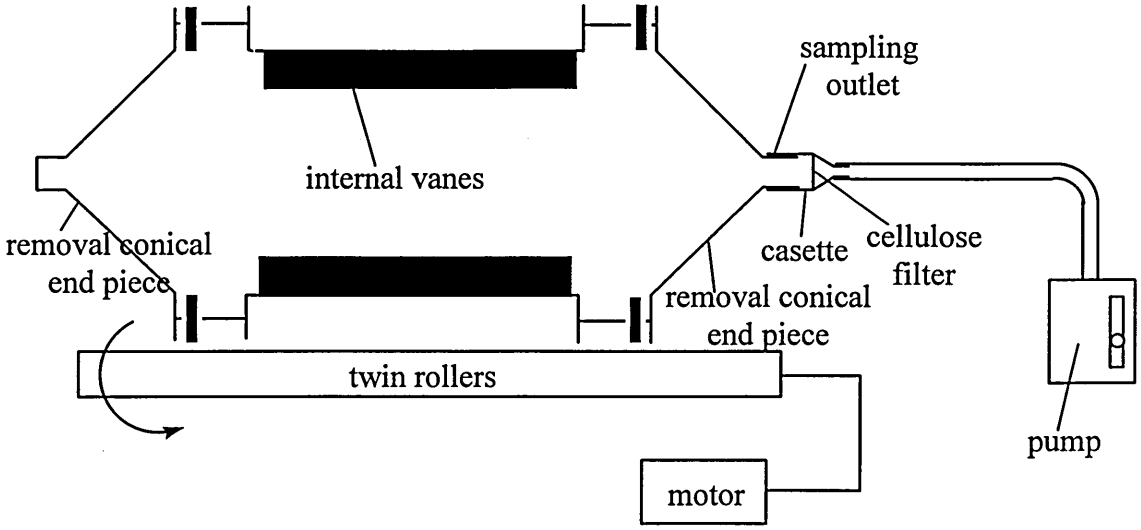

Figure 4.3. Schema of the rotating drum dustiness tester.

4.4.2. Procedure for running a test.

Before performing a test, a control blank filter is run when the drum tester without sample inside, rotates during 2 minutes. The sample under study is then placed in the centre of the cylinder. The drum is closed and sealed. A new cassette containing a cellulose filter (22 diameter, 0.8 μm pore size) is connected to the pump. The air flow rate of the pump is about 2.5 l/min. The motor which rotates the drum at 20 revolutions per minute, is switched on. Dust and fibres produced inside the drum are collected on cellulose filters fitted in cassettes which are change every 2 minutes. While the cassette is removed and replaced by another cassette, the pump and the motor which rotates the drum, are switched off.

The filters including the blank sample are removed and cut in half. One half of the filter is treated using the acetone triacetin method and the fibres are counted using the phase contrast optical microscopic (PCM) method (see chapter 1). The concentration of fibres released in fibres/ml is calculated using the formula (see chapter 1 for more details):

$$C = (1000\ N\ D^2 / V\ n\ d^2) \qquad 3.1$$

where N is the number of fibres counted, n is the number of graticules area examined, D is the diameter of the exposed filter area (22 mm), d is the diameter of the Walton Beckett graticule (100 μm) and V (in litres) is the volume of air sampled (5 l).

The rotating drum dust generation tester was used to evaluate the effectiveness of wetting agents to suppress dust from asbestos containing materials. The wet material under study needed to be compared with the dry material and two sets of experiments were run. When the dry material possesses different weights, a correction is applied on the formula of the concentration of fibres released. The correction factor is the ratio of the dry and wet sample weights.

[1] G.Burdett and G.Revell. Wet Removal of Asbestos: Final Report. Internal report, IR/L/MF/95/08, Health and Safety Laboratory, 11 pp, 1995.

[2] S.K.Brown. Am. Ind. Hyg. Assoc. J., 51, 384-389, 1990.

[3] R.Blundell-Shaw and G.Revell. Report into the Penetration Rates of Wetting and Encapsulating Agents through Asbestos Containing Materials. Internal report, IR/L/DI/94/06, Health and Safety Laboratory, 26 pp, 1994.

[4] J.E.Mark, H.R.Allcock and R.West. Inorganic Polymers, Ed. J.E.Mark, Prentice Hall Advanced Reference Series, 272 pp, 1992.

[5] M.J.Owen. Chemtech, 11, 288-292, 1981.

[6] D.Narula. Jalca, 90, 93-98, 1995.

[7] S.K.Brown. Am. Hyg. Assoc. J., 52, 363-371, 1991.

[8] G.Burdett, G.Revell and J.Brammer. HSL Protocol for Dustiness Measurements of Fibreous Materials. Internal report, IR/L/MF/96/06, Health and Safety Laboratory, 1996.

[9] R.Atkinson. Measurements of Asbestos Realesed from Different Asbestos Containing Materials. Internal report, 43 pp, 1995.

CHAPTER 5

RAMAN SPECTRA OF INORGANIC FIBRES

5. Raman spectra of inorganic fibres.

5.1. Introduction.

Organic fibres possess a diameter of about 10-100 μm. Such fibres are easily identify by Raman or infrared microspectroscopy. An example is given in figure 5.1, for a propylene fibre. The infrared spectrum was obtained in transmission mode. The fibre was flattened in order to improve the signal to noise ratio and reduce diffraction effects[1]. No sample preparation was necessary for Raman analysis. The fibre was simply placed on a quartz slide. The two spectra are very similar, showing bands due to:

- CH stretching vibrations (3000-2840 cm^{-1}).
- CH bending vibrations of methyl group and methylene scissoring (1370-1470 cm^{-1}).
- hydrocarbon methylene twisting and wagging (1150-1350 cm^{-1}).
- methylene rocking vibration (about 720 cm^{-1}).

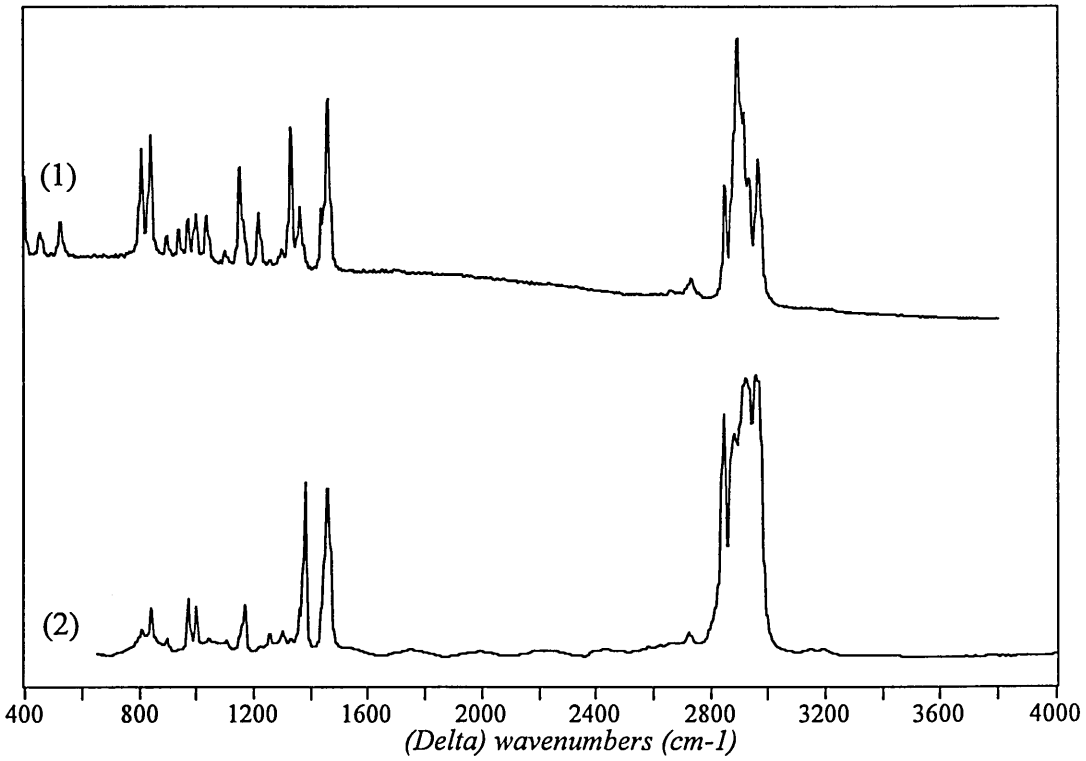

Figure 5.1: Spectra of a polypropylene fibre. (1) infrared spectrum, flattened fibre on KBr, transmission mode, resolution = 4 cm^{-1}, t=500 s; (2) Raman spectrum, fibre on quartz slide, red laser, X 50 objective, $T_{tot} \approx 9$ min.

However, the spectra show differences in intensity or numbers of bands. Indeed, in infrared spectroscopy, vibrations which involve a change of dipole moment (μ) of the molecule are observed, whereas those related to a change of the induced dipole moment through the polarisability (α) are observed in Raman spectroscopy.

Raman microspectroscopy possesses a better spatial resolution than infrared and permits the analysis of particles of 1-2 μm in size without any sample preparation instead of at least 10 μm in the case of infrared. Therefore, Raman microscopy seems to be a more appropriate technique than infrared for the study of inorganic fibres such as asbestos since the fibres can split into thinner fibres of 1 μm or less.

The data were collected using the continuous extended scanning technique. Therefore, for all spectra shown in this chapter, the total exposure time is calculated from the formula[2] : $T_{tot} \approx (1 + \text{total scan range / average static window length}) \times T_{ex}$; with T_{ex}, the exposure time.

5.2. Raman spectra of five asbestos reference standards and some of their non-fibrous analogues.

5.2.1. Introduction.

Five types of asbestos are chain silicates in the amphibole group, while the last one, chrysotile, is a sheet silicate in the serpentine group. Moreover, all asbestos fibres can occur with non-fibrous habit as mineral fragments which are non-asbestos varieties. The discrimination between asbestos fibres and non-asbestiform fragments is based on visual criterion using optical microscopy or Scanning Electron Microscopy. The characteristics of the asbestiform habit are listed in chapter 1.

Five asbestos reference standards (amosite, fibrous anthophyllite, chrysotile, crocidolite and fibrous tremolite) and some of their non-fibrous analogues (grunerite, lizardite, riebeckite and tremolite) were analysed by Raman spectroscopy in order to find out if it was possible:

- firstly, to discriminate one type of asbestos from another.
- secondly, to differentiate the asbestos fibres from the mineral fragments.

5.2.2. Materials and method.

The asbestos fibres and mineral fragments were provided by the Health and Safety Laboratory, Sheffield. The asbestos reference standards are representative of typical asbestos types of amphiboles and serpentine minerals. The asbestos minerals may be associated with non-asbestos analogues among the amphibole minerals or with

non-asbestos serpentine minerals such as antigorite. The five asbestos samples analysed by Raman microspectroscopy contain small amounts of impurities. In amosite fibres from Penge Mine (South Africa), there are a few quartz and graphite particles present. The fibrous anthophyllite sample from Karelia (Finland), contains talc and chlorite. Chrysotile contains small amount of quartz and iron oxide particles. The crocidolite fibres from Coretsi Mine (South Africa), are occasionally intergrown with fine grains of iron oxides and grains of iron hydroxides. Small quartz particles can also be found. Tremolite fibres from Saltworks Mine, Death Valley (California, USA), contains calcite and talc.

For Raman analysis, the hazardous asbestos fibres of each type mentioned above were encapsulated between a quartz slide and a quartz window while the mineral fragments were just deposited on a quartz slide. The quartz is an ideal substrate for Raman spectroscopy since its spectrum does not show a fluorescence background and presents only few weak broad bands at low wavenumbers. However, the thin quartz window (0.22 mm thick) on top of the fibres, necessary for the health and safety risk aspect, reduces the signal to noise ratio. Moreover, asbestos scatters visible light weakly in comparison to organic materials which results in longer acquisition times.

The laser was focused on closely packed bundles of fibres or crystals. Indeed, the fluorescence background is less important when the asbestos fibres are closely packed rather than when they do not show particular arrangement. The Raman spectra of five reference asbestos fibres in comparison with some of their non-fibrous analogues were obtained using the 633 nm line of helium neon laser and the 785 nm line of near infrared laser for chrysotile only. The instrument was set up in microprobe mode using a slit width of 50 μm and a CCD area of 15x576 pixels.

5.2.3. Results.

The spectra display sharp bands in the 200-1200 cm^{-1} and 3500-3800 cm^{-1} region (figure 5.2.a to 5.2.e). The characteristic peaks are listed in table 1 with a general possible assignments[3]. The precise assignments is not very well known or understood from literature because the chemistry and structure of asbestos is rather complex.

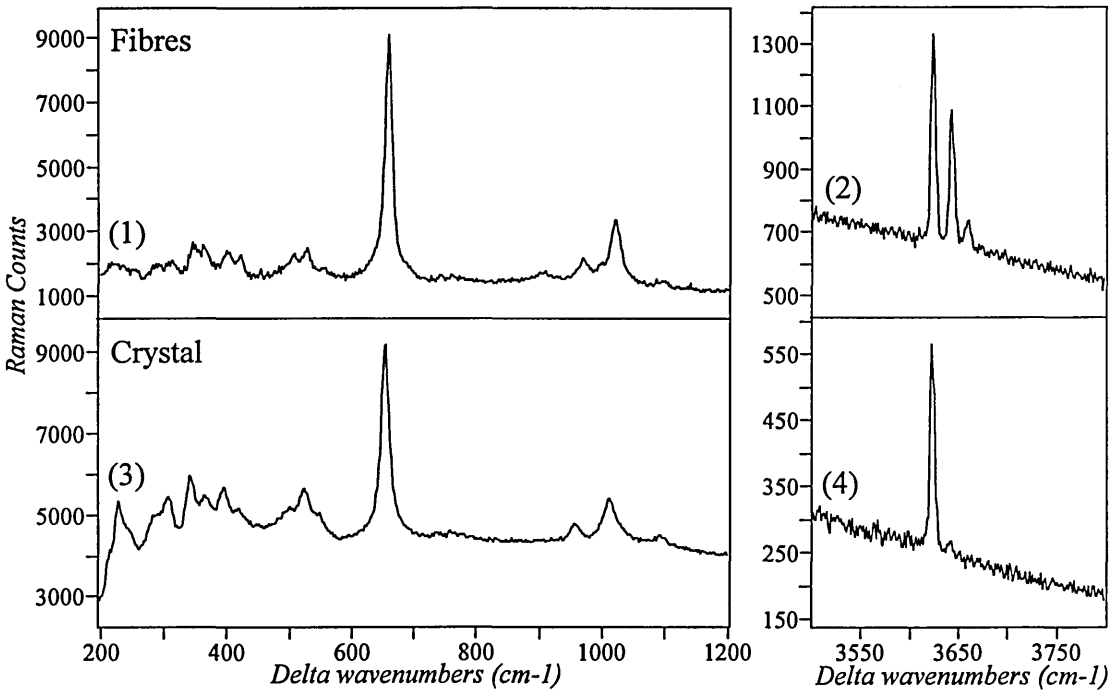

Figure 5.2.a: Raman spectrum of reference amosite fibres in comparison with reference grunerite crystal. (1) amosite, red laser, X 50 objective, $T_{tot} \approx 22.4$ min; (2) amosite, red laser, X 50 objective, $T_{tot} \approx 11.1$ min; (3) grunerite, red laser, X50 objective, $T_{tot} \approx 15.8$ min; (4) grunerite, red laser, X 50 objective, $T_{tot} \approx 3.1$ min. - Quartz subtraction applied on spectrum (1).

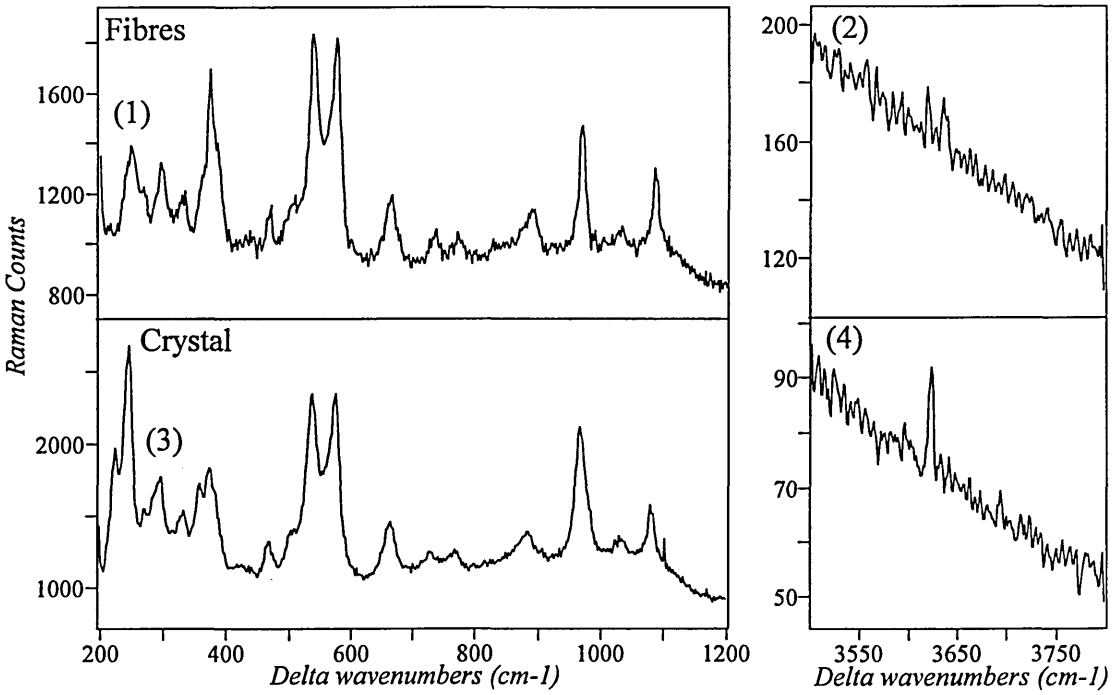

Figure 5.2.b: Raman spectrum of reference crocidolite fibres in comparison with reference riebeckite crystal. (1) crocidolite, red laser, X 50 objective, $T_{tot} \approx 27.7$ min; (2) crocidolite, red laser, X 50 objective, $T_{tot} \approx 11.1$ min; (3) riebeckite, red laser, X 50 objective, $T_{tot} \approx 7.9$ min; (4) riebeckite, red laser, X 50 objective, $T_{tot} \approx 3.1$ min. - Quartz subtraction applied on spectrum (1); smoothing function (Savitsky Golay, degree 2, 11 points) applied on spectra (2) and (4).

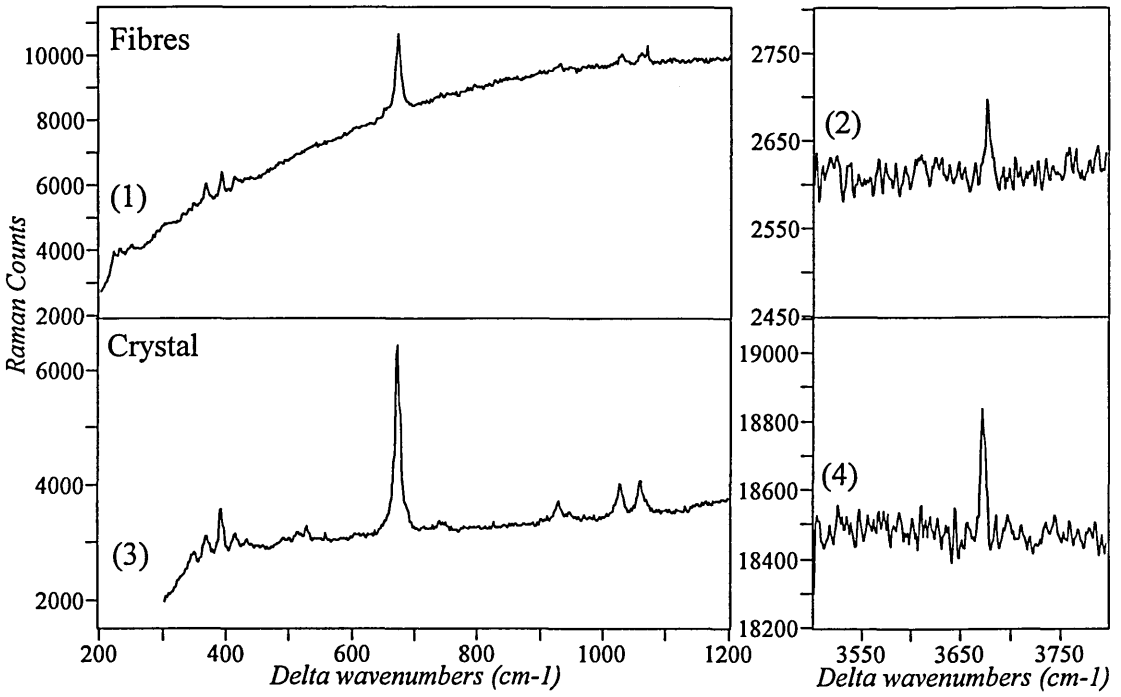

Figure 5.2.c: Raman spectrum of reference tremolite fibres in comparison with reference tremolite crystal. (1) fibrous tremolite, red laser, X 50 objective, $T_{tot} \approx 23.1$ min; (2) fibrous tremolite, red laser, X 50 objective, $T_{tot} \approx 15.8$ min; (3) tremolite, red laser, X 50 objective, $T_{tot} \approx 2.2$ min; (4) tremolite, red laser, X 50 objective, $T_{tot} \approx 3.8$ min. - Quartz subtraction applied on spectrum (1); baseline correction and smoothing function (Savitsky Golay, degree 2, 11 points) applied on spectra (2) and (4).

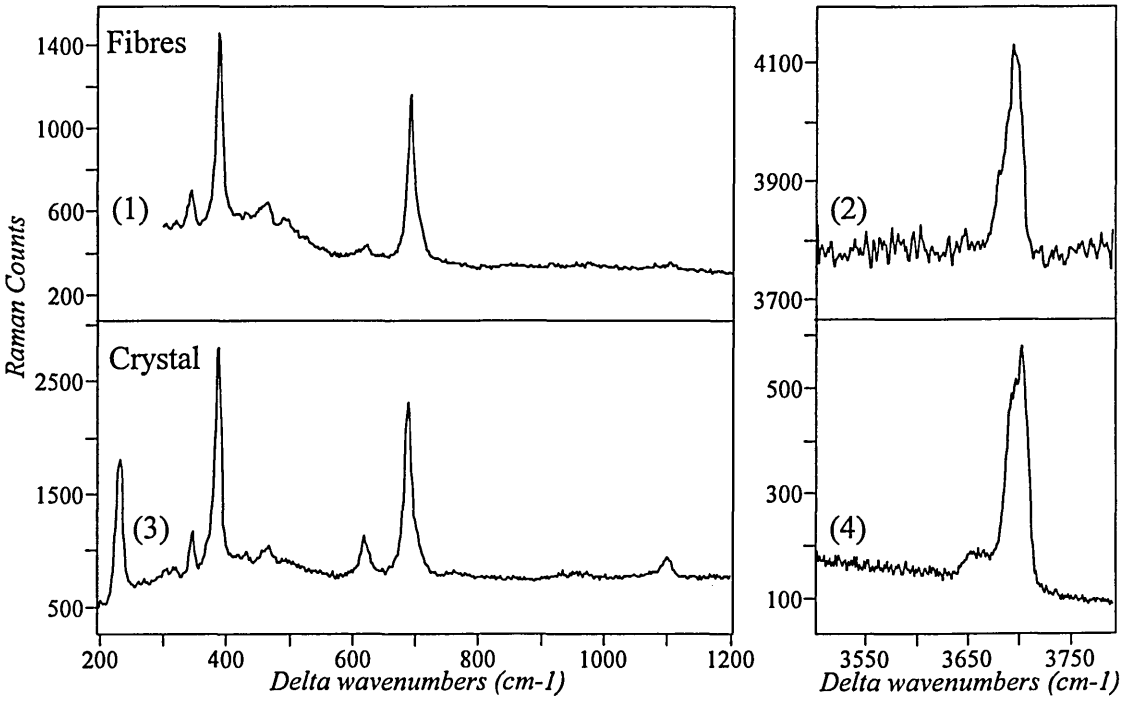

Figure 5.2.d: Raman spectrum of reference chrysotile fibres in comparison with reference lizardite crystal. (1) chrysotile, infrared laser, X 20 objective, $T_{tot} \approx 4.3$ min; (2) chrysotile, red laser, X 50 objective, $T_{tot} \approx 11.1$ min; (3) lizardite, red laser, X 50 objective, $T_{tot} \approx 7.9$ min; (4) lizardite, red laser, X 50 objective, $T_{tot} \approx 3.1$ min. - Quartz subtraction applied on spectrum (1); baseline correction and smoothing function (Savitsky Golay, degree 2, 11 points) applied on spectrum (2).

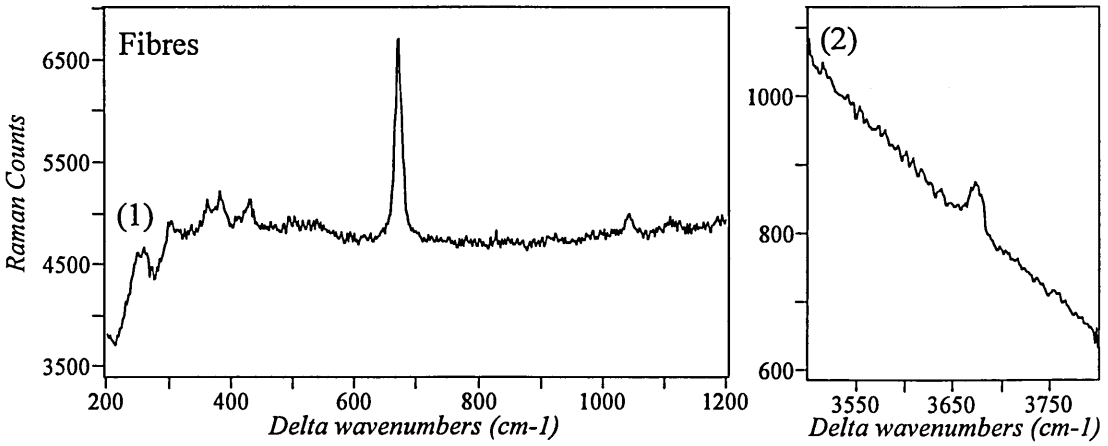

Figure 5.2.e: Raman spectrum of reference anthophyllite. (1) fibrous anthophyllite, red laser, X 50 objective, $T_{tot} \approx 23.1$ min; (2) fibrous anthophyllite, red laser, X 50 objective, $T_{tot} \approx 15.8$ min. - Quartz subtraction applied on spectrum (1); smoothing function (Savitsky Golay, degree 2, 11 points) applied on spectrum (2).

The asbestos spectra are significantly different and possess their own features in such a way it is possible to discriminate one type of asbestos from another as in infrared spectroscopy[4,5]. Actinolite is the only asbestos that was not studied and exhibits a very similar spectrum to tremolite[6]. There are several important advantages of using Raman spectroscopy on asbestos fibres. Firstly, the Raman bands have narrower band widths and are therefore more characteristics than infrared bands. Secondly, in general, the Raman spectra extend to lower wavenumbers, 200 cm^{-1} instead of 400 cm^{-1} in the case of conventional mid-infrared spectroscopy. Thirdly, there is little or no sample preparation. The fibres do not need to be ground with an alkali halide.

All of the five asbestos references show a band between 660 cm^{-1} and 690 cm^{-1} characteristic of the Si bridging -O-Si symmetric stretching vibration. This band can be used as an initial help for discrimination. It appears at about 690 cm^{-1} for chrysotile, at about 670 cm^{-1} for anthophyllite and tremolite and at about 660 cm^{-1} for amosite and crocidolite. However, each asbestos spectrum exhibits also their own bands used for identification. A very strong band at about 390 cm^{-1} assigned to a metal-oxygen vibration occurs in the chrysotile spectrum. For crocidolite, four bands at 577 cm^{-1}, 539 cm^{-1}, 374 cm^{-1} and 969 cm^{-1} are taken as the main features. Amosite and anthophyllite show bands at 1020 cm^{-1} and 1040 cm^{-1} respectively. The tremolite spectrum displays two bands at 1060 and 1030 cm^{-1} (Si-O-Si stretching vibrations) and several bands between 410 and 350 cm^{-1} (metal oxygen vibration modes).

	Si-bridging O-Si stretching modes $\bar{\nu}$ / cm^{-1}	Non bridging Si-O stretching modes $\bar{\nu}$ / cm^{-1}	Si-O-Si deformation modes $\bar{\nu}$ / cm^{-1}	Metal-oxygen modes $\bar{\nu}$ / cm^{-1}	OH stretching modes $\bar{\nu}$ / cm^{-1}
Amosite	1093 (vw) 658 (vs) 555 (vw) 528 (m)	1020 (s) 968 (m) 903 (vw)	506 (w)	421 (m) 401 (m) 364 (m) 349 (m) 309 (w) 287 (w)	three bands: 3656 3639 3623
Anthophyllite	671 (vs) 1042 (m)			430 (m) 410 (w) 384 (m) 362 (m) 336 (vw) 304 (m) 260	3674
Chrysotile	1105 (vw) 692 (vs) 623 (w)			465 (m) 432 (vw) 389 (vs) 345 (s) 321 (vw) 304 (vw)	3700 3685 (sh)
Crocidolite	1085 (s) 1032 (m) 664 (s) 577 (vs) 539 (vs)	969 (vs) 891 (s) 772 (m) 737 (m)	509 (w)	469 (m) 374 (vs) 332 (m) 297 (s) 249 (s) 271	Two bands: 3637 3620
Tremolite	1061 (m) 1028 (m) 672 (vs)	928 (w)		414 (w) 393 (m) 369 (m) 349 (vw) 251 (w) 222 (w) 232 (w)	3677

Key: vs, very strong; s, strong; w, weak; vw, very weak; sh, shoulder.
Table 5.1: Table of wavenumbers and assignments for the Raman spectra of asbestos fibres.

The Raman spectrum of amosite is similar to that of Lewis et al.[3]. The band at 903 cm^{-1} also observed in the spectrum of Lewis et al, is not present in our grunerite spectrum. It might arise from an impurity or more simply be too weak in grunerite spectrum. The band at 1093 cm^{-1} is not observed in the spectrum of Lewis et al., whereas it appears in both of our fibrous and non-fibrous spectra. The Raman spectra of crocidolite and chrysotile are in good agreement with those of Lewis et al and Delhaye et al[3,7]. The Lewis et al. spectrum of chrysotile clearly presents a very strong band at

about 690 cm^{-1}. However, it was reported in the text and table, by mistake, at 670 cm^{-1}. For tremolite fibres the spectrum, using the 633 nm excitation, is in agreement with those of Blaha et al using the 514 nm excitation but the fluorescence background is higher in our spectrum[8]. Our anthophyllite spectrum is in good agreement with those of Delhaye et al and Blaha et al[7,9]. It is also close to the spectrum reported by Lewis et al[3] as tremolite, but which is probably anthophyllite.

The Raman spectra of asbestos fibres and their non-fibrous form were also compared. It is difficult to find any important differences except for some cases in the OH stretching region. Amosite and crocidolite show three (3656(very strong), 3639(very strong), 3623(medium) cm^{-1}) and two (3637(weak), 3620 (weak) cm^{-1}) bands while grunerite and riebeckite presents only two (3642 (weak), 3623 (very strong) cm^{-1}) and one (3624 (weak) cm^{-1}) bands respectively.

5.3. Raman spectra of tremolite reference standard in comparison with its non-fibrous analogue.

5.3.1. Introduction.

A more extensive study on both fibrous and non-fibrous tremolite was performed in order to find out if there was any difference in the Raman spectra corresponding to the difference in morphology. Indeed, the spectra of asbestos fibres and non-asbestiform fragments, both, show only one band in the OH stretching modes region.

5.3.2. Materials and method.

The instrument was set up in confocal mode using a slit width closed down to 15 μm and a CCD area of 4x576 pixels. The confocal mode was used in order to maximise the spectral resolution (it is about 2.5 cm^{-1}). Therefore, because of the resulting loss of photons, a reasonable signal to noise ratio could be obtained when the laser (633 nm excitation) was focused on large crystals of tremolite and bundles of tremolite fibres using the X 50 objective and a long acquisition time was used. The same parameters (time acquisition, objective) were applied for all the spectra and all the spectra were recorded the same day.

The tremolite and tremolite fibrous samples came from Edenite and Death valley respectively. The crystals and fibres were attached on cellulose filter.

5.3.3. Results.

The OH region shows in both cases only one band. The spectra of the fibrous and non-fibrous tremolite show a difference in the half width of the 670 cm^{-1} band, corresponding to the Si bridging-O-Si stretching vibration, and more significantly in the half width of the metal-oxygen bands at 390 cm^{-1} (figure 5.3.a to 5.3.c). The half width of the 670 cm^{-1} was measured after applying a baseline between 600 and 720 cm^{-1}. The half width of the more intense band at 392 cm^{-1} was measured after applying a baseline between 320 cm^{-1} and 460 cm^{-1} and fitting the four bands at 415, 392, 371 and 347 cm^{-1} (figure 5.3.d).

The bands used for the curve fitting were 100 % Lorentzian.

The plots, showing the position and half width of the two bands at about 670 and 390 cm^{-1}, for six different tremolite crystals and fibres are given in figures 5.4.a to 5.4.d.

Figure 5.4.a.

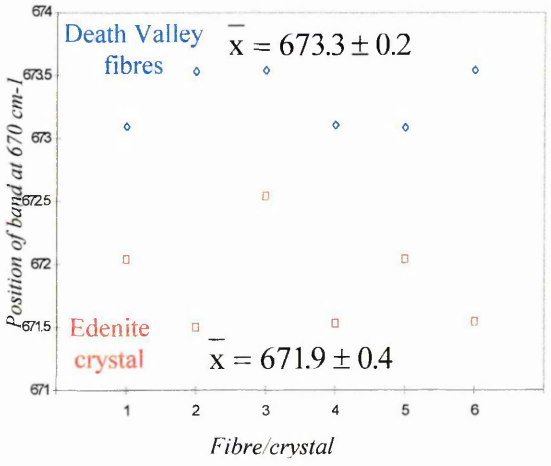

Figure 5.4.b.

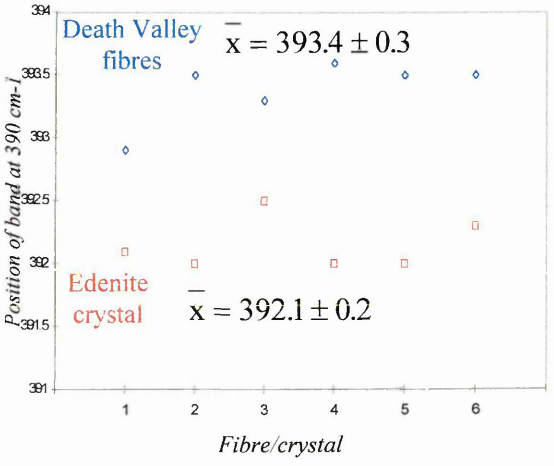

Figure 5.4.c.

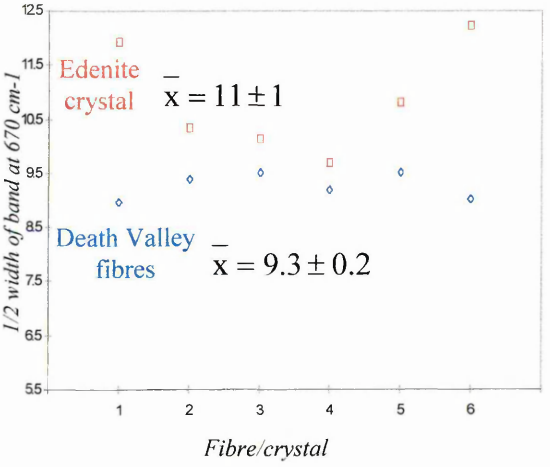

Figure 5.4.d.

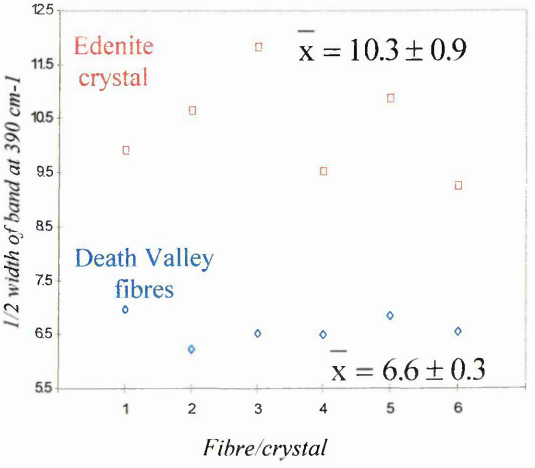

Figure 5.4: Position of the tremolite bands at ~ 670 and 390 cm^{-1} (5.4.a and 5.4.b); width at half height of the tremolite bands at ~ 670 and 390 cm^{-1} (5.4.c and 5.4.d) for six different fibres and crystals.

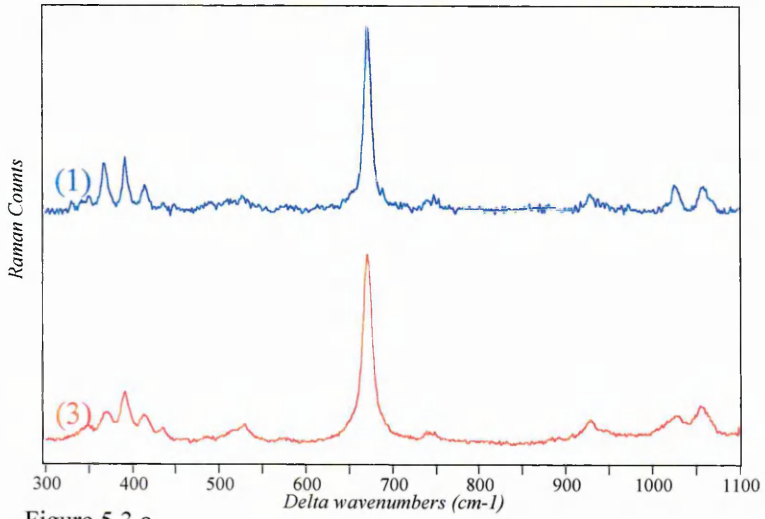

Figure 5.3.a

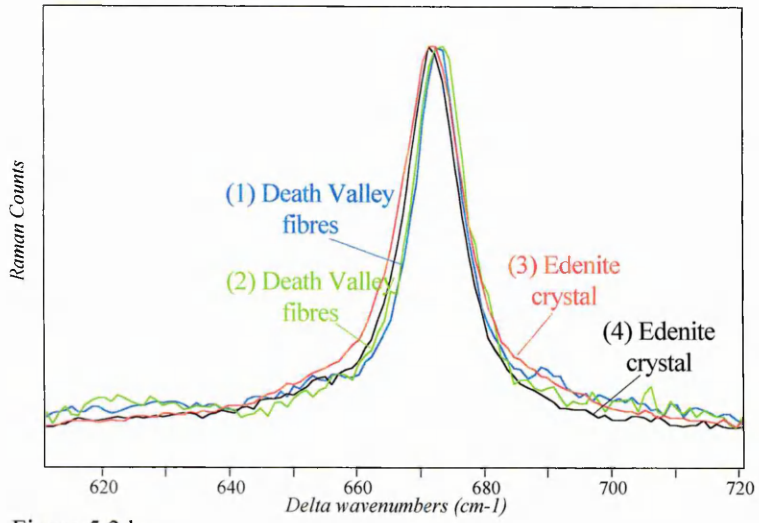

Figure 5.3.b.

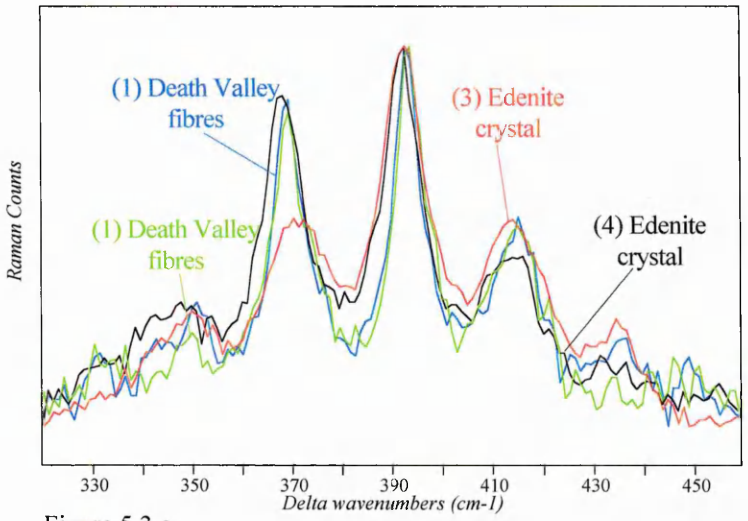

Figure 5.3.c

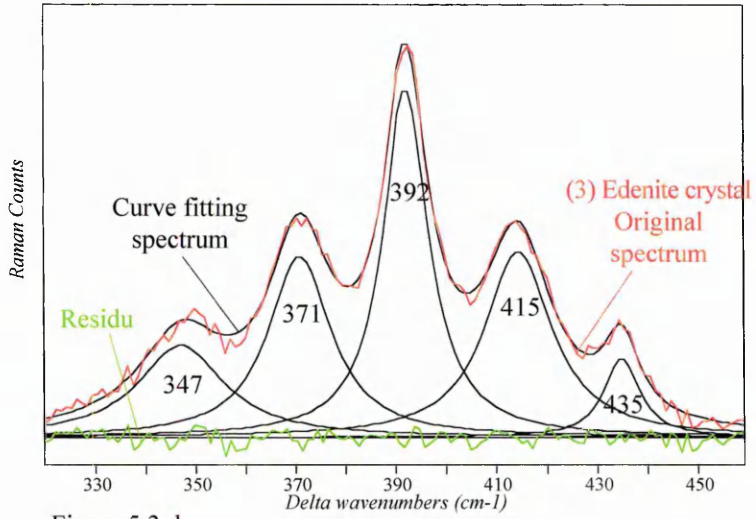

Figure 5.3.d

Figure 5.3.a: Raman spectra of (1) Death Valley fibres and (3) Edenite crystals. Baseline correction and cellulose filter subtraction applied on spectra (1) and (3).

Figure 5.3.b. 670 cm^{-1} Raman band for Death Valley fibres ((1), (2)) and Edenite crystals ((3), (4)). Baseline correction between 610 -720 cm^{-1} applied on spectra (1) to (4).

Figure 5.3.c: 320-460 cm^{-1} region for Death Valley fibres ((1), (2)) and Edenite crystals ((3), (4)). Baseline correction between 320-460 cm^{-1} applied on spectra (1) to (4).

Figure 5.3.d: Curve fitting in the 320-460 cm^{-1} region of spectrum (3) with four Lorentzian bands. Baseline correction between 610 -720 cm^{-1} applied on spectrum (3).

Parameters for data collection: red laser, X 50 objective, $T_{tot} \approx 23.5$ min.

		Position mean value (cm^{-1})	Half width mean value (cm^{-1})
Edenite crystal	Band 1	392.1 ± 0.2	10.3 ± 0.9
	Band 2	671.9 ± 0.4	11 ± 1
Death Valley fibres	Band 1	393.4 ± 0.3	6.6 ± 0.3
	Band 2	673.3 ± 0.2	9.3 ± 0.2

Table 5.2: Mean value of the position and half width of the bands at 670 and 390 cm^{-1} for tremolite fibres and crystals.

The half width mean values for the 670 and 390 cm^{-1} bands is about 1.2 and 1.6 larger in the case of Edenite crystals than Death Valley fibres. The difference in half width between the fibres and the crystals is more important for the 390 cm^{-1} band than the 670 cm^{-1}. A small bands shift of about 1.3 cm^{-1} is also observed between the crystals and the fibres (table 5.2).

The Raman band widths in crystalline solids are relatively sharp, mainly due to the anharmonicity of the molecular vibrations[10] . Two principal reasons can explain the difference in the band widths between the fibrous and non-fibrous tremolite.
Firstly, defects, impurities or vacancies in the crystal lattice results in broadening the Raman bands[11]. It would mean that the number of defects in Edenite is more important than in Death Valley sample. Moreover, the metal-oxygen vibration band at 393 cm^{-1} is more sensitive to the broadening effect. The metal-oxygen vibration may be more perturbed by the defects than the Si bridging -O-Si stretching vibration.
Secondly, an increase in temperature results in a linear increase in the band widths[12]. It could be possible that the laser locally heats the Edenite crystals more than the Death Valley fibres due to the shape differences.

The next step would be to investigate samples from different sources.

5.4. Raman spectra of reference fibres on cellulose filters.

5.4.1. Introduction.

At Health and Safety Laboratory, the asbestos fibres are routinely analysed by polarised light microscopy (PLM) after a tentative identification by stereo microscopy. The fibres are placed on a microscope slide into an appropriate drop of refractive index (RI) liquid which must match the RI of the fibre as explained in chapter 1. Five high dispersion liquids are used in general for the identification of the six types of asbestos

fibres. The same RI liquid is used for the identification of fibrous anthophyllite and fibrous tremolite. Therefore, it could be difficult with the PLM technique to distinguish between tremolite and anthophyllite and a SEM/EDX analysis should be performed.

For fibre counting, the inorganic fibres are collected on cellulose filters. Indeed, a measured volume of air is drawn through a membrane filter which is then mounted on a microscope slide using the acetone triacetin method as explained in chapter 1. Fibres are then counted using phase contrast microscopy in order to calculate the concentration of fibres.

The identification of asbestos fibres by PLM involves many sample preparations. However, Raman microspectroscopy is a more straight forward analysis technique. For this reason, a Raman study of some reference inorganic fibres on filters was investigated in order to:

- firstly, find out if it was possible to analyse individual fibres on membrane filters.
- secondly, establish the detection limit of the spectrometer. In other words, determine the smallest fibre which could be identified.

Fibres especially asbestos, attached on membrane filters, before and after the acetone triacetin treatment (see chapter 1), were analysed by Raman spectroscopy. Moreover, an infrared microspectroscopic analysis in transmission and reflectance mode of asbestos fibres on cellulose filters was attempted.

5.4.2. Materials and methods.

The five asbestos reference standards, described at the beginning of the chapter, were placed on cellulose filters using a pump by drawing a volume of air through the membrane filters. The filters display fibres with different diameter sizes (figure 5.5). All Raman spectra were obtained using the X 100 objective and the 633 nm excitation, except for chrysotile where the 785 nm line was employed. The laser was focused on fibres having diameter from 1 to 5 μm.

An infrared spectrum of amosite fibres, in reflectance mode, with a resolution of 4 cm^{-1} was also recorded. The infrared beam was focused on a bundle of fibres using a microscope.

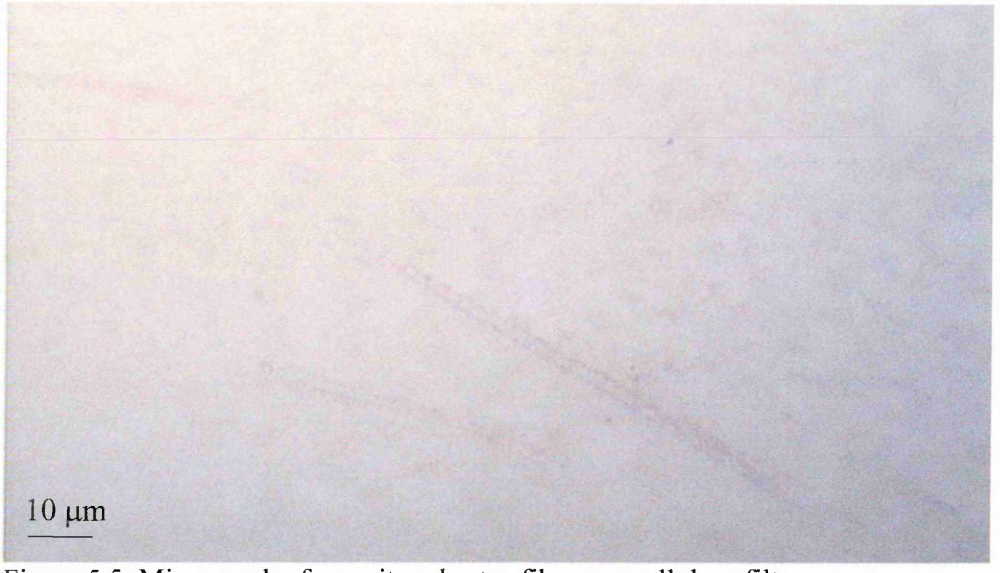

Figure 5.5: Micrograph of amosite asbestos fibres on cellulose filter.

Amosite reference fibres on a filter treated with the acetone triacetin method for fibre counting were also analysed by Raman microspectroscopy using the 633 nm excitation. The cellulose filter was collapsed and cleared on a glass slide using hot acetone. Two drops of glycerol triacetate were then applied and a quartz cover slip (0.22 mm) was mounted as explained in chapter 1.

Some inorganic fibres such as rock wool, mineral wool and microquartz fibres, provided by the Health and Safety Laboratory, also placed on cellulose filters, were analysed by Raman microspectroscopy using the 633 nm excitation. The spectra were obtained using the X 50 objective, since the individual fibres have a diameter as large as 20 μm (figure 5.6).

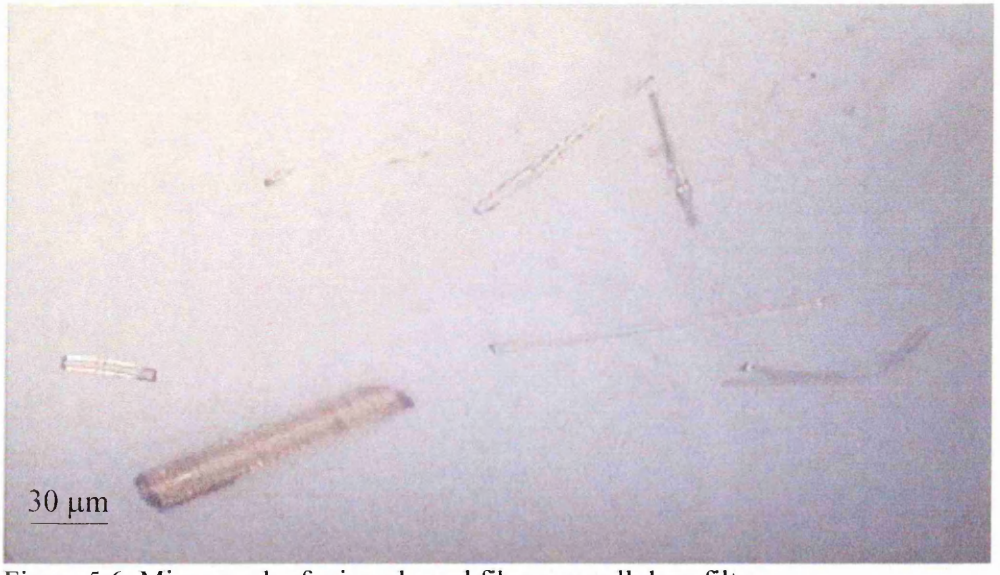

Figure 5.6: Micrograph of mineral wool fibres on cellulose filter.

5.4.3. Results.

Even if the Raman spectrum of the cellulose filter alone gives strong bands, it does not present a fluorescence background. Spectra of the asbestos fibres on the filter show bands associated with the filter. This is not a problem, since the filter spectrum can be easily removed by subtraction. An example is given, in figure 5.7, for an amosite fibre having a diameter of 3 μm. When the size of the fibres becomes smaller, the part of the cellulose filter in the spectrum increases and the information from the asbestos fibres becomes poorer. This is specially true for fibres having small diameters of about 1-2 μm. Nevertheless, after subtraction of the filter, the main features from asbestos are still present (figure 5.8).

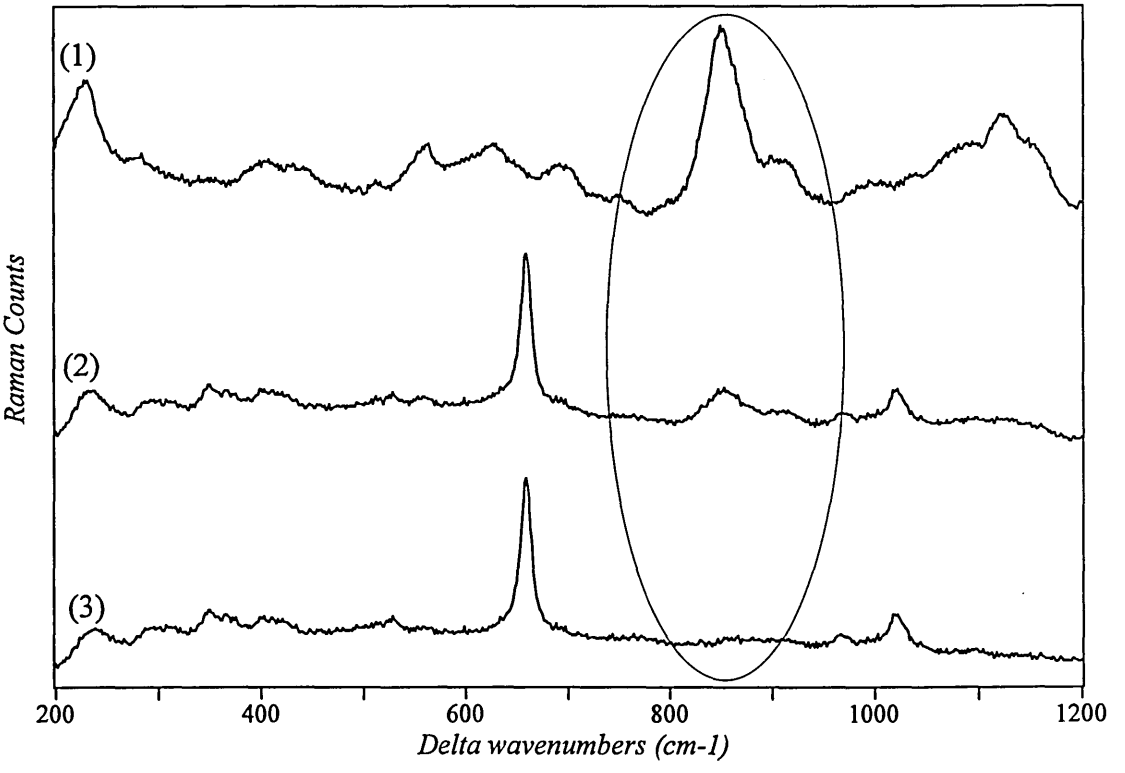

Figure 5.7: Subtraction process of Raman spectra. (1) cellulose filter; (2) amosite fibre of 3 μm of diameter, red laser, X 100 objective, $T_{tot} \approx 27.7$ min; (3) subtraction: (3)=(2)-0.17 (1).

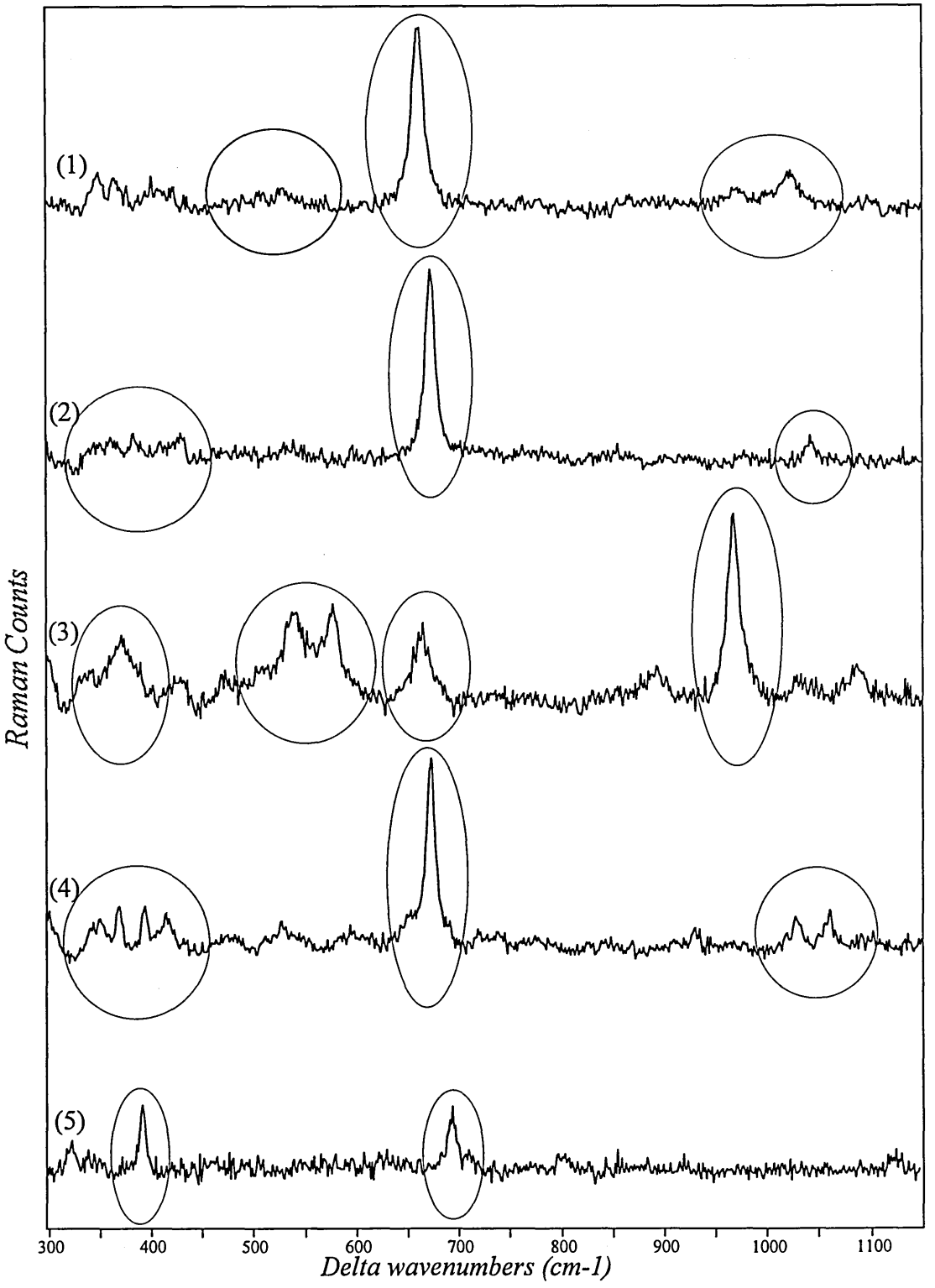

Figure 5.8: Raman spectra of reference fibres on cellulose filters. (1) amosite fibre of 1 μm of diameter, red laser, X 100 objective, $T_{tot} \approx 27.7$ min; (2) anthophyllite fibre of <2 μm of diameter, red laser, X 100 objective, $T_{tot} \approx 27.7$ min; (3) crocidolite fibre of 1 μm of diameter, red laser, X 100 objective, $T_{tot} \approx 27.7$ min; (4) tremolite fibre of <2 μm of diameter, red laser, X 100 objective, $T_{tot} \approx 27.7$ min; (5) chrysotile fibre of 1 μm of diameter, near infrared laser, X 100 objective, $T_{tot} \approx 44.9$ min.
Cellulose filter subtraction and baseline applied on spectra (1) to (5).

The direct infrared spectrum of a bundle of fibres having a 20 μm of diameter on a filter placed on a gold slide was collected in reflectance mode and ratio with the filter background (figure 5.9). The spectrum obtained is clearly not characteristic of that of asbestos from the literature[4,5]. In transmission mode, the filter alone is too thick and not transparent, giving a saturated spectrum.

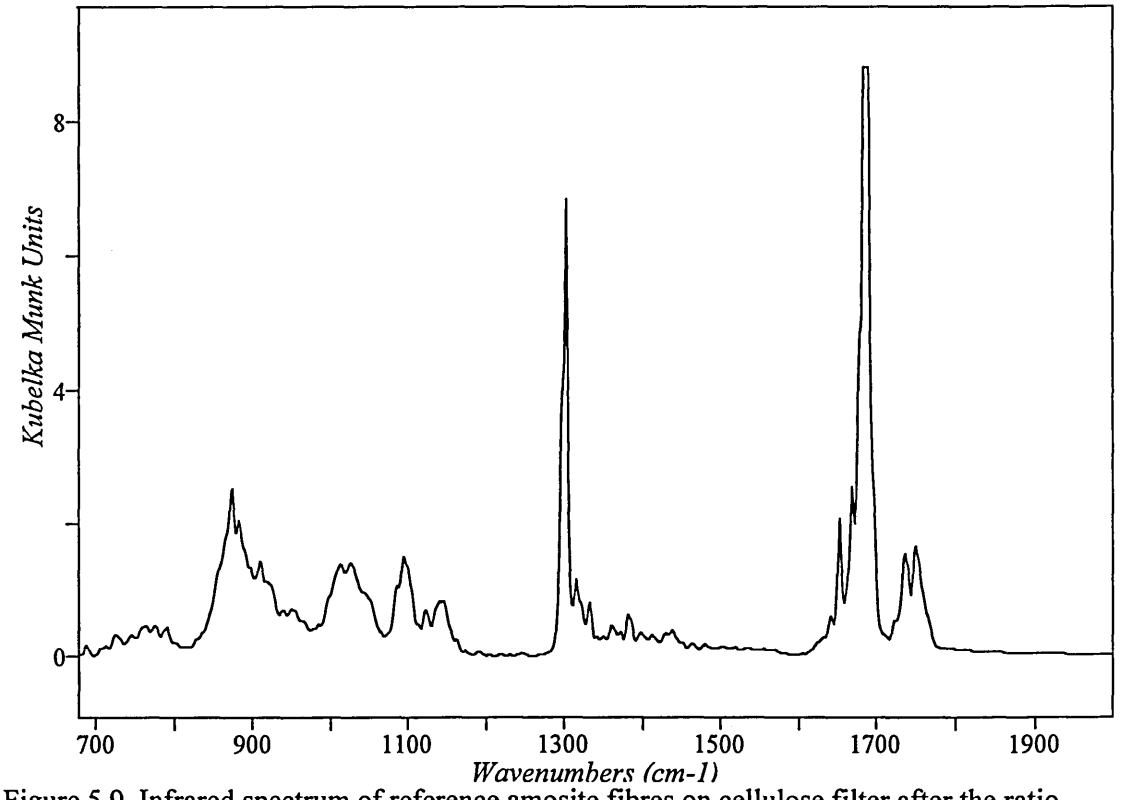

Figure 5.9. Infrared spectrum of reference amosite fibres on cellulose filter after the ratio amosite fibres on filter/filter alone. Bundle of fibres of 20 μm of diameter. Reflectance mode, resolution=4 cm^{-1}, t=500 s.

From the sample treated with the acetone triacetin method, the laser was focused on a fibre having a diameter of 4 μm, using the X 50 objective. In fact, the light had to travel through the quartz slide and the glycerol triacetate, resulting in a Raman spectrum without any band from the asbestos fibre (figure 5.10). Even a quartz slide alone on top of a fibre is going to reduce considerably if it is not to suppress the signal from the fibre.

The spectrum of a reference amosite fibre having a diameter of 3.5 μm and treated with the acetone triacetin method but without any quartz window, was also collected. The background from the filter , acetone and glycerol triacetate was removed by subtraction. The final spectrum displays a strong band at 660 cm^{-1} assigned to the

Si bridging-O-Si stretching vibration and a very weak band at 1020 cm^{-1}, both characteristic of amosite (figure 5.10). However, such treatment for PLM analysis seems to reduce the signal to noise ratio of asbestos spectra.

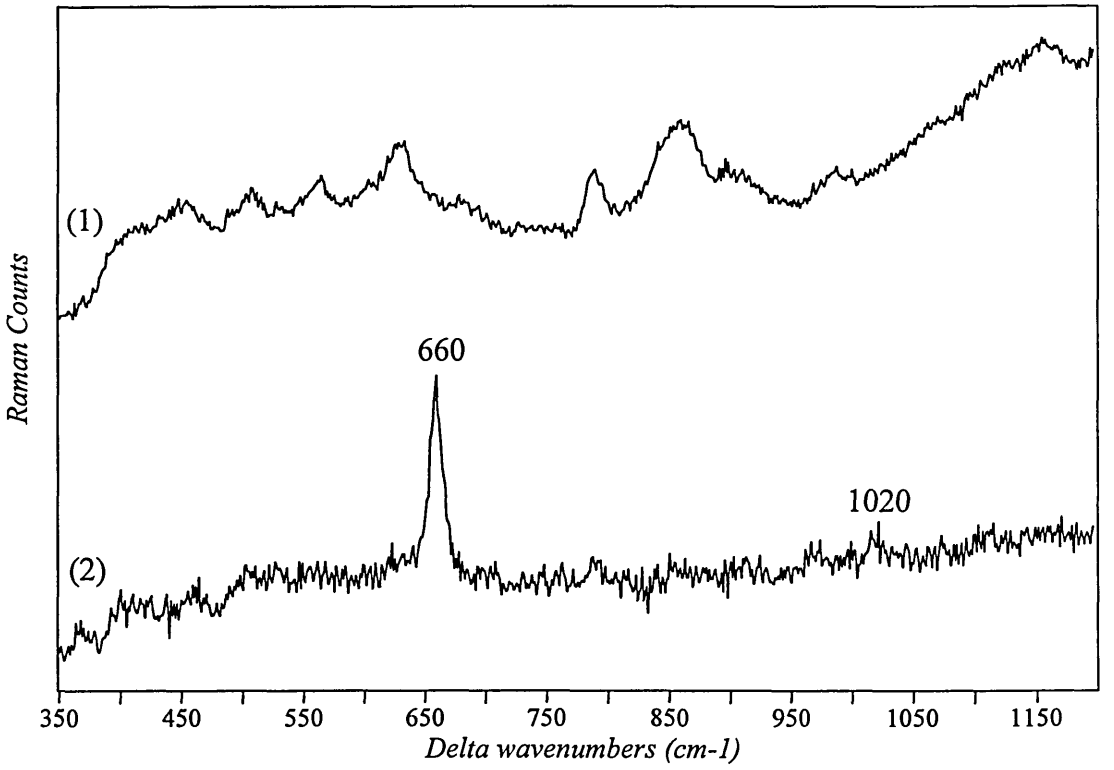

Figure 5.10: Raman spectra of reference amosite fibres treated with the acetone triacetin method. (1) fibre of 4 μm of diameter with a quartz slide on top, red laser, X 50 objective, $T_{tot} \approx 6.3$ min; (2) fibre of 3.5 μm of diameter without quartz slide on top, X 100 objective, red laser, $T_{tot} \approx 18.9$ min.
Background (treated cellulose filter and quartz) subtraction applied on spectrum (2).

The Raman spectra of the rock wool, mineral wool and microquartz fibres, on cellulose filters, were also successfully obtained (figure 5.11 and 5.12). The usual process of filter subtraction was also applied. However, the spectra show a profile totally different from the asbestos fibres. Indeed, the spectra show broad bands in contrast with the sharp bands of asbestos. The broadening effect of bands is due to the elimination of non-bridging oxygen and the introduction of more disorder in the glass network[13]. Mineral wool and rock wool fibres show the same spectra with a strong broad band at about 950 cm^{-1} and a band at 550 cm^{-1} (figure 5.11). These spectra are characteristic of glass spectra and fit very well with the Raman spectra of a lunar glass and a lunar volcanic glass bead recorded by Sweet et al[13] and Wang et al[14] respectively.

In bulk alkali and alkaline earth glasses, the Raman bands found in the 400-700 cm^{-1} region are due to Si-O-Si linkages between the silicate tetrahedra[15]. In the 800-1200 cm^{-1}, the bands are associated with the Si-O stretching vibrations of SiO_4 units[15,16]. The main bands generally appear near 1100, 1000, 900 and 850 cm^{-1} and are assigned to Si-O stretching vibrations of SiO_4 groups with 1, 2, 3 and 4 nonbridging oxygen respectively. Indeed, the addition of alkali and alkaline earth ions in the silicate network creates non-bridging oxygen. The low frequency of Si-O stretching (950 cm^{-1}) vibration in wool fibres could be due to the presence of high content of non-bridging oxygen[13,14]. Indeed, the band position is closer to that of orthosilicate than of network forming silicate. Moreover, the mineral and rock wool fibres have a relatively high content of aluminium. We know that the addition of aluminium in the silicate network of glasses, broadens and smears the bands due to the introduction of more non-equivalent bond lengths and angles between SiO_4 tetrahedra[13,16]. This could explain the broad bands in our spectra.

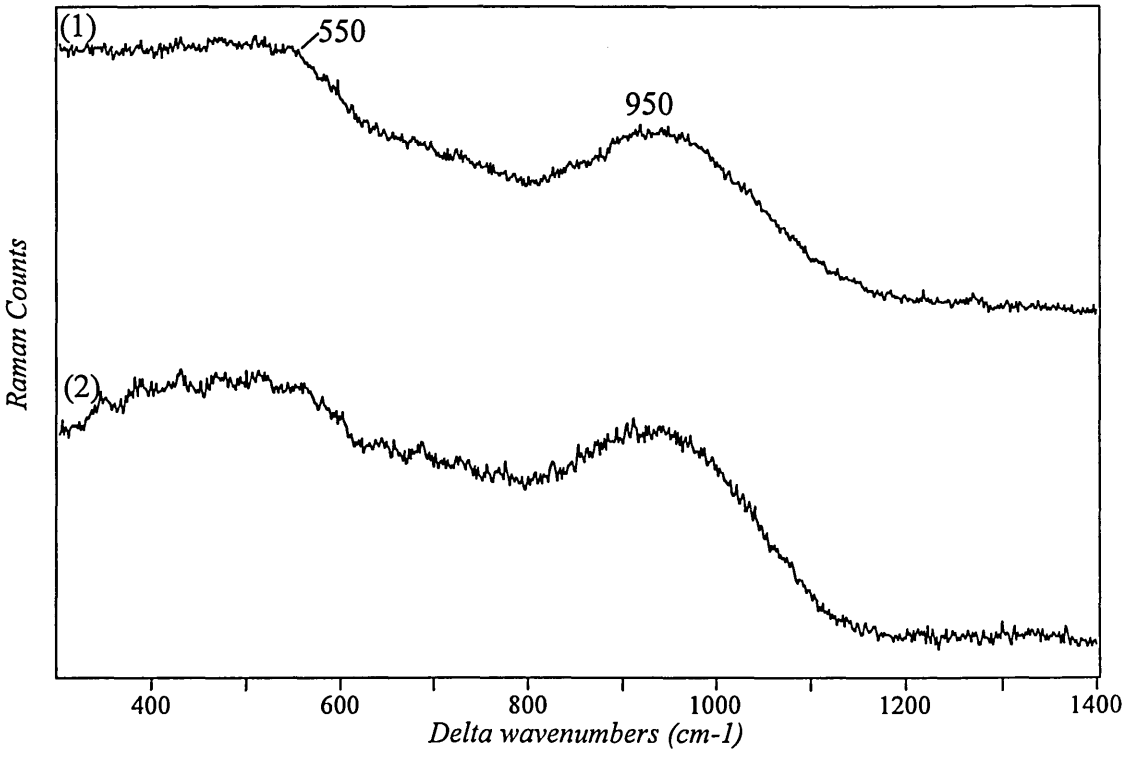

Figure 5.11: Raman spectra of MMVF. (1) mineral wool fibre of 8 µm of diameter, red laser, X 50 objective, $T_{tot} \approx 14$ min; (2) rock wool fibre of 36 µm of diameter, red laser, X 50 objective, $T_{tot} \approx 14$ min.
Cellulose filter subtraction applied on spectra (1) and (2).

The Raman spectrum of the microquartz fibres, in comparison with the spectrum of a quartz slide, shows weak bands (figure 5.12) and only two bands at 490 and 800 cm^{-1} can be clearly observed. The SiO_4 vitreous spectrum is characteristic of a disordered network of SiO_4 completely polymerised by sharing the four oxygen.

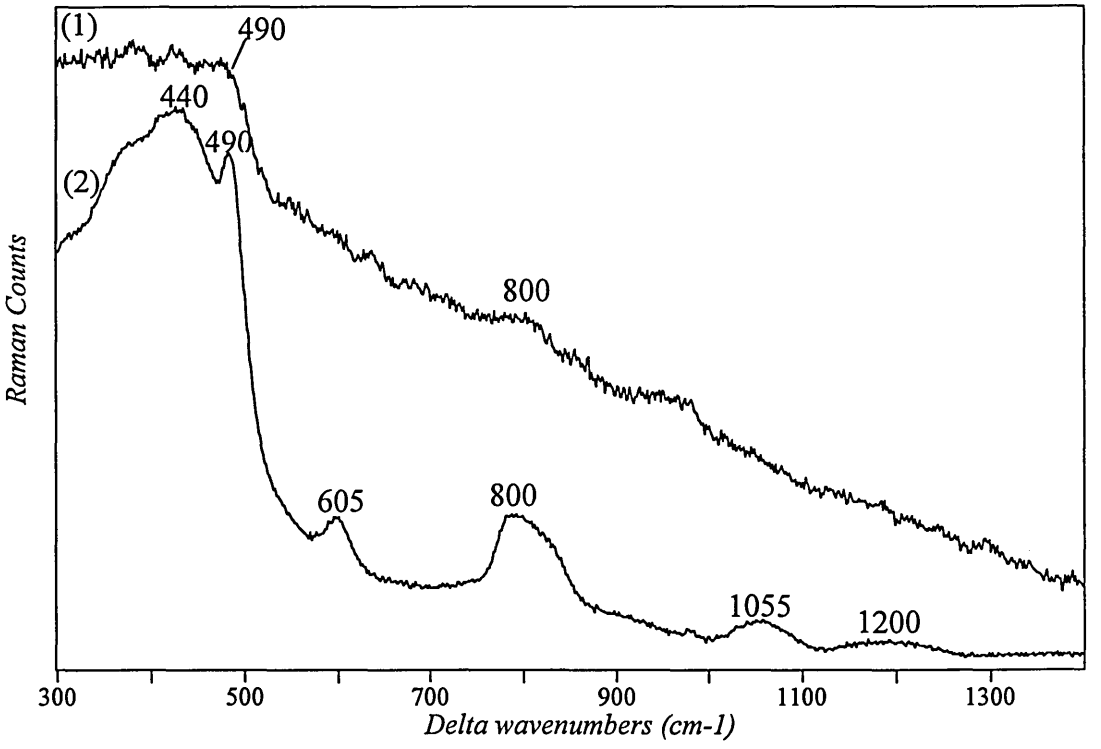

Figure 5.12: Raman spectrum of a quartz fibre in comparison with a quartz slide. (1) microquartz fibre of 10 μm of diameter, red laser, X 50 objective, $T_{tot} \approx 17.4$ min; (2) quartz slide - Cellulose filter subtraction applied on spectrum (1).

Thus, Raman microspectroscopy is a powerful technique allowing the direct identification of pure inorganic fibres on cellulose filters especially asbestos fibres as small as 1 μm of diameter. The next step, now, is the attempted identification of unknown fibres from real "industrial" samples like waste asbestos samples from buildings ceilings, walls or pipe insulation.

5.5. Identification of unknown fibres and other particles on cellulose filter by Raman microspectroscopy.

5.5.1. Introduction.

The fibres and particles under study were:

- either, directly collected on cellulose filters from air monitoring measurements (figure 5.13).

- or, placed on filter from bulk materials using a pump or a rotating drum tester.

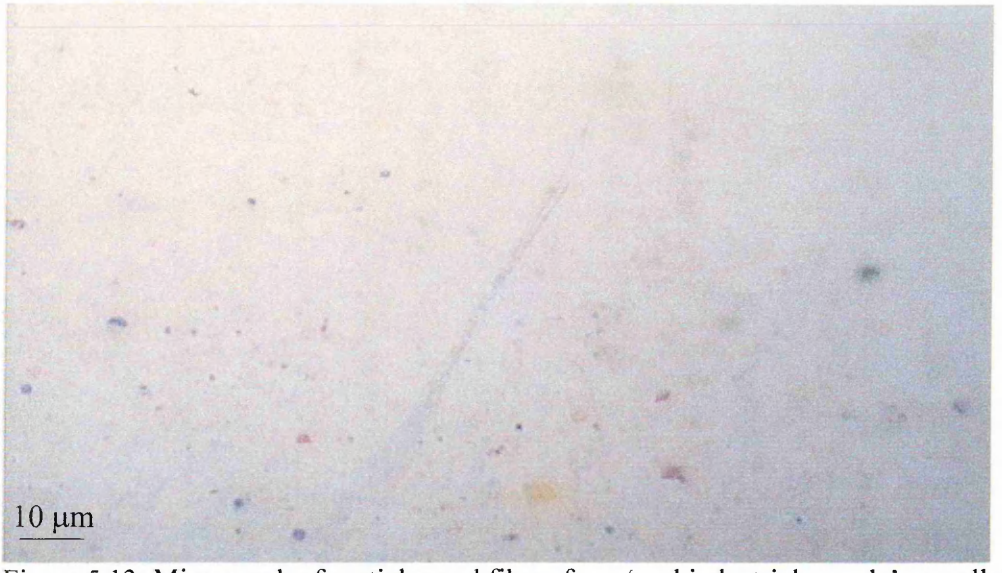

Figure 5.13: Micrograph of particles and fibres from 'real industrial sample' on cellulose filter.

The instrument was set up in microprobe mode using a slit width of 50 µm and a CCD area of 15x576 pixels. The usual process of filter subtraction was applied. In some cases, a baseline correction and a smoothing function were applied in order to improve the quality of the spectra. In the following paragraphs, the spectra of unknown fibres are presented in comparison with reference asbestos. Sometimes, the sample was left under the laser for few minutes in order to diminish the fluorescence background.

5.5.2. Insulation material from the ICI industrial site at Middlesborough.

5.5.2.1. Materials and methods.

Bulk samples from an insulation pipe on the ICI industrial site in Middlesborough were collected for Raman analysis. The insulation was composed of two layers. The first, a yellow material, was apparently mainly a calcium silicate layer. The second, a grey material, was the inner layer containing asbestos fibres. A sample from each layers was then placed on cellulose filters. In this case, a small amount of the bulk samples were placed on a clean glass slide. The particles or fibres were separated using tweezers and collected by directly pressing the filters on top of them.

The laser (633 nm excitation) was focused on particles, bundles and individual fibres using the X 50 and X 100 objectives depending on the size of the mineral investigated.

5.5.2.2. Results.

First layer. Calcium silicate.

From the investigation of several particles, two types of spectra were collected (figure 5.14). The spectra, obtained from yellowish particles, show three bands at 1084 (very strong), 711 (weak) and 280 (medium) cm^{-1}, characteristic of calcium carbonate[17]. These types of particles appear in large majority in the first layer. The spectra, obtained from transparent particles, exhibit a strong band at 460 cm^{-1} as well as weak bands at 350 and 260 cm^{-1} which are typical bands from SiO_2[7,18]. These types of particles are present in only small numbers. However, none of the particles were identified as dicalcium silicate (C_2S)* or tricalcium silicate (C_3S)*[19,20]. Indeed, none of the Raman spectra from the yellow particles show bands from silicates.

The calcium silicate material, was also analysed by infrared spectroscopy using the Golden Gate (attenuated total reflection (ATR) unit) in order to obtain complementary information (figure 5.15). The diffuse reflectance infrared Fourier transform spectra (DRIFTS) of C_3S, silicate calcium hydrate (C-S-H*) and $CaCO_3$ are reported in the literature[21]. The C_3S spectrum shows strong bands (having maxima at 940, 908 and 883 cm^{-1}) in the 800-1200 cm^{-1} region and a sharp band at 813 cm^{-1} characteristic of Si-O stretching vibrations as well as a band at 527 cm^{-1}, assigned to the out of plane bending vibration of SiO_4. The bands below 500 cm^{-1} characteristic of C_3S are assigned to the in plane bending vibrations of SiO_4. In the case of the C-S-H spectrum, the band at 940 cm^{-1} shifts towards high frequency and becomes sharper. The 500 cm^{-1} band disappears and a new band can be observed at 460 cm^{-1}. Moreover, the C-S-H and C_3S spectra show bands in the 1300-1600 cm^{-1} region. These bands are also present in the $CaCO_3$ spectrum with high intensity and are due to antisymmetric stretching vibration of C-O. The $CaCO_3$ spectrum exhibits other bands at 874 cm^{-1} (out of plane bending of C-O) and 712 cm^{-1} (angular bending of O-C-O) as well as two bands at 1795 and 2512 cm^{-1} which are probably overtone and a combination bands respectively.

Our infrared spectrum is very similar to the DRIFTS spectrum of calcium silicate hydrate (C-S-H)* even if no water band can be observed. The bands

* mineralogical notation used in cement chemistry. C=CaO, S=SiO_2 and H=H_2O.

characteristic of $CaCO_3$ are also present, with the exception of the overtone and combination bands.

In the literature, the Raman spectrum of C-S-H shows two broad bands not well separated at about 650 cm^{-1} and a carbonation band at 1090 cm^{-1} when exposed to the air[19,20,22]. Indeed, CO_2 can react with calcium silicate or calcium silicate hydrate resulting in carbonation. In fact, one part of the calcium silicate or calcium hydrate probably adsorbed the CO_2 from the air. It should also be noted that the bands associated with C-S-H are weak due to the poor crystallinity of C-S-H and therefore quartz and $CaCO_3$ analysed from the yellow outer layer may also come from impurities.

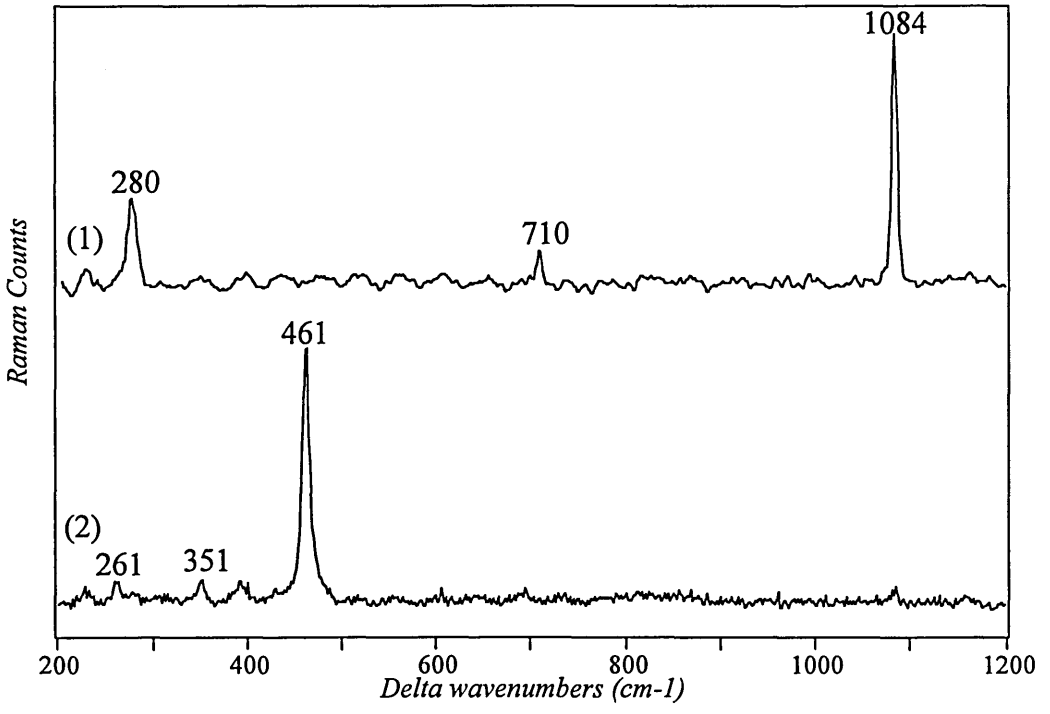

Figure 5.14: Raman spectra of particles from the yellow outer layer. (1) yellow particle, red laser, X 50 objective, $T_{tot} \approx 1.5$ min; (2) transparent particle of 10 µm size, red laser, X 100 objective, Ttot ≈ 6.7 min.
Baseline correction applied on spectra (1) and (2), smoothing function (Savitsky Golay, degree 2, 13 points) applied on spectrum (1).

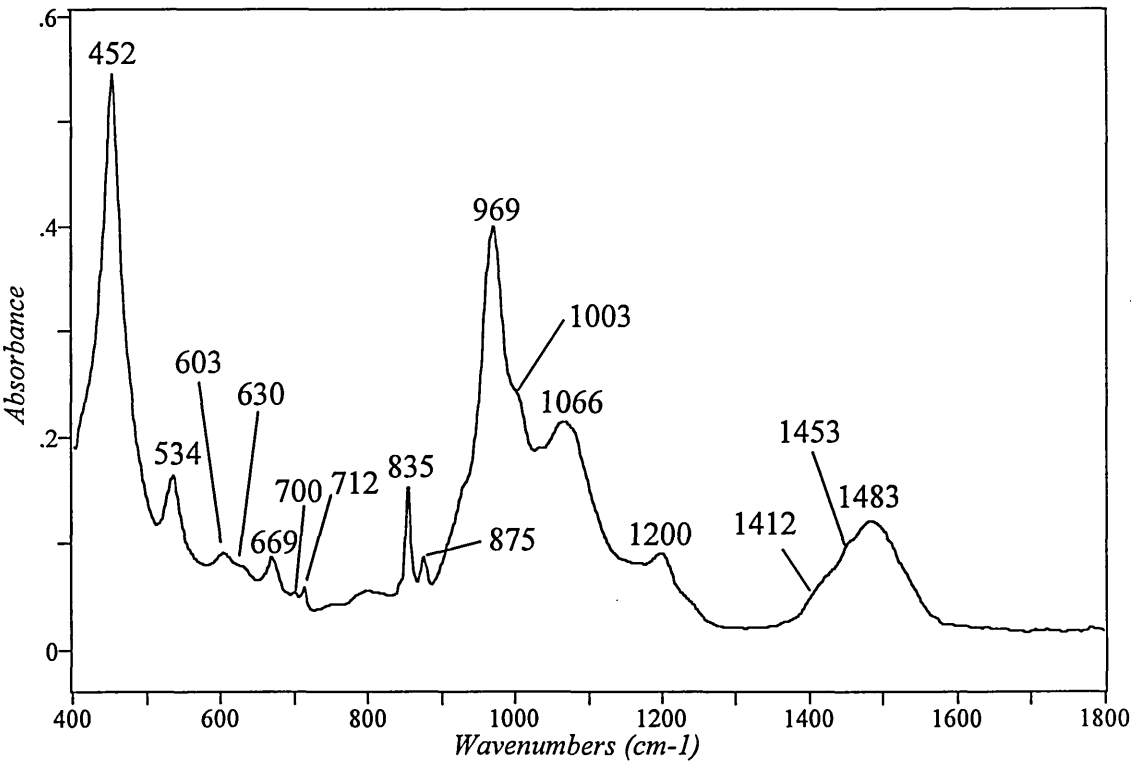

Figure 5.15: Infrared spectrum, from the Golden Gate (ATR unit) of calcium silicate, resolution=4 cm^{-1}, t=128 s.

Second layer. Material containing asbestos.

On the cellulose filter, a large amount of individual as well as bundles of fibres could be observed with the optical microscope. The Raman spectra of individual fibres as small as 2.5 μm in diameter and bundles of fibres of 44 μm in diameter were collected using the X 100 and X 50 objective respectively (figure 5.16). These fibres are identified without any ambiguity as asbestos fibres more specifically amosite fibres, in accordance with the amosite reference spectrum . Indeed, they both, show the characteristic features from amosite which are the strong band at 660 cm^{-1} corresponding to the Si bridging -O-Si stretching vibration as well as other bands at 1020 and 528 cm^{-1}.

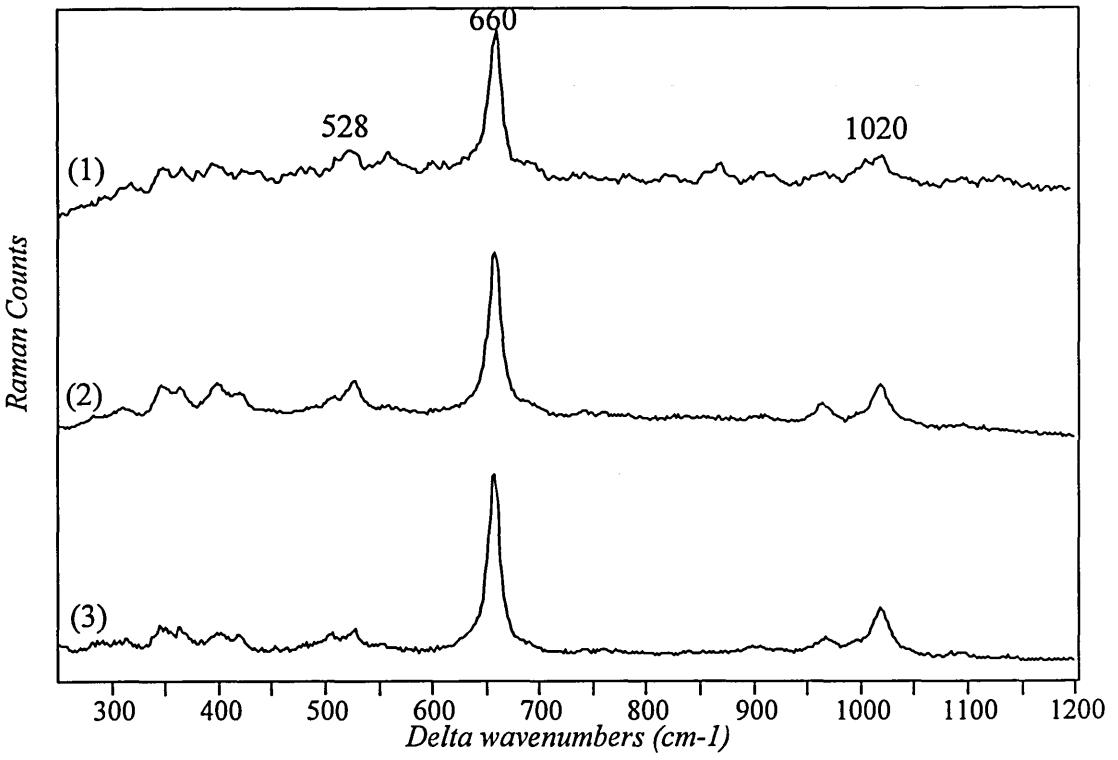

Figure 5.16: Raman spectra of unknown fibres from the grey inner layer in comparison with amosite reference. (1) fibre of 2.5 μm of diameter, red laser, X 100 objective, $T_{tot} \approx 20.2$ min; (2) fibres bundle of 44 μm of diameter, red laser, X 50 objective, $T_{tot} \approx 4.5$ min; (3) amosite reference.
Cellulose filter subtraction, applied on spectra (1) and (2), smoothing function (Savitsky Golay, degree 2, 9 points) applied on spectrum (1).

It should be noted that the spectrum of the bundle of fibres using the X 50 objective is a very high quality spectrum. The acquisition time was not very long. In fact, such quality can be explained by:

-firstly, the number of scattered photons, which is collected, is greater using the X 50 objective than the X 100.

- secondly, the number of scattered photons, which is produced from a large sample is greater than from a very small (few micrometers) sample.

- thirdly, the amount of other materials considered to be "impurities", on the fibres may be small.

Indeed, the bands are very well resolved and those, having a weak intensity, are still observed.

Spectra of particles associated with the material containing asbestos were also collected (figure 5.17), using the X 50 objective since their size is larger than 5 μm.

Calcium carbonate (spectrum (1) figure 5.17) was again identified.

Gypsum ($CaSO_4\ 2H_20$) (spectrum (2), figure 5.17) was found showing a Raman spectrum with a very strong band at 1006 cm^{-1} characteristic of the symmetric stretching vibration of SO_4^{2-} as well as other medium intensity bands at 1133, 670, 616, 494 and 412 cm^{-1}[23]. Indeed, gypsum is very common in insulation materials containing asbestos.

Phosphate, probably hydroxyapatite ($Ca_5OH(PO_4)_3$) (spectrum (3), figure 5.17) was also present, since the Raman spectrum shows a strong band at 962 cm^{-1} characteristic of the symmetric stretching vibration of the phosphate group[24,25].

Finally, aluminium nitride (spectrum (4) figure 5.17) was identified, since the spectrum of the hot pressed compound exhibits strong bands at 659, 614 and 911 cm^{-1}[26].

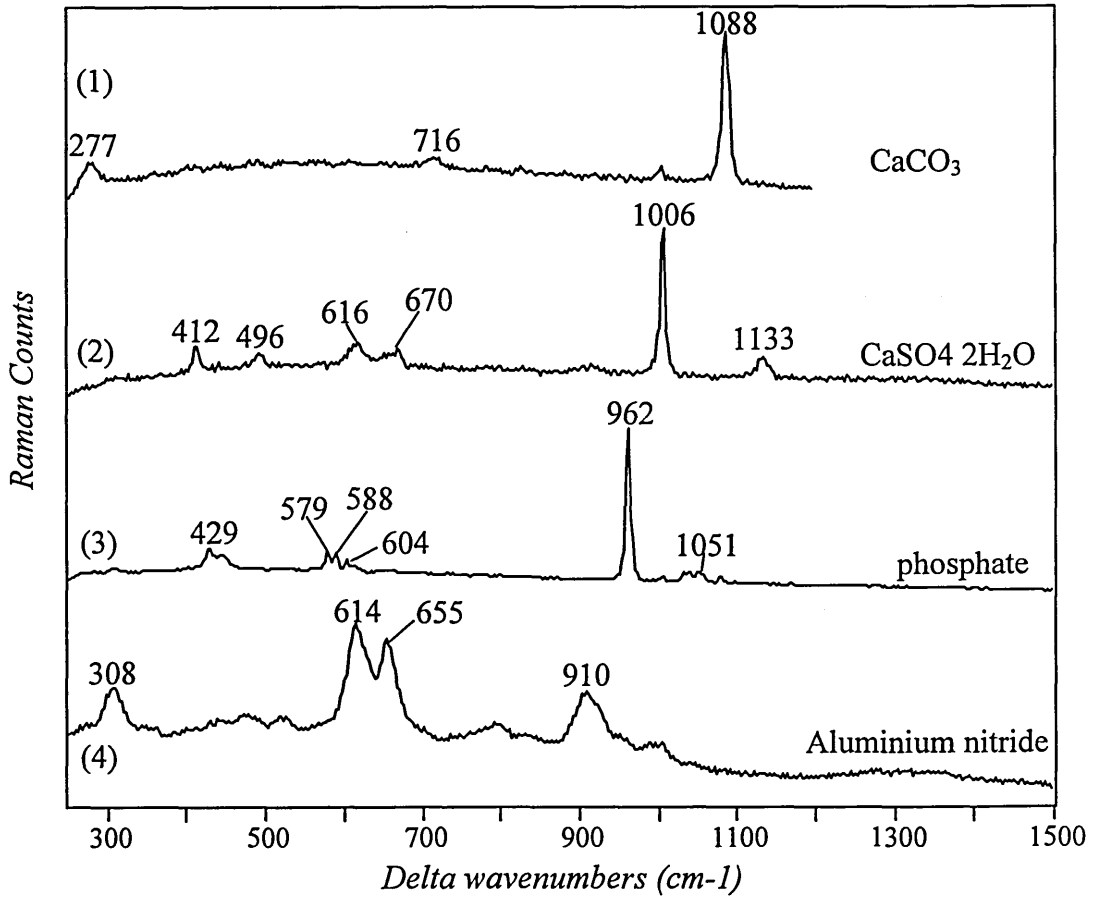

Figure 5.17: Raman spectra of unknown particles from the grey inner layer. (1) brown particle, red laser, X 20 objective, $T_{tot} \approx 27$ s; (2) transparent particle of 7 μm size, red laser, X 50 objective, $T_{tot} \approx 32$ s; (3) transparent particle of 16 μm size, red laser, X 50 objective, $T_{tot} \approx 97$ s; (4) transparent particle of 80x40 μm size, red laser, X 50 objective, $T_{tot} \approx 5.4$ min. Cellulose filter subtraction applied on spectra (1) to (4).

5.5.3. Other unknown fibres on cellulose filters identified as amosite.

5.5.3.1. Materials and methods.

Other samples on cellulose filters from asbestos containing materials were provided by the Health and Safety Laboratory. In this case, the fibres were collected on filters from bulk samples using a rotating drum.

The red laser was focused on individual fibres using the X 50 objective.

5.5.3.2. Results.

The spectra of unknown fibres as small as 1.5 and 1 μm show the bands characteristic of amosite at 660, 1020 and 530 cm^{-1} (figure 5.18).

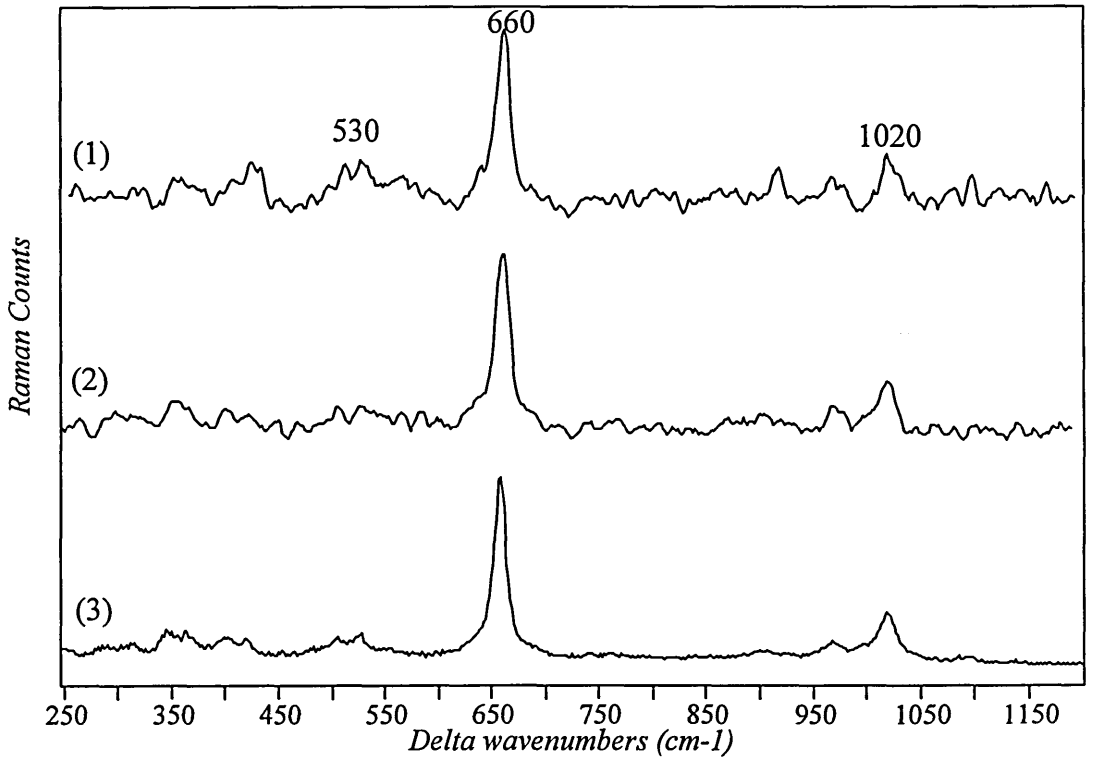

Figure 5.18: Raman spectra of unknown fibres in comparison with amosite reference. (1) fibre of 1.5 μm of diameter, red laser, X 100 objective, $T_{tot} \approx 65.2$ min; (2) fibre of 1 μm of diameter, red laser, X 100 objective, $T_{tot} \approx 44.9$ min; (3) amosite reference.
Cellulose filter subtraction, baseline correction applied on spectra (1) and (2), smoothing function (Savitsky Golay, degree 2, 11 and 9 points) applied on spectra (1) and (2).

5.5.4. Old Lucas Building. Birmingham.

5.5.4.1. Materials and methods.

This building possessed a variety of asbestos containing materials which were removed before demolition. The sample on cellulose filter from air monitoring

measurements was provided by the Health and Safety Laboratory. It came from airborne dust sampled near "Limpet" sprayed asbestos on steel posts. The laser was focused on individual fibres using the 633 nm excitation and X 100 objective.

5.5.4.2. Results.

The Raman spectrum of a fibre as small as 1-1.5 μm, clearly shows strong bands at 970, 575, 540 and 375 cm^{-1} as well as other medium bands at 665, 890 and 1085 cm^{-1} (figure 5.19). These bands are unambiguously attributed to crocidolite spectrum. Crocidolite are probably the easiest asbestos fibres to identify due to a spectrum exhibiting a large number of intense bands.

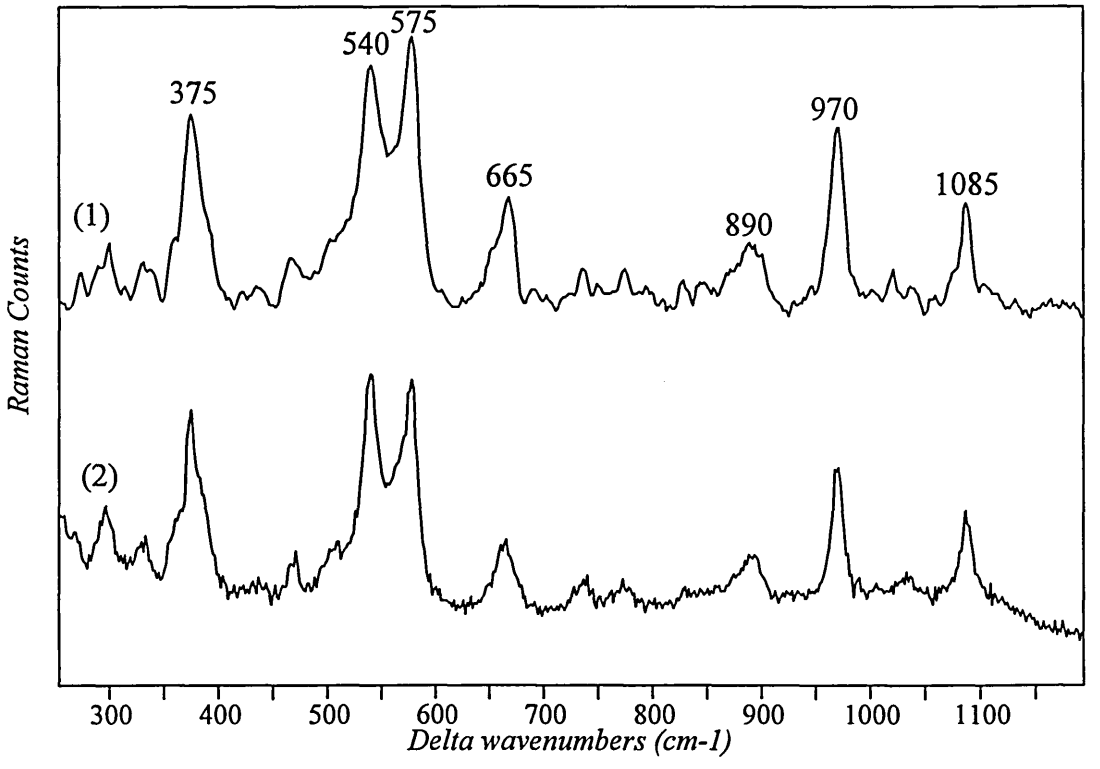

Figure 5.19: Raman spectrum of a unknown fibre in comparison with crocidolite reference. (1) fibre of 1-1.5 μm of diameter, red laser, X 100 objective, $T_{tot} \approx 19.6$ min; (2) crocidolite reference.
Cellulose filter subtraction, baseline correction and smoothing function (Savitsky Golay, degree 2, 11 points) applied on spectrum (1).

5.5.5. Asbestos containing materials from a building in Bristol.

5.5.5.1. Materials and methods.

An insulation material containing asbestos from a building in Bristol was provided by Asbestostrip Innovations for Raman analysis. The fibres and particles were placed on a cellulose filter by breaking and splitting up small amount of materials with tweezers on top of a filter connected with a weak pump. A near infrared laser was focused on individual fibres using the X 100 objective.

5.5.5.2. Results.

The spectra of unknown fibres having a diameter of 1.5 and 4 μm show strong bands at 690 cm^{-1} assigned to the Si bridging-O-Si stretching vibration and at 390 cm^{-1} corresponding to a metal-oxygen vibration (figure 5.20). These bands are characteristic of chrysotile spectra. Weaker bands are also observed in the spectrum of the fibre having the largest diameter. A band at 1120 cm^{-1}, probably from the matrix of the material, can be observed.

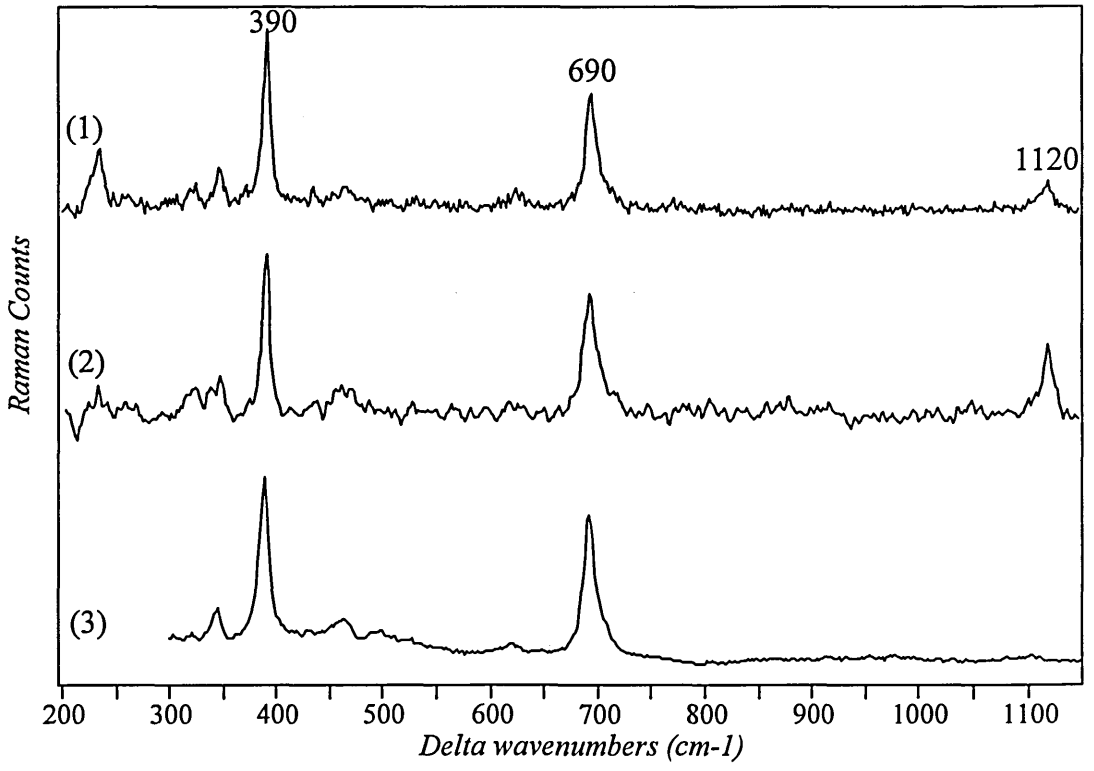

Figure 5.20: Raman spectra of unknown fibres in comparison with chrysotile reference. (1) fibre of 4 μm of diameter, near infrared laser, X 100 objective, $T_{tot} \approx 35.9$ min; (2) fibre of 1.5 μm of diameter, near infrared laser, X 100 objective, $T_{tot} \approx 44.9$ min; (3) chrysotile reference. Cellulose filter subtraction, baseline correction applied on spectra (1) and (2), smoothing function (Savitsky Golay, degree 2, 11 points) applied on spectrum (2).

5.5.6. Asbestos fibres associated with African clay crafts manufacture.

5.5.6.1. Materials and methods.

A whitish light fibrous material, suspected of being asbestos, is used in pot making by local crafts people in and around a village in Botswana. This fibrous material is removed from the ground, pounded in a mortar and then winnowed. The material is then mixed with a reddish brown loamy soil and worked in by hand to produce a clay-like material, which is formed into pots, dried and fired. The finished pots are sold to tourists. These processes are carried out in the open, in an area also used for domestic cooking, with children playing close by. No precautions are taken to avoid breathing in the fibres, apart from occasionally covering the nose and mouth with a headsquare.

The fibrous material was analysed by polarised light microscopy (PLM), scanning electron microscopy (SEM), energy dispersive X-ray analysis (EDX) and infrared and Raman microspectroscopy.

For PLM analysis, the fibres were placed on a glass slide, immersed in a liquid of known refractive index (1.605) and covered with a glass slip.

For SEM analysis, the fibres were mounted on stubs with double-sided adhesive tape and coated with gold. They were examined using a Leica S430 SEM, 10 Kv accelerating voltage and 10 picoamps probe current.

The EDX analysis was carried out on uncoated fibres at 20 Kv accelerating voltage and 600 picoamps probe current.

For infrared analysis, a small bundle of fibres was crushed between diamond windows in a compression cell. The spectrum was obtained using a Nicolet 5 DXC FTIR spectrometer coupled with a Spectra-Tech IR PLAN research grade microscope in transmission mode. The area of interest was defined using "redundant apertures" above and below the sample.

For Raman analysis, the white fibrous material was placed on a cellulose filter using a pump. A X 100 and X 50 objectives were used to collect the Raman spectra of individual and bundles of fibres. The Raman spectra were recorded with a 632.8 nm excitation laser.

5.5.6.2. Results.

The analysis by polarised light microscopy showed that the white fibre bundles

are either tremolite or anthophyllite asbestos. In mass, the white colour suggests that the fibres are tremolite because South African commercially mined anthophyllite is yellowish in colour and slightly pleochroic when viewed under polarised light.

The infrared spectrum showed intense absorption bands at approximately 1100 cm^{-1} and 800 cm^{-1} and is indicative of Si-O stretching modes.

The SEM micrograph showed straight fibres and the EDX analysis suggested that the fibres were either fibrous actinolite or fibrous tremolite.

The Raman spectra collected on an individual fibre of 2 μm in diameter and on a bundle of fibres (figure 5.21) show an intense band at 672 cm^{-1} (corresponding to the Si bridging-O-Si stretching mode) and less intense bands at 1057, 1027, 928, 410, 391, and 368 cm^{-1}. These are characteristic of asbestos tremolite fibres. However, the spectrum of actinolite reported in the literature is very similar to the spectrum of tremolite[6]. Nevertheless, from Raman and PLM analysis, the white fibrous material is identify unambiguously as tremolite fibres.

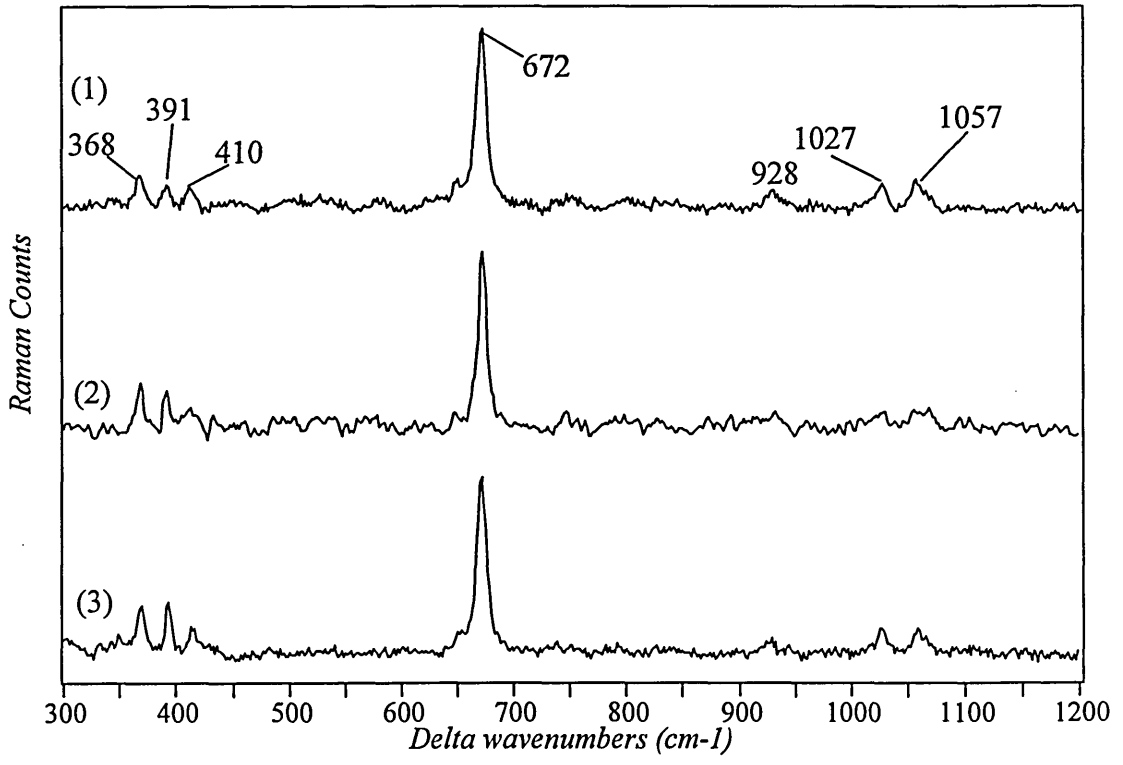

Figure 5.21: Raman spectra of unknown fibres in comparison with tremolite reference. (1) bundle of fibres, red laser, X 50 objective, $T_{tot} \approx 8.8$ min; (2) fibre of 2.5 μm of diameter, red laser, X 100 objective, $T_{tot} \approx 20$ min; (3) tremolite reference.
Cellulose filter subtraction, baseline correction applied on spectra (1) and (2), smoothing function (Savitsky Golay, degree 2, 9 points) applied on spectrum (2).

5.5.7. Other minerals on cellulose filters.

5.5.7.1. Materials and method.

Since other minerals or inorganic compounds are associated with asbestos in insulation materials, not only fibres but also particles are going to be present on cellulose filters. These particles can have sizes in the 5-100 μm range. A red laser was focused on different particles using the X 50 or X 100 objective. The accumulation time was much shorter than in the case of asbestos. In some cases, the laser power was reduced using an attenuation filter in order to avoid the thermal degradation of the particles.

5.5.7.2. Results.

Sulphate and carbonate are common particles associated with insulation materials and were successfully identified previously (figure 5.17). Other inorganic particles a few μm in size (on cellulose filters) such as oxides, are also easily identify using Raman microspectroscopy since their spectra display sharp distinctive bands (figure 5.22)[27,28].

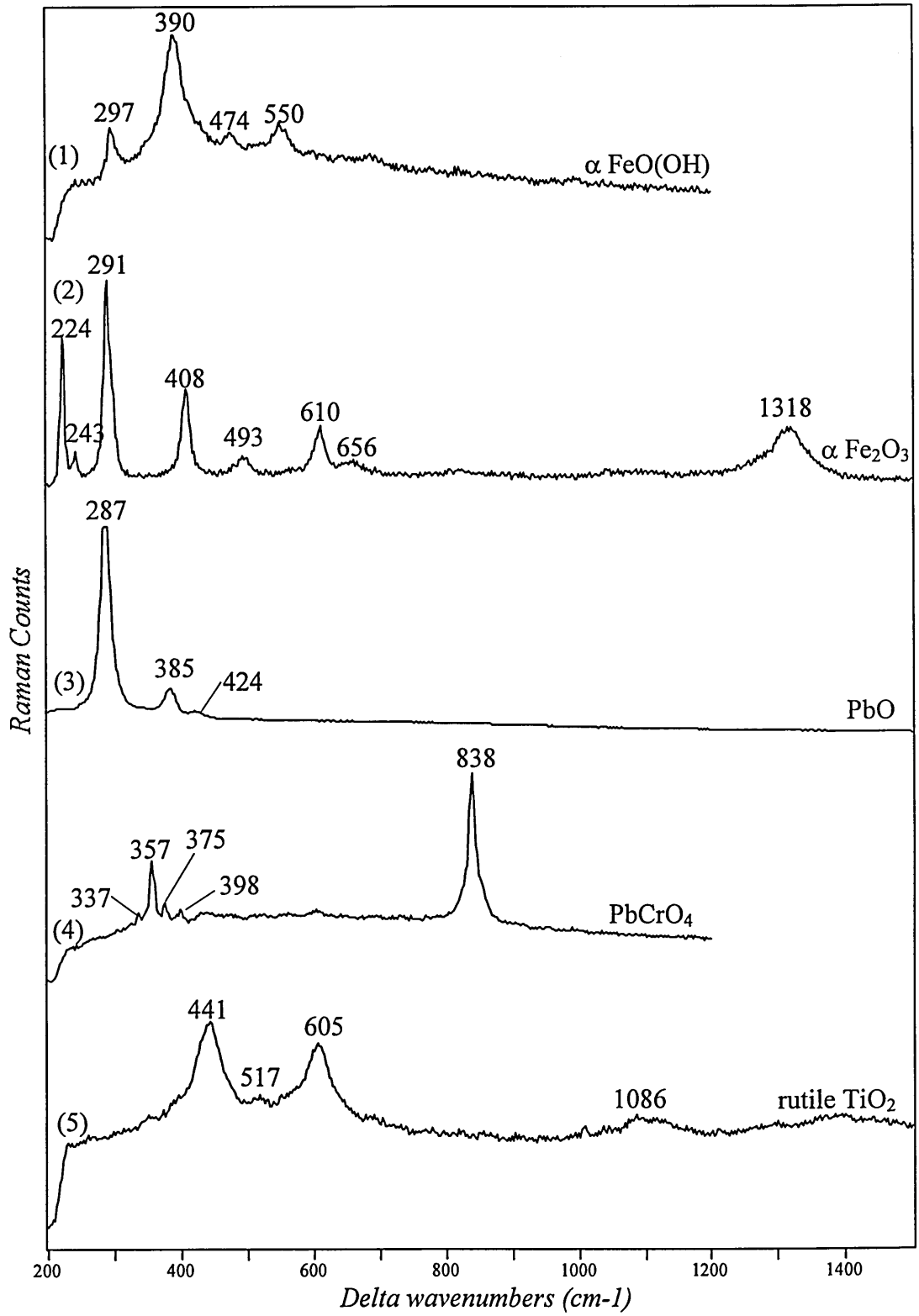

Figure 5.22: Raman spectra of unknown particles. (1) red particle of 7x5 μm size, red laser: 25 % attenuation, X 100 objective, $T_{tot} \approx 270$ s; (2) black-white particle of 15x3 μm size, red laser: 25 % attenuation, X 100 objective, $T_{tot} \approx 32$ s; (3) yellow particle of 14 μm size, red laser: 25 % attenuation, X 50 objective, $T_{tot} \approx 42$ s; (4) yellow particle of 5 μm size, red laser: 25 % attenuation, X 100 objective, $T_{tot} \approx 170$ s; (5) white particle of 4 μm size, red laser, X 100 objective, $T_{tot} \approx 336$ s.

5.6. Raman spectra of coal and diesel particles.

5.6.1. Introduction.

In coal mines, the use of diesel oil powered equipment produces diesel exhaust particles. Coal and diesel are, both, carbonaceous material. However, diesel particles are suspected to be carcinogenic. It is therefore necessary to monitor the concentration of diesel particles in coal mines. But, a technique such as scanning electron microscopy coupled with EDX is not able to distinguish diesel particles from coal particles.

Diesel oil exhaust is chemically complex and contains hundred of different particles. However, its main component is diesel particulate matter (DPM) which is composed of organic and elemental carbon, adsorbed and condensed hydrocarbon and sulphate[29]. Polycyclic aromatic hydrocarbons (PAHs) are associated with DPM and are also suspected to have a role in cancer initiation. However, they are present in low concentration and are not unique to diesel exhaust. DPM are formed during combustion and diesel exhaust particles are very small between 0.001 and 0.08 μm. These particles accumulate by condensation or coagulation to form particle of 0.2 μm in diameter with 90 % of the particles less than 1.0 μm in size[29]. In contrast, coal particles have size typically greater than 1 μm in diameter.

At present, two methods are used to determine the concentration of diesel exhaust particles in coal mines[29]. The first method is gravimetric analysis, which is based on size selection and determines the mass concentration for different size fractions. The other method, the elemental carbon analysis, is more sensitive and is a temperature based thermal optical method. It measures only the concentration of elemental carbon which is 40 to 60 % of DPM mass.

Scientists are looking for a more sensitive and reliable method. Since Raman spectroscopy is an easy tool to characterise the structure of carbon such as graphite, diamond and amorphous carbon[30], it was used to analyse coal and diesel particles. This study was focused on the carbon spectra.

5.6.2. Materials and methods.

Pure coal particles were deposited on quartz filters in the laboratory conditions while diesel particles were directly collected from a car also on a quartz filter. The spectra were obtained using the X 50 objective and the 633 nm excitation. The power of the laser was attenuated down to 10 % in order to avoid the degradation by heat of the particles. Therefore, the laser power at the sample was about 0.5 mW. The spectra were collected from particles having a size distribution between 10 and 45 μm.

5.6.3. Results.

The carbon spectra from coal and diesel particles were analysed and compared. The spectrum of the filter gives weak bands only at low frequency which does not interfere with the carbon spectra. Therefore, it was not necessary to subtract the filter from the original spectra.

A baseline correction using a polynomial function was applied on coal and diesel spectra before curve fitting in the 800-2100 cm^{-1} region (figure 5.23a and 5.23d)[31-34]. Four Lorentzian bands were introduced, two bands related to carbon, a shoulder at about 1200 cm^{-1} and a band at about 1505 cm^{-1} necessary to obtain a good fit.

The Raman spectra of diesel and coal particles are similar to the Raman spectra of some types of disordered carbon (figure 5.23c and 5.23.d). They show a narrow band at about 1595 cm^{-1} and a broad band at about 1340 cm^{-1}. The band at 1595 cm^{-1} is related to the 1580 cm^{-1} band of graphite, called G band, which is attributed to C-C in plane stretching vibration. With the increase of disorder in crystalline graphite, the 1580 cm^{-1} band broadens and moves to higher frequency and a new band appears at 1350 cm^{-1}. The band at 1340 cm^{-1} is related to the band at 1350 cm^{-1} band, called D band, which is attributed to defects present in structural units and disorder. This band is induced by structural defects. Moreover, the relative intensity of the D to G bands is correlated with a structural correlation length (L_a) which corresponds to the size of well-ordered domains (i.e. the crystallite size).

The position and width at half peak height of the G and D bands were measured for ten particles of coal and diesel particles (figure 5.24.a to 5.25.d). The ratio of the intensity of the 1340 cm^{-1} band to the intensity of the 1595 cm^{-1} band was also studied (figure 5.25).

Figure 5.2.3.a

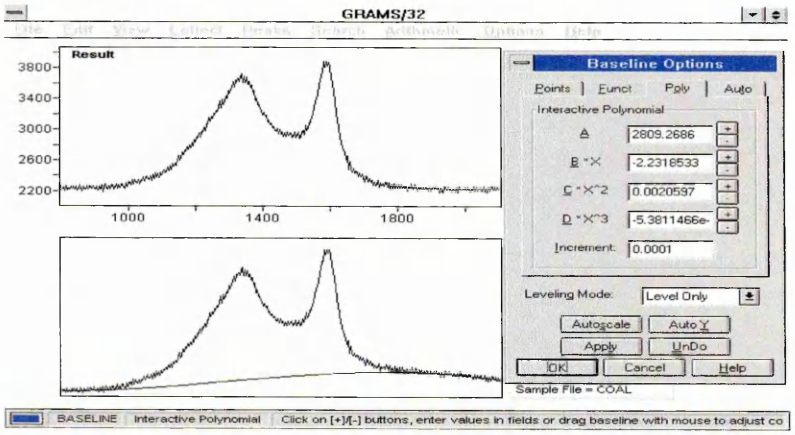

Figure 5.2.3.b

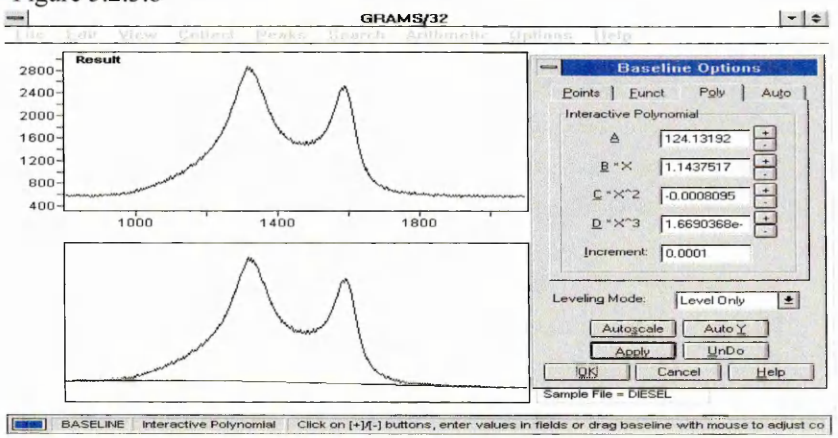

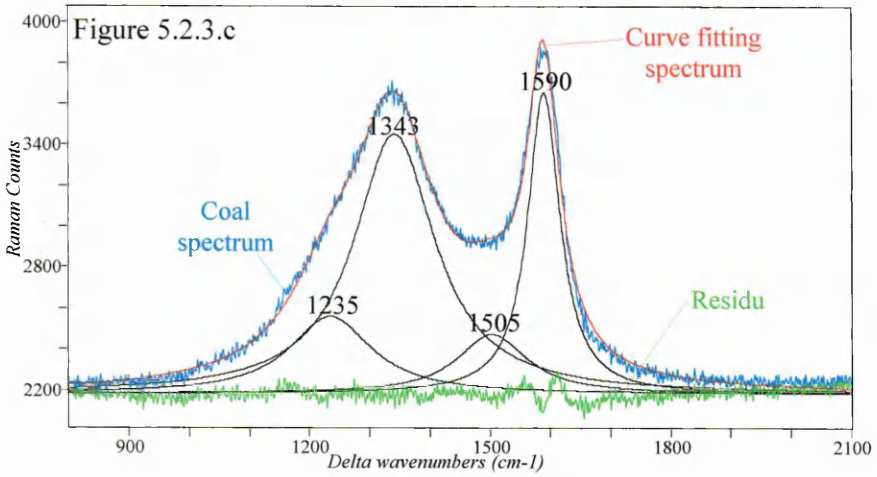

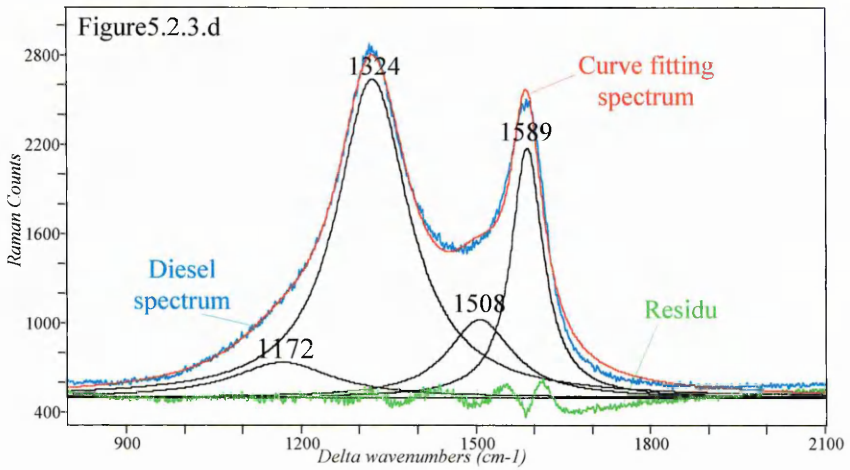

Figures 5.2.3.a. and 5.2.3.b. Baseline correction on coal and diesel spectra using a polynomial function.
Figures 5.2.3.c and 5.2.3.d. Curve fitting, in the 800-2000 cm^{-1} region, with four Lorentzian bands on coal and diesel spectra.
Figure 5.2.3.c. Raman spectrum of a coal particle (10 x 40 µm size), red laser: 10 % attenuation, X 50 objective, T tot ≈ 86 s. Figure 5.2.3.d. Raman spectrum of a diesel particle (10 x 40 µm size), red laser: 10 % attenuation, X 50 objective, T tot ≈ 5.7 min.

Figure 5.24.a.

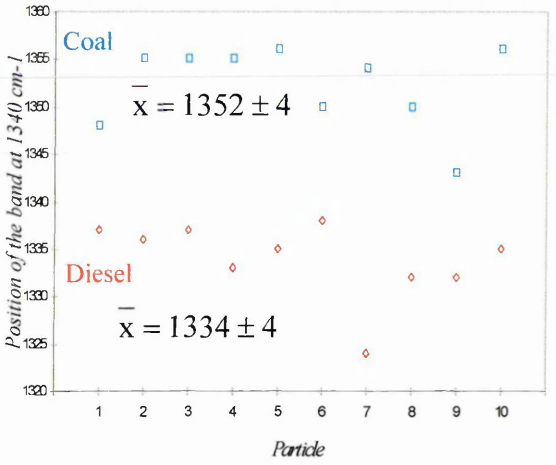

Figure 5.24.b

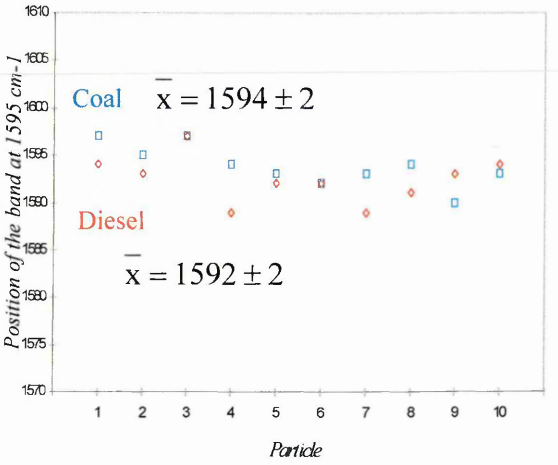

Figure 5.24.c.

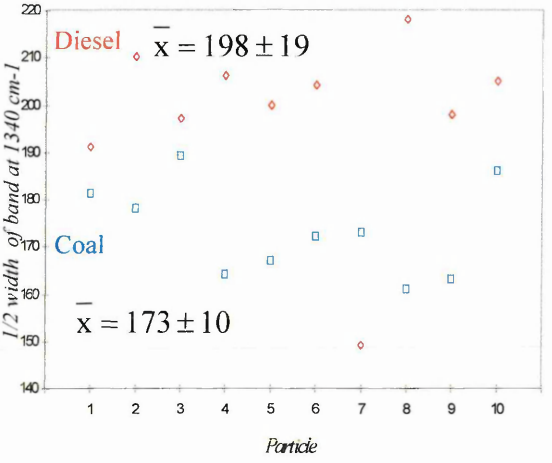

Figure 5.24.d.

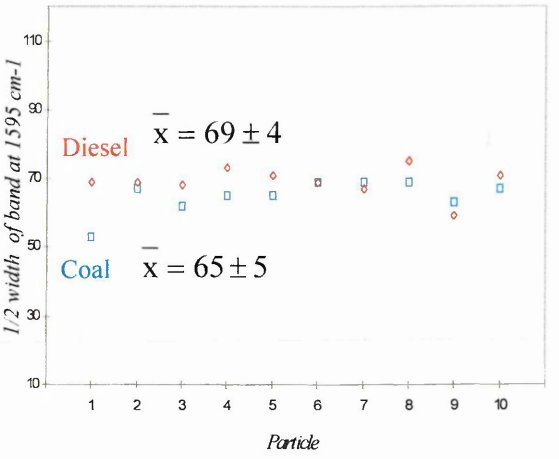

Figures 5.24.a to 5.24.d: Position of the bands at ~ 1340 and 1595 cm^{-1} (5.24.a and 5.24.b); width at half height of the bands at ~ 1340 and 1595 cm^{-1} (5.24.c and 5.24.d) for ten different coals and diesel particles.

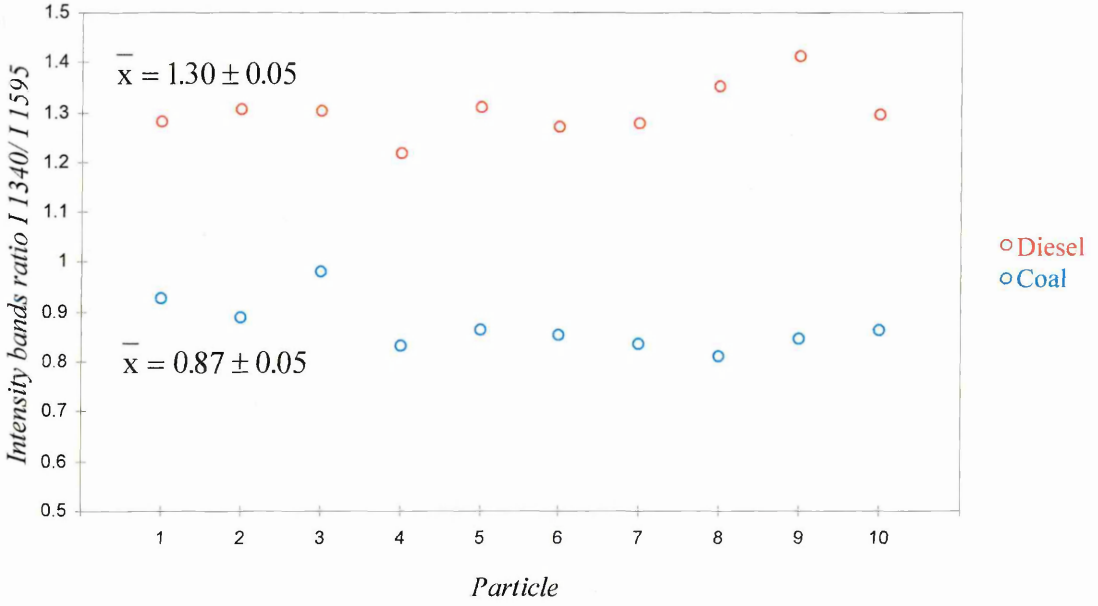

Figure 5.25: Ratio of the intensity of the 1340 cm^{-1} band to the intensity of the 1595 cm^{-1} band for ten different coal and diesel particles.

The G band at 1595 cm^{-1} appears to be relatively constant. Indeed, the difference in band position and width at half height between coal and diesel particles is relatively small, 2 cm^{-1} and 4 cm^{-1} respectively. These differences are more significant in the case of the D band at 1340 cm^{-1} (18 cm^{-1} and 25 cm^{-1} respectively). This is due to the introduction of a shoulder band at 1235 cm^{-1} which seems to be more important and occurs at higher frequency in the coal than diesel spectra. The D and G bands follow the same general tendency which are a higher frequency and a lower half width for coal than diesel bands. The intensity ratio of the D to the G band for coal and diesel is significantly different with mean values of 0.87 ± 0.05 and 1.30 ± 0.05 respectively. This intensity ratio difference between DPM and coal particles was previously observed by L.Suhartono et al[35].

We know, that the relative intensity of D to G bands varies as the inverse of the crystallite size and the Raman bands broaden as the size of well ordered domains decreases. Therefore, the carbon from diesel exhaust particles seem to show more disorder in the structure than coal particles which probably have larger crystallite size. Another marker for disorder is the increase in frequency of the G band. However, in our case, the frequency difference between coal and diesel is rather small and might not be significant enough to discriminate the particles.

There is a difference in the carbon Raman spectra of diesel and coal particles, especially from the intensity ratio of the D to G bands. The carbon structure of diesel exhaust particles seem to be more disordered than coal particles. The next step would be to investigate samples from different sources as well as mixed coal/diesel samples.

5.7. Gunshot residues.

5.7.1. Introduction.

In criminal cases, the identification of the gun and ammunition is very important. The investigation of the particles, left on the victim and weapon, after the gunshot gives information about the distance and direction of the shooting as well as the distribution of the gunshot residues. Such particles are usually identified by X-ray fluorescence (XRF), optical emission spectroscopy (OES), atomic absorption spectroscopy (AAS), neutron activation analysis and scanning electron microscopy (SEM) coupled with

energy disperse X-ray analysis (EDX)[36]. These techniques allow the determination of the shooting distance. The distribution of gunshot residues can be performed using Zeeman atomic absorption spectroscopy (DZ-AAS)[37]. These are, however, elemental techniques and do not give any information about the associated (molecular) anions present.

The ammunition is a cartridge which basically consists of the bullet, the case, the propellants and the primer. The primer is a mixture of explosives used to ignite the propellants. The propellants, which are in general compounds such as nitro-glycerine or nitro-cellulose, combust and produce a gas with high pressure. This high pressure drives the bullet out of the barrel. When a gun is fired, a complex cloud of chemicals leaves the barrel. These compounds comprise incompletely burned propellant particles, metallic components of the bullet and characteristic particles of elements originating from the primer, the bullet, the propellant and the propellant additives.

The gunshot residues have sizes from about 1 to more than 100 μm. The objective is the identification of particles of gunshot residues from firings on paper substrates in order to deduce the oxidation state(s) of the species involved and provide further information on the nature of the anions present.

5.7.2. Materials and Methods.

The gunshot residues came from a Heckler & Koch pistol of 9 mm calibre along with GECO ammunition (Luger, calibre 9 mm). The firing distances on paper substrates were 10, 20 or 30 centimetres. The main primer components, for the gunshot examined in this work, are: $C_6H_3N_3OPb$, $Ba(NO_3)_2$ and Sb_2S_3. During the firing process, the temperature reaches 2000°C-4000°C and the following compounds may be expected in the gunshot residues: BaO, PbO or PbO_2, Sb_2O_3 or Sb_2O_4. Compounds of the metals which comprise the bullet and barrel of the gun such as copper, zinc, iron and aluminium may be also expected.

The paper substrates, holding the gunshot residues, were cut into small strips in order to allow the radial distribution from the centre to be measured (figure 5.26). The strips were flattened before analysis and placed on quartz slides.

The reference materials were obtained from Aldrich (PbO, 99%) and from stocks held in the Materials Research Institute or division of chemistry at Sheffield Hallam University ($BaCO_3$ and $BaSO_4$).

The Raman instrument was set up with a slit open to 50 μm and a CCD area of 15 x 576 pixels. The Raman spectra were recorded with a 632.8 nm excitation laser. X 100 and X 50 objectives were used to collect the Raman spectra of individual particles.

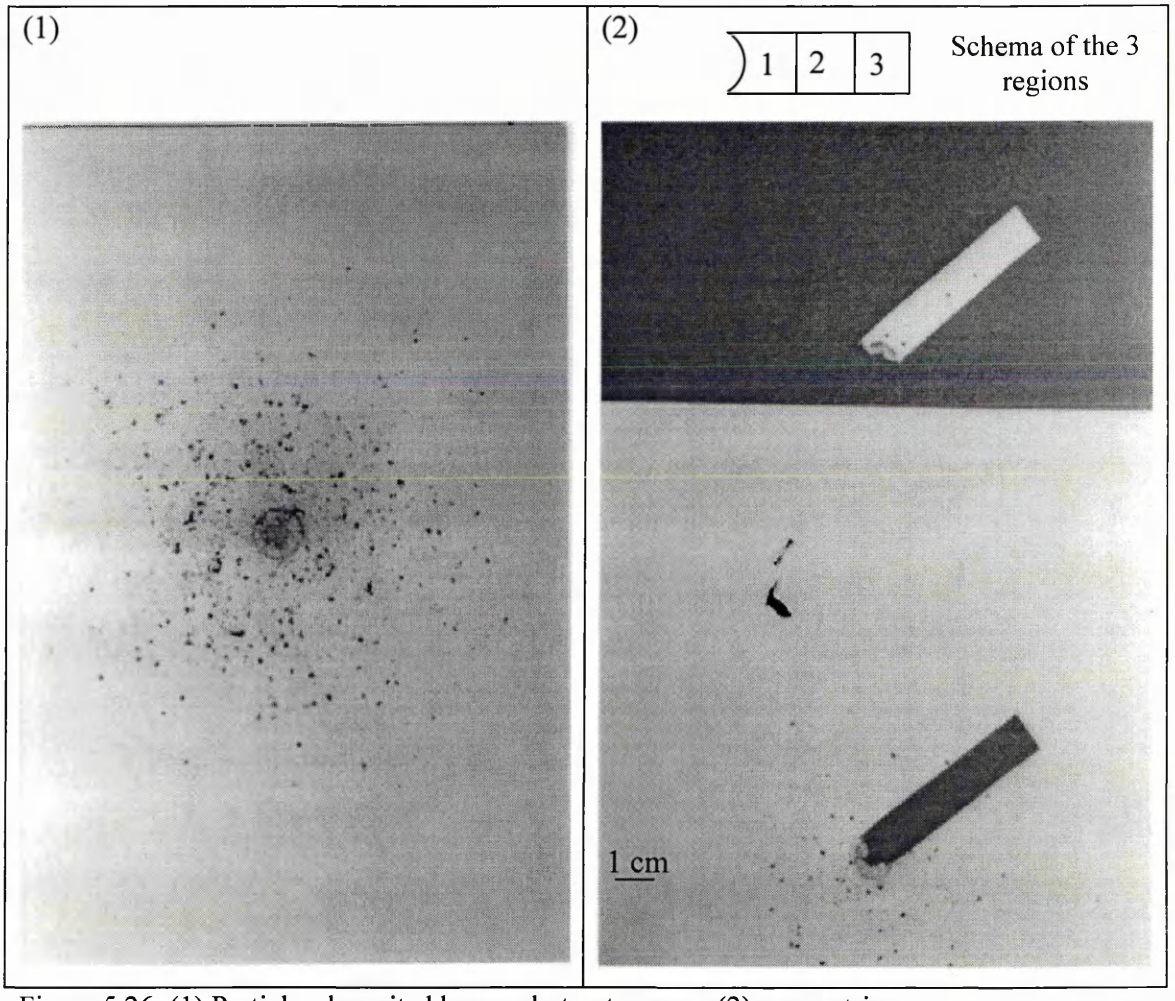

Figure 5.26: (1) Particles deposited by gunshot onto paper; (2) paper strip.

5.7.3. Results.

The Raman bands from the paper substrate in the spectra of gunshot residues were weak and easily removed by spectral subtraction. The Raman spectrum of the paper substrate alone is given in figure 5.27.

Figure 5.27: Raman spectrum of paper substrate, red laser.

Many particles found among the gunshot residues were composed of carbon (figure 5.28). The spectrum, in figure 5.28, shows a first order band at 1575 cm^{-1} and second order bands (from 2350 to 3350 cm^{-1}) characteristic of pure carbon graphite as well as a band at 1366 cm^{-1} due to the introduction of disorder in graphite[38]. It probably comes from organic materials combusted at high temperature.

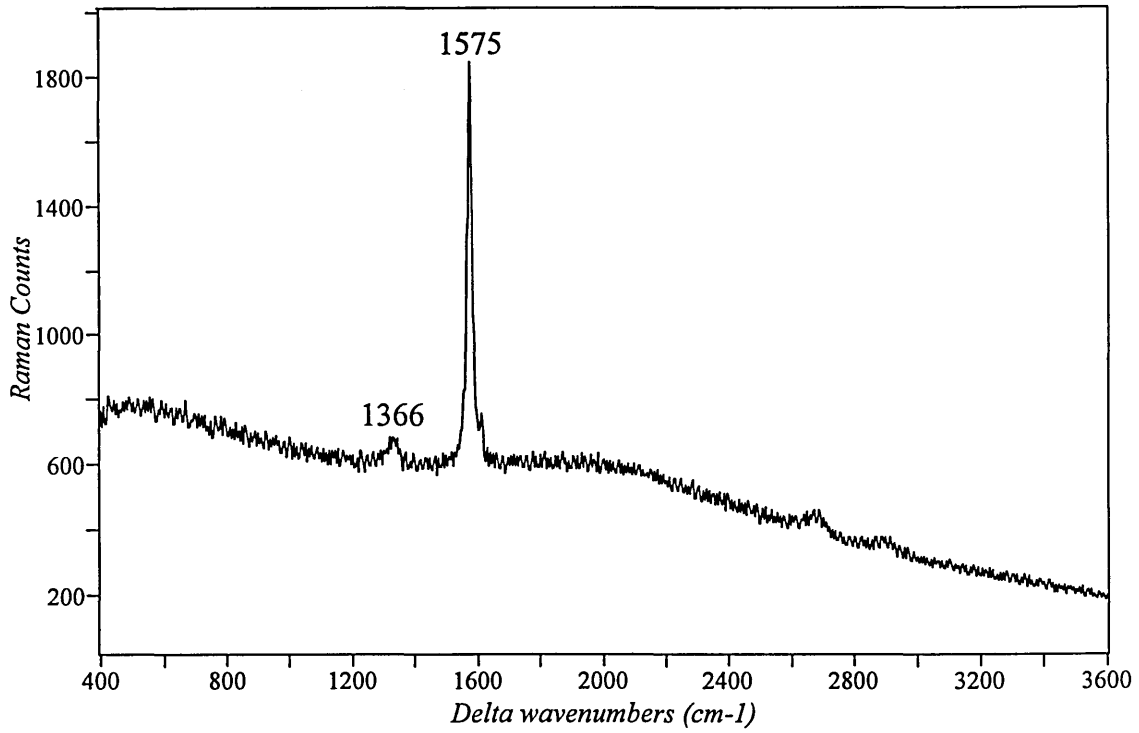

Figure 5.28: Raman spectrum of a particle of 8 μm size, red laser, X 100 objective, $T_{tot} \approx 22.7$ min.

The particles were analysed in three regions called 1, 2 and 3 (figure 5.26). All particles under study, had sizes between 5 and 15 μm and tended to have a blackish colour but often with a white centre. We have examined the Raman spectra of particles found in regions 1, 2 and 3 of the paper sample. A spectrum of the particles found in region 1, compared with the spectrum of the barium carbonate reference material, is given in figure 5.29[39]. It shows bands at 1055 and 689 cm^{-1} characteristic of the symmetric stretching and in plane bending vibrations of the CO_3^{2-} ion. It is clear that the barium carbonate anion is the most commonly observed material in this region. The carbonate is probably formed from BaO in the air either during, or after, the gunshot.

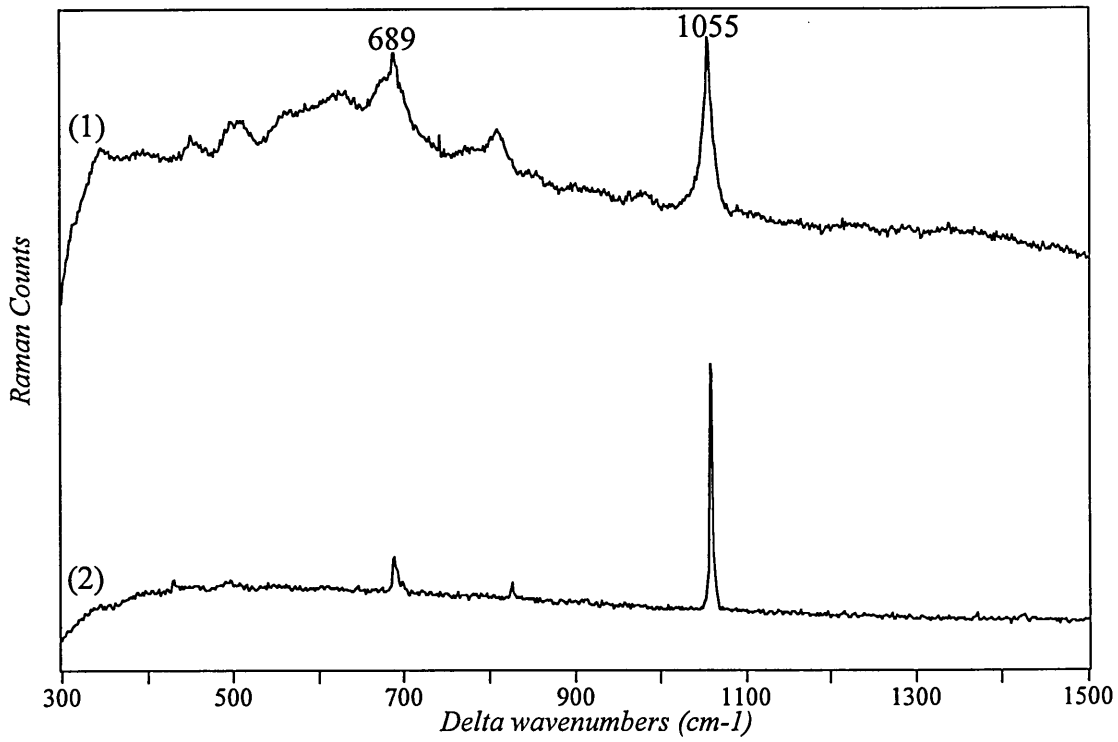

Figure 5.29: Raman spectrum of a unknown particle, from region 1, in comparison with $BaCO_3$. (1) particle of 5 μm size, red laser, X 50 objective, $T_{tot} \approx 10.5$ min; (2) $BaCO_3$ reference. Cellulose filter subtraction applied on spectrum (1).

The spectra from particles in region 2 (figure 5.30) exhibits two bands at about 1060 cm^{-1} and 980 cm^{-1} arising from the symmetric stretching vibration of the CO_3^{2-} ion and the stretching vibration of the SO_4^{2-} group respectively. It is clear that, in this region particles containing the carbonate anion and the sulphate anion (figure 5.31), probably lead sulphate (see table 5.3), may be observed[40,41]. But it is also clear that the particles comprise mixtures of such materials. For example, oxides of lead are probably present, but this cannot be confirmed, because of the extreme breadth of the bands below 600 cm^{-1} in many of the spectra. The broad feature extending from 700 cm^{-1} to 350 cm^{-1} in many of the spectra from regions 2 (figure 5.30) and 3 (figure 5.32) is most likely to be associated with mixed iron oxides, even though it is not totally clear from whence the elemental iron arises[42,43].

$BaCO_3$ $\bar{\nu}$ / cm^{-1}	$BaSO_4$ $\bar{\nu}$ / cm^{-1}	$PbSO_4$ [5] $\bar{\nu}$ / cm^{-1}	PbO orthorhombic $\bar{\nu}$ / cm^{-1}
1060 (s)	1142 (w)	1158 (w)	340 (s)
690 (m)	987 (s)	1065 (w)	291 (m)
	645 (w)	981 (s)	
	616 (w)	443 (m)	
	461 (m)	454 (m)	
	452 (m)	608 (w)	
		644 (w)	

Table 5.3: Wavenumbers ($\bar{\nu}$) and intensities of Raman bands of some inorganic ions. (s: strong, m: medium, w: weak)

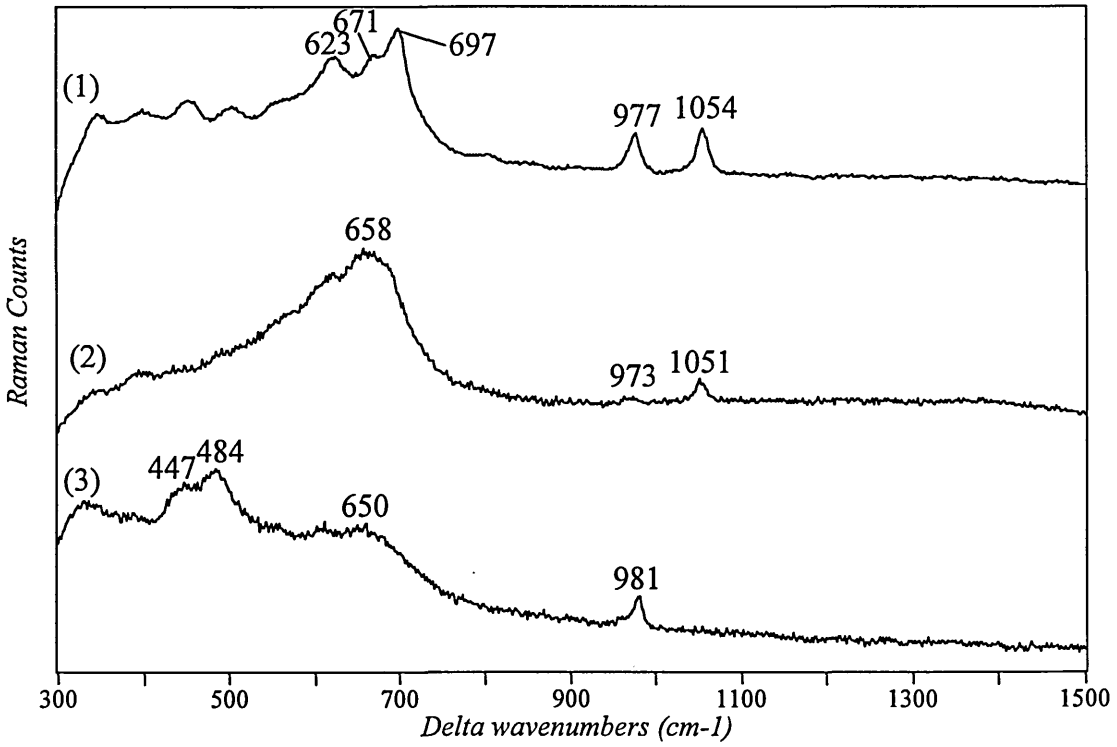

Figure 5.30: Raman spectra of unknown particles from region 2. (1) particle of 8 μm size, red laser, X 50 objective, T_{tot} ≈10.5 min; (2) particle of 15 μm of size, red laser, X 100 objective, T_{tot} ≈ 1.7 min; (3) particle of 5 μm size, red laser, X 100 objective, T_{tot} ≈19 min; Cellulose filter subtraction applied on spectra (1) to (3).

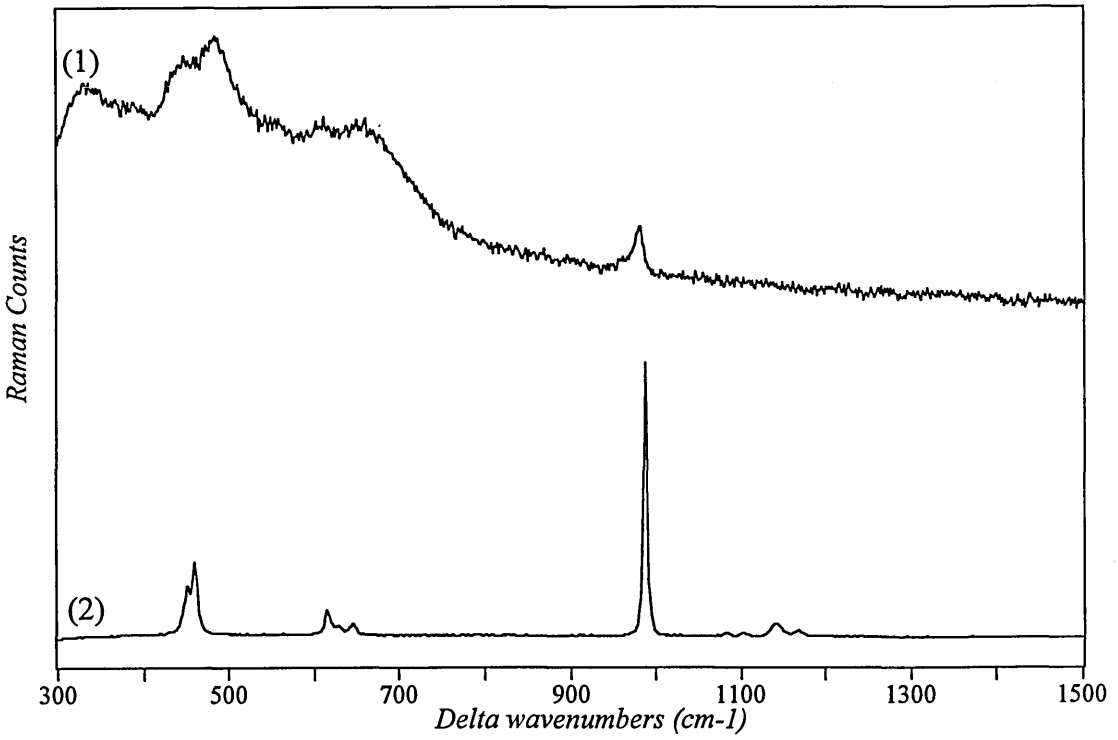

Figure 5.31: Raman spectra of a unknown particle from region 2 (1) in comparison with $BaSO_4$ (2) - Cellulose filter subtraction applied on spectrum (1).

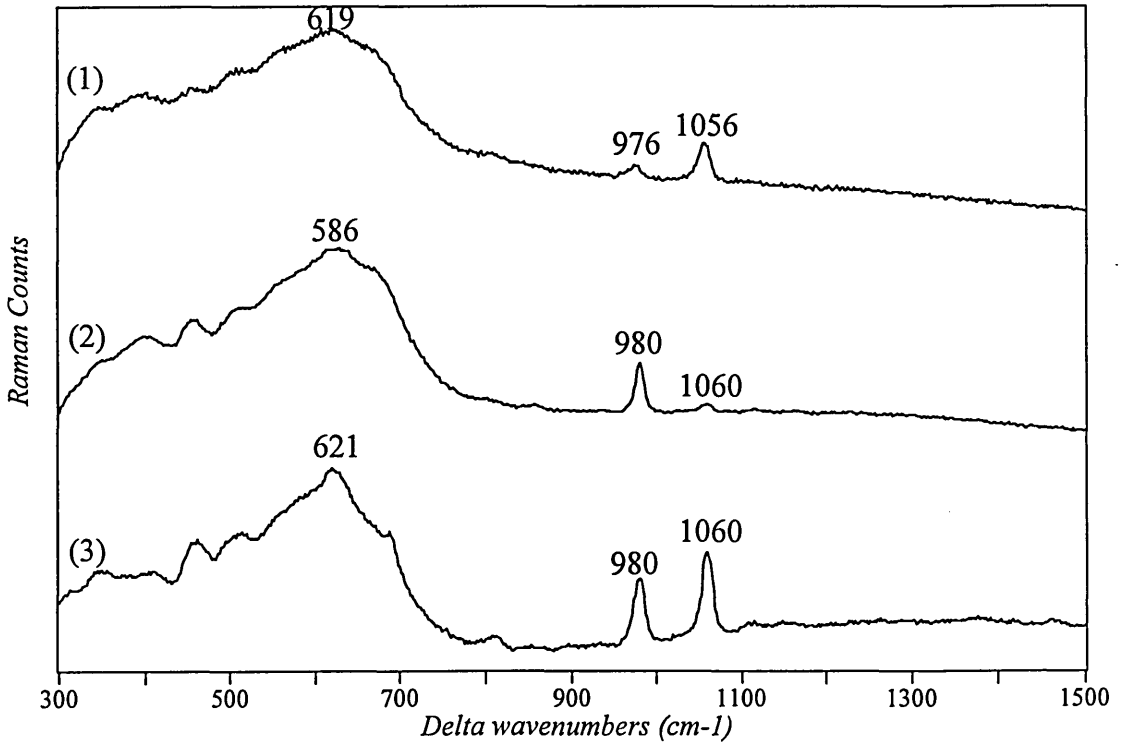

Figure 5.32: Raman spectra of unknown particles from region 3. (1) particle of 6 μm size, red laser, X 50 objective, $T_{tot} \approx 2.1$ min; (2) particle of 5 μm of size, red laser, X 50 objective, $T_{tot} \approx 10.5$ min; (3) particle of 4 μm size, red laser, X 50 objective, $T_{tot} \approx 21.1$ min; Cellulose filter subtraction applied on spectra (1) to (3).

A number of particles in region 3 of the substrate also show definitive evidence for the presence of orthorhombic lead oxides[44] (figure 5.33) as well as carbonate and sulphate anions. Indeed almost all the particles in regions 2 and 3 of the substrate contain multiple components.

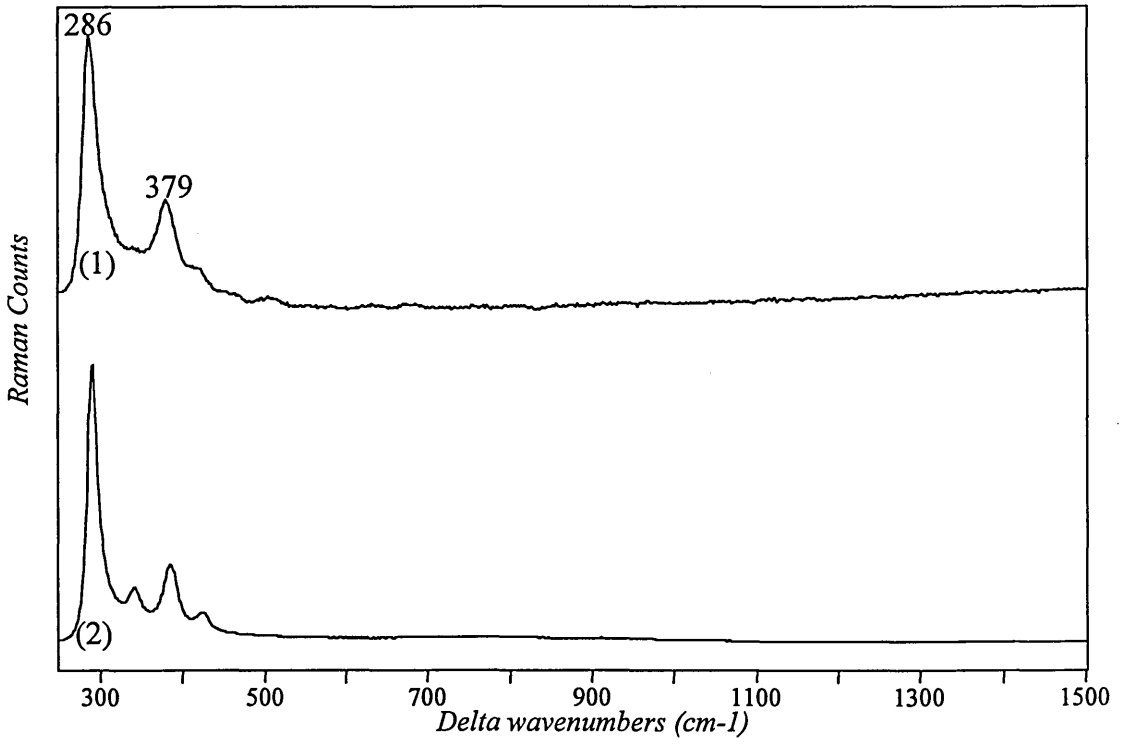

Figure 5.33: Raman spectrum of a unknown particle, from region 3, in comparison with orthorhombic PbO. (1) particle of 4 μm size, red laser, X 50 objective, $T_{tot} \approx 2.1$ min;
(2) orthorhombic PbO reference.
Cellulose filter subtraction applied on spectrum (1).

These results are consistent with the SEM/EDX spectra obtained for the same particles at the Bundeskriminalamt in Wiesbaden, Germany. The principal conclusion of that study was the gunshot residues consist of elemental lead, barium, antimony and possibly with some particles containing a little copper (not detected here). It was suggested using EDX that antimony appears only in combination with barium and/or lead and that the concentration is very small[45]. This explains why we are unable to confirm the presence of antimony oxides in the presence of barium carbonate, lead sulphate and lead oxide. One interesting feature of the Raman data is that it is clear that many of the gunshot residues contain material which is microcrystalline. The spectra thus show definite evidence of one particular crystal structure (for example, orthorhombic PbO) and stoichiometry. This leads to potentially richer Raman spectra with more opportunities for the detection of a particular crystal lattice.

The particles identified by Raman microspectroscopy consist mainly of carbon particles, $BaCO_3$ especially in region 1, mixtures of compounds such as: $BaCO_3$, $PbSO_4$, PbO and iron oxides, in regions 2 and 3, PbO alone in region 3. The broad band from 700 to 350 cm^{-1} in many of the spectra has been attributed to mixed iron or iron/chromium oxides.

5.8. Conclusion.

Five asbestos reference standards (amosite, fibrous anthophyllite, chrysotile, crocidolite and fibrous tremolite) and some of their non-fibrous analogues (grunerite, lizardite, riebeckite and tremolite) were analysed by Raman spectroscopy. The spectra are significantly different and possess their own features in such a way it is possible to discriminate one type of asbestos from another as in infrared spectroscopy. The Raman spectra of asbestos fibres and their non-fibrous form were also compared. It is difficult to find any important differences except for some cases in the OH stretching region such as amosite and crocidolite.

A more extensive study on tremolite fibrous and tremolite was performed and showed differences in the band widths and positions of the 670 and 390 cm^{-1} bands. These changes may be explained by a difference in the number of defects or in the local laser heat.

An important conclusion is that, Raman microspectroscopy is a powerful technique for the direct identification of pure inorganic fibres on cellulose filters especially asbestos fibres as small as 1 μm in diameter. The technique also allows the identification of unknown fibres, on cellulose filters, from real "industrial" samples such as waste asbestos samples from buildings ceilings, walls or pipe insulation. Moreover, other inorganic particles on cellulose filters can be identified very easily.

Raman microscopy was also used to discriminate coal and diesel particles. It was found that, the most significant feature is the difference in the intensity ratio of the D to G bands in the carbon Raman spectra of diesel and coal particles. This difference is probably due to a more disordered carbon structure in the case of diesel particles than of coal.

Another field of interest, concerning the discrimination of μm size particles, was the investigation of gunshot residues. The particles identified by Raman microspectroscopy consist mainly of carbon particles, $BaCO_3$, mixtures of compounds such as: $BaCO_3$, $PbSO_4$, PbO and iron oxides as well as PbO alone. The broad band from 700 to 350 cm^{-1} in many of the spectra was attributed to mixed iron or iron/chromium oxides.

[1] E.G.Bartick. In The Design, Sample Handling, and Applications of Infrared Microscopes, Ed. P.B.Roush, American Society for Testing and Materials, Philadelphia, 64-73, 1987.
[2] C.Dyer and B.J.E. Smith. J. Raman Spectrosc., 26, 777-785, 1995.
[3] I.R.Lewis, N.C.Chaffin, M.E.Gunter and P.R.Griffiths. Spectrochim. Acta, 52A, 315-328, 1996.
[4] M.J.Luys, G.De Roy, E.F.Vansant and F.Adams. J. Chem. Soc. Faraday Trans.1, 78, 3561-3571, 1982.
[5] A.Marconi. Ann. Ist. Sup. Sanità, 19, 629-638, 1983.
[6] A.Wang, P.Dhamelincourt and G.Turrell. Appl. Spectrosc., 42, 1441-1450, 1988.
[7] M.Delhaye, P.Dhamelincourt and F.Wallart. Toxicol. and Environm. Chem. Rev., 3, 73-87, 1979.
[8] J.J.Blaha and G.J.Rosasco. Anal. Chem., 50, 892-896, 1978.
[9] J.J.Blaha, E.S.Etz and W.C.Cunningham. Scanning Electron Microsc.I, SEM Inc, 1, 93-102, 1979.
[10] G.Turrell. In Raman Microscopy Developments and Applications, Eds. G.Turrell and J.Corset, 1-23, 1996.
[11] S.Brawer. Phys. Rev., 11B, 3173-3194, 1975.
[12] R.Loudon. Adv. Phys., 13, 423-482, 1964.
[13] W.B.White. Infrared and Raman Spectroscopy of Lunar and Terrestrial Minerals, Ed. C.Karr Jr, Academic Press, New York, 325-358, 1974.
[14] A.Wang, B.L.Jolliff and L.A.Haskin. J. Goephys. Res., 100, 189-199, 1995.
[15] C.T.Ho, W.C.LaCourse, R.A.Condrate Sr. and A.Jillavenkatesa. Mater. Lett., 23, 237-240, 1995.
[16] P.F.McMillan, J.Dubessy and R.Hemley. In Raman Microscopy Developments and Applications, Eds. G.Turrell and J.Corset, 289-365, 1996.
[17] R.G.Herman, C.E.Bogdan, A.J.Sommer and D.R.Simpson. Appl. Spectrosc., 41, 437-440, 1987.
[18] A.Wang, J.Han, L.Guo, J.Yu and P.Zeng. Appl. Spectrosc., 48, 959-968, 1994.
[19] M.Tarrida, M.Madon, B.Le Rolland and P.Colombet. Advn. Cem. Bas. Mat., 2, 15-20, 1995.
[20] M.Conjeaud and H.Boyer. Cem. Concr. Res., 10, 61-70, 1980.
[21] A.H.Delgado, R.M.Paroli and J.J.Beaudoin. Appl. Spectrosc., 50, 970-976, 1996.
[22] J.Bensted. J. Am. Cer. Soc., 59, 140-143, 1976.
[23] G.C.Kosztolanyi, J.Mullis and M.Weidmann. Chem. Geol., 61, 19-28, 1987.
[24] C.Kontoyannis, N.C.Bouropoulos and P.G.Koutsoukos. Appl. Spectrosc., 51, 1205-1209, 1997.
[25] V.R.Kodati, G.E.Tomasi, J.L.Turumin and A.T.Tu. Appl. Spectrosc., 45, 581-583, 1991.
[26] Renishaw library, Grams/32 software, Library Search, 1991-1996.
[27] D.L.A.De Faria, S.Venâcio Silva and M.T.De Oliveira. J.Raman Spectrosc., 28, 873-878, 1997.
[28] A.H.Kuptsov. J. Forensic Sci., 39, 305-318, 1994.

[29] B.K.Cantrell and W.F.Watts Jr. Appl. Occup. Environ. Hyg., 12, 1019-1026, 1997.
[30] J.R.Dennison, M.Holtz, G.Swain. Spectroscopy, 11, 38-46, 1996.
[31] P.D.Green, C.A.Johnson and K.M.Thomas. Fuel, 62, 1013-1023, 1983.
[32] H.J.Scheibe, D.Drescher and P.Alers. Fresenius J. Anal. Chem., 353, 695-697, 1995.
[33] B.Wopenka. Earth Planet. Sci. Lett., 88, 221-231, 1988.
[34] Z.Zheng and X.Chen. Sci. China, Ser. B, 38, 97-106, 1995.
[35] L.Suhartono, B.C.Cornilsen, J.H.Johnson and D.H.Carlson. Appl. Occup. Environ. Hyg., 11, 790-798, 1997.
[36] W.Lichtenberg. Forensic Sci. Rev, 2, 37-62, 1990.
[37] H.W.Wenz, W.J.Lichtenberg and H.Katterwe. Fresenius J. Anal. Chem., 341, 155-165, 1991.
[38] J.D.Pasteris and B.Wopenka. Can. Mineral., 29, 1-9, 1991.
[39] I.A Degen and G.A Newman, Spectrochim. Acta, 49A, 859-887,1993.
[40] K.R Bullock, G.M Trischan and R.G Burrow. J. Electrochem. Soc, 130, 1283-1289, 1983.
[41] Y.Koshino and A.Narukawa. Analyst, 119, 2473-2475,1994.
[42] M.Thieme and D.Scharnweber. Corros. Sci., 34, 363-381,1993.
[43] M.Thieme. Corros. Sci., 34, 1557-1560, 1993.
[44] D.A Ciomartan, R.J.H Clark, L.J.McDonald and M.Odlyha. J. Chem. Soc. Dalton Trans., 18, 3639-3645, 1996.
[45] C.Gliwitzky. In Ausarbeitung und Bewertung von Verfahren zur ortsselektiven Sicherung und Vermessung von Schmauchanhaftungen an der Schusshand. Diploma thesis, FH- Fresenius, Wiesbaden (1992).

CHAPTER 6

ESTABLISHMENT OF A RAMAN METHOD FOR THE INVESTIGATION OF THE WETTING PROCESS ON INORGANIC FIBRES AND OTHER MATERIALS

6. Establishment of a Raman method for the investigation of the wetting process on inorganic fibres and other materials.

6.1. Introduction.

Today, asbestos containing materials in public buildings, chemical industries and schools represent a potential health hazard and are being progressively removed. But, the hazards increase during this process as the materials are disturbed. It has been found that, the spraying and injection of wetting or encapsulating agents inside the materials considerably reduce the concentration of fibres released in the atmosphere. Wetting and encapsulating agents and systems of injection were therefore developed in order to reduce the risks associated with asbestos removal or comply with the HSE regulations.

Wetting and encapsulating agents are generally developed from 'hands on' experience rather than from the study of the chemistry and properties of asbestos containing materials. They need to be efficient and non-toxic, but also cheap. The cheapest one is probably water which proved to be as good as other wetting agent but non applicable due to its fast rate of evaporation. However, a lot of agents are water based products. Two types of wetting agent are often found on the market for the use at ambient and high temperatures (such as insulation on very hot pipes and boilers).

Basic laboratory experiments were performed in order to establish a Raman method for the coverage measurements of wetting and encapsulating agents on fibres and particles. We were interested to find out the possibilities of Raman microspectroscopy in the determination of the amount and distribution of wetting and encapsulating agents on individual fibres. Indeed, Raman microspectroscopy was shown to be a very powerful technique for the identification of μm size fibres with little or no sample preparation. Hazardous fibres such as asbestos were successfully analysed on cellulose filters. In this chapter, the fibres and particles were also transferred, after wetting, on such filters for Raman analysis or in some cases directly wetted and analysed on the filters. The subtraction process of cellulose filter was applied on all asbestos spectra in this chapter. The spectra were collected using the red laser with the X 50 and X 100 objective which give an illuminated spot of about 4 and 1-2 μm respectively.

Inorganic fibres such as asbestos and man-made mineral fibres as well as calcium silicate (a material very often found in the composition of insulation containing asbestos) were the main materials under investigation. The two principal modes of wetting were the spraying with an aerosol spray gun and the capillary action. Three commercial agents were studied in this project: astrip and hotstrip provided by Asbestostrip Innovations and penetrant n°1 from Eppert Europe Limited. The full details of the agents are given in chapter 3.

Penetrant n°1 is a white solution or emulsion in water of unknown composition. It is an encapsulating agent. The infrared and Raman spectra display bands characteristics of n-alkanes and C-Cl stretching vibrations.

Astrip, designed by B.P Chemicals, is a clear wetting agent mainly made of polyalkylene glycol (50 % in weight) and water (39.7% in weight).

Hotstrip is a clear wetting agent made of pure polydimethylsiloxane (PDMS), used in high temperature conditions.

Silicone emulsions in water were also investigated containing 60 % of silicone for 40 % of water by weight. The idea was to produce a better quality product than Astrip and be able to use these emulsions to wet dense asbestos containing materials, such as those with high levels of calcium silicate.

All spectra shown in this chapter were also collected using the continuous extended scanning technique. The total exposure time was then calculated from the formula[1] : $T_{tot} \approx (1 + \text{total scan range / average static window length}) \times T_{ex}$; with T_{ex}, the exposure time.

6.2. Reference asbestos fibres.

6.2.1. Spraying of commercial wetting agents on asbestos fibres attached to cellulose filters.

6.2.1.1. Penetrant n°1.

6.2.1.1.1. Materials and methods.

Amosite and crocidolite reference fibres attached to cellulose filter were wetted with penetrant n°1 using an aerosol spray gun. Three sprays (one failure, two successful) were applied on amosite fibres at a distance of 20-30 cm and two (one failure, one successful) on crocidolite fibres. The Raman spectra were collected along the fibres

using the X 100 and X 50 objectives. The instrument was set up in microprobe mode using a slit width of 50 μm and a CCD area of 15 x 576 pixels.

6.2.1.1.2. Results.

The aerosol spray gun creates small homogeneous drops of about 5 μm.

- *Amosite*

The spraying of the encapsulating agent from the aerosol spray gun created small drops which took the shape of the fibres. These drops along the fibres were clearly observed under the optical microscope (figures 6.1.a to 6.1.c).

The Raman spectra collected along a fibre having a diameter of 2.5 μm show bands from amosite as well as bands from the encapsulating agent (figure 6.2). Moreover, the relative area of penetrant n°1 compared to amosite bands varies. This variation is indicative of a difference in the amount of encapsulating agent on the surface of the fibres. This amount is generally maximum on drops which are observed on the micrographs. On the other hand, some spectra exhibit only bands from the amosite characteristic of uncovered areas on the fibres. In fact, different level of coverage and areas without encapsulating agent were found and semi quantified. The quantification is based on area ratio of the encapsulating agent to the amosite bands. However, the amosite bands interfere with the wetting agent bands in some part of the wet asbestos spectra. The curve fitting method was applied in order to separate the bands into individual components. Two regions were fitted using Lorentzian bands (figure 6.3):

- the 560-720 cm^{-1} region, introducing one band for amosite and four bands for the encapsulating agent.
- the 1390-1510 cm^{-1} region, introducing two bands for the encapsulating agent.

Two graphs were then plotted (figure 6.4):

- the ratio of the area of the encapsulating agent bands at 560-720 to the amosite band at 660 cm^{-1} against distance along the fibre.
- the ratio of the area of the encapsulating agent bands at 1390-1510 to the amosite band at 660 cm^{-1} against distance along the fibre.

Figure 6.1a.

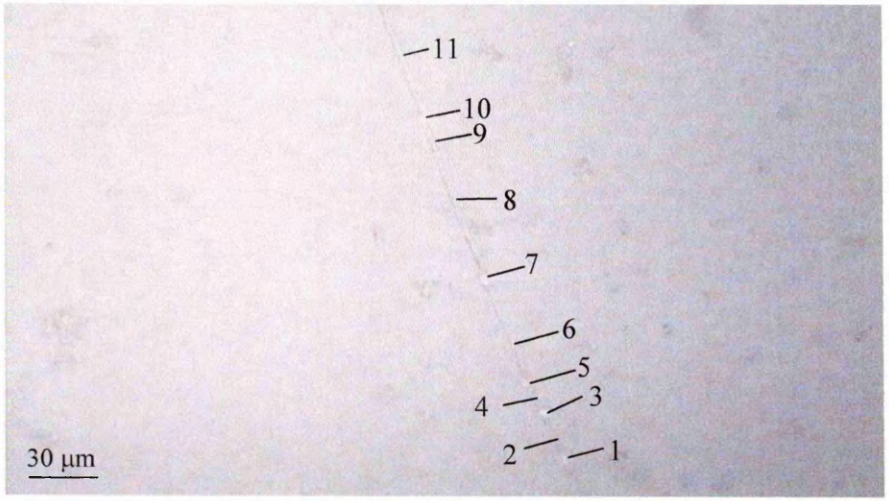

Figure 6.1.a to 6.1.c: Micrograph of a wet amosite fibre on cellulose filter. The X 20 objective was used to collect the picture 6.1.a and the X 50 objective to collect the pictures 6.1.b and 6.1.c.

Figure 6.1.b.

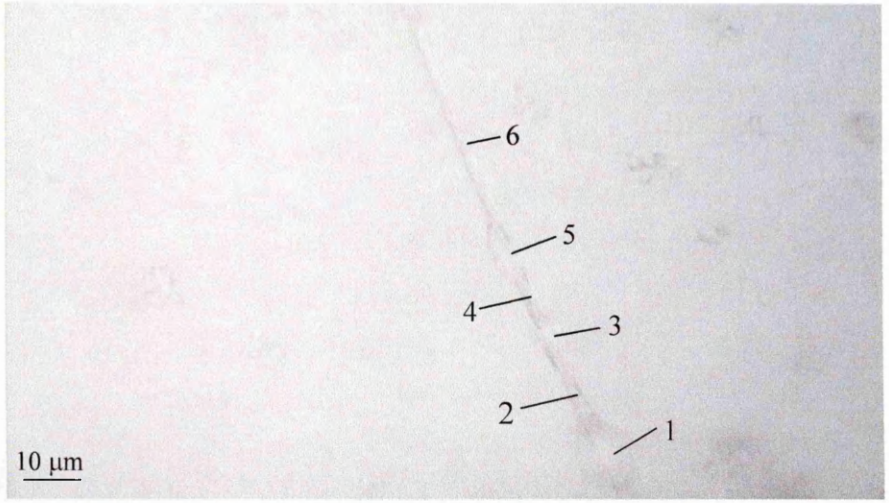

Figure 6.1.c.

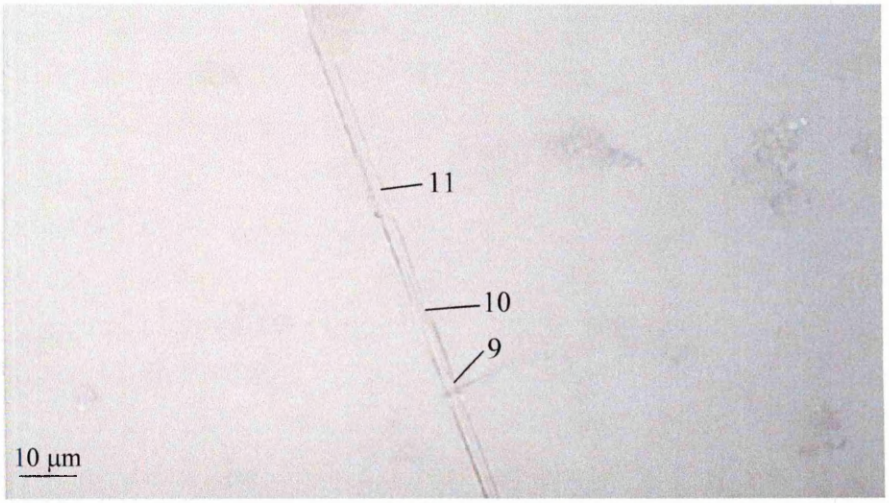

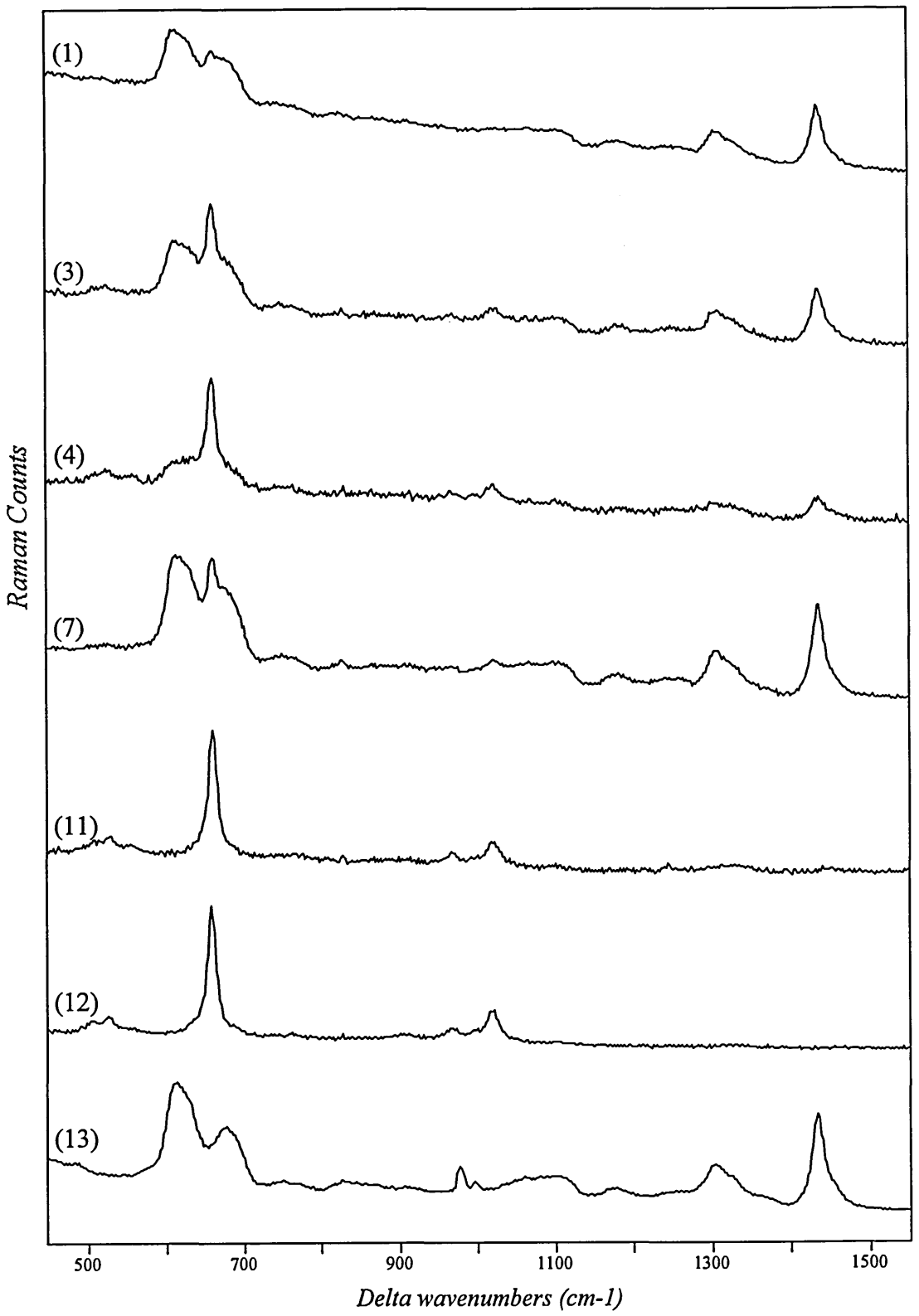

Figure 6.2: Raman spectra collected along a wet amosite fibre in comparison with amosite and penetrant n°1. (1) to (11) wet amosite fibre of 2.5 µm of diameter (positions 1 to 11 shown in figures 6.1.a to 6.1.c), red laser, X 100 objective, $T_{tot} \approx 14.8$ min; (12) amosite reference; (13) penetrant n°1.
Cellulose filter subtraction applied on spectra (1) to (11).

Figure 6.3.a.

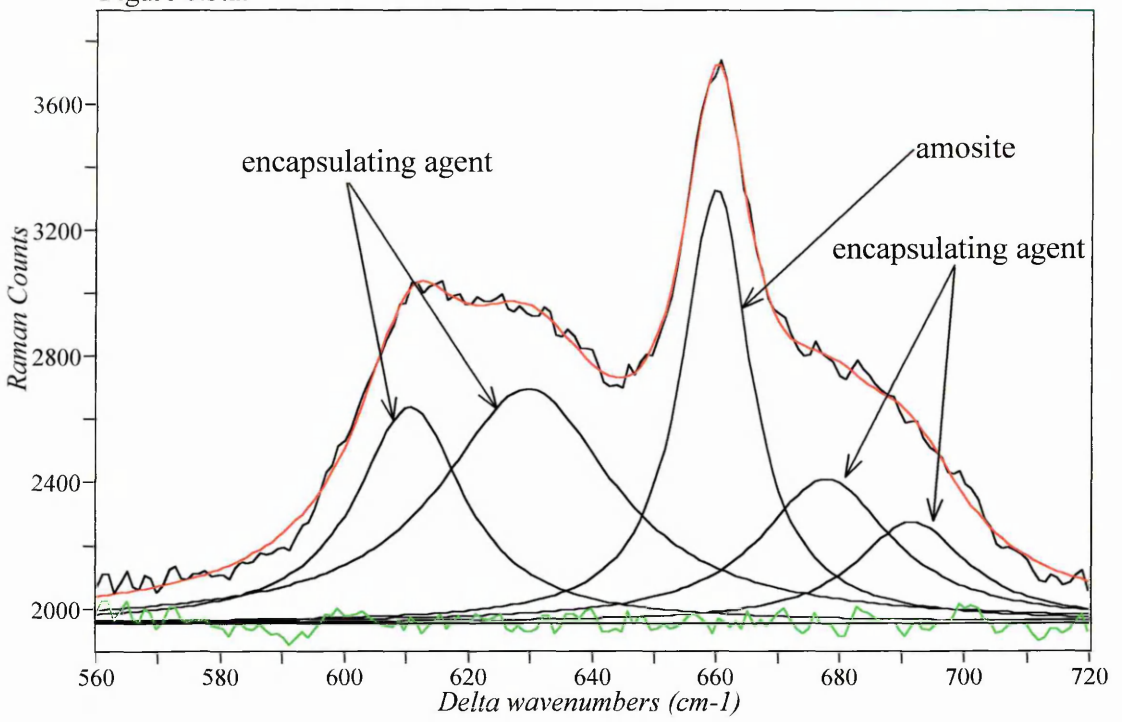

Figure 6.3.b.

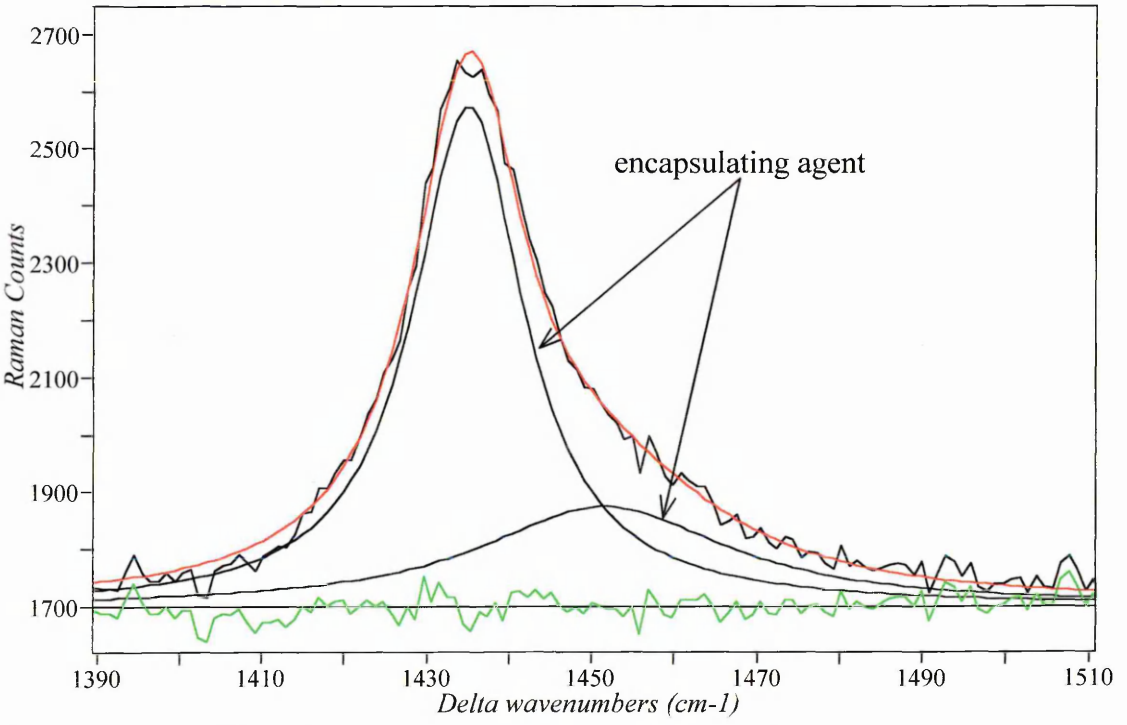

Figure 6.3: Curve fitting of spectrum 3, in figure 6.2, introducing Lorentzian bands from the encapsulating agent and amosite.
Figure 6.3.a. Curve fitting in the 560-720 cm^{-1} region; figure 6.3.b. curve fitting in the 1390-1510 cm^{-1} region.

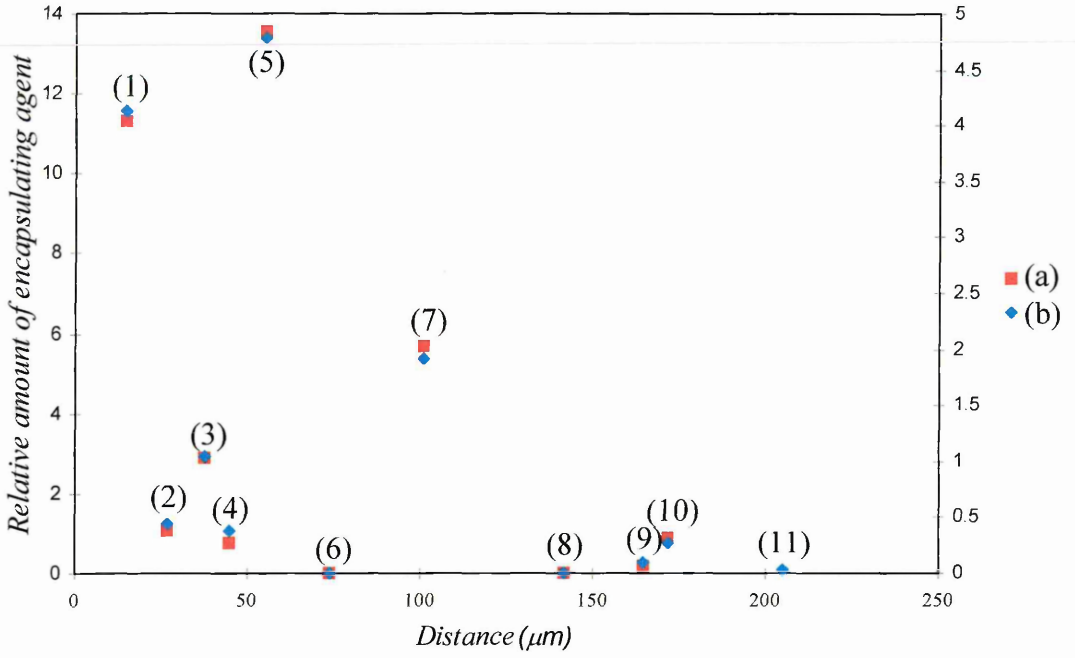

Figure 6.4: Plot of the relative amount of encapsulating agent along an amosite fibre (figures 6.1), calculated from area bands ratio (spectra 1 to 11 in figure 6.2).
(a). ratio of the encapsulating agent bands at 560-720 cm^{-1} to the 660 amosite band.
(b). ratio of the encapsulating agent bands at 1390-1510 cm^{-1} to the 660 amosite band.

The two graphs of the relative amount of encapsulating agent along an amosite fibre match each other confirming a good curve fitting. They also fit with the optical micrographs. The drops on the pictures appears as points with maximum values on the plots whereas uncoated areas with minimum or nil values. The plots show an heterogeneous random coverage. This coverage is made of an alternation of coated and uncoated areas.

• ***Crocidolite.***

The micrograh of a wet crocidolite fibre coated with penetrant n°1, given in figure 6.5, do not show proper drops but patches like diffuse areas. The Raman spectra confirmed the presence of encapsulating agent along the fibre (figure 6.6). As amosite, the relative amount of penetrant n°1 along the crocidolite fibre was measured. The curve fitting method was also applied in order to separate the crocidolite from the encapsulating agent bands. Three regions were fitted (figure 6.7) using Lorentzian bands:

- the 480-720 cm^{-1} region, introducing four bands for crocidolite and four bands for the encapsulating agent which include one crocidolite band.

- the 935-1010 cm^{-1} region introducing two bands for crocidolite.
- the 1390-1510 cm^{-1} region, introducing two bands for the encapsulating agent.

Two graphs were then plotted (figure 6.8):
- the ratio of the area of the encapsulating agent bands at 1390-1510 to the crocidolite bands at 480-625 against distance along the fibre.
- the ratio of the area of the encapsulating agent bands at 1390-1510 to the crocidolite bands at 935-1010 against distance along the fibre.

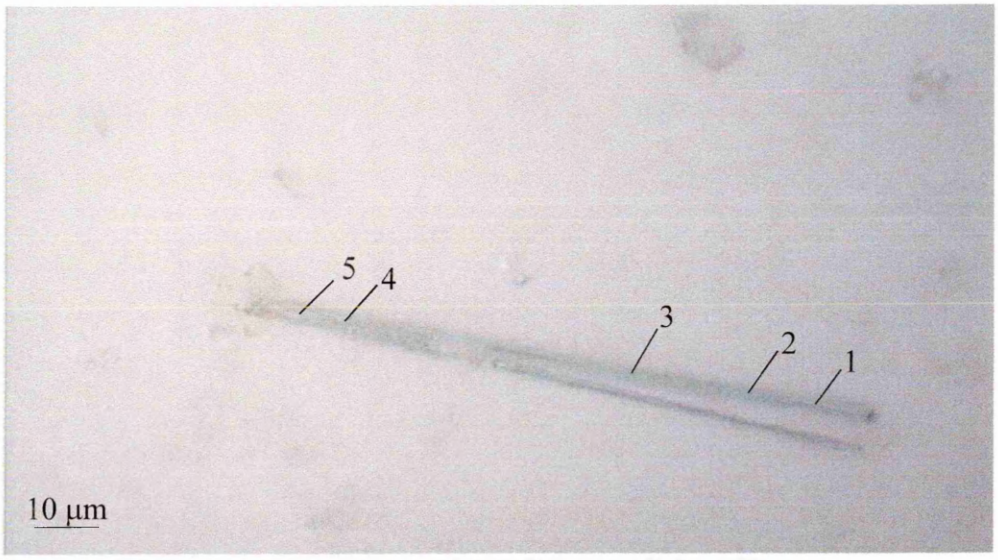

Figure 6.5: Micrograph of a wet crocidolite fibre on cellulose filter.

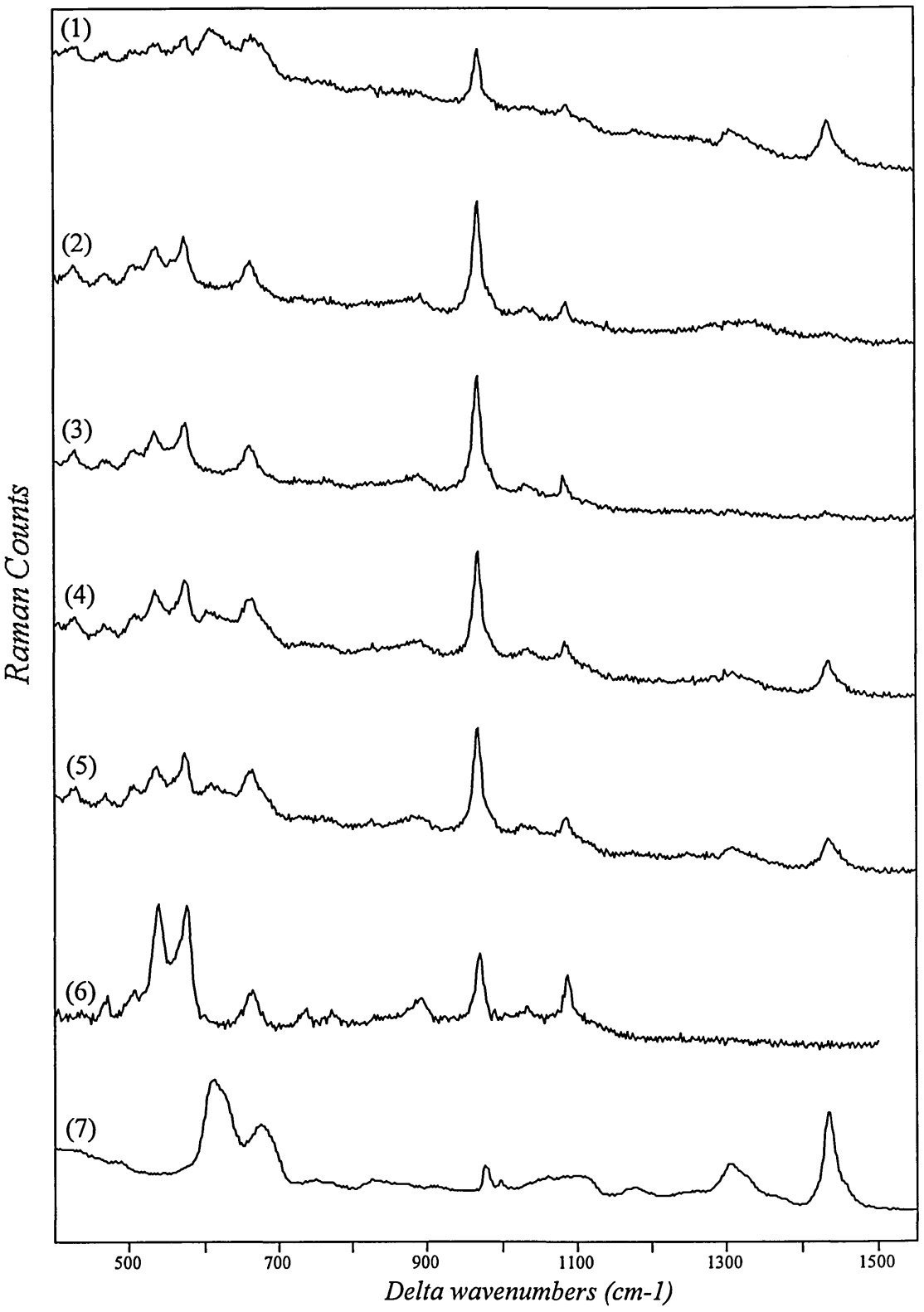

Figure 6.6: Raman spectra collected along a wet crocidolite fibre in comparison with crocidolite and penetrant n°1. (1) to (5) wet crocidolite fibre of 3-4 μm of diameter to 1-2 μm when the fibre is split, (positions 1 to 5 shown in figure 6.5), red laser, X 100 objective, $T_{tot} \approx 15.1$ min; (6) crocidolite reference; (7) penetrant n°1.
Cellulose filter subtraction applied on spectra (1) to (5).

Figure 6.7.a.

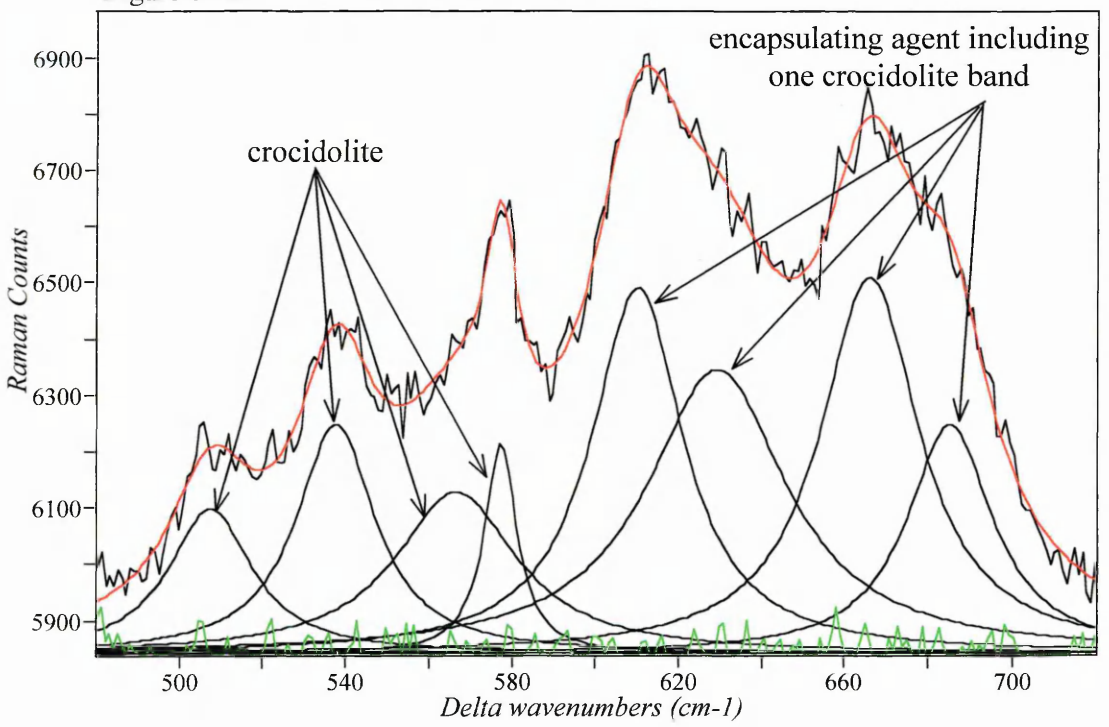

Figure 6.7.a.

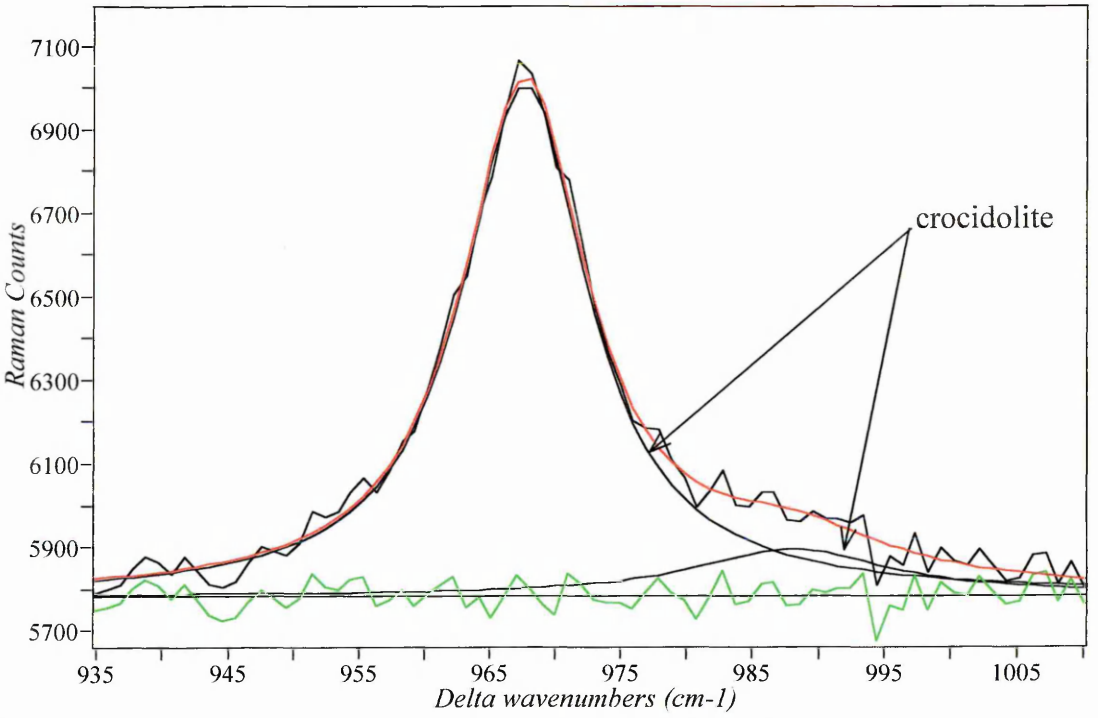

Figure 6.7: Curve fitting of spectrum 1, in figure 6.6, introducing Lorentzian bands from the encapsulating agent and crocidolite.
Figure 6.7.a. Curve fitting in the 480-720 cm^{-1} region; figure 6.7.b. curve fitting in the 935-1010 cm^{-1} region.

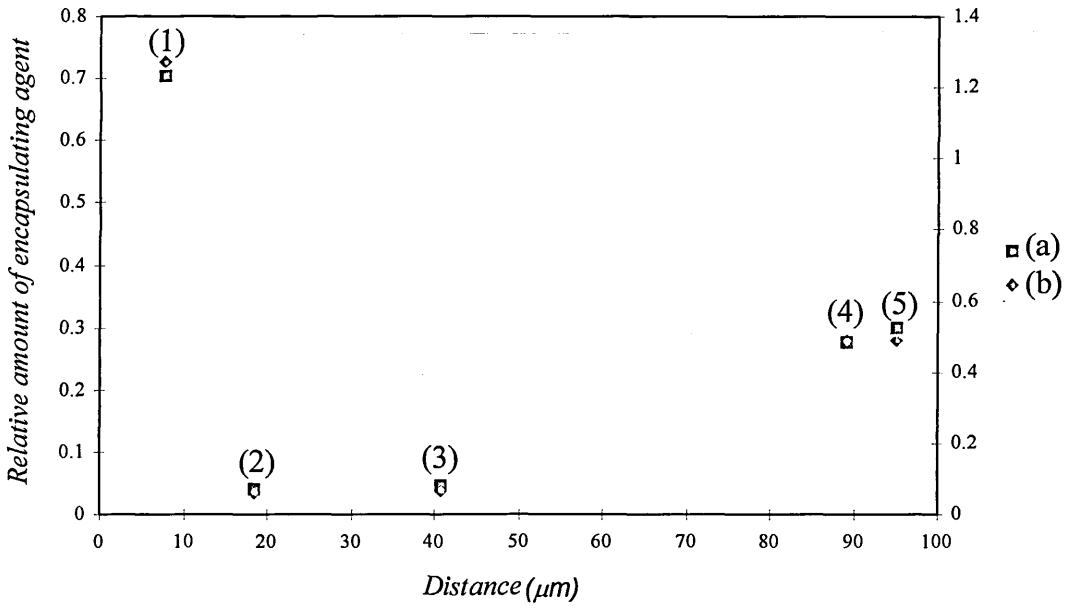

Figure 6.8: Plot of the relative amount of encapsulating agent along a crocidolite fibre (figure 6.5), calculated from area bands ratio (spectra 1 to 5 in figure 6.6).
(a). ratio of the encapsulating agent bands at 1390-1510 cm^{-1} to the crocidolite bands at 480-600 cm^{-1}.
(b). ratio of the encapsulating agent bands at 1390-1510 cm^{-1} to the crocidolite bands at 935-1010 cm^{-1}.

The two graphs of the relative amount of encapsulating agent along the fibre also match each other confirming a good curve fitting. Different level of coverage was found on crocidolite fibre but with fewer disparities than the previous amosite case since no drops were observed.

Drops formed on crocidolite fibres were also observed under the optical microscope.

A Raman spectrum was collected from a 9.5 x 6 μm drop surrounding a crocidolite fibre having a diameter of 1 μm (figure 6.9). In this case, the spectrum shows only bands from the encapsulating agent (figure 6.10). Indeed, most of the scattered light comes from the penetrant n°1 rather than the crocidolite.

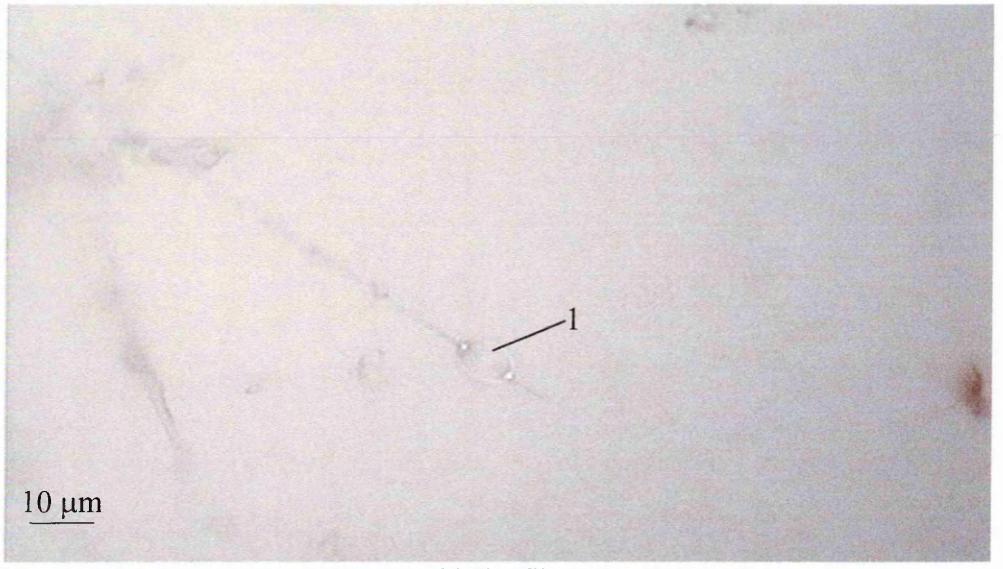

Figure 6.9: Micrograph of a wet crocidolite fibre on cellulose filter.

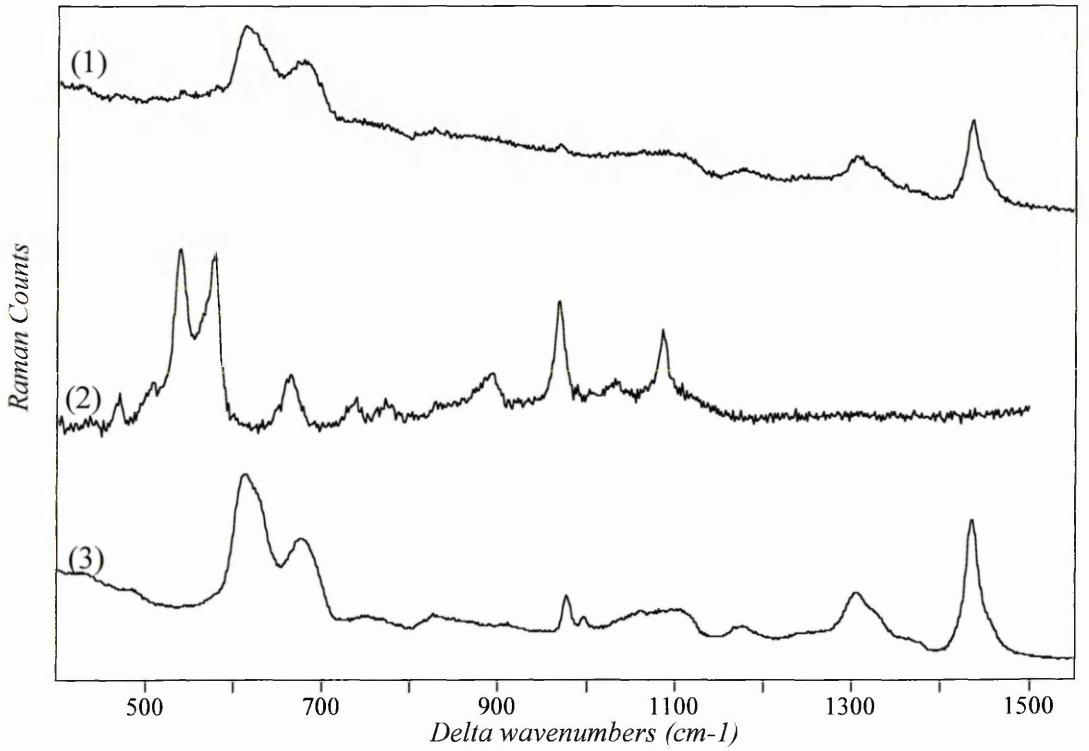

Figure 6.10: Raman spectrum collected on a wet crocidolite fibre in comparison with crocidolite and penetrant n°1. (1) wet crocidolite fibre of 1 µm of diameter surrounded by a drop of 9.5 x 6 µm size from the encapsulating agent (figure 6.9), red laser, X 100 objective, $T_{tot} \approx 7.5$ min; (2) crocidolite reference; (3) penetrant $n^0 1$.
Cellulose filter subtraction applied on spectrum (1).

A Raman spectrum was collected from a 5 µm drop on a bundle of crocidolite fibres (figure 6.11). The spectrum displays not only bands from the encapsulating agent but also from asbestos (figure 6.12). The drop probably penetrated partially inside the bundle and took place around the individual fibres of the bundle.

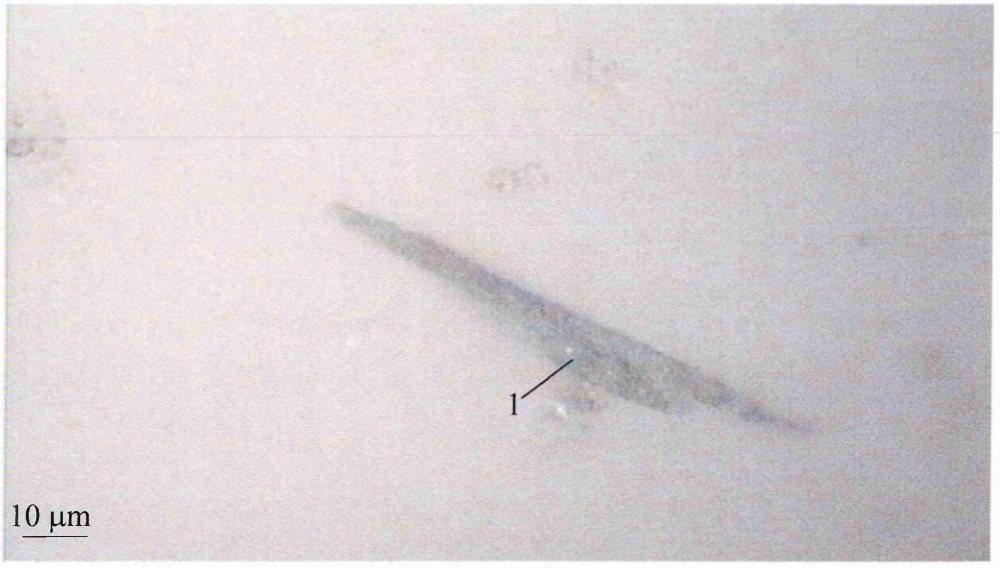

Figure 6.11: Micrograph of a wet crocidolite fibre on cellulose filter.

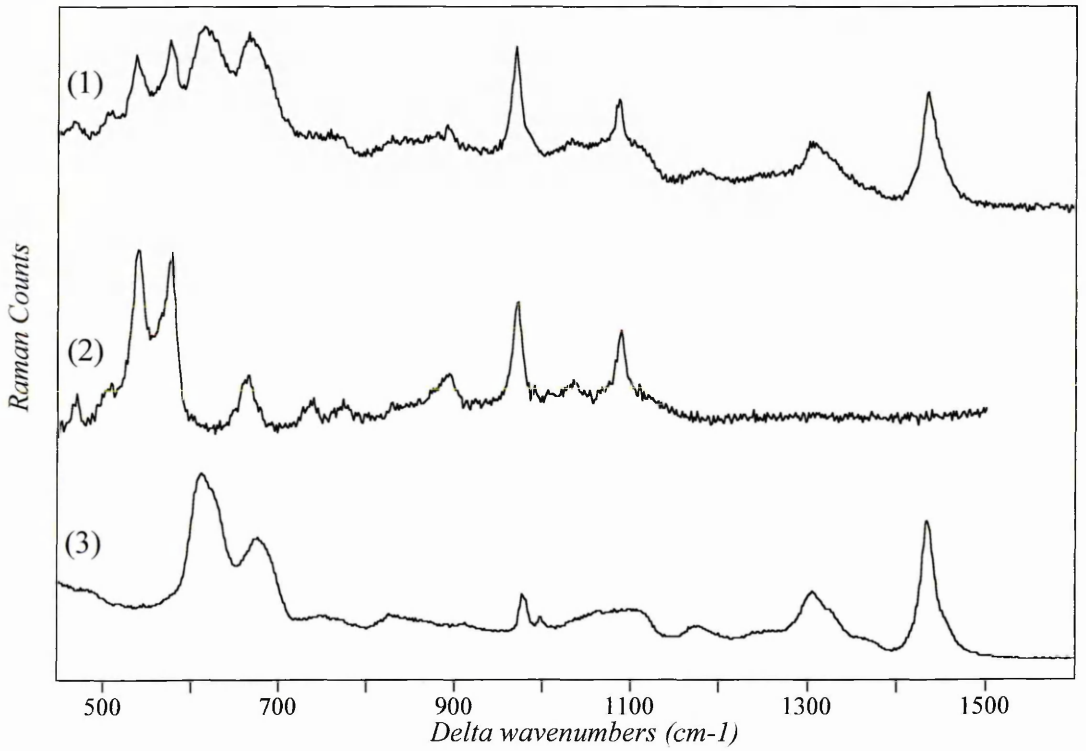

Figure 6.12: Raman spectrum collected on a wet bundle of crocidolite fibres in comparison with crocidolite and penetrant n°1. (1) wet bundle of crocidolite fibres with a drop of 5 µm size on the surface (figure 6.11), red laser, X 100 objective, $T_{tot} \approx 25.6$ min; (2) crocidolite reference; (3) penetrant n°1.
Cellulose filter subtraction applied on spectra (1).

It is to be noted that, sometimes, a variation in relative band intensity of crocidolite was observed such as on the spectra collected from two distinctive wet fibres (figures 6.6 and 6.12). Therefore, the comparison of the amount of encapsulating agent on these two fibres becomes difficult. Indeed, two different evaluations can be found

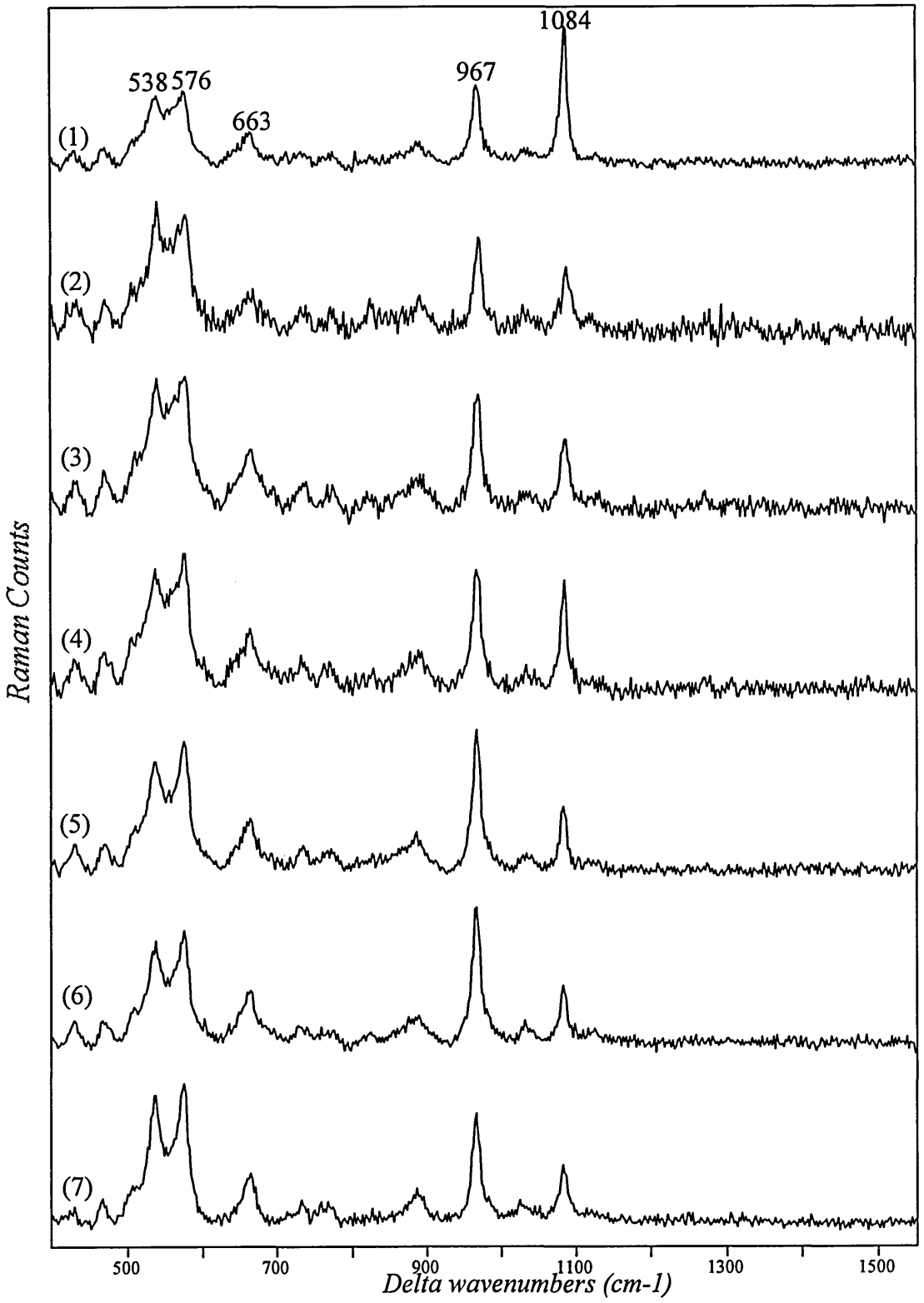

Figure 6.13: Raman spectra collected on reference crocidolite fibres (1) fibre 1, of 4 μm of diameter, position 1 on the fibre, red laser, X 100 objective, $T_{tot} \approx 22.4$ min; (2) fibre 1, position 2 on the fibre, red laser, X 100 objective, $T_{tot} \approx 22.4$ min; (3) fibre 1, position 3 on the fibre, red laser, X 100 objective, $T_{tot} \approx 22.4$ min; (4) fibre 2, of 8 μm of diameter, red laser, X 100 objective, $T_{tot} \approx 22.4$ min; (5) fibre 3, of 4 μm of diameter, position 1 on the fibre, red laser, X 100 objective, $T_{tot} \approx 22.4$ min; (6) fibre 3, position 2 on the fibre, red laser, X 100 objective, $T_{tot} \approx 22.4$ min; (7) fibre 4, of 7 μm of diameter, red laser, X 100 objective, $T_{tot} \approx 22.4$ min. Cellulose filter subtraction and baseline correction applied on spectra (1) to (7).

depending on the choice of the crocidolite band (1084 or 576-536 cm^{-1} bands) to calculate the area ratio of the encapsulating agent to the asbestos bands. Nevertheless, the relative amount of encapsulating agent along an individual wet fibre was successfully assessed (figure 6.8) since in this case, no variation in the crocidolite bands occurs as a function of the laser position on the fibre.

However, spectra collected on uncoated reference crocidolite fibres may show sometimes a relative variation in bands intensity both from one fibre to another, and also along the same fibre (figure 6.13). The relative intensity of the three bands at 576, 538 and 663 cm^{-1} are rather constant relative of each other. The variations mainly arise from the 1084, 967 and 576-538 cm^{-1} bands (figures 6.14). It is well known that crocidolite fibres can present locally strained areas[2]. Amphibole fibres also show chemical and structural variations along the fibres. These differences might explain the variation in relative band intensity, especially along an individual fibre. However, this variation may also be due to a polarisation effect. Indeed, asbestos fibres possess different refractive index in different direction. Therefore, the Raman bands intensity may change depending on the orientation of the fibres related to the red laser beam which has horizontal polarisation. The analysis of polarised Raman scattering on a single crocidolite fibre confirms the polarisation effect.

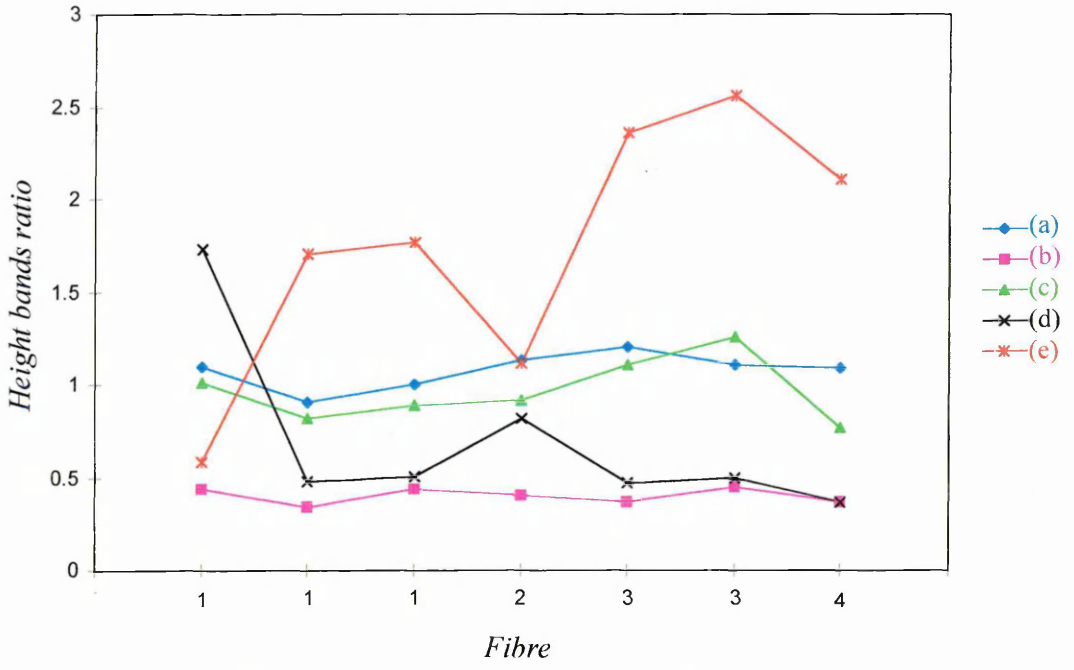

Figure 6.14: Height ratio of crocidolite bands for different fibres or at different positions on the fibres. (a). ratio of 576 to 538; (b). ratio of 663 to 576; (c). ratio of 967 to 576; (d). ratio of 1084 to 576; (e). Ratio of 967 to 1084.

A crocidolite fibre attached to cellulose filter was oriented parallel to the red laser beam. The instrument was set up in microprobe mode and the spectra were collected using the X 100 objective. The parallel polarisation state of Raman scattered light was studied with the half plate and the polariser in place whereas the perpendicular polarisation state was studied with only the polariser in place.

The intensities of the 374, 576-538, 970, 1085 cm^{-1} bands change in relation to each other depending on the polarisation analysis (figure 6.15). The 576-538 and 1085 bands are weak in the parallel polarisation spectrum and intense in the perpendicular polarisation spectrum. The opposite effect appears with the 970 cm^{-1} band.

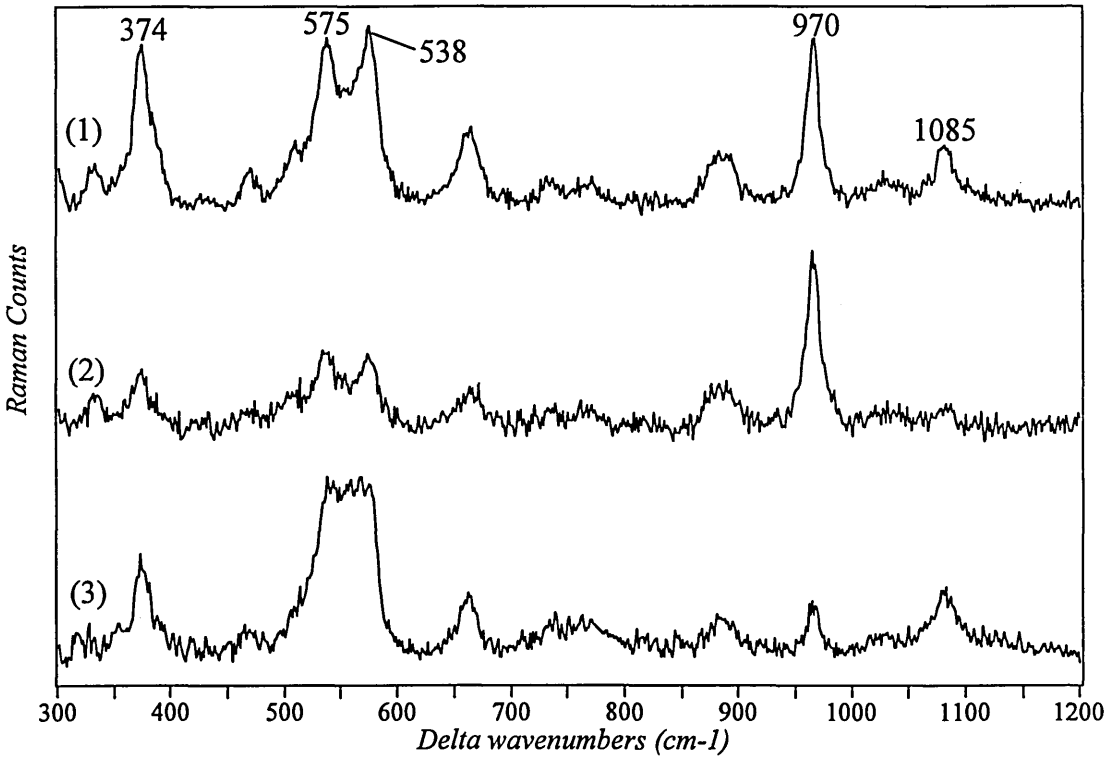

Figure 6.15: Raman spectra collected on a reference crocidolite fibre of 2.5 μm of diameter. (1) red laser, X 100 objective, $T_{tot} \approx 21.0$ min; (2) perpendicular polarisation, red laser, X 100 objective, $T_{tot} \approx 21.0$ min; (3) parallel polarisation, red laser, X 100 objective, $T_{tot} \approx 21.0$ min. Cellulose filter subtraction and baseline correction applied on spectra (1) to (3).

6.2.1.2. Hotstrip.

6.2.1.2.1. Materials and methods.

The same experiment than previously was carried on using a different wetting agent, hotstrip, which is pure PDMS. Amosite and crocidolite fibres attached to cellulose filter were wetted with the aerosol spray gun. Four sprays were applied on crocidolite and three on amosite fibres. The Raman spectra were collected using the

X 100 objective. The instrument was set up in microprobe and confocal modes using a slit width of 50 and 15 μm and a CDD area of 15 x 576 and 4 x 576 pixels respectively.

6.2.1.2.2. Results.

No drops nor wetting agent were observed under the optical microscope. However, all Raman spectra collected on the fibres and cellulose filter show bands from hotstrip which proved a complete wetting including the filter (figure 6.16). Indeed, no uncovered area was found. Unfortunately, in microprobe mode, using the X 100 objective, the spectra of the wet asbestos fibres were not only collected from the fibres but also from the wet filter.

The instrument was then set up in confocal mode in order to reduce the volume of sampling area, especially in the z direction. This arrangement provides a depth resolution of about 2 μm^3. Consequently, the relative volume collected from the fibres is larger than in microprobe mode. A comparison between the confocal and microprobe modes was investigated on wet amosite fibres having a diameter of 4 and 6 μm (figure 6.17). The same parameters were applied for all spectra and the X 100 objective was used.

The signal to noise ratio is considerably reduced in confocal mode especially when the fibres are small because of the resulting loss of photons.

In confocal mode, the contribution of the cellulose filter in the spectrum of a fibre having a diameter of 4 μm is similar to the microprobe mode. The band area ratio of cellulose filter to amosite is about 1.1 in both cases. Nevertheless, the band area ratio of hotstrip to amosite are slightly smaller (1.4) in confocal than in microprobe (2.0) mode. The difference between the two modes is more significant for a fibre having a larger diameter (6 μm). Indeed, the contribution of the cellulose filter in the spectrum and the band area ratio of hotstrip to amosite is about 0.26 and 0.75 in confocal mode, compared with 0.73 and 1.8 in microprobe mode.

In confocal mode the signal to noise ratio is rather poor and the contribution of cellulose filter is only reduced.

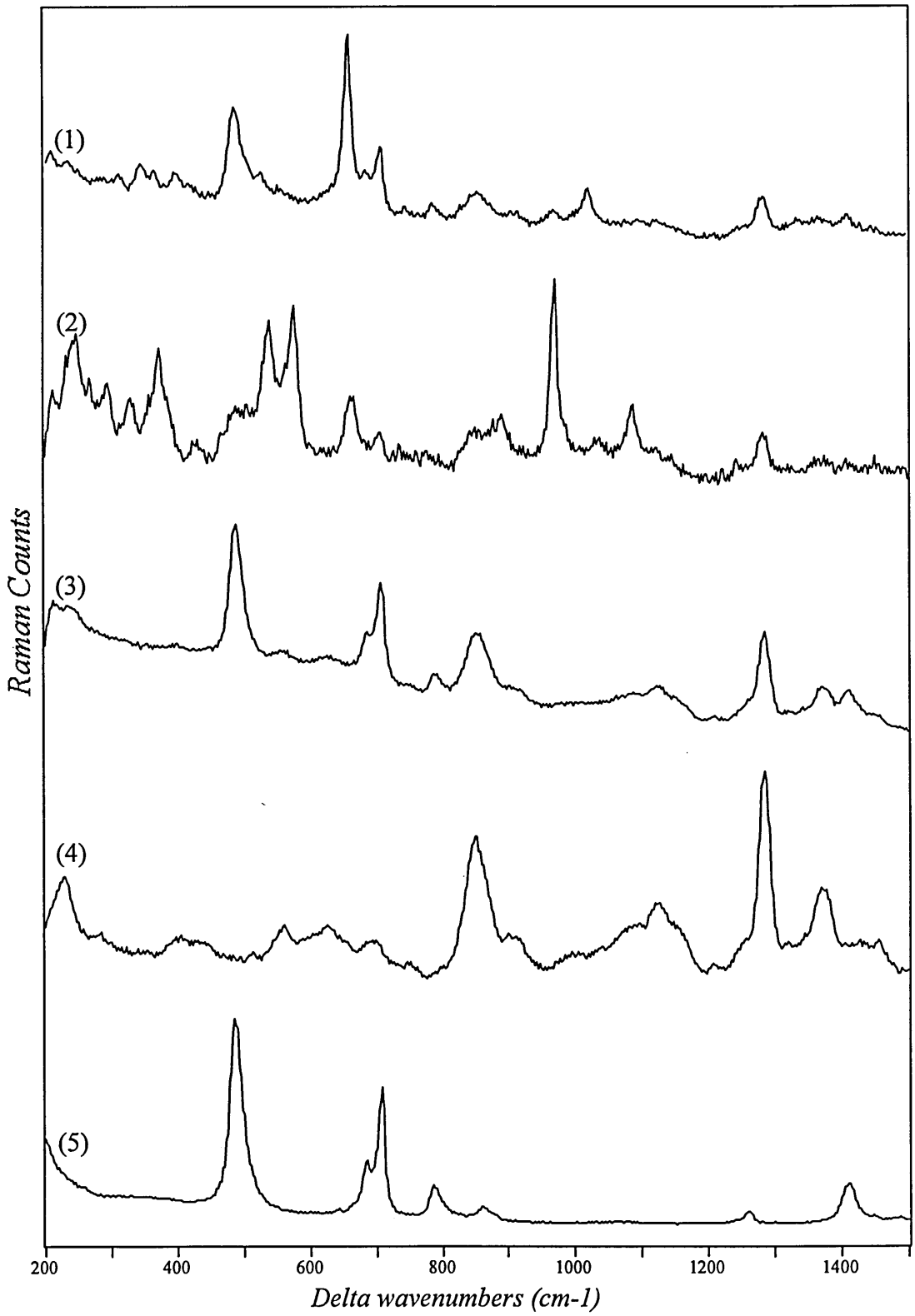

Figure 6.16: Raman spectra collected on wet asbestos fibres and wet cellulose filter in comparison with cellulose filter and hotstrip. (1) wet amosite fibre of 5 μm of diameter, red laser, X 100 objective, $T_{tot} \approx 21.0$ min; (2) wet crocidolite fibre of 5 μm of diameter, red laser, X 100 objective, $T_{tot} \approx 42.1$ min; (3) wet cellulose filter, red laser, X 50 objective, $T_{tot} \approx 3.5$ min; (4) cellulose filter; (5) hotstrip.

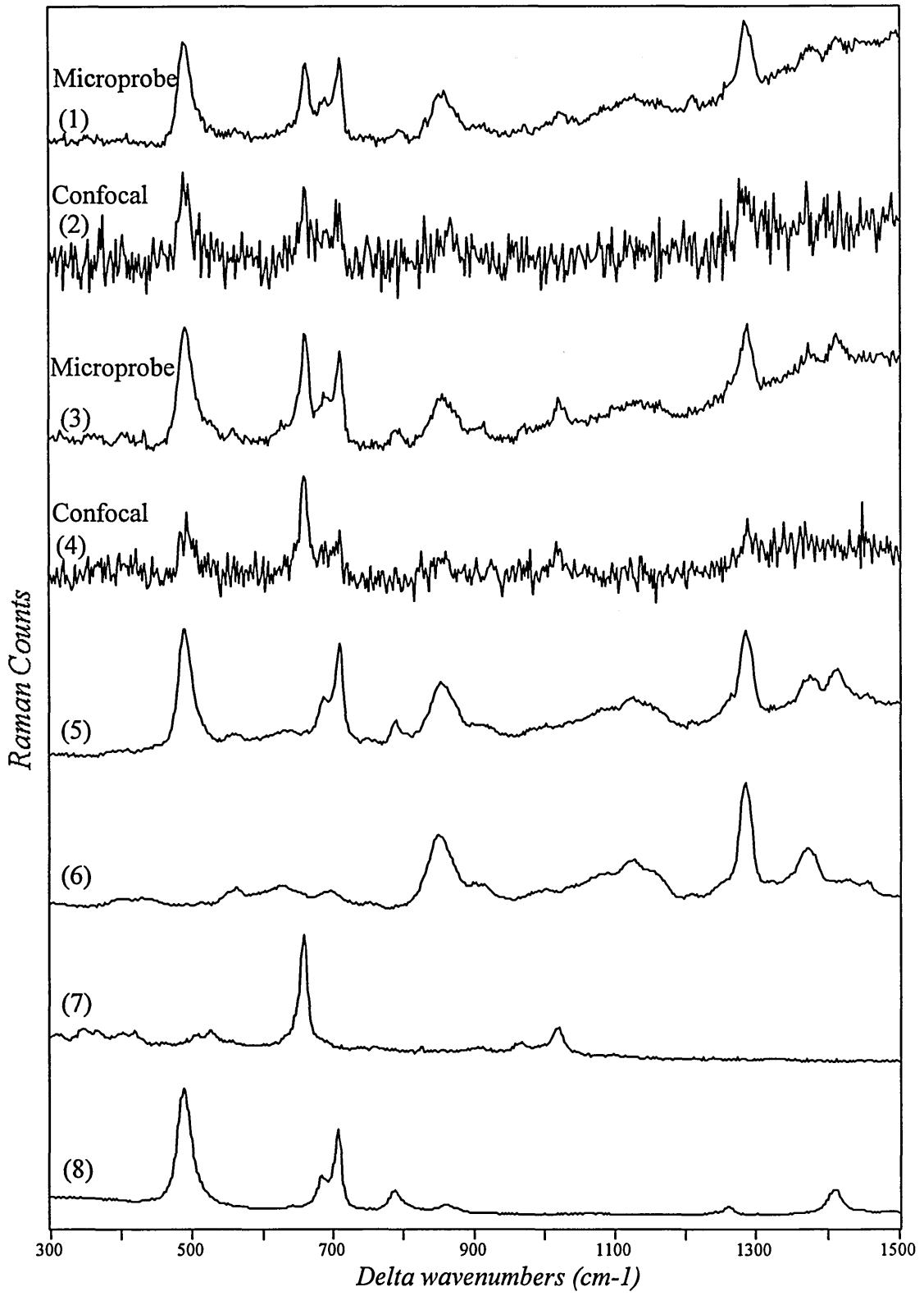

Figure 6.17: Raman spectra collected on wet amosite fibres (using the confocal and microprobe mode) and wet cellulose filter in comparison with cellulose filter, amosite, and hotstrip. (1) wet amosite fibre of 4 μm of diameter, microprobe mode, red laser, X 100 objective, $T_{tot} \approx 43.7$ min; (2) wet amosite fibre of 4 μm of diameter, confocal mode, red laser, X 100 objective, $T_{tot} \approx 43.7$ min; (3) wet amosite fibre of 6 μm of diameter, microprobe mode, red laser, X 100 objective, $T_{tot} \approx 43.7$ min (4) wet amosite fibre of 6 μm of diameter, confocal mode, red laser, X 100 objective, $T_{tot} \approx 43.7$ min; (5) wet cellulose filter, red laser, X 50 objective, $T_{tot} \approx 2.7$ min; (6) cellulose filter; (7) amosite reference, (8) hotstrip.

6.2.2. Spraying of commercial wetting agents on free standing asbestos fibres.

6.2.2.1. Materials and methods.

Reference amosite fibres, in a bottle, were wetted with hotstrip using an aerosol spray gun. The wet fibres were then placed on a glass slide, the fibres split up with tweezers and transferred on a cellulose filter by pressing the filter onto the glass slide. However, this method is hazardous and not reliable. During the spraying process, the fibres 'flew' and after, it was difficult to remove them from the bottle. The Raman spectra were collected with the X 100 and X 50 objectives. The instrument was set up in microprobe mode.

6.2.2.2. Results.

Only very small bands from the wetting agent was observed on one Raman spectrum (figure 6.18).

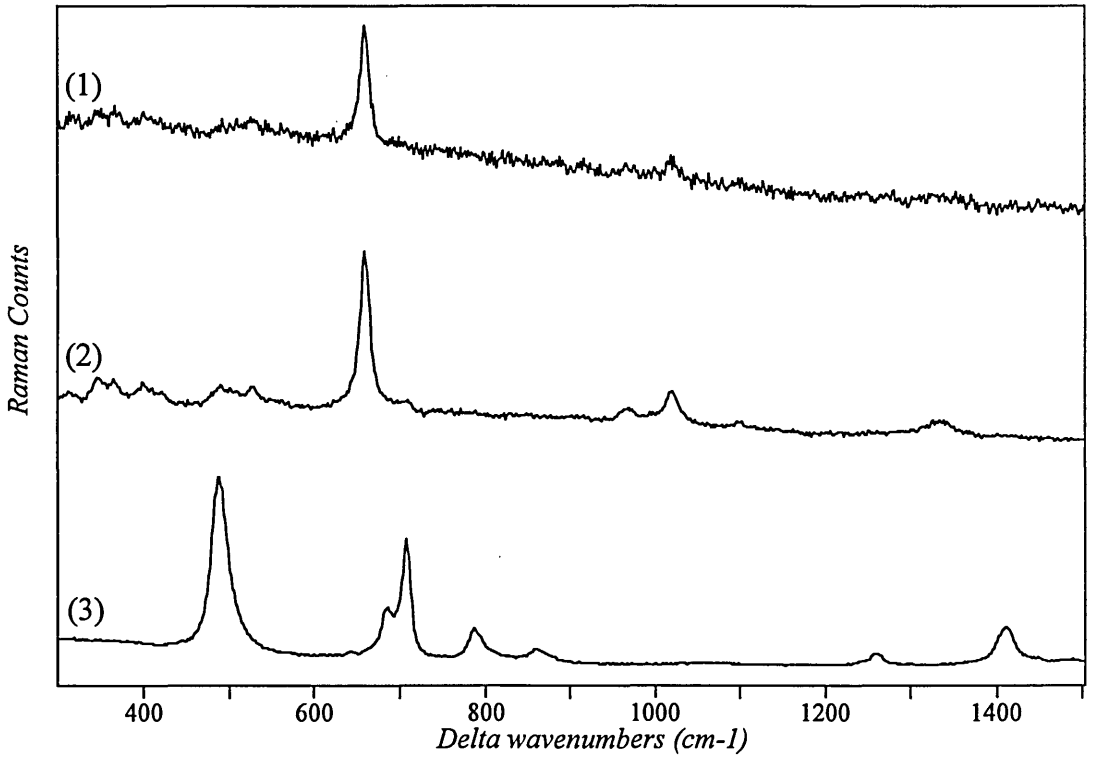

Figure 6.18: Raman spectra collected on wet amosite fibres in comparison with hotstrip. (1) wet amosite fibre of 2 μm of diameter, red laser, X 100 objective, $T_{tot} \approx 15.3$ min; (2) wet bundle of amosite fibres of 40 μm of diameter, red laser, X 50 objective, $T_{tot} \approx 2.6$ min; (3) hotstrip. Cellulose filter subtraction applied on spectra (1) and (2).

6.2.3. Dipping of amosite fibres in a commercial wetting agent.

6.2.3.1. Materials and method.

Reference amosite fibres were dipped in hotstrip. The wetted fibres were then placed on a paper in order to drain the wetting agent. Two days later, the fibres were placed on a glass slide, split up with tweezers and transferred on a cellulose filter by pressing the filter onto the glass slide. The spectra were collected using the X 100 objective and the instrument was set in microprobe mode.

6.2.3.2. Results.

There is no evidence of wetting agent by Raman (figure 6.19).

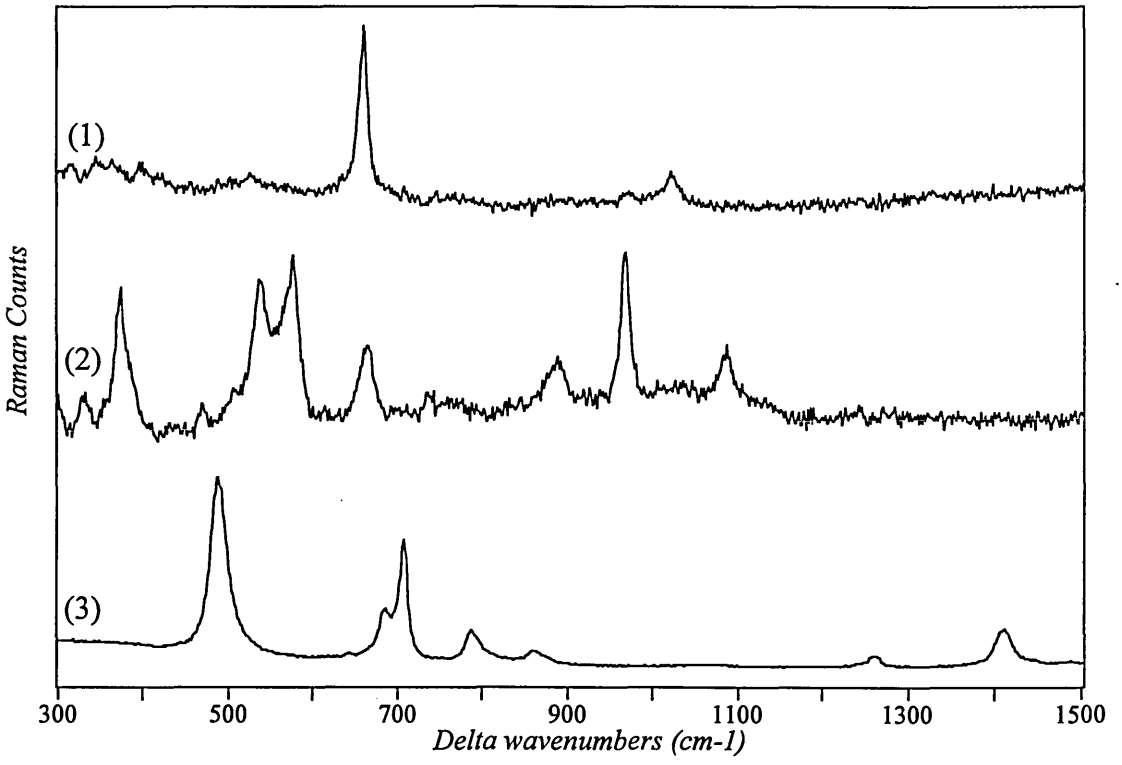

Figure 6.19: Raman spectra collected on wet asbestos fibres in comparison with hotstrip. (1) wet amosite fibre of 5 μm of diameter, red laser, X 100 objective, $T_{tot} \approx 18.1$ min; (2) wet crocidolite fibre of 5 μm of diameter, red laser, X 100 objective, $T_{tot} \approx 18.1$ min; (3) hotstrip. Cellulose filter subtraction applied on spectra (1) and (2).

Hotstrip, which is pure PDMS and penetrant n°1, a water based encapsulating agent show two totally different wetting behaviour. Indeed, when penetrant n°1 was sprayed on asbestos fibres attached to cellulose filter, different types of drops and patches like diffuse areas were observed while no drops were formed from hotstrip on the fibres.

The PDMS consists of:

- the reactive inorganic siloxane backbone associated with high surface energies.
- and the inert organic hydrocarbon having low surface energy.

This explains the very low surface tension (20mN/m) of PDMS[4]. Liquids, with low surface tension, generally, easily wet most solid surfaces giving a zero contact angle. In this case, the force of attraction between the solid and liquid is higher than those between liquid and liquid[5]. One of the PDMS properties is indeed its spreading or 'creep' behaviour[6]. When sprayed on asbestos, PDMS in fact spread around the curve shape of the fibres while the cellulose filter or the paper, which is a porous material absorbed the liquid. On the other hand, the penetrant n°1 probably possesses a high surface tension which generally gives a finite contact angle. In this case, the cohesion between the molecules of the liquid become the dominant forces[5]. Therefore, drops were observed on asbestos giving an adhesional wetting between the fibres and the encapsulating agent.

The fibres were only partially wetted with penetrant n°1, whereas PDMS spread all over the filter.

6.3. Man made vitreous fibres.

6.3.1. Wetting by capillary action.

6.3.1.1. Materials and method.

Cylinders of man made mineral fibres (MMMF) and ceramic fibres were wetted with hotstrip, by capillary action, from the bottom and top of the cylinders. The volume of wetting agent which was used, corresponded to 40 % of the cylinder volume. Samples of fibres taken on top of the cylinders were directly placed on cellulose filter. The spectra were collected using the X 100 and X 50 objective. The instrument was set up in microprobe mode.

6.3.1.2. Results.

The cylinders wetted from the bottom, do not show evidence of hotstrip by Raman or optical microscopy (figures 6.20). The wetting agent clearly remained at the bottom.

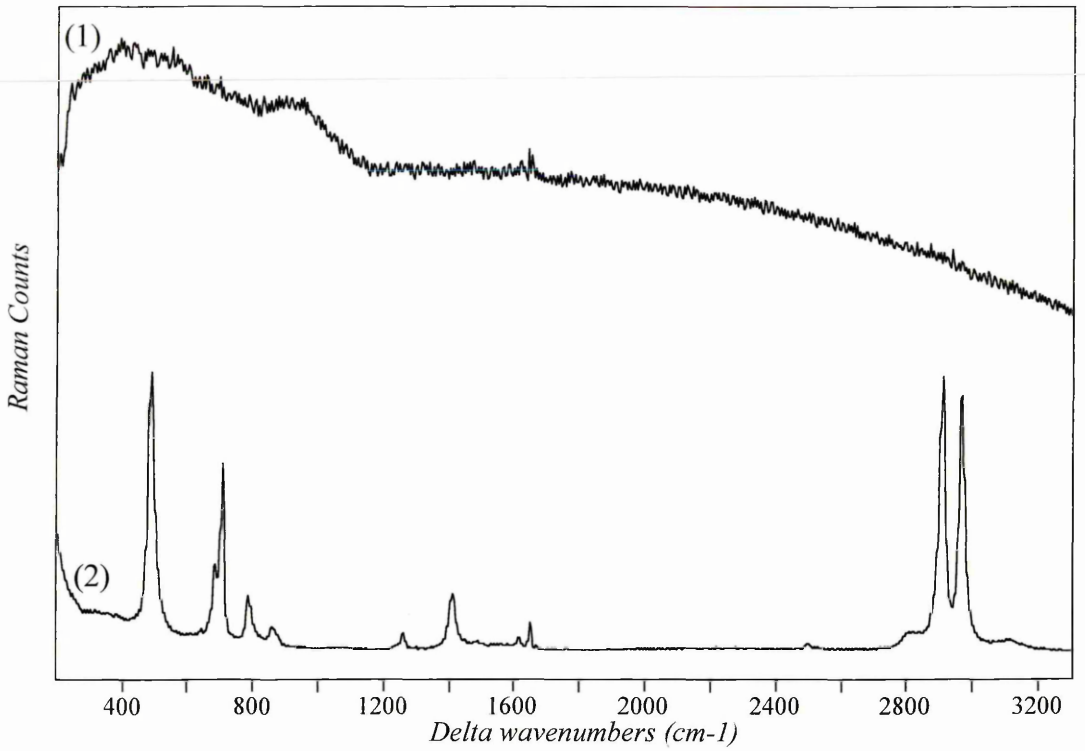

Figure 6.20: Raman spectrum collected on MMMF in comparison with hotstrip. (1) MMMF of 12 µm of diameter, red laser, X 100 objective, $T_{tot} \approx 56.9$ min; (2) hotstrip.
Cellulose filter subtraction applied on spectrum (1).

In the case of the cylinders wetted from the top, the Raman spectra display strong bands from the wetting agent. The micrograph of a typical wet fibre showing two different contrasting areas is given in figure 6.21. Two spectra were collected from these areas, showing, both, the presence of wetting agent around the fibre (figure 6.22).

Mineral fibres display broad bands in their Raman spectra making more difficult the estimation of the relative coverage of wetting agent along the fibres.

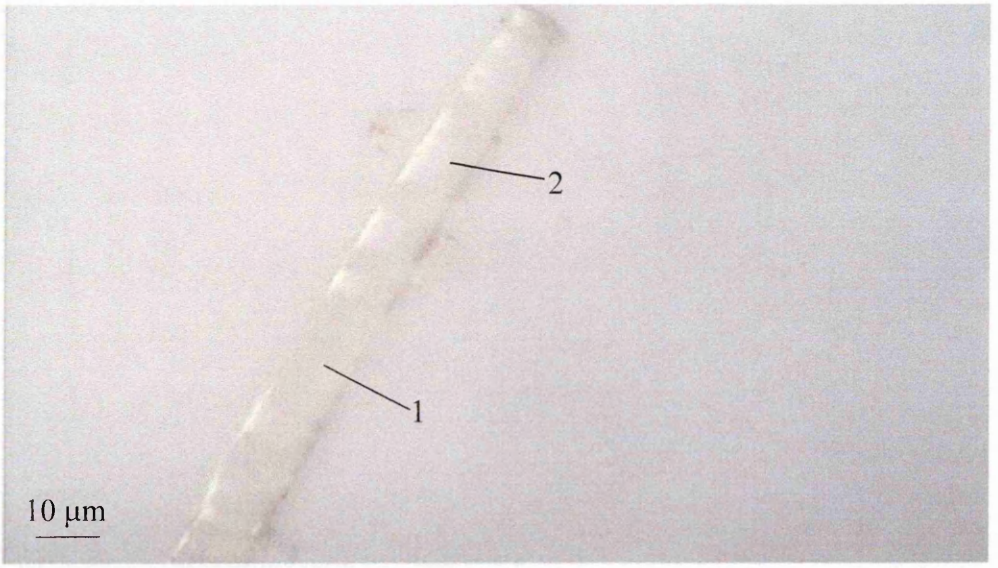

Figure 6.21: Micrograph of a wet MMMF.

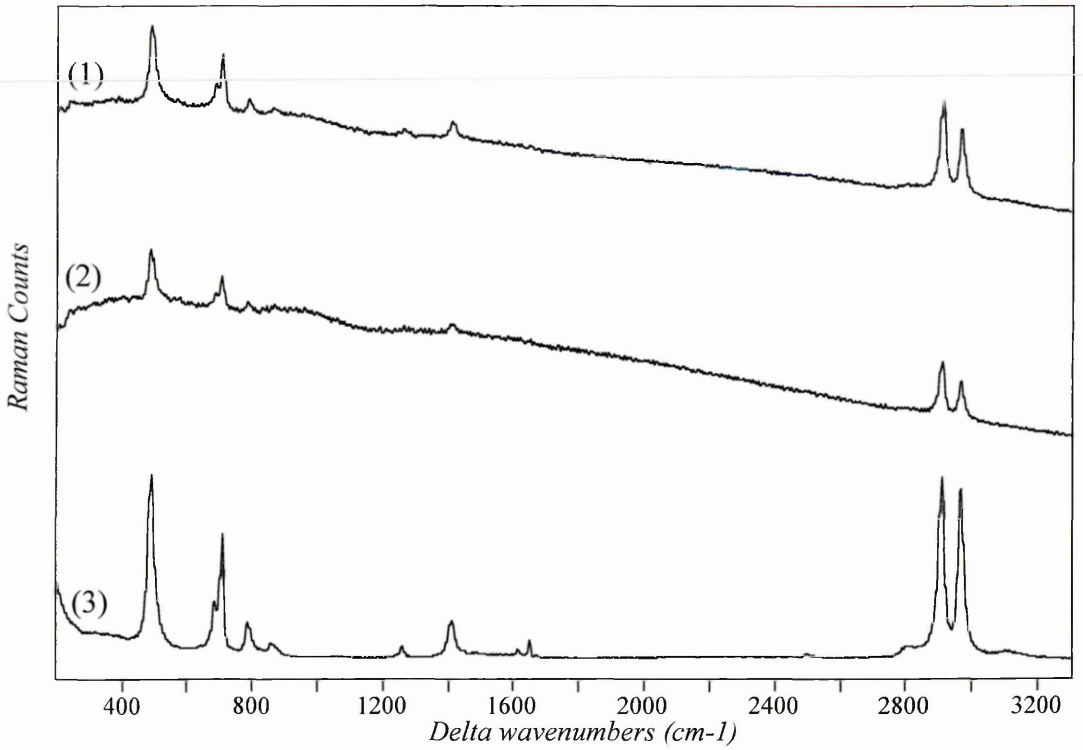

Figure 6.22: Raman spectra collected on a wet MMMF in comparison with hotstrip. (1) and (2) wet MMMF of 10 μm of diameter (position 1 and 2 shown in figure 6.21), red laser, X 50 objective, $T_{tot} \approx 6.3$ min; (3) hotstrip - Cellulose filter subtraction applied on spectra (1) and (2).

It is to be noted that no drops were observed on the fibres attached to cellulose filter. On the other hand, single fibres, not very well attached to the filter, exhibit drops around them. But, if the red laser is focused on a drop, this one moves along the fibre or totally disappears (figure 6.23).

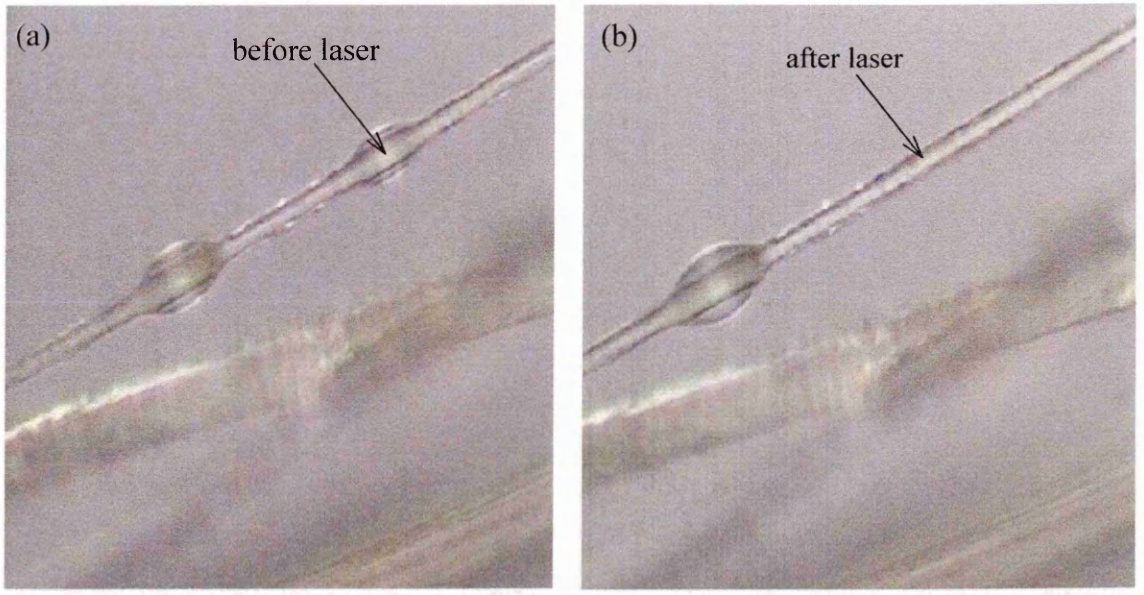

Figure 6.23: Micrograph of a wet MMMF before (a) and after (b) laser heating.

The same results and conclusions were obtained for ceramic fibres.

PDMS did not penetrate the MMMF cylinders. The liquid is drained at the bottom of the cylinder. In this case, the capillary wetting process is limited since the size of voids between fibres are too great for the liquid to bridge.

6.4. Calcium silicate.

6.4.1. Wetting by capillary action using commercial wetting agents and emulsions.

6.4.1.1. Wetting agents.

6.4.1.1.1. Materials and method.

Cylinders of calcium silicate were wetted with astrip and hotstrip, by capillary action. Astrip was diluted before used. Samples taken on top and bottom of the wet materials were directly placed on cellulose filters. The spectra were collected using the X 50 and X 100 objectives. The instrument was set in microprobe mode.

6.4.1.1.2. Results.

As shown in chapter 5, the calcium silicate material gives spectra characteristic of $CaCO_3$ (sharp band at 1085 cm^{-1}) and quartz (sharp band at 465 cm^{-1}). The carbonate bands may be due to a surface reaction of calcium silicate or hydrated calcium silicate with CO_2 from air. $CaCO_3$ and quartz may also arise from impurities. It should also be noted that the bands associated with hydrated calcium silicate (C-S-H) are weak due to its poor crystallinity. In fact, only one part of the material of calcium silicate or hydrated calcium silicate probably adsorbed the CO_2 from the air.

- ***Hotstrip.***

A cylinder of calcium silicate was wetted with hotstrip from the top of the cylinder, and then placed at 270°C in an oven. The volume of wetting agent which was used, corresponded to 50 % of the cylinder volume. Before heating, the wetting agent remained at the bottom but after heating, hotstrip was completely adsorbed.

There is Raman evidence of hotstrip at the top of the cylinder.

A cylinder of calcium silicate was wetted with hotstrip from the bottom at room temperature. The volume of wetting agent which was used, corresponded to 60 % of the cylinder volume. After sometime, hotstrip was completely adsorbed.

A spectrum from a sample taken on top of the cylinders clearly proves the presence and diffusion of hotstrip in all the material (figure 6.24).

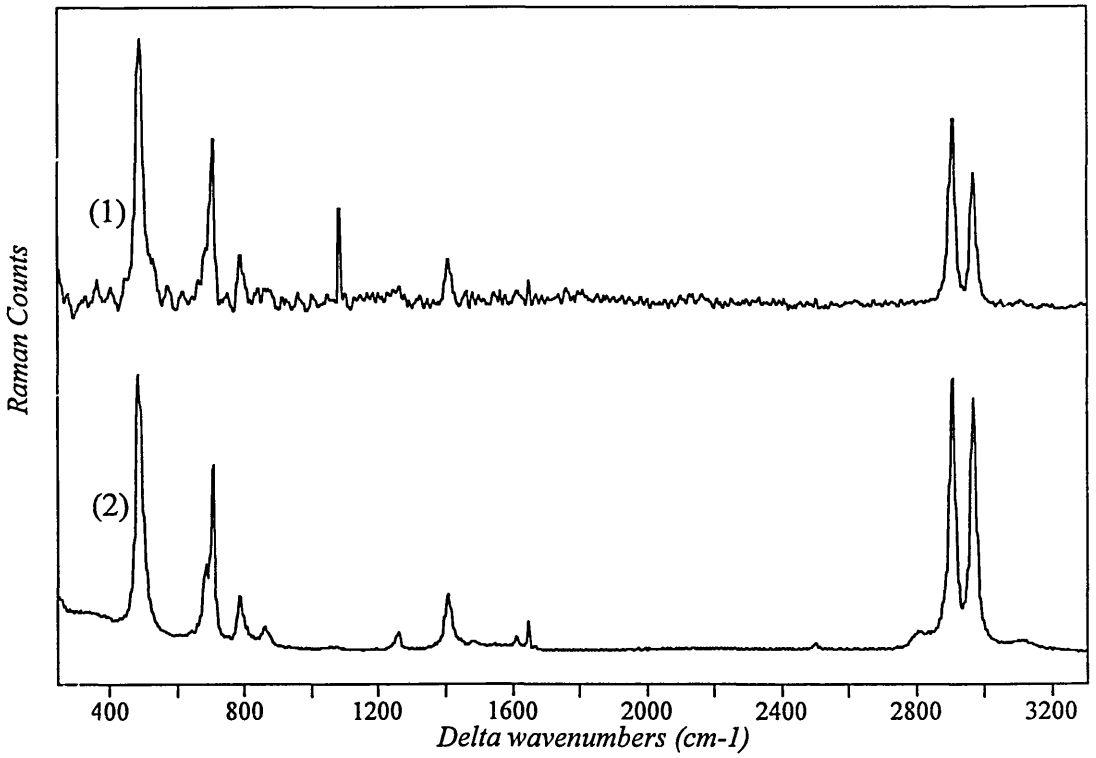

Figure 6.24: Raman spectrum collected on a wet particle in comparison with hotstrip. (1) particle of 12 µm of diameter, red laser, X 100 objective, $T_{tot} \approx 3.8$ min; (2) hotstrip. Cellulose filter subtraction and smoothing function (Savitsky Golay, degree 2, 21 points) applied on spectrum (1).

• ***Astrip.***

Pieces of calcium silicate were wetted with astrip at different dilution from the bottom. The volume of wetting agent which was used corresponded to 60 % of the cylinder volume. Solutions of astrip in water at concentrations of 1 volume of astrip for 10 and 15 volumes of water were applied.

The Raman spectra of particles taken at the bottom and top of the materials display clearly bands from the wetting agent (figure 6.25). The solution diffused into the material up to the top. The bands in the spectra of the material wetted with the more diluted solution are rather weak and at the limit of detection.

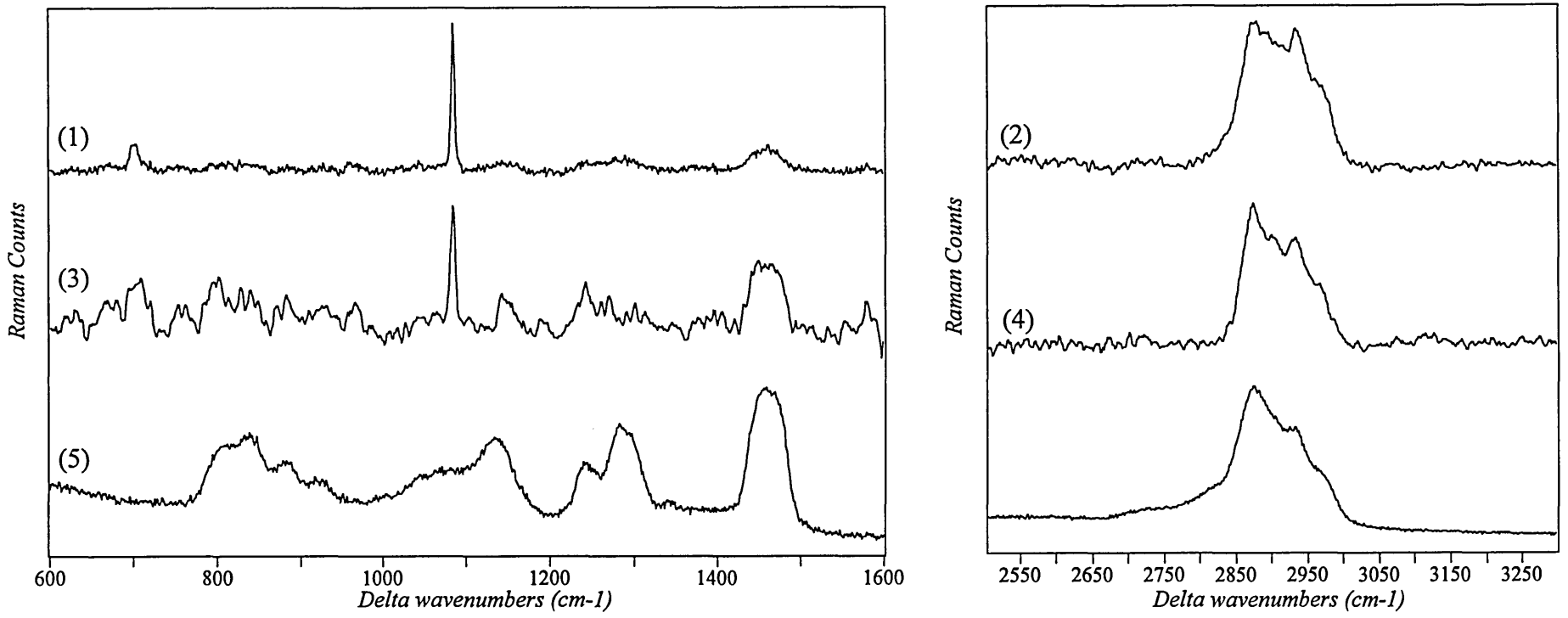

Figure 6.25: Raman spectra collected on particles from a wet cylinder in comparison with astrip (1/10). (1) and (2) particle from the bottom of the cylinder, red laser, X 50 objective, (1) $T_{tot} \approx 5.7$ min, (2) $T_{tot} \approx 5.9$ min; (3) and (4) particle from the top of the cylinder, red laser, X 50 objective, (3) $T_{tot} \approx 3.4$ min, (4) $T_{tot} \approx 5.9$ min; (5) astrip.
Cellulose filter subtraction and baseline correction applied on spectra (1) to (4), smoothing function (Savitsky Golay, degree 2, 11, 15 and 19 points) applied on spectra (2) (3) and (4) respectively.

Both astrip and hotstrip wetted the calcium silicate material very well. Nevertheless, the shape of calcium silicate particles is different than that of man made mineral fibres. The calcium silicate material is a porous solid which possesses spaces between the particles. These spaces are arrays of capillaries through which the liquid can penetrate and air can escape[7].

6.4.1.2. Emulsions.

6.4.1.2.1. Materials and method.

Pieces of calcium silicate were wetted with silicone emulsions by capillary action from the bottom and then cut in three parts. Different volumes of emulsions at different concentration were applied. Samples were directly placed on cellulose filter for Raman analysis. The spectra were collected using the X 50 and X 100 objectives. The instrument was set up in microprobe mode.

6.4.1.2.2. Results.

The volumes of silicone emulsions which were used, corresponded to 50 % and 60% of the volume of the calcium silicate material. The original silicone emulsions contain 40 % of water in weight. Nevertheless, more diluted emulsions, from one volume of the original emulsions for 10 to 20 volumes of water, were applied.

The visible liquid front reaching the top of the pieces was an indication of a complete wetting.

The wetting agent was detected in the lower part of the calcium silicate materials. The particles are mainly covered with the silicone particles only in the first and or the beginning of the second part of the material (figure 6.26). The rest of the material was mainly wetted with water since the spectra do not show silicone bands. The calcium silicate material seems to act like a chromatography column which separates water from silicone. The silicone is left at the bottom part of the material while water diffuses up to the top.

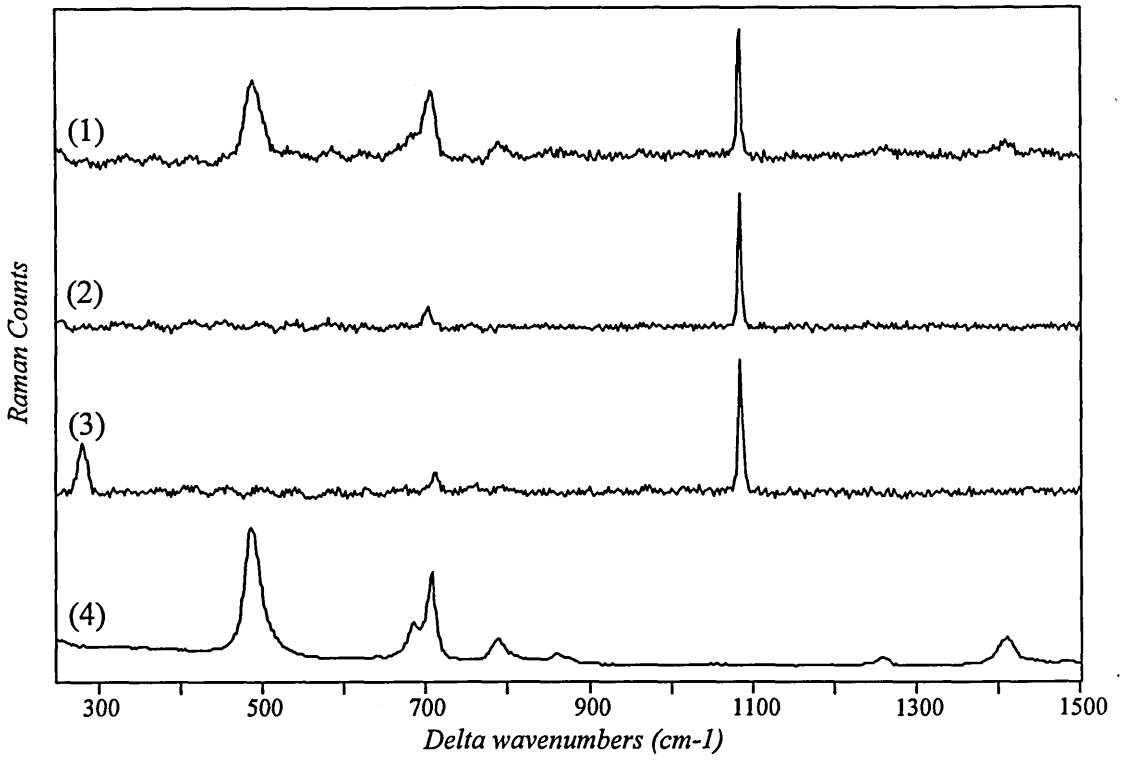

Figure 6.26: Raman spectra collected on particles from a wet cylinder in comparison with the silicone emulsion (1/10, 50% in volume). (1) particle of 12 μm size from the first part of the cylinder, red laser, X 50 objective, $T_{tot} \approx 7.6$ min; (2) particle of 30 μm size from the second part of the cylinder, red laser, X 50 objective, $T_{tot} \approx 7.6$ min; (3) particle of 10 μm size from the third part of the cylinder, red laser, X 50 objective, $T_{tot} \approx 38$s; (4) emulsion.
Cellulose filter subtraction and baseline correction applied on spectrum (1) to (3).

6.5. Conclusion.

Inorganic fibres such as asbestos and man made mineral fibres as well as calcium silicate were the main materials investigated in the wetting process. The fibres and particles were transferred, after wetting, on cellulose filters for Raman analysis or in some cases directly wetted and analysed on the filters. The two principal modes of wetting were the spraying with an aerosol and the capillary action.

The coverage measurements of wetting agents on fibres and particles, on a few μm scale, was successfully achieved by Raman microspectroscopy. The amount and distribution of wetting and encapsulating agents along individual fibres were estimated from the area bands ratio of wetting and encapsulating agent to asbestos. These measurements correlated very well with the micrographs of wet fibres.

Important information on the ability of these liquids to wet or spread on inorganic fibres and other types of materials such as calcium silicate was also obtained. Hotstrip, which is pure PDMS and penetrant n°1, a water based encapsulating agent show two totally different wetting abilities. Indeed, when penetrant n°1 was sprayed on asbestos fibres attached to cellulose filter, different types of drops and patches like diffuse areas were observed while no drops were formed from hotstrip on the fibres. When sprayed on asbestos, PDMS spread and drained around the curve shape of the fibres while the cellulose filter or the paper, which is a porous material absorbed the liquid. This behaviour was explained by the fact that PDMS has a low surface tension and a very small contact angle. On the other hand, the penetrant n°1, possesses probably a high surface tension giving a much higher contact angle. Therefore, drops were observed on asbestos showing adhesional wetting between the fibres and the encapsulating agent.

The fibres were only partially wetted with penetrant n°1 whereas PDMS spread all over the filter.

PDMS did not successfully wet the cylinders of man made mineral and ceramic fibres. The liquid was drained at the bottom of the cylinder. In this case, the capillary wetting process is limited since the size of voids between fibres are too great for the liquid to bridge.

Astrip and hotstrip wetted both very well the calcium silicate materials. The shape of calcium silicate particles is totally different than that of man made mineral fibres. Indeed, the calcium silicate material is a porous solid which has spaces between the particles. The liquid penetrated through these capillaries while air escaped.

The silicone emulsions wetted heterogeneous the calcium silicate materials leaving the silicone at the bottom while water diffused up to the top. The silicone emulsions were not used as a wetting agent for wet asbestos removal process.

[1] C.Dyer and B.J.E. Smith. J. Raman Spectrosc., 26, 777-785, 1995.
[2] T.F.Bergin. Microscope, 39, 287-298, 1991.
[3] K.P.J.Williams, G.D.Pitt, D.N.Batchelder and B.J.Kip. Appl. Spectrosc., 48, 232-235, 1994.
[4] D.Narula. Jalca, 90, 93-98, 1995.
[5] D.J.Shaw. Introduction to Colloid and Surface Chemistry, 4 th Ed., Butterworth Heinemann, 306 pp, 1991.
[6] M.J.Owen. Chemtech, 11, 288-292, 1981.
[7] M.J.Jaycock and G.D.Parfitt. Chemistry of Interfaces, Ellis Horwood Limited Ed., John Wiley and Sons, New York, 279 pp, 1981.

CHAPTER 7

RAMAN MICROSPECTROSCOPY FOR THE INVESTIGATION OF THE WETTING PROCESS ON ASBESTOS CONTAINING MATERIALS

7. Raman microspectroscopy for the investigation of the wetting process on asbestos containing materials.

7.1. Introduction.

The coverage measurements of wetting agent on fibres and particles from basic laboratory experiments were successfully achieved by Raman microspectroscopy in chapter 6. The distribution and amount of wetting agent were estimated from the variation of relative area of Raman bands of a given wetting agent on reference asbestos fibres. The Raman method for the investigation of the wetting process on inorganic fibres and other particles was applied, in this chapter, on insulation and asbestos containing materials in order to establish a correlation between the Raman experiments and the effectiveness of wetting agent to suppress dust.

The asbestos containing materials under investigation were:
- either directly collected from industrial removal site after wetting.
- or wetted by capillary action in laboratory conditions and then tested in a rotating drum which estimated the concentration of fibres released during disturbance of the material.

Only hotstrip, which is pure PDMS, was used for the wetting of asbestos containing material.

Some spectra shown in this chapter were collected using the continuous extended scanning technique. The total exposure time was calculated from the formula[1] : $T_{tot} \approx (1 + \text{total scan range / average static window length}) \times T_{ex}$; with T_{ex}, the exposure time. Other spectra were collected using the static scanning technique where the acquisition time (T_{aq}) corresponded to the total exposure time.

7.2. Asbestos site removal.

7.2.1. Materials and method.

The wetting and removal process was carried out in Middlesborough for a chemical company by Asbestostrip Innovations. Two meters of an asbestos lagging on a pipe at high temperature was wetted with hotstrip, before removal, in order to prevent the release of fibres. The 12 inch pipe reached a temperature of 270°C. The 4 inch thick lagging was mainly composed of calcium silicate and asbestos. The wetting agent was directly injected inside the lagging, at a rate of 70-80 ml/min from each needles, using a needle system (2 sets of 15 needles) placed as shown in figure 7.1. 18 litres of hotstrip was injected for an insulation volume of 25 litres over four and half hours. A pressure of

3 bar was applied at the liquid in order to obtain a 2 bar pressure at the needles. The wetting process was monitored by inspection of the lagging asbestos.

The samples collected during removal, were placed on a glass slide, the fibres and particles were split up with tweezers and transferred on a cellulose filter by pressing the filter onto a glass slide. The Raman spectra were collected with the X 50 and X 100 objectives using the red laser. The instrument was set up in microprobe mode.

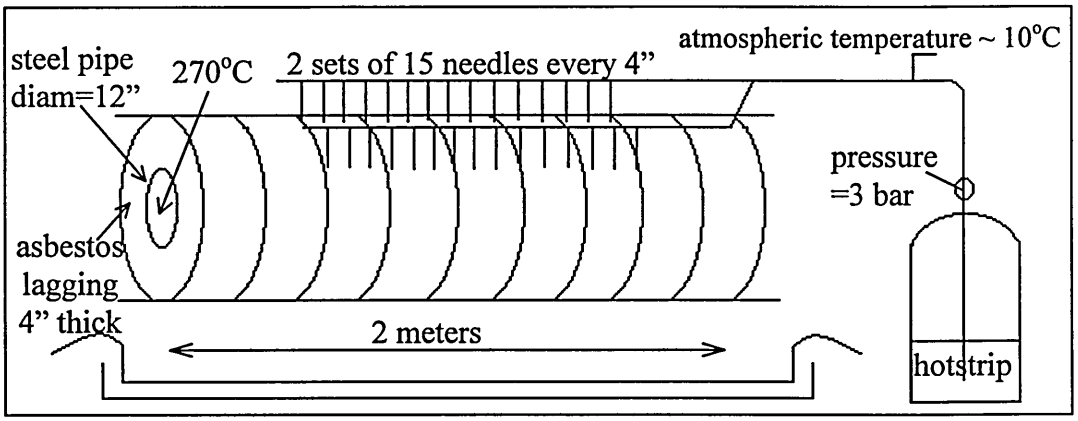

Figure 7.1. schema of the asbestos removal site in Middlesborough.

7.2.2. Results.

After inspection, the removal process was rapidly stopped since the lagging was only partially wet. Nevertheless, two samples collected from the lagging were analysed. One seemed wet while the other seemed dry.

The fibres were identified as amosite fibres. Indeed, the spectra show characteristic features from amosite which are the strong band at 660 cm^{-1} corresponding to the Si bridging-O-Si stretching vibration as well as other bands at 1020 and 528 cm^{-1} (figure 7.3).

As shown previously, the Raman spectra of particles are not characteristic of calcium silicate but calcium carbonate and quartz due to a partial carbonation of the silicate surface. Indeed, the spectrum (1) given in figure 7.2, is characteristic of quartz (showing a strong band at 463 cm^{-1}) associated with CO_3^{2-} (showing a band at 1084 cm^{-1}).

- ***"Dry" sample.***

There is no evidence of wetting agent on the spectra of particles and fibres (figures 7.2 and 7.3) from the "dry" sample, confirming the partial wetting of the asbestos lagging. No drops of wetting agent were observed under the optical microscope.

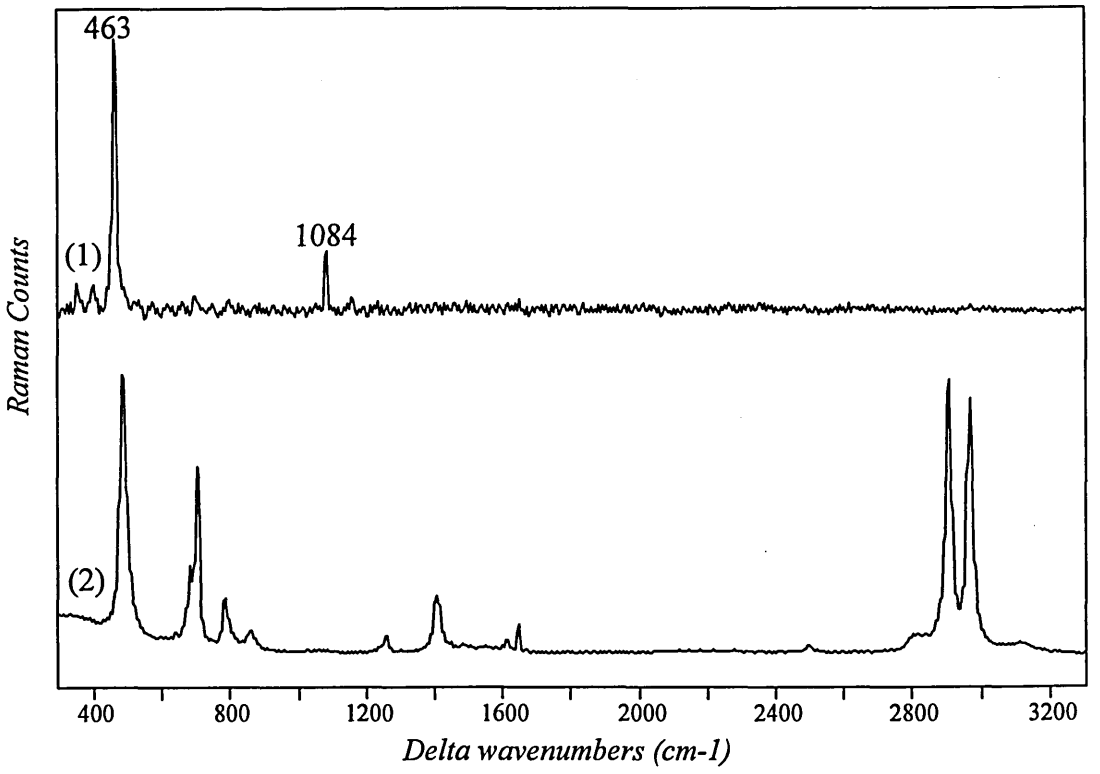

Figure 7.2: Raman spectrum collected on a particle in comparison with hotstrip. (1) particle of 25 μm size, red laser, X 50 objective, $T_{tot} \approx 4.4$ min; (2) hotstrip.
Cellulose filter subtraction and baseline correction applied on spectrum (1).

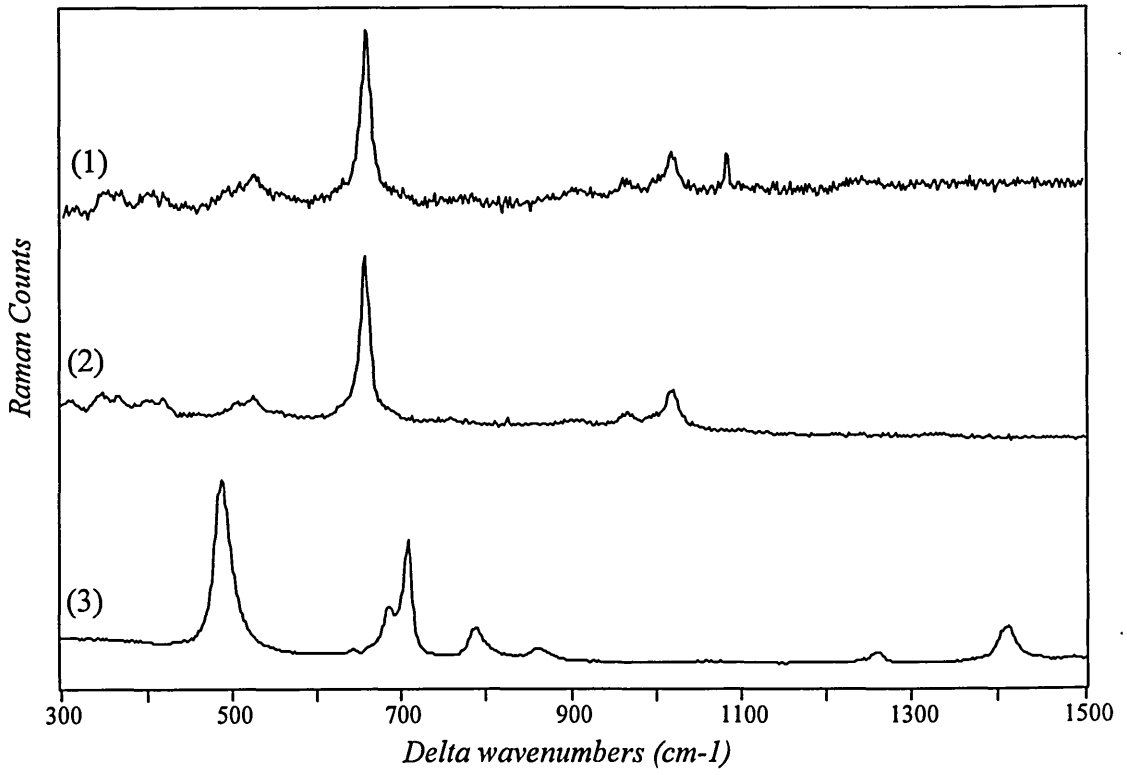

Figure 7.3: Raman spectrum collected on a fibre in comparison with amosite and hotstrip.
(1) fibre of 3 μm of diameter, red laser, X 100 objective, $T_{tot} \approx 31.6$ min; (2) amosite; (3) hotstrip.
Cellulose filter subtraction applied on spectrum (1).

• *"Wet" sample.*

The spectra collected on particles and fibres from the "wet" sample exhibit bands characteristic of PDMS (figures 7.4, 7.6 and 7.9). Neither drop nor wetting agent were observed under the optical microscope.

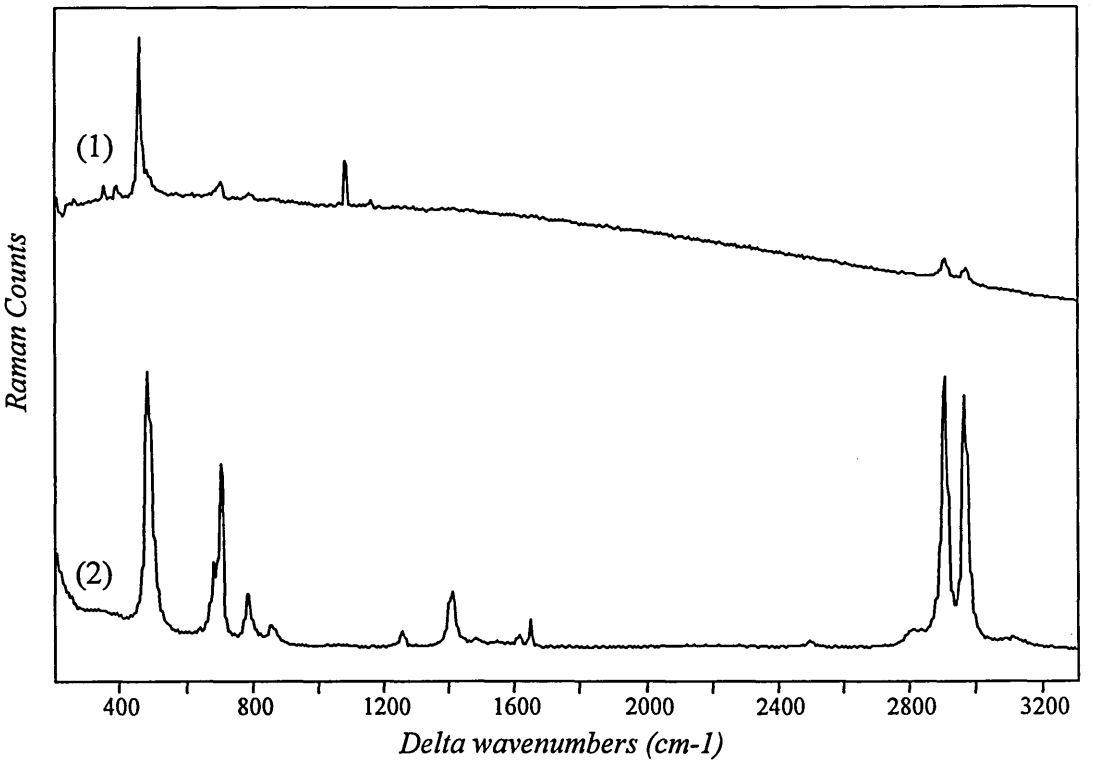

Figure 7.4: Raman spectrum collected on a wet particle in comparison with hotstrip. (1) wet particle of 8x34 μm of size, red laser, X 50 objective, $T_{tot} \approx 15.2$ min; (2) hotstrip. Cellulose filter subtraction applied on spectrum (1).

Coverage measurements of wetting agent along individual fibres were measured using the same method established in chapter 6, which is based on area ratio of the wetting agent to the asbestos bands. Since the amosite bands interfered with the wetting agent bands in some parts of the wet asbestos spectra, the curve fitting method was also applied in order to separate the bands into individual components.

The micrograph of a wet fibre coated with hotstrip is given in figure 7.5 where no drops nor wetting agent are observed. However, the Raman spectra confirm the presence of wetting agent on the amosite fibre (figure 7.6). The relative amount of hotstrip along the fibre was measured. Two regions were fitted using Lorentzian bands after applying a 3 point binomial smoothing function (figures 7.7):

- the 600-745 cm^{-1} region, introducing one band for amosite and two bands for the wetting agent.
- the 440-560 cm^{-1} region, introducing two bands, one of which corresponding to the wetting agent. The second band is an interference due to the notch filters.

A graph was then plotted (figure 7.8) giving the ratio of the area of the wetting agent band at 490 cm^{-1} to the amosite band at 660 cm^{-1} against distance along the fibre.

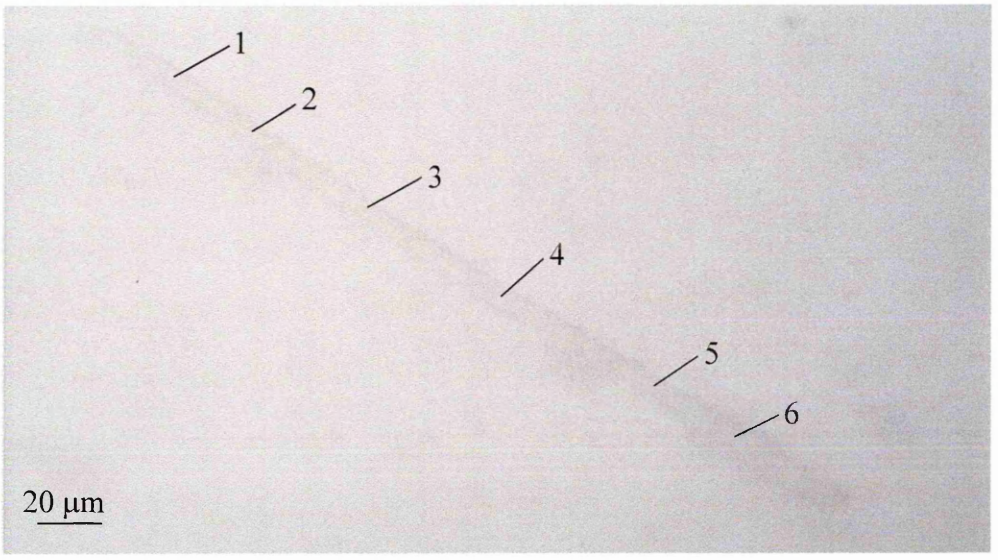

Figure 7.5: Micrograph of a wet fibre.

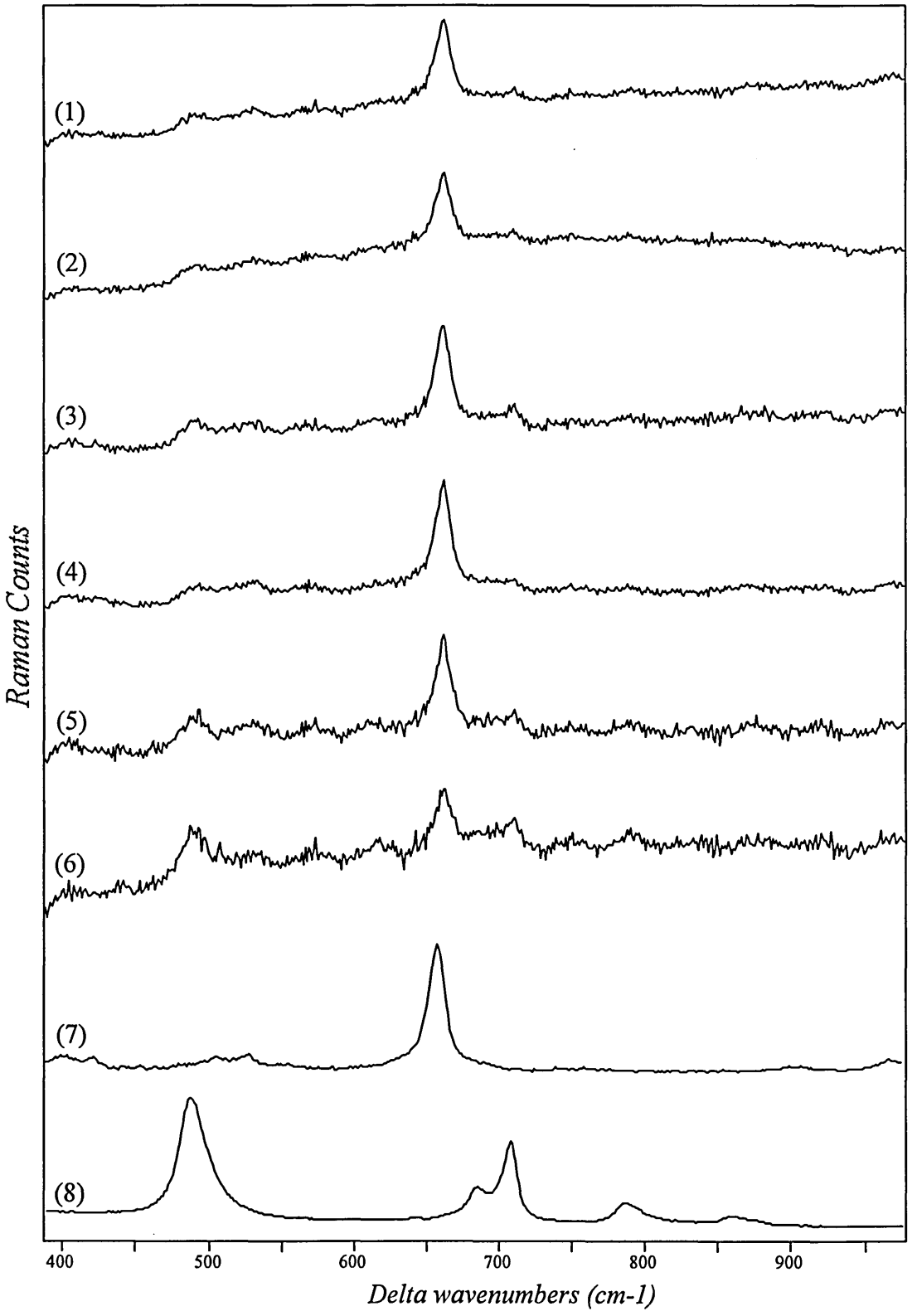

Figure 7.6: Raman spectra collected along a wet fibre in comparison with amosite and hotstrip. (1) to (6) wet fibre of 2 μm of diameter (positions 1 to 6 shown in figure 7.5), red laser, X 100 objective, $T_{aq} \approx 10$ min; (7) amosite reference; (8) hotstrip.
Cellulose filter subtraction applied on spectra (1) to (6).

Figure 7.7.a.

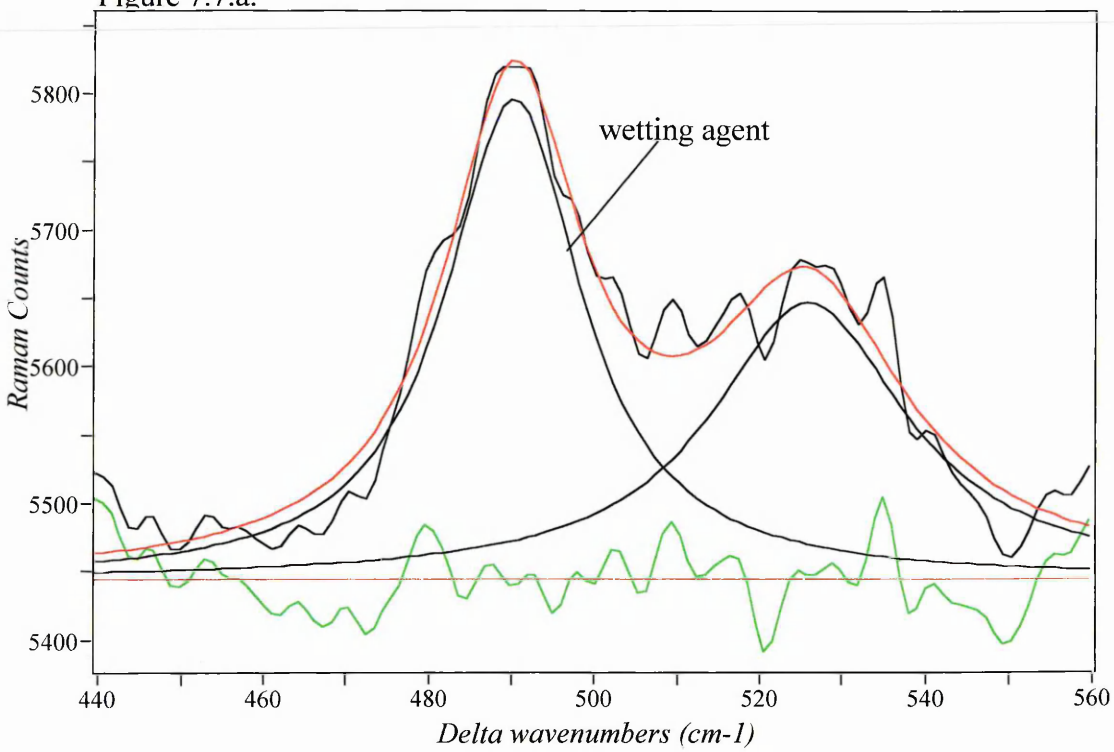

Figure 7.7.b.

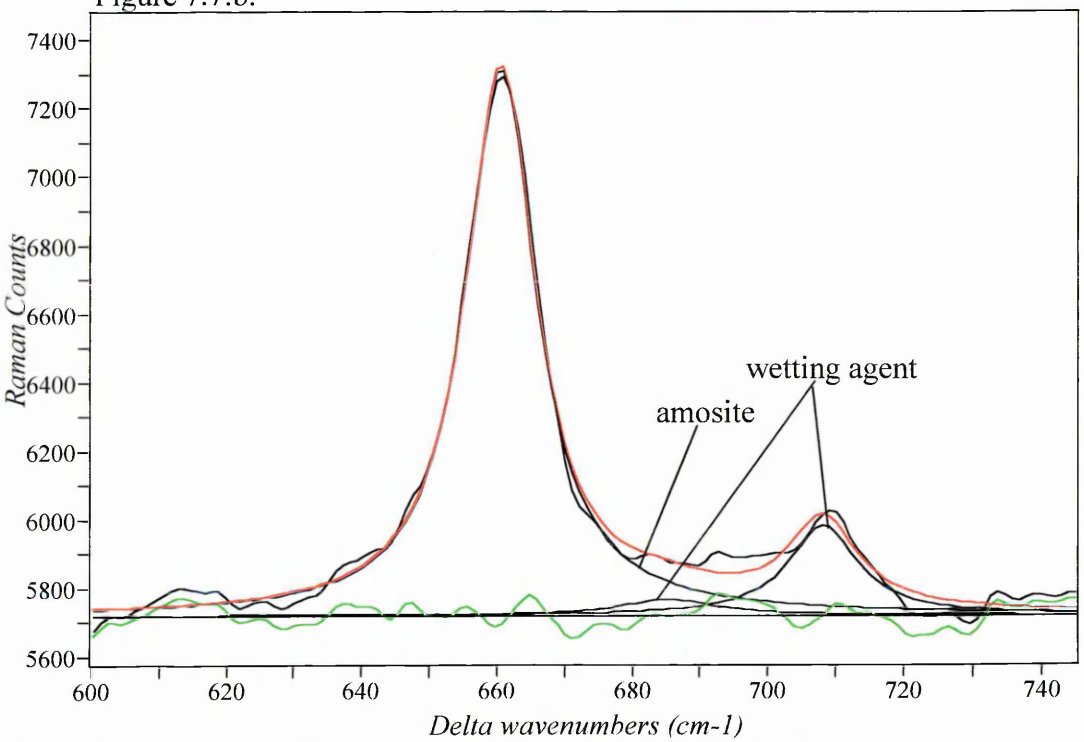

Figure 7.7: Curve fitting of spectrum (3) in figure 7.6 after applying binomial smoothing, introducing Lorentzian bands from the wetting agent and amosite.
Figure 7.7.a. Curve fitting in the 440-560 cm^{-1} region; figure 7.7.b. curve fitting in the 600-745 cm^{-1}.

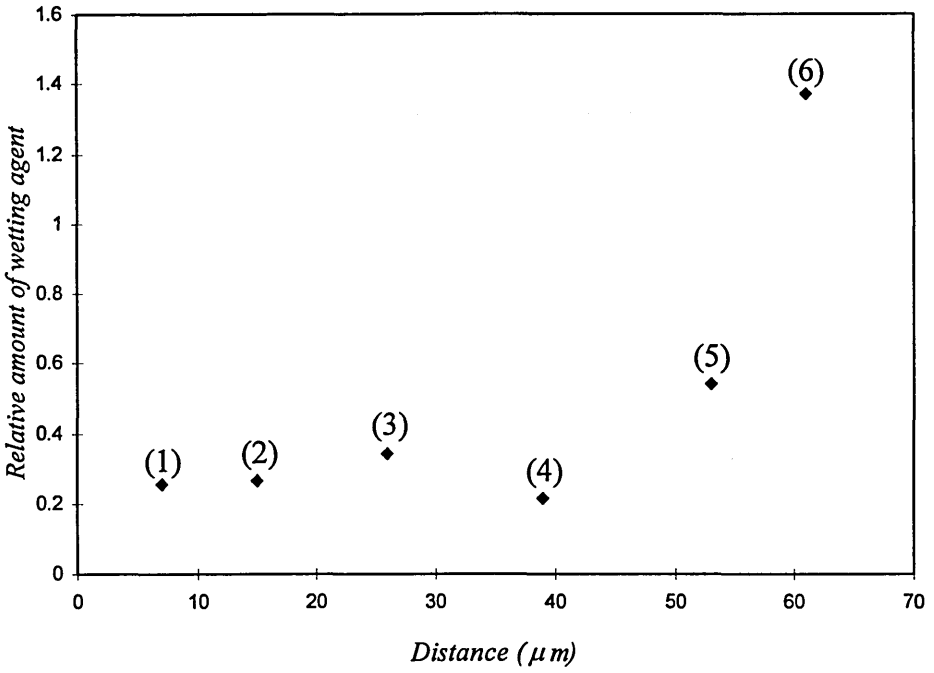

Figure 7.8: Plot of the relative amount of wetting agent along a fibre (figure 7.5) calculated from area bands ratio (spectra 1 to 6 in figure 7.6) of the wetting agent band at 490 cm^{-1} to the amosite at 660 cm^{-1}.

The plot of the relative amount of wetting agent along the fibre shows a rather heterogeneous coverage since the values of the area bands ratio are comprised between 0.2 and 1.4. However, most of these values are found in the 0.2 to 0.6 range.

The micrograph of another wet fibre coated with hotstrip is given in figure 7.10. The Raman spectra confirmed the presence of wetting agent on the amosite fibre (figure 7.9). However, a band at 465 cm^{-1} appears on the spectra characteristic of quartz demonstrating the presence of small impurities on the fibre. The relative amount of hotstrip along the fibre was also measured. Two regions were fitted using Lorentzian bands (figures 7.11):

- the 745-600 cm^{-1} region introducing one band for amosite and two bands for the wetting agent.
- the 440-560 cm^{-1} region introducing three bands, two of which corresponding to the wetting agent and quartz. The last band is an interference due to the notch filters.

A graph was then plotted (figure 7.12) giving the area ratio of the wetting agent band at 490 cm^{-1} to the amosite band at 660 cm^{-1} against distance along the fibre.

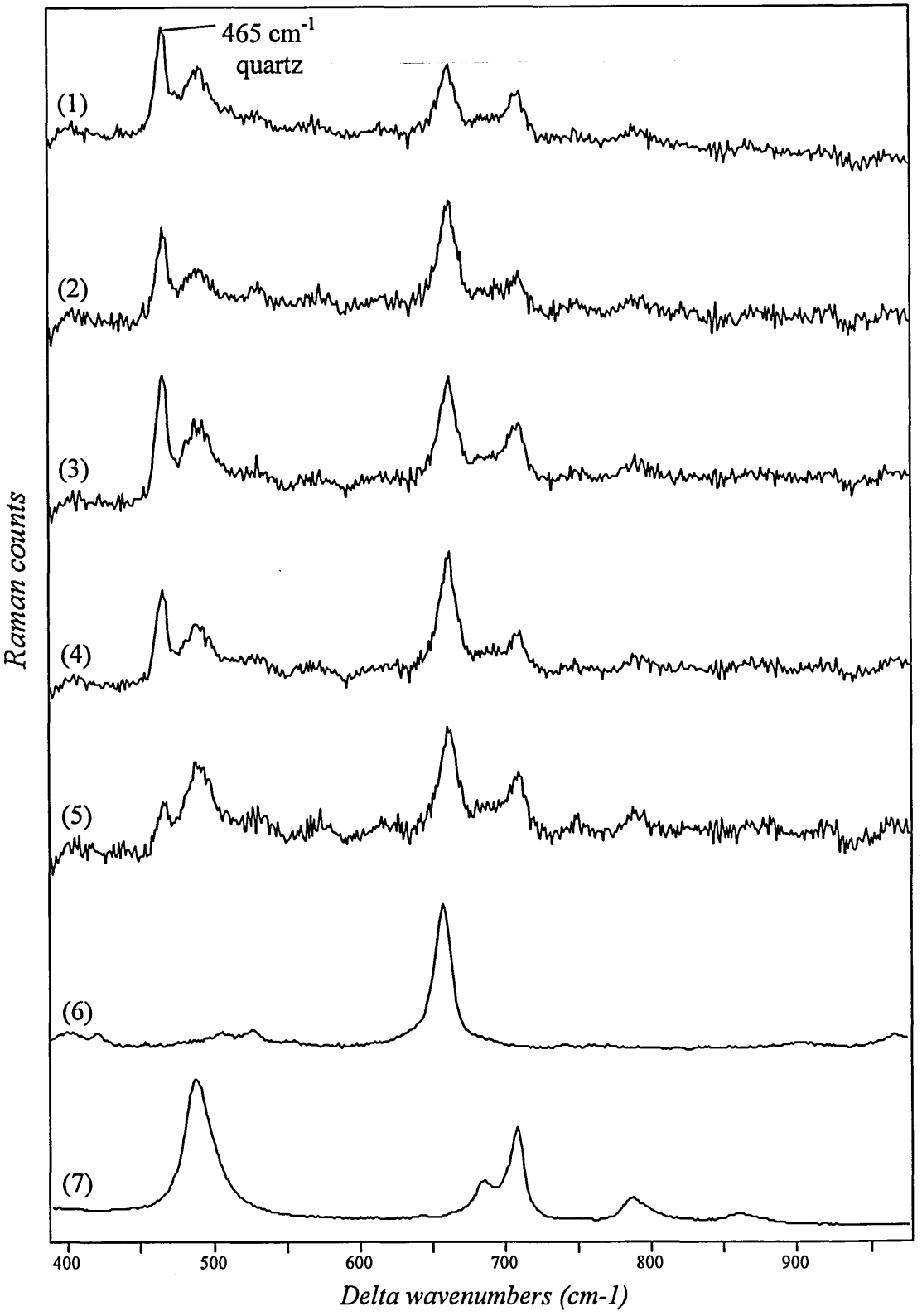

Figure 7.9: Raman spectra collected along a wet fibre in comparison with amosite and hotstrip. (1) to (5) wet fibre of 3 μm of diameter (positions 1 to 5 shown in figure 7.10), red laser, X 100 objective, $T_{aq} \approx 6.7$ min; (6) amosite reference; (7) hotstrip.
Cellulose filter subtraction applied on spectra (1) to (5).

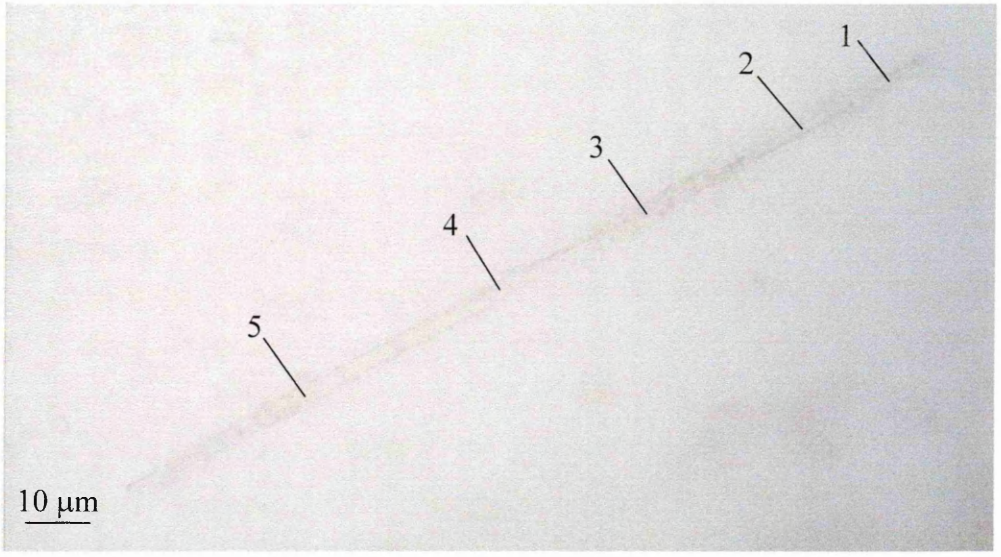

Figure 7.10: micrograph of a wet fibre.

Figure 7.11.a.

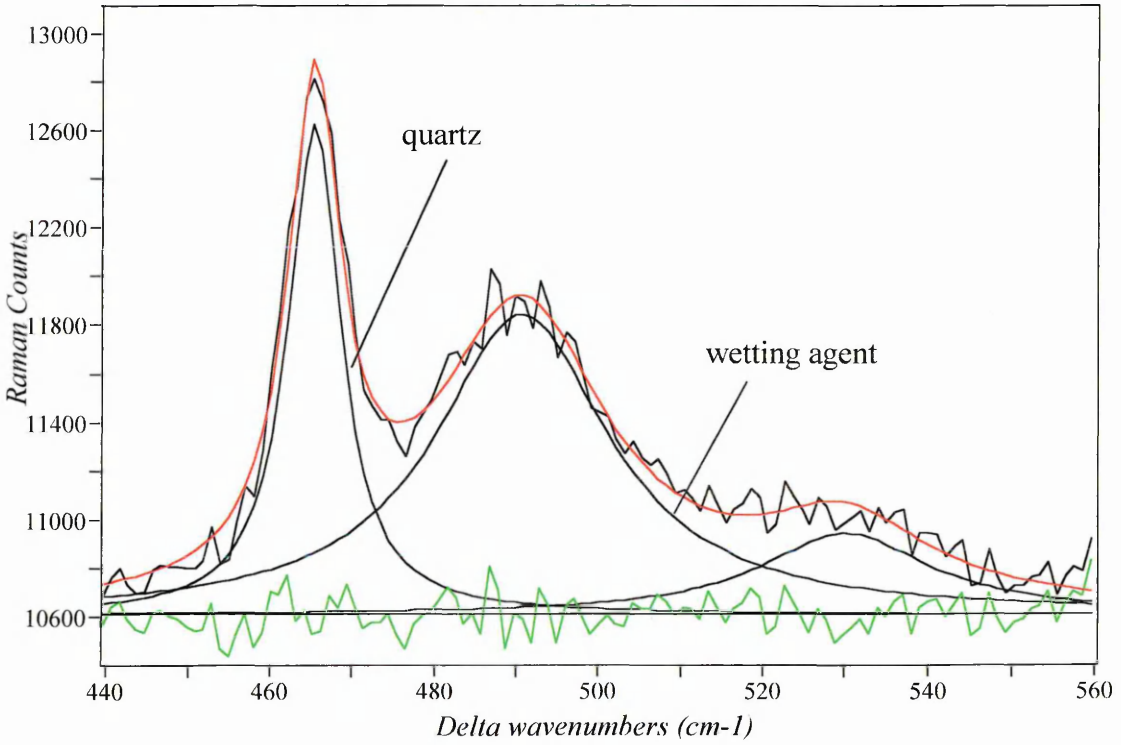

Figure 7.11.b.

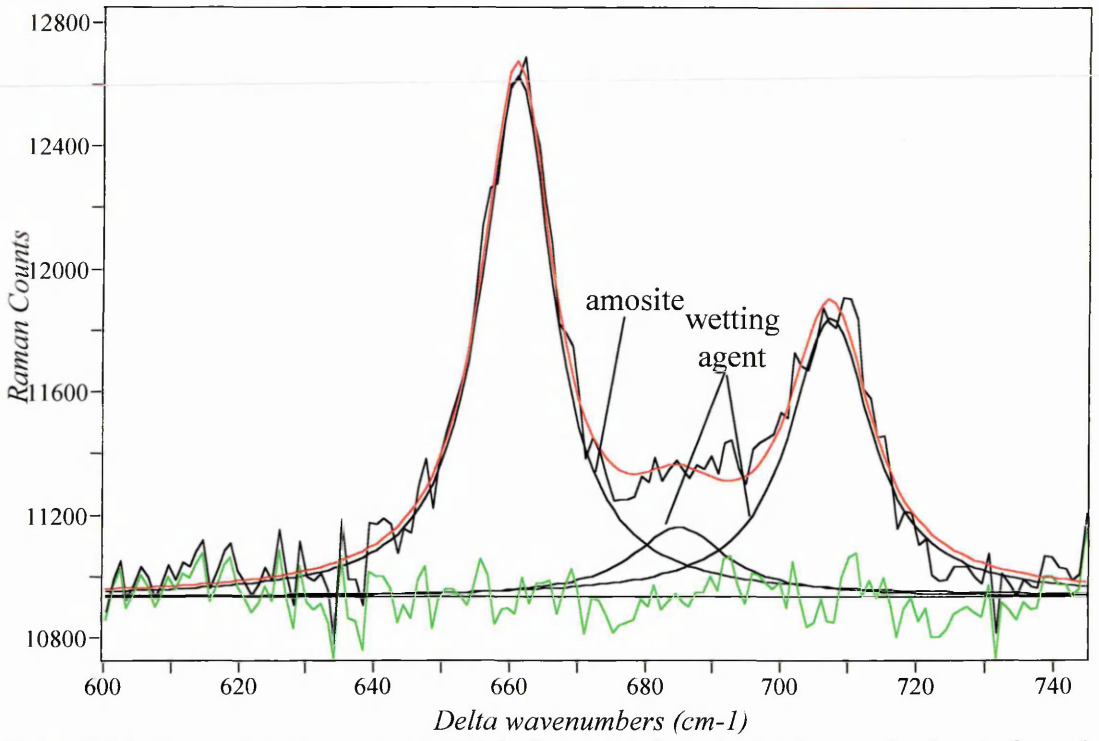

Figure 7.11: Curve fitting of spectrum (3) in figure 7.9, introducing Lorentzian bands from the wetting agent, amosite and quartz.
Figure 7.11.a. Curve fitting in the 440-560 cm^{-1} region; figure 7.11.b. curve fitting in the 600-745 cm^{-1}.

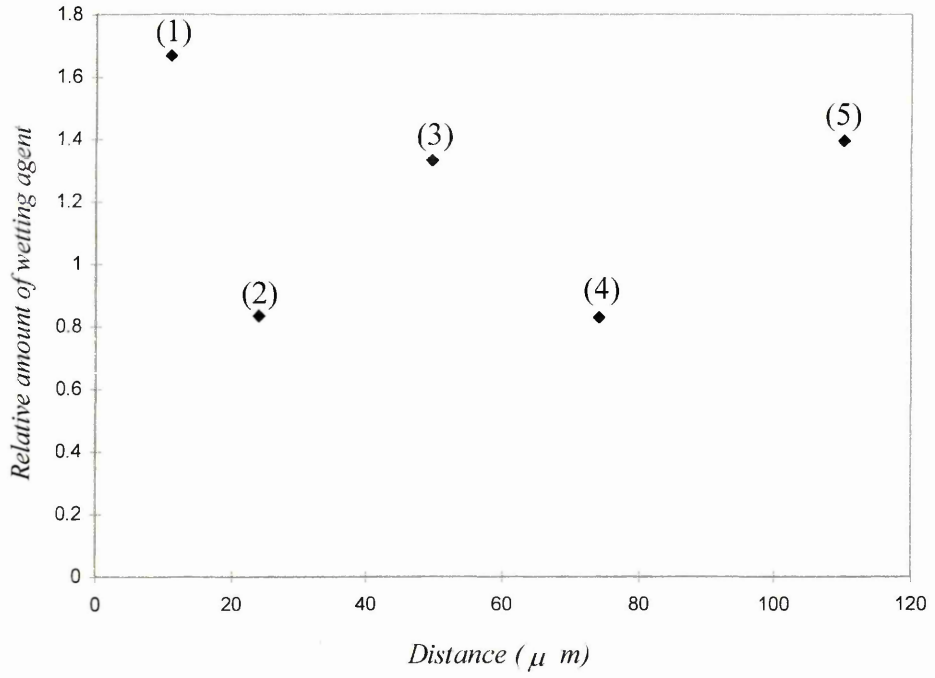

Figure 7.12: Plot of the relative amount of wetting agent along a fibre (figure 7.10) calculated from area bands ratio (spectra 1 to 5 in figure 7.9) of the wetting agent band at 490 cm^{-1} to the amosite at 660 cm^{-1}.

The plot of the relative amount of wetting agent along the fibres contaminated with quartz shows also a complete coverage but with higher values of the area bands ratio than in the previous case. These values were between 0.8 and 1.7. This may be due to a change in the surface morphology. Indeed, the quartz impurities may be fine particles which provide a rough surface where PDMS drains off less easily than a smooth curved surface like pure fibre.

Raman microspectroscopy gave evidence of completely wet as well as dry areas in the insulation material. This incomplete wetting may be due to:
-the quantity of PDMS which was not sufficient.
- more probably, a lack of time for the diffusion of the liquid through the insulation.

7.3. Rotating drum dust generation tester.

7.3.1. Cementitious material containing asbestos.

7.3.1.1. Materials and methods.

A cementitious material containing asbestos was wetted with hotstrip by capillary action from the bottom. The approximate volume of the material was 8.5 cm^3. The amount of wetting agent which was used (2g), corresponded to 24.5 % of the material volume.

Samples taken on top and bottom of the material were directly placed on cellulose filters after splitting up fibres and particles with tweezers. The Raman spectra were collected with the X 50 and X 100 objectives using the red and green laser. The red laser was installed on a new spectrometer. The notch filters, optics and CCD camera are slightly different in order to obtain a higher performance. The green laser remained on the usual instrument. The instrument was set up in microprobe mode.

The concentration of fibres produced by disturbing the wet material in reference with a dry material was measured using a rotating drum tester[2,3]. The running and set up of the tester was explained in chapter 4.

7.3.1.2. Results.

7.3.1.2.1. Raman microspectroscopy.

This cementitious material possessed a low level of fibres. Particles rather than fibres were mainly observed on the filters. These particles were principally identified as $CaCO_3$ showing characteristic bands at 1087, 713 and 280 cm^{-1} (figure 7.13 and 7.15). The spectra of the fibres display strong bands at 660 cm^{-1} and weaker bands at 1020 and 530 cm^{-1} which were attributed to amosite asbestos (figure 7.14).

The Raman spectra, using the red laser, collected on fibres and particles from the bottom of the wet cementitious material show bands from hotstrip as well as different level of coverage and uncovered areas (figure 7.13 and 7.14). However, the bands intensity from hotstrip were generally rather weak on the $CaCO_3$ particles and asbestos fibres spectra.

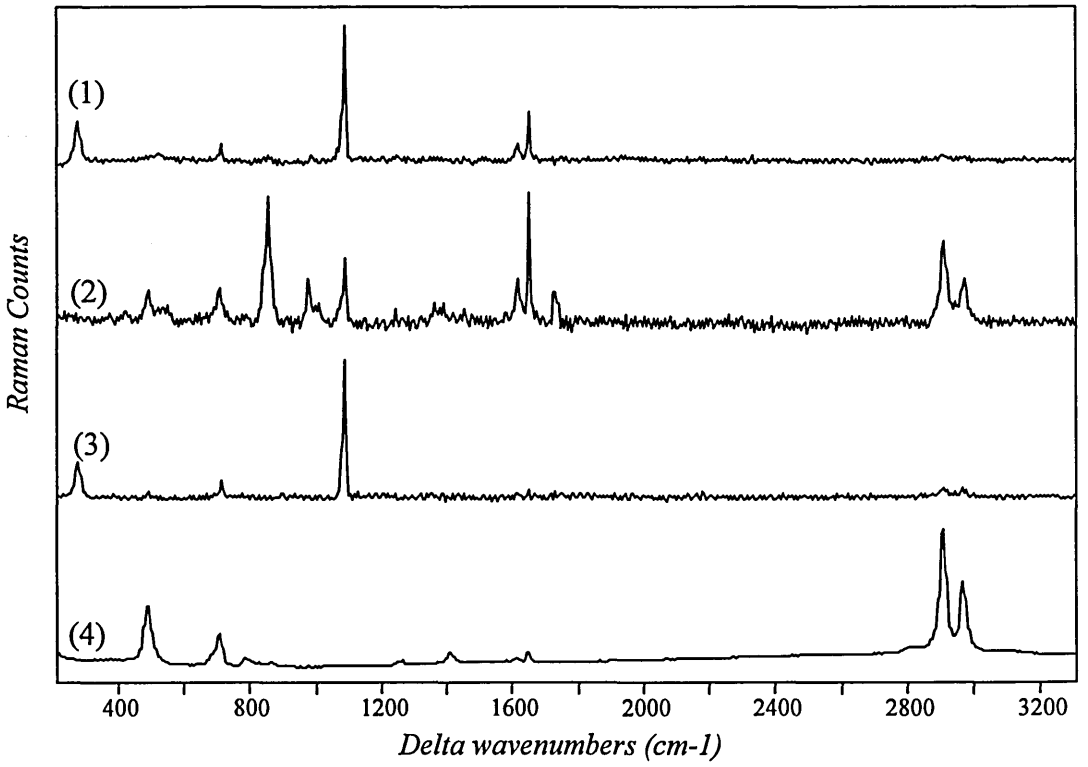

Figure 7.13: Raman spectra collected on particles from the bottom of the wet material in comparison with hotstrip. (1) particle of 40x16 µm size, red laser, X 50 objective, $T_{tot} \approx 3.9$ min; (2) particle of 40 µm size, red laser, X 50 objective, $T_{tot} \approx 7.8$ min; (3) particle of 80x40 µm size, red laser, X 50 objective, $T_{tot} \approx 1.9$ min; (4) hotstrip.
Cellulose filter subtraction and baseline correction applied on spectra (1) to (3).

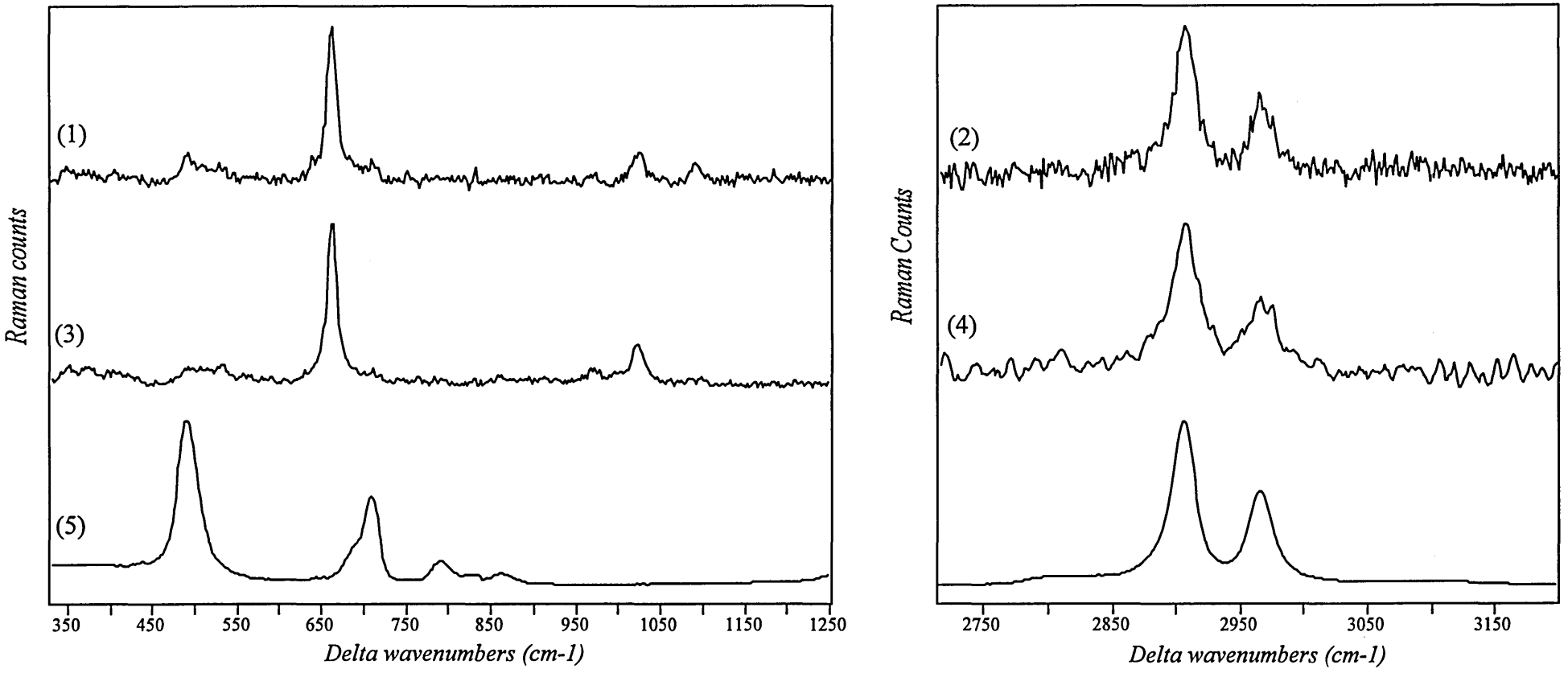

Figure 7.14: Raman spectra collected on a bundle of fibres from the bottom of the wet material, in comparison with hotstrip. (1) and (2) fibres bundle of 7 µm of diameter, position 1, red laser, X 100 objective, (1) $T_{tot} \approx 38.1$ min, (2) $T_{tot} \approx 27.7$ min; (3) and (4) position 2, red laser, X 100 objective, (3) $T_{tot} \approx 38.1$ min, (4) $T_{tot} \approx 27.7$ min; (5) hotstrip.
Cellulose filter subtraction and baseline correction applied on spectra (1) to (4), smoothing function (Savitsky Golay, degree 2, 11 points) applied on spectrum (4).

The Raman spectra collected on particles from the top of the wet cementitious material show also bands from hotstrip (figure 7.15) which proves the presence and diffusion of hotstrip in all the material.

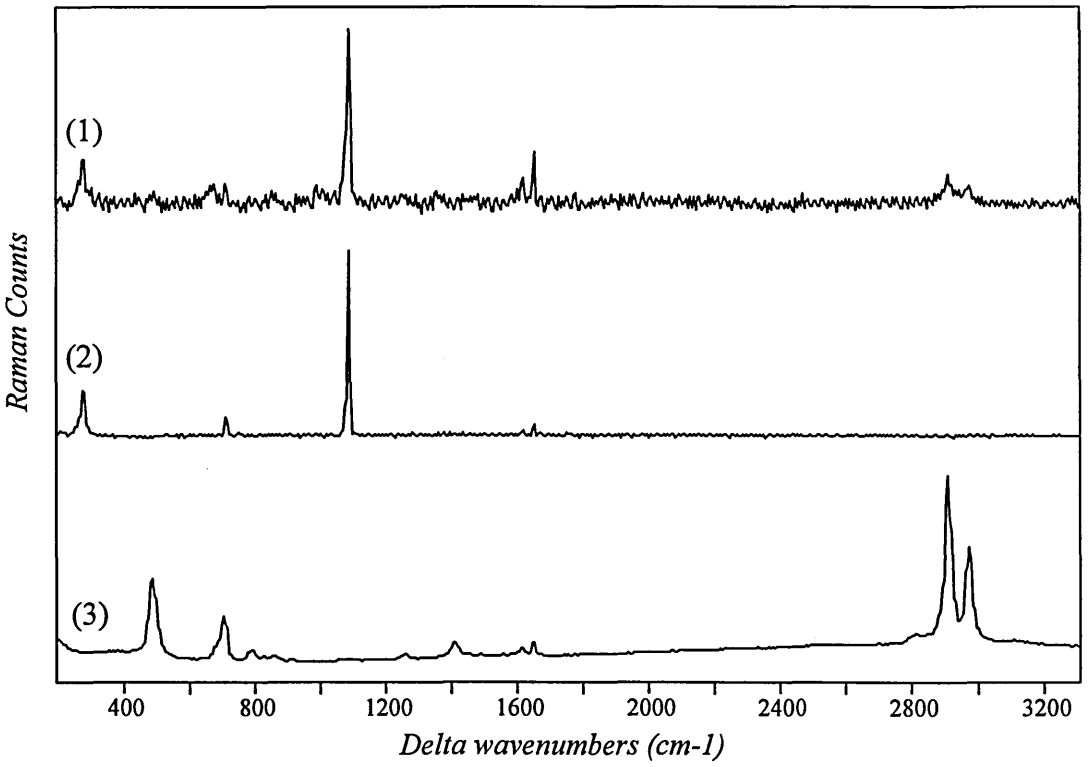

Figure 7.15: Raman spectra collected on particles from the top of the wet material in comparison with hotstrip. (1) particle of 70x50 μm size, red laser, X 50 objective, $T_{tot} \approx 9.1$ min; (2) particle of 50x40 μm size, red laser, X 50 objective, $T_{tot} \approx 5.2$ min (3) hotstrip. Cellulose filter subtraction and baseline correction applied on spectra (1) and (2).

The Raman spectra, using the green laser, collected on particles from the bottom and top of the wet cementitious material show also a complete diffusion of the wetting agent through the material as well as different coverage level of hotstrip on the particles (figures 7.16 and 7.17). However, the wetting agent spectrum exhibits different relative intensity bands ratio. The bands characteristic of the CH stretching vibrations are more intense than the other wetting agent bands. It has to be noted that the red laser has a horizontal polarisation since the green laser possesses a vertical polarisation. Therefore, this change in relative band intensities may be due to an orientation of the PDMS on quartz slide (substrate used to collect the reference spectrum) and on the fibres and particles.

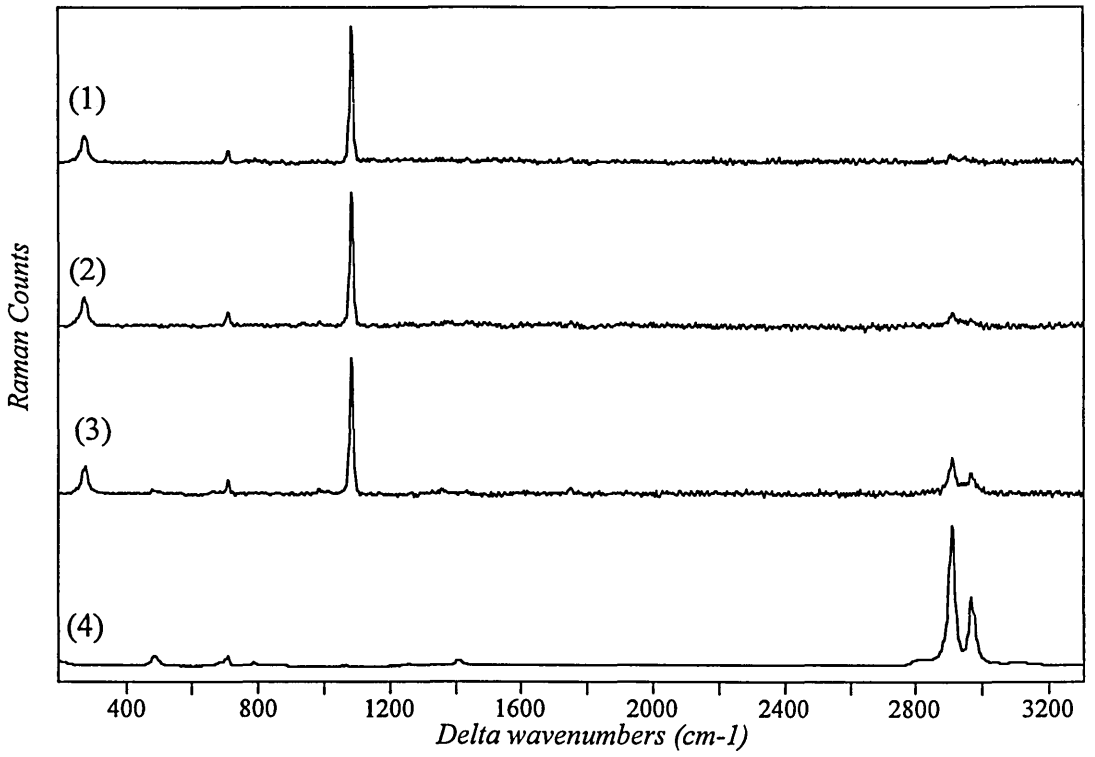

Figure 7.16: Raman spectra collected on particles from the bottom of the wet material in comparison with hotstrip. (1) particle, green laser, X 50 objective, $T_{tot} \approx 2.7$ min; (2) particle of 110x70 μm size, green laser, X 50 objective, $T_{tot} \approx 3.3$ min; (3) particle of 14 μm size, green laser, X 50 objective, $T_{tot} \approx 4.0$ min; (4) hotstrip.
Cellulose filter subtraction and baseline correction applied on spectra (1) to (3).

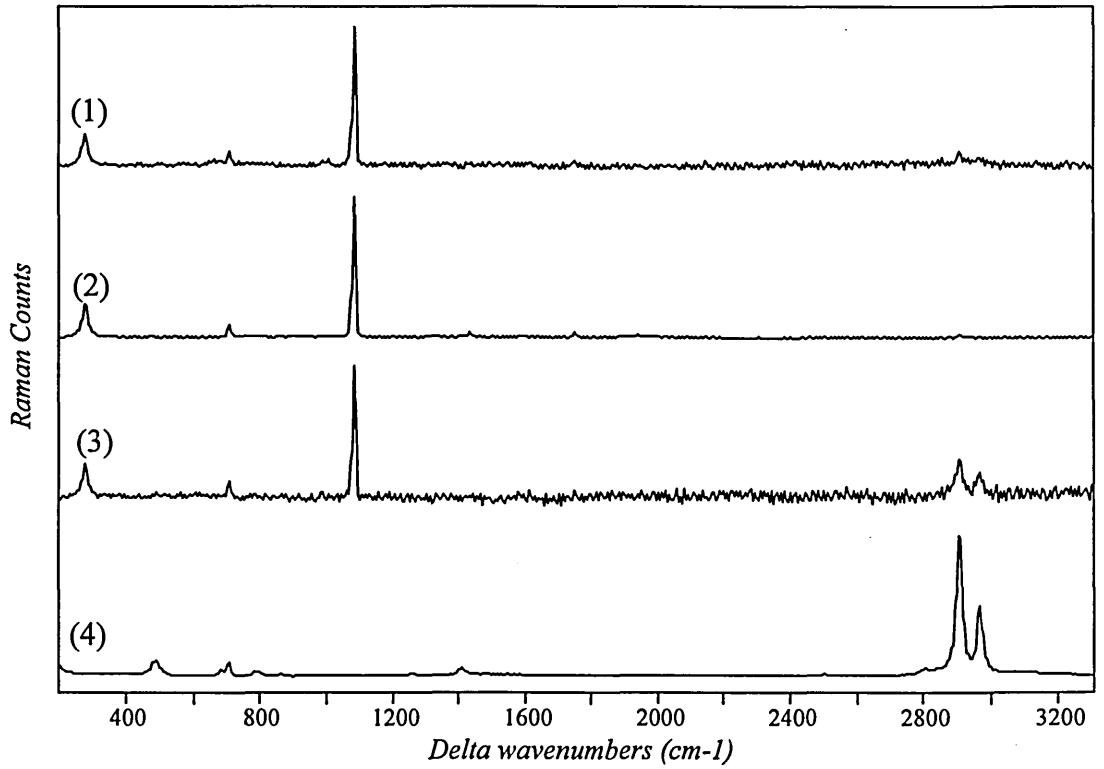

Figure 7.17: Raman spectra collected on particles from the top of the wet material in comparison with hotstrip. (1) particle of 70x30 μm size, green laser, X 50 objective, $T_{tot} \approx 5.3$ min; (2) particle of 50 μm size, green laser, X 50 objective, $T_{tot} \approx 6.6$ min; (3) particle, green laser, X 50 objective, $T_{tot} \approx 2.7$ min; (4) hotstrip.
Cellulose filter subtraction and baseline correction applied on spectra (1) to (3).

The wetting agent diffused in all the cementitious material. Indeed, this material is a porous solid which possesses arrays of capillaries through which the liquid can penetrate[4].

7.3.1.2.2. Rotating drum tester.

The cementitious materials were difficult to break up. Moreover, during the rotating drum experiment, the concentration of dust released from the dry material was relatively low. Nevertheless, the number of fibres generated from the wet material was considerably reduced comparing to the dry material (figure 7.18). After the rotating drum experiment, two large pieces of the wet material were recovered. The maximum of fibres generated from the dry material reached 13 fibres/ml after 4 minutes while less than 1 fibre/ ml was produced from the wet material. This indicates a nearly complete suppression of fibres after wetting.

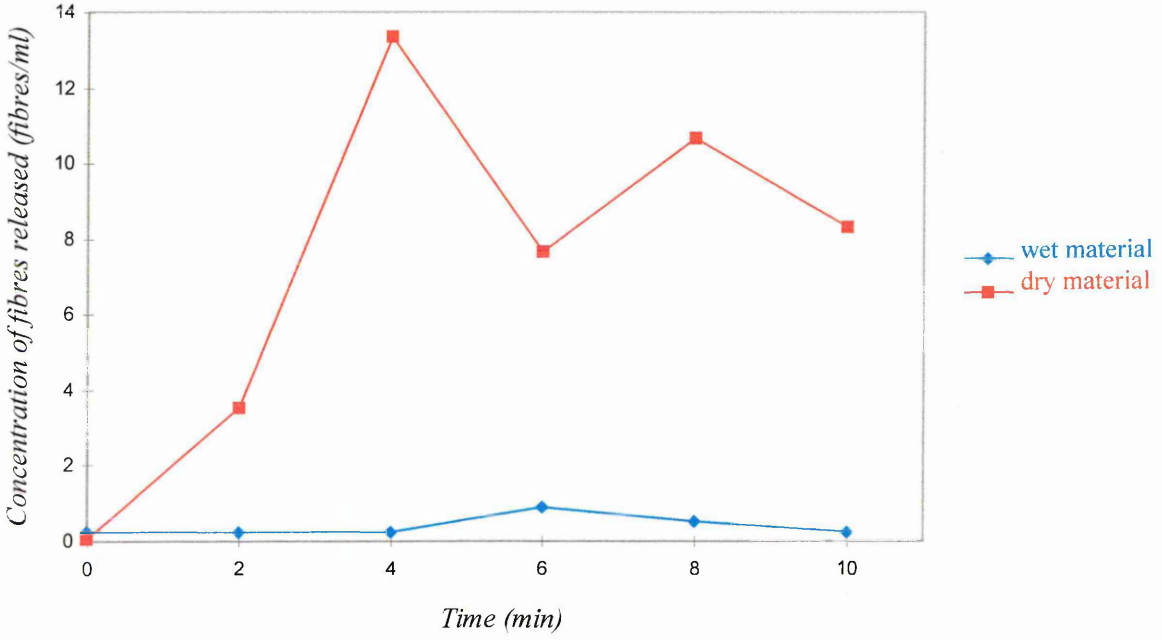

Figure 7.18.: Concentration of fibres released from a wet and dry materials during the drum rotating test against time.

The Raman experiments fit very well with the rotating drum test showing both a complete wetting and diffusion of PDMS through the material.

7.3.2. Friable material containing asbestos.

7.3.2.1. Materials and methods.

A friable material containing a high concentration of asbestos fibres, from an insulation board, was wetted with hotstrip by capillary action from the bottom. The approximate volume of this material was 25 cm^3 corresponding to a weight of 5.6g. The

amount of wetting agent which was used (5g) corresponded to 21% of the material volume. The material was difficult to wet since only about 30 % seemed wet at the bottom. Three samples from the bottom, middle and top, were taken before the rotating drum experiment, and directly placed on cellulose filters by pressing the filters onto the material. In the case of the bottom sample, the filter was also wet. The Raman spectra were collected with the X 50 and X 100 objectives on the new spectrometer using the red laser. The instrument was set up in microprobe mode.

The concentration of fibres produced by disturbing the wet material in reference with a dry sample was measured using the rotating drum tester.

7.3.2.2. Results.

7.3.2.2.1. Raman microspectroscopy.

The material was mainly composed of fibres identified as amosite since the spectra display characteristic bands at 660, 1020 and 530 cm^{-1} (figure 7.20 to 7.22). Other particles, brown grey, which could cover the fibres were observed and identified as some type of oxides (figure 7.19).

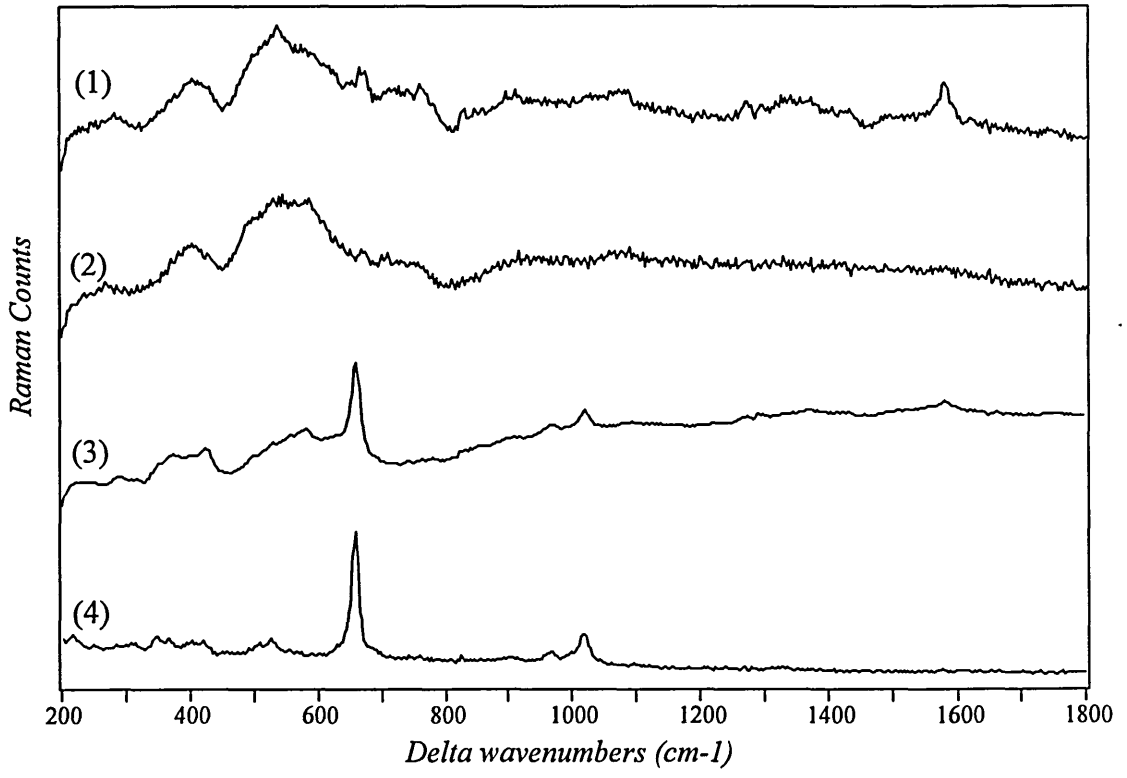

Figure 7.19: Raman spectra collected on particles in comparison with a fibre from the insulation and amosite. (1) grey brown particle of 12x8 µm size, red laser: 25 % attenuation, X 50 objective, $T_{tot} \approx 50.8$ min; (2) grey brown particle of 16x10 µm size, red laser: 25 % attenuation, X 50 objective, $T_{tot} \approx 51.7$ min; (3) fibre of 6 µm of diameter, red laser, X 100 objective, $T_{tot} \approx 25.9$ min - Cellulose filter subtraction applied on spectra (1) to (3).

The bottom of the wet material was completely saturated with liquid. Raman spectra collected on fibres and cellulose filter show strong bands from hotstrip which proved a complete wetting (figure 7.20) of the bottom of the material. However, the spectra of the wet asbestos fibres were not only collected from the fibres but also from the wet filter.

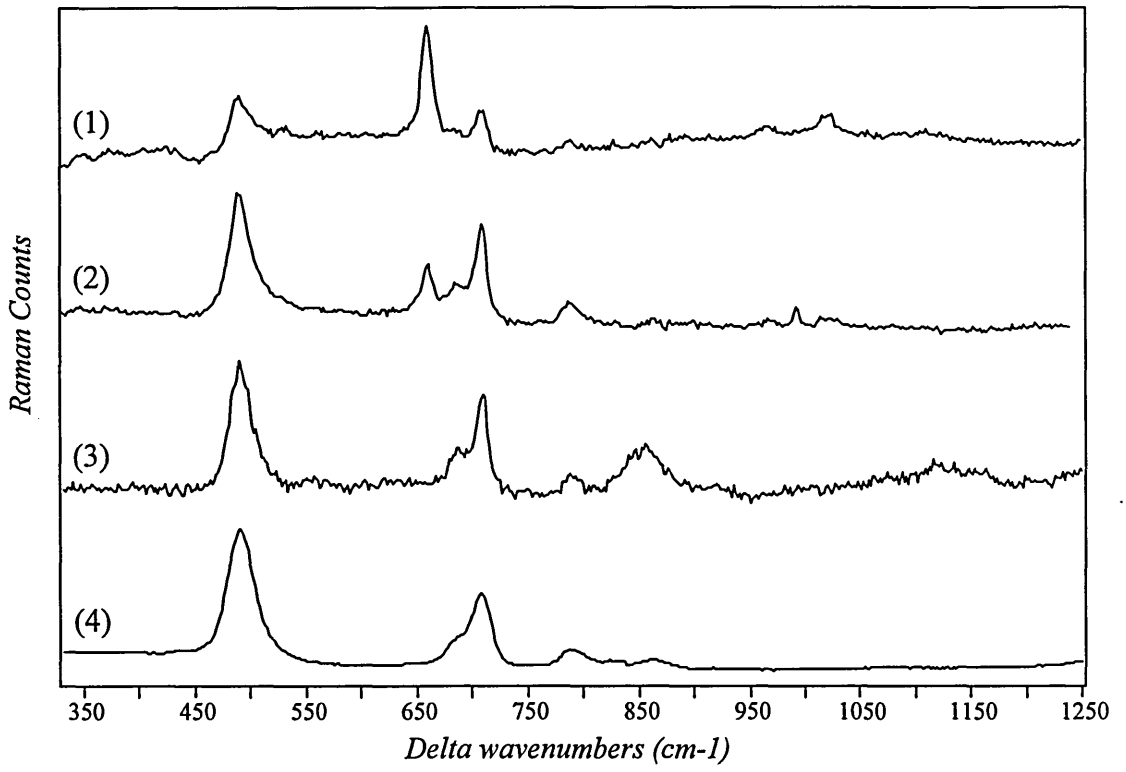

Figure 7.20: Raman spectra collected on fibres and filter from the bottom of the wet material, in comparison with hotstrip. (1) fibre of 2 μm of diameter, position 1, red laser, X 100 objective, $T_{aq} \approx 13.3$ min; (2) position 2, red laser, X 100 objective, $T_{aq} \approx 13.3$ min; (3) wet cellulose filter; (4) hotstrip - Cellulose filter subtraction applied on spectra (1) and (2).

The fibres collected directly on the filter from the bottom of the material were then transferred on another dry filter by pressing it on top of the wet filter. The bands of the wetting agent are not as strong as they were on the wet cellulose filter. On the other hand, some spectra exhibit only bands from the asbestos fibres characteristic of uncovered areas (figure 7.21). As shown in chapter 6, the wetting agent around the fibres drained off and was absorbed by the filter. This rheological phenomenon was explained by the low surface tension and spreading behaviour of PDMS[4,5].

The Raman spectra of the fibres from the middle of the wet material show only bands characteristic of asbestos, which prove the absence of hotstrip in the middle part of the material (figure 7.22). The fibres from the top of the wet material were also uncoated. The wetting agent clearly remained at the bottom of this friable material.

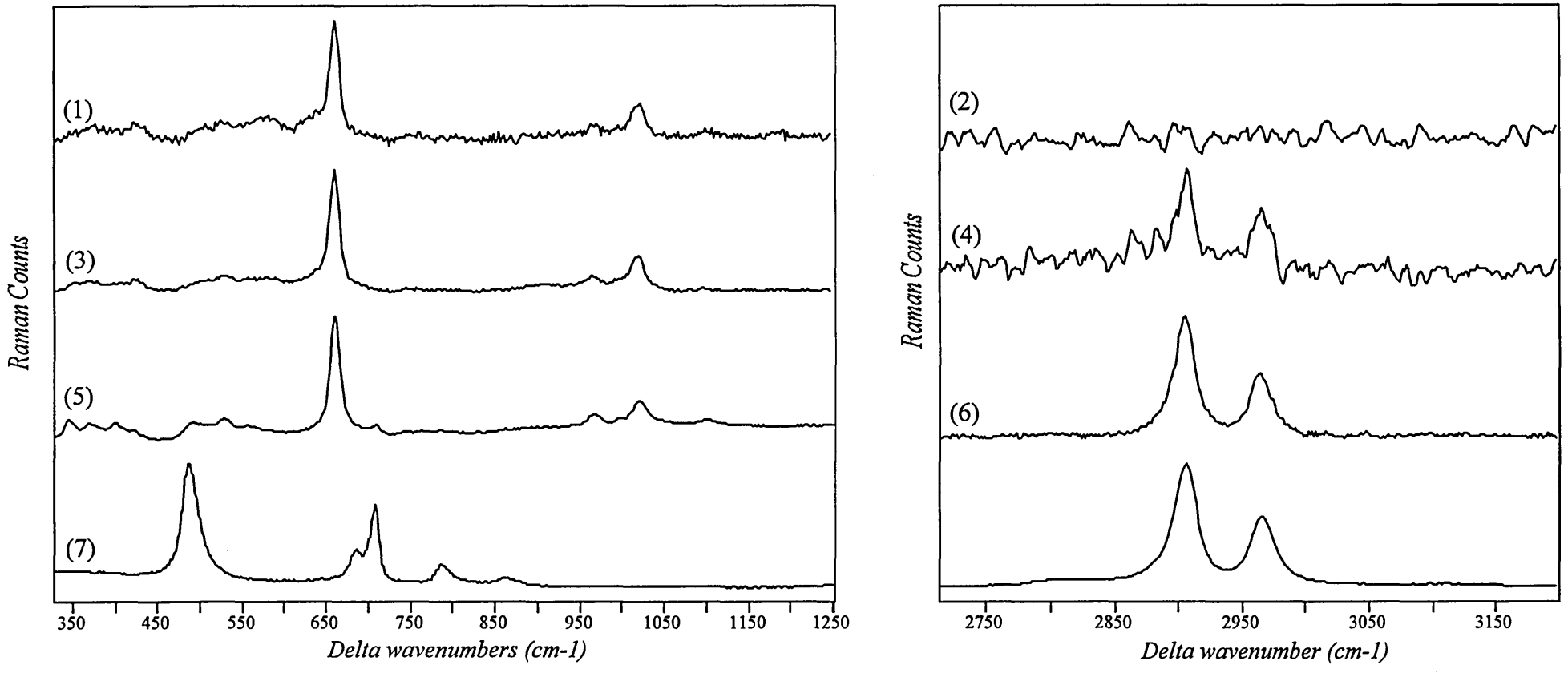

Figure 7.21: Raman spectra collected on fibres from the bottom of the wet material (after transfer on another filter), in comparison with hotstrip. (1) and (2) fibre of 6 µm of diameter, position 1, red laser, X 50 objective, $T_{aq} \approx 2.5$ min; (3) and (4) position 2, red laser, X 50 objective, $T_{aq} \approx 2.5$ min; (5) and (6) bundle of fibres of 16 µm of diameter, red laser, X 50 objective, (5) $T_{tot} \approx 19.0$ min, (6) $T_{aq} \approx 5.0$ min; (7) hotstrip.
Cellulose filter subtraction and baseline correction applied on spectra (1) to (6), smoothing function (Savitsky Golay, degree 2, 13 points) applied on spectra (2) and (4).

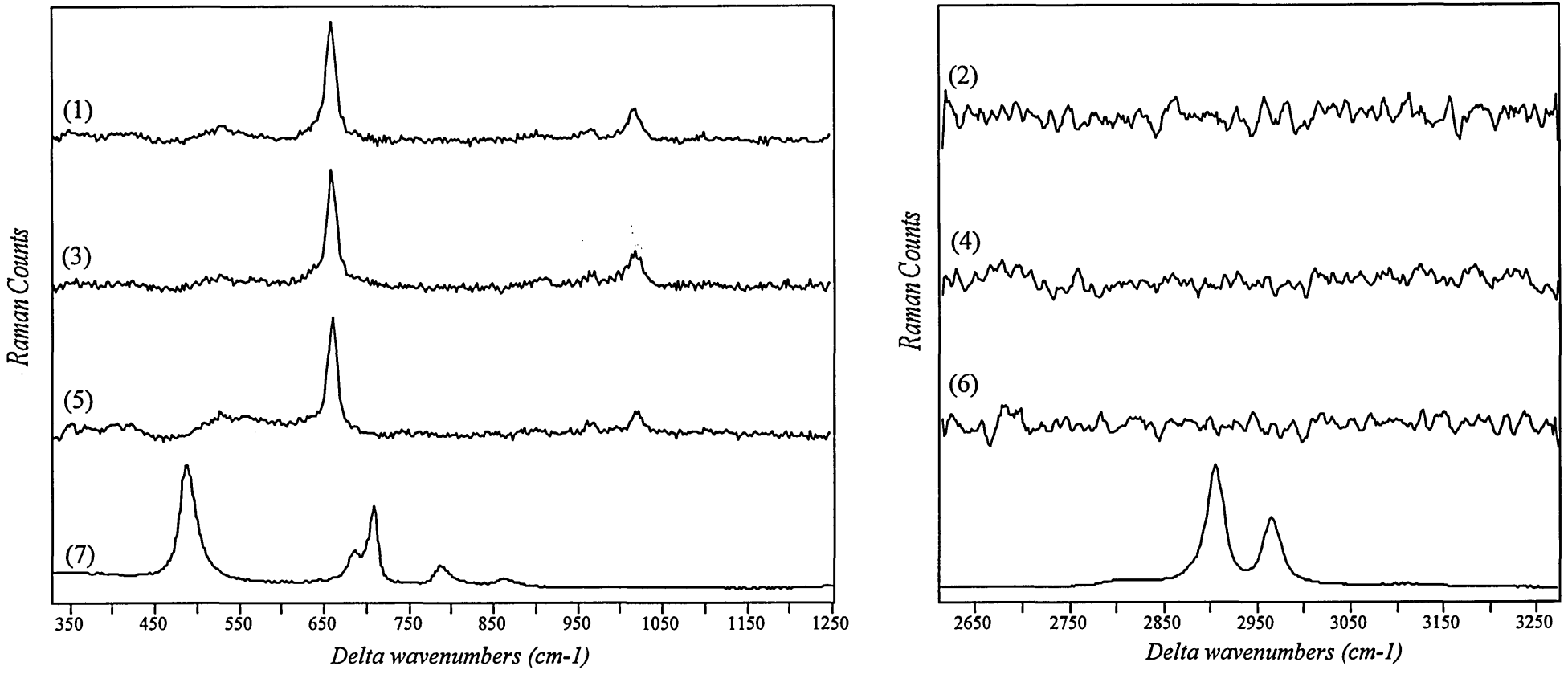

Figure 7.22: Raman spectra collected on fibres from the middle of the wet sample, in comparison with hotstrip. (1) and (2) fibre of 6 μm of diameter, red laser, X 100 objective, $T_{aq} \approx 13.3$ min; (3) and (4) fibre of 3.5 μm of diameter, red laser, X 100 objective, $T_{aq} \approx 13.3$ min; (5) and (6) fibre of 6 μm of diameter, red laser, X 100 objective, $T_{aq} \approx 13.3$ min; (7) hotstrip.
Cellulose filter subtraction and baseline correction applied on spectra (1) to (6), smoothing function (Savitsky Golay, degree 2, 13 points) applied on spectra (2), (4)and (6).

As found in chapter 6 for man-made mineral fibres, PDMS did not penetrate through the material which was mainly composed of fibres. The fact that the liquid was drained at the bottom may be due to a more limited capillary wetting process since the size of voids between fibres are too great for the liquid to bridge.

7.3.2.2.2. Rotating drum tester.

The friable material easily broke up. During the rotating drum experiment, the wet and dry materials were split up into very small pieces. The concentration of dust, mainly fibres, released from the dry material was rather high compared to the cementitious material (35 times higher). However, the level of fibres generated from the wet material still remain extremely high (figure 7.23). The number of fibres produced from the dry material reached 480 fibres/ml after 8 minutes while 340 fibres/ml were released from the wet material. This indicates an unsuccessful suppression of dust after wetting.

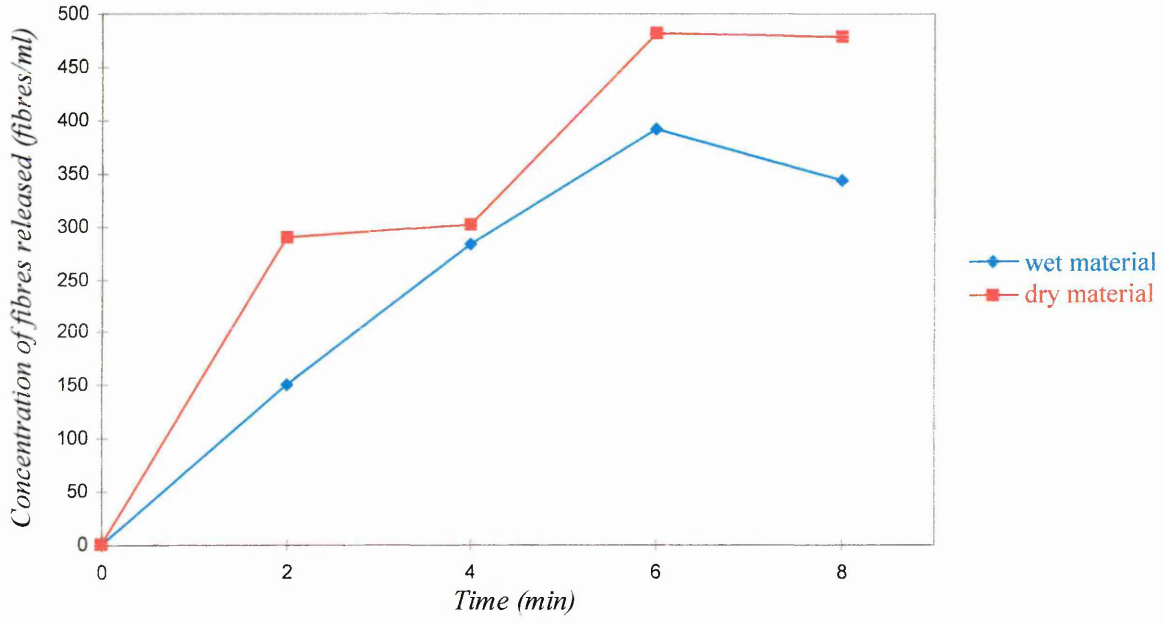

Figure 7.23: Concentration of fibres released from a wet and dry materials during the drum rotating test against time.

The Raman experiments fit also in this case with the rotating drum test showing both a partial wetting of the fibrous material.

7.4. Conclusion.

Asbestos containing materials wetted by PDMS were investigated in this chapter. These materials were either directly collected from an industrial removal site after wetting or wetted by capillary action in laboratory conditions and then tested in a rotating drum which estimated the concentration of fibres released during disturbance of the material.

The coverage measurements of wetting agent on fibres and particles from asbestos containing materials were successfully achieved by Raman microspectroscopy. The distribution and amount of wetting agent along fibres were estimated from the variation of area bands ratio of wetting agent to asbestos. These measurements correlated very well with the observation made on the asbestos removal site and rotating drum tests.

The wetting behaviour of PDMS on asbestos containing materials was as expected from chapter 6.

Asbestos fibres from a wet sample collected on an asbestos removal site, showed a complete coverage. However, the amount of wetting agent on a fibre contaminated with quartz particles was found more important than in the case of a non-contaminated fibre. The quartz impurities might provide a rough surface where PDMS drains off less easily than a smooth curved surface like pure fibre.

PDMS wetted successfully the cementitious material, a porous solid possessing arrays of capillaries through which the liquid can penetrate.

However, PDMS did not penetrate through the material which was mainly composed of fibres as expected from chapter 6. The liquid drained off at the bottom, probably due to the capillary wetting process which was more limited since the size of voids between fibres are too great for the liquid to bridge.

[1] C.Dyer and B.J.E. Smith. J. Raman Spectrosc., 26, 777-785, 1995.
[2] G.Burdett, G.Revell and J.Brammer. HSL Protocol for Dustiness Measurements of Fibreous Materials. Internal report, IR/L/MF/96/06, Health and Safety Laboratory, 1996.
[3] R.Atkinson. Measurement of Asbestos Releases from Different Asbestos Containing Materials, HSL internal report, 44 pp, 1997.
[4] M.J.Jaycock and G.D.Parfitt. Chemistry of Interfaces, Ellis Horwood Limited Ed., John Wiley and Sons, New York, 279 pp, 1981.
[5] D.Narula. Jalca, 90, 93-98, 1995.

8.1. Conclusion.

Raman microspectroscopy has been shown to be:

- a sensitive technique to the composition of materials, which was used to distinguish between similar species.

- and a very powerful technique for the identification of μm size fibres and particles on paper substrates, with little or no sample preparation. The subtraction process of cellulose filter was successfully applied on the spectra.

These particles were either:

- air pollutants such as inorganic fibres (e.g. asbestos and man made vitreous fibres) and diesel particles which are hazardous carcinogenic particles when airborne.
- or gunshot residues of great importance in criminal cases for the identification of the gun and ammunition.

• The Raman spectra of five asbestos reference fibres have shown significant differences, possessing their own features and allowing the possibility to discriminate one type of asbestos from another.

Each asbestos type and its non-fibrous form displayed very similar spectra except for some cases in the ν(OH) stretching region, such as amosite and crocidolite. Nevertheless, a more extensive study on tremolite fibrous and tremolite showed differences in the band widths and positions of the 670 and 390 cm^{-1} bands. These changes might be explained by a difference in the number of defects or by local laser heating.

• Raman microspectroscopy allowed the direct identification of:

- pure inorganic fibres on cellulose filters, especially asbestos fibres as small as 1 μm of diameter.
- unknown fibres, on cellulose filters, from real "industrial" samples like waste asbestos samples from buildings ceilings, walls or pipe insulation.
- other inorganic particles on cellulose filters.

• Raman microscopy was used to discriminate coal and diesel particles. The most significant feature was the difference in the bands intensity ratio of the D to G carbon bands in the Raman spectra of diesel and coal particles, probably due to a more disordered carbon structure in the case of diesel particles compared with that of coal.

• Finally, gunshot residues were successfully identified by Raman microspectroscopy mainly as carbon particles, $BaCO_3$, PbO and mixtures of compounds such as: $BaCO_3$, $PbSO_4$, PbO. The broad band from 700 to 350 cm^{-1} in many of the spectra was attributed to mixed iron or iron/chromium oxides.

Raman microspectroscopy has also been shown a useful technique for the coverage measurements of wetting agents on fibres and particles, with a few μm spatial resolution. It has provided important information about surface coverage of materials with a spatial resolution between 2 and 4 μm.
Indeed, asbestos containing materials which are now being progressively removed, are wetted before removal in order to reduce the concentration of fibres released in the atmosphere during disturbance.

• The coverage measurements of wetting and encapsulating agents on fibres and particles were established from basic laboratory experiments. The amount and distribution of wetting and encapsulating agents along individual fibres were estimated from the band area ratio in the spectra of the wetting or encapsulating agent and asbestos.

• Several wetting or encapsulating agents, materials and wetting process were investigated in this thesis. The Raman measurements correlated very well with:
- the micrographs of wet fibres from the optical microscope.
- the visual examination of the asbestos lagging on asbestos removal site.
- the estimation of the concentration of fibres realised during disturbance of wet materials (rotating drum tests).

• Important information on the ability of the liquids to wet or spread on inorganic fibres and other types of materials such as calcium silicate was obtained.

Wetting agents having a low surface tension and a very small contact angle, show weak adhesion forces between liquid and fibres. This liquid drained off easily on smooth curved surface such as fibres, and spread easily also on flat surfaces. The spraying of such liquid onto inorganic fibre surfaces resulted in good coverage while the wetting by capillary action remains difficult if the material is not porous.

On the other hand, wetting agents which possess a higher surface tension and higher contact angle, show strong adhesion wetting liquid and fibres. The spraying of such liquid covered the surfaces of inorganic fibres in a heterogeneous manner, leaving drops.

It was also shown that emulsions such as silicone, wetted heterogeneous calcium silicate materials leaving the silicone at the bottom while water diffused up to the top.

Porous solid such as calcium silicate, possess arrays of capillaries through which liquids can penetrate. However, in materials mainly composed of fibres, the capillary wetting process is more limited since the size of voids between fibres is too great for liquids to "bridge".

8.2. Future work.

Raman microspectroscopy has been shown to be a very powerful technique for the identification of μm size asbestos fibres. It would be also interesting to study degraded asbestos which may appear in insulation materials.

The carbon spectra from coal and diesel particles displayed differences especially from the band intensity ratios. The next step would be to investigate samples from different sources, as well as mixed coal/diesel samples. The identification of other compounds associated with carbon in coal and diesel particles (such as polycyclic aromatic hydrocarbons (PAHs) in the case of diesel particles) could also be used as criteria of discrimination. This should be investigated.

Wetting and encapsulating agents studied are generally developed from "hands on experience" rather than from the study of chemistry and properties of asbestos containing materials. A study of the adsorption of molecules such as probe molecules (or surfactants) in regards with the chemical and surface properties of insulation materials, by Raman microspectroscopy, would allow the development of a better wetting agent. This would involve using fibres of known properties, the variation in surfactant type and pH in order to achieve chemical matching with the material under investigation.

LIST OF ABBREVIATIONS:

AAS: Atomic Absorption Spectroscopy.

ATR: Attenuated Total Reflection.

CAWR: Control of Asbestos at Work Regulations.

CCD: Charge Coupled Device.

DRIFTS: Diffuse Reflectance Infrared Fourier Transform Spectroscopy.

EDX: Energy Dispersive X ray.

DPM: Diesel Particulate Matter.

HSE: Health and Safety Laboratory.

HSL: Health and Safety Laboratory.

HNF: Holographic Notch Filters.

MIR DR: Mid Infrared Diffuse Reflection.

MMMF: Man Made Mineral Fibres.

MMVF: Man Made Vitreous Fibres.

NA: Numerical Aperture.

NIR DR: Near Infrared Diffuse Reflection.

OES: Optical Emission Spectroscopy.

PAHs: Polycyclic Aromatic Hydrocarbons.

PCM: Phase Contrast Microscopy.

PLM: Polarised Light Microscopy.

RI: Refractive index.

SEM: Scanning Electron Microscopy.

TEM: Transmission Electron Microscopy.

XRF: X Ray Fluorescence.

CONFERENCES ATTENDED:

1. Microspectrometry Applications Group (MAG) Meeting: Sample Preparation and Data Handling.
At Reading Scientific Services Ltd, UK.
1 May 1996.

2. Infrared and Raman Discussion Group (IRDG) and IRDG 3rd Martin and Willis Prize Meeting for Students.
At Glaxo Wellcome Medicines Research Centre, Stevenage, UK.
16-17 October 1996.

3. Microspectrometry Applications Group (MAG) Meeting.
At Zeneca Specialities, Backley, Manchester, UK.
5 November 1996.

4. Microspectrometry Applications Group (MAG) Meeting: 3rd MAG Award for Young Microspectroscopist.
At Perkin Elmer Ltd., Seer Green, Buckinghamshire, UK.
30 April 1997.

5. Infrared and Raman Discussion Group (IRDG).
At Leeds University, Leeds, UK.
31 March- 1 April 1998.

6. XVIth International Conference on Raman Spectroscopy, ICORS'98.
Presented by the University of Pretoria at the University of Cape Town, South Africa.
6-11 September 1998.

PAPERS PUBLISHED:

1. Asbestos Fibre Identification by Raman Microspectroscopy.

D. Bard, J. Yarwood and B. Tylee.

Journal of Raman Spectroscopy, (28), 803-809, 1997.

2. Raman Microscopic Identification of Gunshot Residues.

S. Stich, D. Bard, L.Gros, W. Wenz, J. Yarwood and K. Williams.

In press.

3. Microscopic Identification of Asbestos Fibres Associated with African Clay Crafts Manufacture.

K.K.Peterson, D.Bard, N.Garrington, J.Yarwood and B.Tylee.

Submitted to Annals of Occupational Hygiene (1998).